Synthesis and Tribology of Sialon/TiB_2 Ceramic Composites

Alan Hywel Jones

Thesis submitted for the award of
Doctor of Philosophy

Department of Physics
Centre for Advanced Materials

September 1997

For Gramps
(1919-1997)

Contents

List of Figures

List of Tables

Key to Symbols and Abbreviations

Symbol/Abbrev.	
γ	fracture energy
α_x	coefficient of thermal expansion, x denotes of particle (p) or matrix (m)
a	diagonal length of Vickers indent
c	crack length
c'	crack length for K_{ic} measurement
d	sliding distance in wear test
D	diameter of ball mill
E	Young's Modulus
$H_k(x)$	Knoop hardness (x=load used)
HPx	refers to hot pressing or a material that has been hot pressed x=vol% TiB_2
$H_v(x)$	Vickers Hardness (x=load used)
IRS	In-situ reaction sintering
k	wear coefficient
K_{ic}	Fracture toughness or critical stress intensity factor
LPS	liquid phase sintering
μ	coefficient of friction
ν	Poisson's Ratio
P_0	maximum pressure at axis of spherical on flat contact
PSx	pressureless sintering or a material that has been pressureless sintered, x= vol% TiB_2
ρ	density
R	radius of pin
r	diameter of wear scar or contact area.
RH	relative humidity
σ	stress (subscript identifies type)
V	linear sliding velocity in wear test
W	applied load in wear test
ω	rotational speed of ball mill

Acknowledgements

I would like to acknowledge the financial support of EPSRC and Cookson Syalon plc. who have generously funded this project.

I have received help and support from many people during the course of this PhD. I would like to thank Prof. Mike Lewis for all his input as supervisor on the project and Dr John Lumby for his willingness to impart with knowledge and advice from his many years of experience (of both ceramics and rugby!). I would also like to thank my colleagues and all the technical staff from the department who have assisted in the project in some way. Special thanks go to Steve York, Steve Carpenter and Gerald Smith for all their help, patience and friendship.

I would also like to thank all my friends, both in the physics department and else where, who have made my time spent at Warwick a thoroughly enjoyable and rewarding one. Finally I would like to thank my parents for supporting me throughout my whole academic career. I dedicate this work to my grandfather who died before he could see its completion.

Declaration

This thesis is entirely my own work unless otherwise referenced and has not been submitted for the award of a degree at any other university. The thesis is set out as per the guidelines issued by the Warwick Graduate School (Sept 96).

Parts of this work have appeared in the following publication:

H. Jones, R.J. Lumby, F. Hong and M.H. Lewis, "Ceramic Matrix Composites via In-situ Reaction Sintering", British Ceramic Proceedings No. 53, pp221-232, Novel Synthesis and Processing of Ceramics, Ed F.R. Sale, Institute of Materials, 1994.

Summary

The inclusion of TiB_2 particles in a Si_3N_4 or sialon matrix has the potential to improve the materials properties over those of the Si_3N_4 alone. The combination of the excellent properties of sialon and the high hardness of the TiB_2 makes these materials potentially suitable for tribological applications. This research has investigated the use of chemical reactions that can take place during sintering to synthesise TiB_2 from TiN and BN. The reactions not only produce TiB_2 but simultaneously synthesise the matrix material. The sialon matrix is used as a flexible receptor for excess nitrogen and oxygen.

Using such reactions, sialon/TiB_2 composites were successfully produced by both hot pressing and pressureless sintering. It was shown that these materials achieve densities close to the theoretical and contain only the required phases of TiB_2 and β sialon. Pressureless sintered materials also contain residual sintering aid as an intergranular phase.

The composites were characterised with respect to their microstructure, hardness, fracture toughness and tribological properties. A specially designed wear test apparatus was constructed for the tribological testing. The pin-on-disc apparatus was capable of testing the small volumes of material (minimum diameter of disc ~15mm) typically produced at the development stage.

The materials were found to have high hardness and reasonable fracture toughness which was attributed primarily to the properties of the matrix phase with some possible toughening from the presence of TiB_2. Tribological testing revealed high dry sliding coefficients of friction (μ) for the composites sliding on themselves and reasonable values for the wear coefficient (k) were measured. Wear was found to be dominated by tribochemical reactions forming tribofilms which act to reduce wear of the disc. However, the presence of TiB_2 was not seen to contribute directly to the tribological properties of these materials and the usefulness of this type of composite is questioned.

Chapter One

Introduction

1. Introduction

Ceramic materials are in common use in everyday life, from tableware to precisely engineered components used in automotive and aircraft engines. In the last 20-30 years the use of ceramics in engineering or structural applications has become more widespread[1]. This has been a consequence of several factors;

- increased demand for high performance components to replace metals,
- improved raw materials, processing and machining methods,
- property improvements brought about by an improved understanding of the processes involved in the formation of ceramics and how microscopic material properties influence macroscopic mechanical properties.

Ceramics provide strong, hard, stiff, light-weight components capable of withstanding high temperatures and operating in corrosive environments. The combination of these properties offers performance improvement and cost saving in many applications. The "holy grail" for many years has been the concept of the all-ceramic gas turbine[2] but many other applications such as turbocharge rotors, roller cams, heat exchangers, cutting tools, extrusion dies and biomedical implants have all used ceramics successfully.

However, the application of ceramics to many more structural applications is still limited by their brittle behaviour, poor tolerance to flaws, problems in processing and production and their relatively low resistance to crack initiation and propagation. Another major obstacle to the widespread replacement of metal alloy components with ceramic alternatives has been their cost.

1.1 Description of the Research

The research has been based on the development of a ceramic composite system via a novel production route. The composite material, based upon two well

established ceramics, offers improvements in material properties and in the method of production.

The composite material is a particulate reinforced ceramic matrix composite. The matrix material is sialon[3], reinforced by the addition of titanium diboride (TiB_2) particles.

The potential advantages of this material are;

- Improved hardness and/or fracture toughness over comparable materials
- Possible applications in tribological areas especially in chemically corrosive, high temperature environments (e.g. cutting inserts, extrusion dies.).

The production technique, called *in-situ reaction sintering*, offers several advantages over traditional production methods. It has the potential to be cost saving by using cheaper starting materials which can be handled more conveniently. It may also allow the production of microstructures not readily achievable via traditional methods.

Broadly stated the objectives of this research are therefore:

1. The production of sialon/TiB_2 ceramic matrix composites by in-situ reaction sintering using both hot pressing and pressureless sintering.
2. The measurement of key engineering properties of these composites.
3. The design and construction of a wear test apparatus. Most conventional wear test apparatus use large specimens (e.g. discs of > 50mm diameter). Because of the limited size of materials produced at a development level the apparatus should be capable of testing small samples (e.g. <25mm diameter).

1.2 An Overview of Ceramic Materials

There are many types of ceramic materials; in the following sections these are defined and classified by the applications in which they are used.

1.2.1 Classification of Ceramic Materials

The definition of a ceramic material is not an easy one to make. A common perception is that a ceramic is an inorganic, non metallic material usually produced by a heating process and that they are hard, brittle materials with poor heat and electrical conduction and that they are non-magnetic. For example, the following material groups are traditionally thought of as ceramics:

Materials	Examples
oxides	SiO_2, Al_2O_3
carbides	SiC, TiC
nitrides	Si_3N_4, AlN
borides	TiB_2, ZrB_2

Table 1.1 Material groups commonly regarded as ceramics

Traditional Ceramics

The raw materials from which ceramic materials are formed come from a range of sources, including minerals and organic products such as rice husks. Many of these raw materials are still used today, with some refinement, in the production of traditional ceramics which is still the largest section of the ceramic industry. Products range through whiteware, brick, cement, abrasives and glassware all of which are in common, everyday usage.

Refractories

Another large proportion of the ceramic industry is concerned with refractory materials. These materials are designed and used primarily for their ability to function at high temperatures, where metals are not suitable, and their insulating properties allow isolation of high temperature components and processes. Typically they are of a complex multiphased composition. They can range from fire-clay refractories used in basic furnace brick production to silica refractories used because of their higher tolerance to (compressive) loading and high purity

alumina, used because of its resistance to chemical attack. They should be regarded as separate from structural ceramics discussed in 1.2.2 because they are not suitable for use where there may be significant applied stress.

1.2.2 Structural or Engineering Ceramic Materials

In the last 50-60 years the scientific study of ceramic materials has led to a much better understanding of their processing and materials properties and this has facilitated the refinement of naturally occurring minerals and the synthesis of new compositions. These new high purity, chemically controlled materials, often referred to as technical, engineering or structural ceramics, are of highly controlled composition and structure and have been designed to meet the demands of modern applications in the automotive and aeronautical industries. Modern ceramic materials can be split into several groups, depending upon their composition, properties or applications but many cross the borders between these distinctions.

Examples include oxide ceramics (such as Al_2O_3, ZrO_2, MgO), magnetic ceramics (such as $PbFe_{12}O_{19}$, $ZnFe_2O_4$), ferroelectric ceramics ($BaTiO_3$) and the nitrides, carbides and borides used in structural applications such as bearings, cutting tools, extrusion dies and turborotors (Si_3N_4, SiC, BN, B_4C, TiB_2). It is this later group of ceramics upon which this research is based.

1.3 Production of Ceramics

There are several routes to producing the raw materials from which structural ceramics are synthesised. In this work commercially available powders are used for purity, consistency and quality reasons.

Firstly, powders with appropriate properties for shaping and sintering must be selected from the available grades, taking into consideration particle size and purity. These powders are processed to form a consolidated, shaped component from the powder, followed by firing to achieve full density and the required microstructure. Since a material's properties are strongly related to

microstructure and composition, the proper understanding and control of the processes involved in densification and microstructure development are essential for the successful production of ceramic components.

1.3.1 Powder and Precursor Processing.

The choice of raw materials and the way in which they are processed can have significant effects on the properties of the finished product. The strength of ceramics is usually determined by the presence of internal flaws (see section 1.4.1). Other properties, such as creep and oxidation, are strongly influenced by the chemical composition of the finished product. Many of the strength limiting flaws typically found in densified ceramics are introduced by, or a consequence of, the powder precursors and their processing. Chemistry and composition is influenced by the purity of the starting powders. For example, in Si_3N_4 densified with MgO the creep resistance is severely affected in the presence of Ca impurities[4] which lower the softening point of the intergranular phase but, when Y_2O_3 is used as a densification aid, the Ca is absorbed into the crystalline phase by solid solution and the effect is much less pronounced[5].

Most conventional fabrication techniques begin with fine powders which require consolidation and shaping before firing to produce dense materials with the required composition. To achieve this, the powders should be of a range of particle sizes to allow close packing and the elimination of as much porosity as possible at the consolidation stage. Small particle sizes are desirable because of the increased surface area and the accompanying increase in the driving force for densification (i.e. the reduction of free surface energy). This is especially important when using pressureless sintering fabrication routes or when small grain sized microstructures are preferred. High surface areas also increase the reactivity of the powders which is important when using reactions between the powders, during the sintering process, to synthesise components of the composite structure.

Consolidation and shaping form the powders into as tightly packed structures as possible in the required shape. The practical limit of the level of densifcation

achievable by consolidation is governed by the stresses that the consolidated body can withstand[6]. Many consolidation and shaping techniques form stresses in the powder bodies that lead to cracking or deformation that is undesirable in components to be fired. These problems are discussed further in the experimental techniques chapter. Some examples of commonly used consolidation and shaping techniques are uniaxial pressing, isostatic pressing, injection moulding, slip casting, tape casting and extrusion.

1.3.2 Densification Process for Ceramics

Many ceramic materials can be sintered via a thermally activated solid state route. The driving force is the reduction in Gibbs free energy (ΔG) by the replacement of high energy grain surfaces by lower energy grain boundaries. However, for the nitride systems considered in this work the diffusion rates for solid state sintering are extremely low. Higher levels of thermal energy (i.e. an increase in the sintering temperature) lead to the disassociation of Si_3N_4. Densification of Si_3N_4 materials is almost always achieved via a liquid phase sintering route.

1.3.3 Liquid Phase Sintering

There are three general requirements for liquid phase sintering (LPS)[7,8]:

1. a liquid must be present at the sintering temperature,
2. there should be good wetting of the solid by the liquid,
3. the solid must be reasonably soluble in the liquid.

The process of LPS itself is split into 3 stages, I - rearrangement, II - solution-precipitation and III - final pore removal. In stage I a number of simultaneous processes occur; melting, wetting, spreading and redistribution of the liquid phase. Both the solid particles and the liquid are rearranged by capillary forces in the liquid phase situated between particles[9], see Figure 1.1., which can reach levels of 1.2 to 12MPa in silicate liquids .

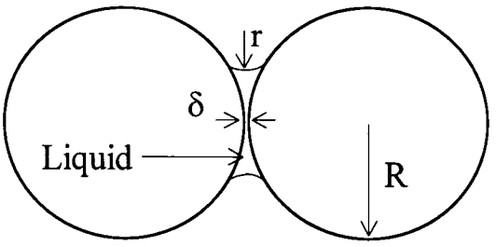

Figure 1.1 Liquid present between two solid spheres exerts a capillary force, pulling them together.

The liquid present between powder particles also acts as a lubricant allowing easy movement of particles. Densification due to rearrangement slows as a close packed structure is formed and movement is inhibited by the impingement of neighbouring particles. Where these contacts are first formed the small contact area causes high stresses which lead to further small increases in densification via plastic deformation and creep. The viscosity of the liquid phase present has a significant effect upon the rate of densification due to rearrangement.

In stage II, solution-precipitation, the solid material is dissolved into the liquid phase and then precipitates out onto existing grains. This process is often accompanied by a phase change such as in Si_3N_4 where α Si_3N_4 dissolves into the liquid and precipitates out as β Si_3N_4. This leads to shrinkage of pores by the build up of precipitated material on the pore walls and grain growth. Differential dissolution takes place according to grain shape and size. Small particles and sharp corners dissolve into the liquid more readily and re-precipitate out onto coarser grains. Hence small particles and sharp corners are eliminated and a coarser grain structure results. This process occurs concurrently with further rearrangement of grains due to capillary forces that are still present. The interconnecting pores, present in the original green body, are isolated as this process occurs forming closed porosity in the powder compact at about 90-95% of the theoretical density.

In stage III gases are usually trapped within the closed pore structure and the vapour pressure within these pores and the reduction in the densification driving force caused by the increase in particle size (i.e.: the reduction of stress at

interfaces) can lead to a halt in densification or bloating as the internal gas pressure of the pore counteracts the driving force for shrinkage. During the final stage of LPS several processes can occur simultaneously such as grain growth and coalescence, pore expansion, diffusion of the liquid into the solid phase, formation of reaction products and phase changes. The effect of these concurrent processes is complicated and not fully understood and empirical methods for producing fully dense materials are commonplace.

In order to densify a material using the processes described above it is common to mix additives with the starting powders that form liquid phases at the sintering temperature. For example, to densify Si_3N_4 and sialons metal oxides such as MgO, Y_2O_3 or Y_2O_3 + Al_2O_3 are used. These additives, while allowing sintering to full density, remain in the structure, normally as amorphous intergranular and grain boundary phases. This is clearly undesirable for high temperature applications as the viscosity of these residual phases at high temperatures can severely effect a material's properties. There has been much work performed on this problem but one approach is to reduce, as much as possible, the amount of additive used.

1.3.4 Hot Pressing (HP)

Hot pressing uses applied pressure during the firing cycle to increase the driving force for sintering. The application of pressure accelerates densification by increasing the contact stress between particles and also aids particle rearrangement, improving packing. It is possible then to use less liquid forming additive if applied pressure is used to compensate for the low levels of capillary forces due to small amounts of liquid. It also lowers the required sintering temperature which has several advantages; firstly, it avoids any stability problems of constituents at high temperatures and secondly it avoids temperatures that may promote unwanted grain growth. Since many of a material's mechanical properties are dependent upon grain size and high density, hot pressing can produce ceramics with excellent mechanical properties. Hot

pressing also minimises residual porosity which leads to stronger materials (see Table 1.2).

Ceramics produced by hot pressing are limited to simple shapes such as discs or tiles and this fact makes it an undesirable technique for the production of complex shaped components as might be needed in many applications.

Material	Sintering Aid	Density (% theoretical)	MOR* @ 22°C	MOR @ 1350°C
HP Si_3N_4	5% MgO	98	587	173
S Si_3N_4	5% MgO	~90	483	138
HP Si_3N_4	6% Y_2O_3	>99	897	669
S Si_3N_4	13% Y_2O_3	~98	587	414

* Modulus of Rupture. S Si_3N_4 = sintered silicon nitride, HP Si_3N_4 =hot pressed silicon nitride.

Table 1.2 Comparison of densities and strengths of Si_3N_4 produced by hot pressing and pressureless sintering.[10]

A variation on hot pressing is hot isostatic pressing (HIP)[11] in which the pressure is applied from all directions during firing. The pressure is applied by an inert gas such as argon or helium and hence the part to be fired must be evacuated and encapsulated in a gas impermeable envelope, usually a high temperature capable glass. HIPing is suitable for near net shape production and produced higher densities than pressureless sintering. However, due to the high specifications of the equipment and the difficulty in glass encapsulation HIPing is often prohibitively expensive.

1.3.5 Pressureless Sintering

The hardness of most ceramic materials is in fact an impediment when complex shapes are needed because of the difficulty and cost of diamond machining to final dimensions. It is desirable then to sinter shapes that require the minimum of machining after densification. Pressureless sintering can produce such components by using increased amounts of sintering aids to form enough liquid phase to promote sintering without applied pressure. This is aided by using very fine starting powders (i.e. large surface areas) which increases the capillary

forces and the driving force for the replacement of free surface with particle contacts (i.e.: grain boundaries). Pressureless sintering provides a reproducible shrinkage in components on densification hence careful green body formation can produce components which require very little machining to achieve the final shape and tolerances. It is however, a more complex process than hot pressing and not only must composition, particle size, temperature and time be controlled but other factors such as atmosphere, furnace design and materials used in the furnace, placement of the specimen and all the powder processing steps prior to sintering can have significant effects upon the results.

The large amount of residual sintering aid can significantly influence the materials properties and several methods have been used to tailor the properties of these phases to provide optimum properties. For example, use can be made of the crystallisation of the residual amorphous phase either during cooling or by post production heat treatment. The ability to crystallise the amorphous phase depends strongly on the composition and the homogeneity of the glass.

1.3.6 In-situ Reaction Sintering (IRS)

This research uses a technique called in-situ reaction sintering (IRS) to produce the required phases and microstructures of the ceramic composite. Traditional methods add secondary phases in powder form at the powder preparation stage. IRS synthesises the required phase through chemical reactions during the sintering process. This approach uses raw materials that react producing the compounds required in the composite. A novel application of this approach is the use of reactions that not only produce the secondary phase but whose by-products contribute to the simultaneous synthesis of the matrix phase.

	Reaction	ΔG J/mol (2000K)	Composite
1	$3TiO_2 + 4AlN + 3C = 3TiC + 2Al_2O_3$	-2.75×10^5	TiC/Al_2O_3
2	$Ti_2O_3 + 2AlN = 2TiN + Al_2O_3$	-2.51×10^6	TiN/Al_2O_3
3	$3B_2O_3 + 3TiO_2 + 10Al = 3TiB_2 + 5Al_2O_3$	-1.01×10^6	TiB_2/Al_2O_3
4	$4TiN + 8BN + 9Si = 4TiB_2 + 3Si_3N_4$	-2.49×10^4*	TiB_2/Si_3N_4
5	$4TiN + 8BN + AlN + 0.5Si_3N_4 + 9Si + 0.5SiO_2 = 4TiB_2 + Si_{11}AlON_{15}$	--	TiB_2/β sialon
6	$B_2O_3 + 3AlN + Si_3N_4 = 2BN + Si_3Al_3O_3N_5$	--	BN/β sialon
7	$2\ TiO_2 + 2B_2O_3 + 10AlN + 5Si = 2TiB_2 + Si_5Al_{10}O_{10}N_{10}$	--	TiB_2/sialon

Table 1.3 Possible reactions for the production of composites via in-situ reaction sintering. (*1500K)

At Warwick a range of possible reactions for producing nitrides and borides in Si_3N_4 and sialon matrices, in which the matrix phase was synthesised simultaneously have been investigated.[12] The viability of the reactions was investigated by using JANAF, the MTDATA program from NPL and from experimental studies.

Table 1.3 presents potential reactions for in-situ reaction sintering. Of particular note are the reactions which produce transition metal nitrides or borides from their oxides or nitrides in sialon matrices. In these cases not only is sialon produced simultaneously but the matrix acts as a flexible receptor for the excess nitrogen/oxygen produced by the reduction/oxidation reactions that take place during synthesis of the second phase. Also of note is that reaction between oxides (no.7), that are always present on the surface of nitride powders, also contribute to the production of matrix and particulate phase.

The use of in-situ reaction sintering in the way described above can lead to several advantages over the direct addition method.

1. The cost of starting materials may be reduced as oxides and nitrides of transition metal compounds are usually cheaper and more readily available than the borides.

2. Unique microstructures may be achievable due to the improved sinterability and the production of particulate phases *during* the sintering process.

3. In some cases, such as for TiB_2, the powder form of the compound can be hazardous and, for safety reasons, can require elaborate handling and processing procedures. Producing TiB_2 in-situ from the less hazardous and more readily available nitrides and borides avoids this problem.

It has been shown that several of the above systems are viable and dense TiN/sialon composites have been produced with high enough volume fractions of TiN that the materials has the potential for electro-discharge machining[13].

The initial aim of the research was the application of the above methods to the production of sialon/TiB_2 composites by the reaction of TiN and BN and the simultaneous production of the sialon matrix. The aim was to optimize the production of sialon/TiB_2 composites by hot pressing and to develop compositions that would be suitable for pressureless sintering.

1.4 Properties of Ceramics

The use of ceramic materials in many applications has been precluded by the limitations imposed by their mechanical properties. In this section the basic properties and limiting factors of ceramics are examined and the solutions offered by the use of ceramic composite materials are discussed.

1.4.1 Failure of brittle materials

One of the most serious problems with ceramic materials is that they exhibit brittle failure under applied stress at room temperature. Unlike metallic systems which can exhibit plastic deformation, ceramics undergo very limited macroscopic plastic deformation under applied stress. This is a consequence of the atomic bonding present in ceramic systems. The similar ionic size and close packed structure of metals allows the dislocation motion necessary for plastic deformation. The mixture of ionic and covalent bonding found in ceramics means that the slip systems necessary for dislocation flow do not exist and therefore large scale plastic deformation does not occur. In order to overcome this limitation it is first necessary to understand the behaviour of ceramic materials under load and the cause of the failure.

In considering this situation the stresses encountered by the material are assumed to be tensile in nature. Even though ceramics tend to be an order of magnitude stronger under compressive stresses, a pure compressive stress is difficult to achieve and failure under compressive modes is usually caused by some element of tensile stress. The failure mode of ceramics can be dependent upon temperature, low temperature tests will exhibit brittle behaviour while high temperature tests may demonstrate some plastic deformation. For simplicity only low temperature behaviour will be discussed here and the focus will be on the behaviour of polycrystalline materials. In polycrystalline ceramic materials the random crystallographic orientation of the grains usually gives rise to isotropic properties even though individual single crystal grains will have anisotropic properties.

Most materials have an elastic region where they behave linearly and reversibly under applied stress, when the yield stress is reached the material reaches its elastic limit and plastic deformation or failure then occurs. Polycrystalline ceramics, when tested in bulk at room temperature, exhibit no significant plastic deformation and will fail in a brittle manner at the yield point. This is due to their complex crystallographic structures and strong directional bonding (e.g.

70% covalent in Si_3N_4) which means that the dislocation movement necessary for plastic flow cannot occur. In plastic materials (i.e. materials in which the movement and flow of dislocations is easily achieved such as metals) any small flaws present in the material have a significant macroscopic plastic zone associated with them and the plastic work done absorbs energy and prevents such flaws developing into running cracks that lead to failure.

In brittle materials, little plastic flow is possible, no such zone is present and very little plastic work is done. In such a situation small flaws catastrophically grow under a critical applied stress, leading to brittle failure. This does not imply that plastic processes do not occur in ceramics, there is a highly localised plastic zone at the crack tip. While some energy is absorbed by plastic deformation resistance to crack propagation is caused primarily by crack shielding processes at the crack tip.

The low observed strengths of brittle ceramics (much lower than theoretically predicted values) was explained by Griffith[14] who suggested that flaws in the material act as stress concentrators and that the separation of surfaces during fracture takes place sequentially rather than simultaneously across the cross section.

Griffith considered an elliptical crack and showed that fracture will occur when,

$$\sigma_f = \left(\frac{E \gamma_0}{A c} \right)^{\frac{1}{2}} \qquad \textbf{Equation 1.1}$$

where σ_f is the critical stress for fracture, E is the Young's modulus, γ_0 is the fracture surface energy and c is half the crack length. A is a constant depending upon the loading geometry, so for plane stress (i.e. stress parallel to the cracks length are zero) $A=\pi/2$ and for plane strain $A=(\pi(1-n2)/2$ where n is Poisson's ratio This is a necessary but not always sufficient condition for cracks to propagate. An important aspect of the Griffith equation is that the failure stress varies inversely with the square root of the crack size.

Ceramic materials, because of the inability of dislocations to move and flow, fail in a brittle manner and are very sensitive to the inherent flaws invariably present in or at the surface of any material. Such flaws, introduced during processing, act as stress concentrators. Fracture is initiated at the most serious flaw present and this leads to the statistical nature of strength in ceramics, i.e. the variation in flaw sizes between test pieces gives rise to differing strength results exhibited by otherwise identical material.

It is the reduction of the number and size of these flaws in the material and the increase in the material's resistance to crack propagation that are the major challenges for the ceramic engineer when designing ceramics to meet the demands of modern applications.

1.4.2 Fracture Toughness

It is extremely difficult to produce materials that do not contain some form of internal flaws. Even a flawless material will accumulate damage during service which will lead to failure. In this case the ability to resist crack growth is an important property in a ceramic material. If the critical stress at which a crack will extend is raised then the ceramic can reach higher stresses before failure. Irwin[15] followed the initial work by Griffith and determined the local stress field at the tip of a sharp crack due to macroscopic externally applied stress. His expression for the stresses around a crack tip included the term K called the stress intensity factor which has the units of $MPa \cdot m^{1/2}$. Irwin showed that, as the applied stress is increased, K reaches a critical level, K_c, at which point the crack propagates unstably, as described by Griffith. This critical stress intensity factor is highly material dependent and is known as the fracture toughness. There are three modes of crack loading, I, II and III describing the differing directions of applied stress on the crack. In brittle materials usually only mode I, the "opening mode" operates (tensile stress normal to the plane of the crack) and hence the fracture toughness is written K_{Ic}. The increase in K_{Ic} is an important goal for many structural ceramics. Wear in many materials is caused by the removal of material by sub-surface cracks propagating under repeated loading.

Improving fracture toughness so that these cracks are more difficult to propagate is one approach to achieving better wear resistance.

1.4.3 Hardness

Ceramic materials are known to have high hardness when compared to metals. However, the definition of hardness is not precise and its measurement may be performed in many different ways. It is not a unique property but is a measure of the material's response to the type of test being performed. Examples of hardness tests are : the scratch test, ploughing tests, damping tests and static indentation tests. The last is the most commonly encountered and consists of a ball, cone or pyramid being forced into the surface and the load per unit area of impression is considered the materials hardness. There are several such tests; Brinell, Rockwell, Vickers and Knoop. The latter two are the most commonly quoted hardness properties for engineering ceramics. The techniques are explained more fully in chapter 3.

There are several parameters that govern a material's hardness. Grain size has been seen to have a significant effect on the measured hardness of polycrystalline ceramic materials when the grain size is comparable to the indent size. Smaller grain sizes give rise to higher hardnesses. Since the indent size is governed by the load applied, the correct load should be used for the grain size being tested. Often it is wise to use a range of loads to examine the variation of hardness with load/indent size. Hence applied load is another parameter in hardness testing. Hardness indents are usually shallow and as such are sensitive to the nature of the surface itself. Special care should therefore be taken when preparing the surface to be tested as many preparation techniques can harden the surface.

In all of the above, the selection of the applied load is of prime importance, too low a load can lead to indents that only sample a small volume of material that may not be representative of the whole microstructure. These shallow indents

are also sensitive to the surface properties Too high a load and local cracking may occur around the indent leading to artificially high hardness values.

The microstructure of polycrystalline ceramic material will determine its hardness by means of grain size, residual stresses, properties of intergranular phases and amount of porosity present. The correct load to use is also governed by these factors, especially grain size.

Increasing hardness can be important for applications where improved wear resistance is important but hardness alone is not the controlling factor in wear and improvements in hardness may well be at the expense of other materials properties such as toughness or flexural strength.

The second objective of this work is to examine the effects of TiB_2 particulate additions on the key engineering properties of the sialon matrix. Because of the physical properties of TiB_2 it is expected that its inclusion will improve the hardness and fracture toughness of the material and these increments may also lead to improved tribological properties.

1.5 Tribology

Materials with high hardness, toughness, high temperature capability and corrosion resistance are ideal candidates for applications where wear is an issue. The types of composites described in this work have the potential to be used in such applications.

The term tribology comes from the Greek tribos meaning rubbing and is the term used to describe the study of "interacting surfaces in relative motion". Its principal constituents are the study of friction and wear of materials.

The tribology of materials has been a topic of investigation for many years but has become increasingly important in the last 30 or so years as the economic drive for more efficient equipment and processes increases. Attention to friction and wear could save developing countries 1.6% of their gross national product ($116 billion in America alone in 1995)[16]. However, despite the universal interest surrounding tribology the discipline has developed in many different directions. The result is widely varied tests and standards for the investigation of anything from test bars and discs in the laboratory to the field testing of engine components. Such a situation has lead to differing results and conclusions on the processes occurring and the measured properties of materials. Before undertaking an investigation into the wear of a material system it is thus necessary to undertake a literature survey of previous work performed on similar systems and to evaluate critically such standards and test procedures that are available before deciding on the type of testing to be carried out.

The hardness, chemical inertness and high temperature stability of structural ceramic materials has led to them being increasingly used for tribological applications especially in corrosive and/or high temperature environments (e.g. engine components, bearings, cutting tools). While there is extensive literature available on the behaviour of metal, metal alloy and composite systems there is far less published material concentrating upon ceramic systems, especially

ceramic composites. However with structural ceramic composites increasingly being considered for the replacement of metals in tribological environments there is a need for research in this area.

1.5.1 Friction

An accepted international definition of friction is:

The resisting force tangential to the common boundary between two bodies when, under the action of an external force, one body moves relative to the surface of the other.[17]

The first laws describing friction are attributed to Amonton[18] in 1699 who noted that:

1. The force of friction is directly proportional to the applied load

2. The force of friction is independent of the *apparent* area of contact.

The same principles had been suggested by Leonardo da Vinci much earlier (1452-1519 but not published until the 17th century). These so called laws, based upon models of surface asperity interlocking, explained the observed behaviour of materials but are inaccurate.

These "laws" gives us the well known expression $F=\mu R$ where F is the frictional force, R is the normal load acting on the apparent contact area and μ is known as the coefficient of friction (μ). Two coefficients are encountered; μ_s the static coefficient of friction, the force required to initialise movement and μ_k, the kinetic or sliding coefficient of friction experienced once the two surfaces are in relative motion. It should be noted that "the coefficient of friction describes the friction system and is a convenience and not a material property."[19]

Friction can be considered both as a microscopic and macroscopic mechanism. The microscopic view deals with the fundamental atomic and molecular

processes which give rise to the frictional force and despite many models and theories there is no global explanation of friction on this scale.

As examples some of the basic theories of the microscopic cause of friction that have been proposed are summarised below:

a) *Mechanical Interlocking*: Amontons and de la Hire (1699), the interlocking of asperities in the contact area, explained the presence of the static coefficient of friction.

b) *Molecular Attraction*: Tomlinson and Hardy (1936) arising from the energy dissipation as molecules from opposing surfaces in intimate contact are "plucked" from their attractive range.

c) *Electrostatic forces*: (1961) a net flow of electrons (in metals) at the interface producing clusters of charge with opposite polarity, holding the surfaces together by electrostatic attraction.

d) *Welding, Shearing and Ploughing*: Bowden and Tabor (1950), to describe metallic friction, high local pressures cause welding and these areas are consequentially sheared. With surfaces of differing hardness ploughing occurs as the harder material deforms and ploughs into the softer surface.

However, all these explanations have since been shown to be incorrect in most respects. In fact friction has been shown to be proportional to the "true" contact area, made up of many small asperity contacts, and is related to the adhesion between the molecules of the two surfaces at these asperities. Recent work suggests that atomic scale friction is caused by the interaction of phonons in the materials, set up by the sliding action of the two surfaces[16]. With work on the fundamental nature of friction still continuing it is thus desirable to approach friction from the macroscopic view point in a particular material system.

The macroscopic view considers friction on the large scale encountered in everyday systems and, despite being a cruder approach, it is commonly encountered when dealing with materials design and engineering where the

emphasis is on applications rather the underlying causes. Most models using the macroscopic approach are dependent on the material system being investigated and hence the treatment of metals and ceramics is substantially different due to the differing material properties.

1.5.2 Wear

The wear of materials involves many diverse phenomena which interact in a complex and mostly unpredictable manner and is in some ways, even less well understood than friction. Wear can be considered as the *progressive removal of material from surfaces caused by the tangential movement of the two surfaces relative to each other*. There have been several types of wear mechanisms[20] identified and described in metallic systems and these can be applied with caution to ceramic materials with appropriate modifications for the differing properties. There are four main classes of wear commonly referred to in the literature:

- **Adhesive wear:** arises from the strong adhesive forces formed by atoms from either surface coming into intimate contact. If the bond formed at the interface is stronger than that with the underlying bulk material some of the surface of one of the pair will be removed forming a wear debris. This wear debris may become re-adhered to one of the original surfaces on further passes or may be removed and become a loose wear debris.

- **Abrasive Wear**: when there is a difference in hardness between the sliding pair then the harder material may plough a groove or series of grooves in the softer material. The process of creating the groove may be by plastic deformation (more common in metallic systems) or by material removal by fracture or grain pull out (predominant in brittle ceramic systems). Wear debris may be produced which can contribute to abrasive wear by impinging on the softer surface and either plastically deforming the surface or producing more wear debris.

- **Corrosive Wear**: reaction between sliding pairs or the presence of an environment that can react with material surfaces under wear conditions leads to corrosive wear. Tribochemical reactions between sliding pairs and/or with elements of the environment (e.g. oxygen or water vapour) give rise to chemical products that commonly form a film of material (referred to here as a tribofilm) on the wear surfaces. This tribofilm can improve or degrade a system's wear performance and wear is dominated by the properties of the film and its interaction with the underlying wear surfaces.

- **Surface Fatigue Wear**: most wear processes consist of a repeated motion such as sliding or rolling over a fixed area or track. Under most conditions a single pass will do little damage to the material, however repeated passes can give rise to surface and subsurface cracks which propagate under repeated loading giving rise to the removal of relatively large fragments of material. The pits and irregular surfaces formed by the removal of these fragments can lead to increased local loading causing yet more severe damage. This effect is most severe if the motion is reciprocal in nature and less pronounced in a unidirectional sliding situation. Due to the brittle nature of ceramic materials fatigue wear is an important consideration.

Other wear mechanisms exist and each is caused by specific conditions such as particles incident at high speed upon a surface (erosion) or the repeated small amplitude oscillation of two surfaces (fretting). Avoiding the condition under which these forms of wear occur is relatively easy in the systems to be considered and therefore they shall not be considered further here.

Some or even all of the above mentioned wear mechanisms may be operative in a tribo-system, dependent upon the material system and the conditions such as load, sliding speed and environment The identification of the mechanism of wear and the occurrence of "wear transformations" are important factors when studying a tribological system. Wear transformations occur when the conditions under which wear is taking place change so as to cause a change in the dominant, rate controlling wear mechanism. For example an increase in the load

or sliding speed may lead to an increased (or even decreased) wear rate, caused by a change in the wear mechanism, which can either be detrimental or advantageous.

The third objective is the design of a test apparatus suitable for determining the tribological behaviour of the composites. While there are many wear testers in use the majority use large volumes of material (typically discs >50mm diameter) and/or many component systems (e.g. ball on 3 flats, 4 balls). A test apparatus suitable for small samples with simple geometries is required (i.e. diameters<25mm, discs and pins).

The study of tribological properties includes the measurement of friction and wear rate, their variation with test parameters and the determination of wear mechanisms.

1.6 References

[1] W.D. Kingery, H.K. Bowen and D.R. Uhlman, "Introduction to ceramics", 2nd Edition, Wiley & Sons, 1991

[2] A.F. Mclean, "Ceramics in small vehicular gas turbines", *Ceramics for High Performance Applications.*, Ed. J.J Burke, A.E. Gorum & R.N. Katz, pp. 9-36

[3] F.F Lange, "Silicon nitride polyphase systems: fabrication, microstructure and properties", Review 247, *International Metals Reviews*, No.1, 1980, pp.1-20

[4] D.W. Richerson and M.E. Washburn, "Hot pressed silicon nitride", U.S. patent No. 3,836,374, Sept. 17. 1974

[5] G.E. Gazza, "Effect of yttria additions on hot pressed Si_3N_4", *Bull. Am. Ceram. Soc.*, **54**, pp.778-781 (1975)

[6] O.J. Whittemore Jr. "Particle compaction" in *Ceramic Processing before firing*, (G.Y. Onoda Jr. & L.L. Hench, eds.), Wiley, New York, 1978, pp.343-55

[7] W.D. Kingery, "Densification during sintering in the presence of a liquid phase. I: Theory", *J. Appl. Phys.*, **30**, pp.301-306 (1959)

[8] W.D. Kingery and M.D. Narasimhan, "Densification during sintering in the presence of a liquid phase. II: Experimental" *J. Appl. Phys.*, **30**, pp.307-10, (1959)

[9] J.W. Cahn & R.B. Heady, "Analysis of capillary forces in liquid-phase sintering of jagged particles", *J. Am. Cearm. Soc.*, **53** [7], pp.406-409, (1970)

[10] D.W. Richerson, "Modern ceramic engineering", 2nd Ed,. Dekker, New York, 1992

[11] R.R. Wills & M.C. Brockway. "Hot isostatic pressing of ceramics", *Proc. Brit. Ceram. Soc.*, **31** [6] 1981.

[12] F. Hong, M.H. Lewis, "Ceramic matrix composites via Insitu Reaction Sintering", *Ceram. Eng. & Sci. Proc.*, **14**, 1993, p131

[13] F. Hong, R.J. Lumby and M.H. Lewis, "TiN /sialon composites via in-situ reaction sintering" *J. Eur. Ceram. Soc.*, **11**, pp.237-39 (1993)

[14] A. A. Griffith, "The phenomena of rupture and flow in solids", *Philos. Trans. R. Soc. Lond.* **A221**, pp163, (1920)

[15] G.R. Irwin, "Fracture and fracture dynamics" *J. Welding,* **32**, pp95s-100s 2nd Feb (1952)

[16] Jacqueline Krim "Friction at the atomic scale", *Scientific American*, Oct. 1996, pp 48-56

[17] ASTM standard G40, "Standard terminology relating to wear and erosion."

[18] G. Amontons, "On the resistance originating in machines" (in French), *Mem. Acad. Roy.*, pp206-22, 1699

[19] G. Salomon, in *Mechanics of Solid Friction*, ed. P.J. Bryant, L. Lavik and G. Salomon, Elsevier, Amsterdam, p. 3

[20] J.T. Burwell, "Survey of possible wear mechanisms", *Wear*, **1**, pp.119-41, (1957)

Chapter Two

Literature Review

2. Literature Review

The objectives of this research (see chapter 1) were to produce ceramic matrix composites with sialon as the matrix phase and TiB_2 as particulate inclusions and to evaluate the key engineering properties with special emphasis on tribological behaviour. This chapter presents a review of the literature with respect to silicon nitride and related materials, ceramic composites and the tribological behaviour of such materials.

2.1 Silicon Nitride Ceramics

The matrix phase (sialon) is a member of the silicon nitride (Si_3N_4) family of materials. Silicon nitride has received much attention over the previous 40 years as a major engineering ceramic[1,2]. In its most common forms, α and β Si_3N_4[3], it exhibits an excellent combination of properties that make it a suitable candidate for many engineering applications (see Table 2.2). It is strong, hard, wear resistant, stable at high temperatures, has good oxidation resistance and has a relatively low coefficient of thermal expansion.

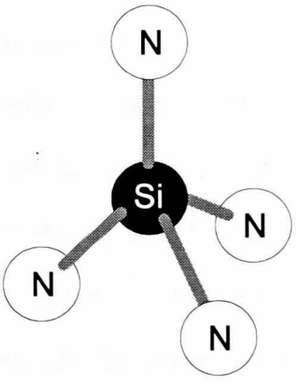

Figure 2.1 The Si_3N_4 tetrahedron

It is a strongly covalent material (70% covalent) which forms tetrahedra with Si at the centre and N atoms at the corners. Each nitrogen corner atom is a member of another 3 tetrahedra to form a continuous network with a hexagonal crystal structure (see Figure 2.1). In β Si_3N_4 the unit cell contains 6 silicons and 8 nitrogens forming tetrahedra in a layered structure in the sequence ABAB. In α

Si_3N_4 the unit cell contains 12 silicon and 16 nitrogen stacked in the sequence ABCD where the layer structure from β Si_3N_4 is stacked with its mirror image, resulting in twice the c-axis lattice spacing. Both α and β forms have a hexagonal crystal structure.

Crystalline Phase	Lattice spacings
α Si_3N_4 (hexagonal)	a = 0.775-0.777 nm, c = 0.516-0.569 nm
β Si_3N_4 (hexagonal)	a = 0.759-0.761 nm, c = 0.271-0.292 nm

Table 2.1 Lattice spacings for α and β Si_3N_4 polymorphs[4]

The phase transformation from α to β Si_3N_4 is reconstructive and takes place at elevated temperatures (1600-1800°C) usually via a solution-precipitation process in a liquid phase.

2.1.1 Densification of Si_3N_4

The properties of polycrystalline Si_3N_4 reach values suitable for engineering application only when the material has been fully densified. However, the highly covalent nature of Si_3N_4 makes it extremely difficult to sinter to full density via a solid state diffusion process, as the diffusion rates, at temperatures where the Si_3N_4 does not disassociate, are very low. Si_3N_4 is densified using liquid forming additives that allow densification and transformation to progress via liquid phase sintering where diffusion rates are much greater. These additives are most commonly those that form silicate-related eutectic liquids when they react with the SiO_2 layer, invariably found on the surface of Si_3N_4 powder. The liquids formed are of the form M-Si-O-N or M-Si-Al-O-N (in the sialon system, discussed in section 2.1.3), where M is a metallic ion. The metallic ion is usually introduced as an oxide and the range of suitable metal oxides is restricted by its stability when in the oxynitride liquid. The reduction reaction:

$$\frac{1}{3}Si_3N_4 + O_2 \rightarrow SiO_2 + \frac{2}{3}N_2 \qquad \textbf{Equation 2.1}$$

has a free energy (ΔG) of ~ -153kcal at 1500°C hence any reaction of the type $2M + O_2 \rightarrow MO$ must have a greater (-ve) ΔG for the metal oxide MO or M_2O_3 to be suitable. Some examples, in ascending order are Ce, Mg, La, Nd, Ca, Be and Y.

The viscosity of the liquid phase plays a major role in the sinterability, with the higher valence oxides providing better sinterability. However, the resulting material can have limited high temperature properties as the residual intergranular phase softens because of its lower viscosity.

For further improved sinterability mixed oxide additives are preferred because of the lowering of the eutectic temperature, e.g. the Y_2O_3 - SiO_2 binary mixture formed when Y_2O_3 is used as an additive has an eutectic at ~1650°C whereas Y_2O_3-Al_2O_3-SiO_2 has a lower eutectic temperature of ~1300°C.

There are several methods of densifying silicon nitride ceramics. The most commonly used are hot pressing and pressureless sintering. Both methods use additives (less in hot pressing and more in pressureless sintering) in the form of metal oxides to aid densification.

Silicon nitride can be successfully hot pressed to full density with sintering aids such as MgO, Li_2O and Y_2O_3[5]. The furnaces are usually heated by radio frequency induction and hence the material is held inside a graphite die and heated to 1600°C to 1800°C under pressures of 15 to 30MPa for times of 1 to 4 hours. Reaction between the die (carbon) and the sample are prevented by coatings or liners of boron nitride (BN) which can also act as a solid lubricant for the removal of samples after pressing. The small amount of additives needed for densification via hot pressing means that hot pressed materials have higher densities and superior mechanical properties. However, component shapes are limited to simple discs or tiles and the production of more complex shapes requires extensive diamond machining due to the hardness of Si_3N_4, making hot pressing an undesirable process for complex shaped components.

Pressureless Sintering can allow more complex shapes to be densified, avoiding the need for machining to final shapes and tolerances. Components are fired at 1700°C to 1800°C under a nitrogen atmosphere. Densification is achieved via the increased amounts of additives forming more liquid phase. The driving force for densification is the reduction of free surface area and hence very fine powders are commonly used to increase this driving force. The increased surface area also provides increased oxide impurities which themselves contribute to the amount and composition of the liquid phase[6]. At higher densification temperatures (>1700°C) Si_3N_4 can disassociate without the presence of an over-pressure of nitrogen. This can be provided either with a simple atmosphere of nitrogen or by surrounding the component in a powder bed of a similar composition that will disassociate and provide the required partial pressures of gaseous species.

Pressureless sintered silicon nitride contains a large amount of residual sintering aid in the microstructure either as vitreous or crystalline intergranular phases. These essentially diphasic materials have properties that can be highly dependent on the type and amount of these residual phases.

2.1.2 Properties of Dense Si_3N_4

Si_3N_4 materials are produced by many manufacturers in many different grades for varying applications[7] so it is only possible to give a broad range of material properties as a guide. Properties are dependent upon phase content, chemical composition, additive chemistry, porosity, microstructure, environmental conditions. Table 2.2 below gives a range of values for some key engineering properties of fully dense β Si_3N_4:

Property	Value (units)
α Si_3N_4 density	3.168-3.188 (g/cc)
β Si_3N_4 density	3.19-3.202 (g/cc)
Coefficient of Thermal Expansion (20-1500°C)	2.9-3.6 (10^{-6} C^{-1})
Thermal Conductivity (at R.T.)	15-50 ($Wm^{-1}K^{-1}$)
Specific Heat	700 (J Kg^{-1} $°C^{-1}$)
Electrical Resistivity (at R.T.)	~10^{13} (Ω cm)
Microhardness (Vickers)	16-22 (GPa)
Young's Modulus (at R.T.)	300 - 330 (GPa)
Flexural Strength (at R.T.)	400 - 1000(MPa)
Fracture Toughness (at R.T.)	3.4 - 8.2 (MPa $m^{½}$)

Table 2.2 Some properties of β Si_3N_4 ceramics (after Zeigler et. al. [4])

In sintering with oxide additives which include Al_2O_3 a certain level of solid substitution of Al for Si and O for N is possible in Si_3N_4. Such materials have now become widely known as "sialons".

2.1.3 The Si-Al-O-N System

Sialon is the acronym given to the phases in the Si-Al-O-N system whose existence was discovered independently at both Newcastle-upon-Tyne, England[8] and in Japan[9,10] in the early 1970s. The research was based upon the reaction sintering of Al_2O_3 and Si_3N_4 and was first described as a stoichiometric mixture of the two which implied a structure containing Si vacancies. This was shown to be incorrect by later work by Lumby et. al. [11]. The accepted view is that it is possible to substitute Al^{3+} ions for Si^{4+} ions provided that charge balance is then maintained by the substitution of O for N in the structure. The cation/anion balance remains at 3:4 and hence for β sialon the β Si_3N_4 crystal structure is maintained and no vacancies/interstitials are formed. This results in a slight enlargement of the β Si_3N_4 structure up to the solid substitution limit given by :

$$Si_{6-z}Al_zO_zN_{8-z}$$

where $0<z<4$.

The change in the lattice parameters is easily detected via x-ray diffraction techniques and this method provides useful information on the level of solid solution in any material produced.

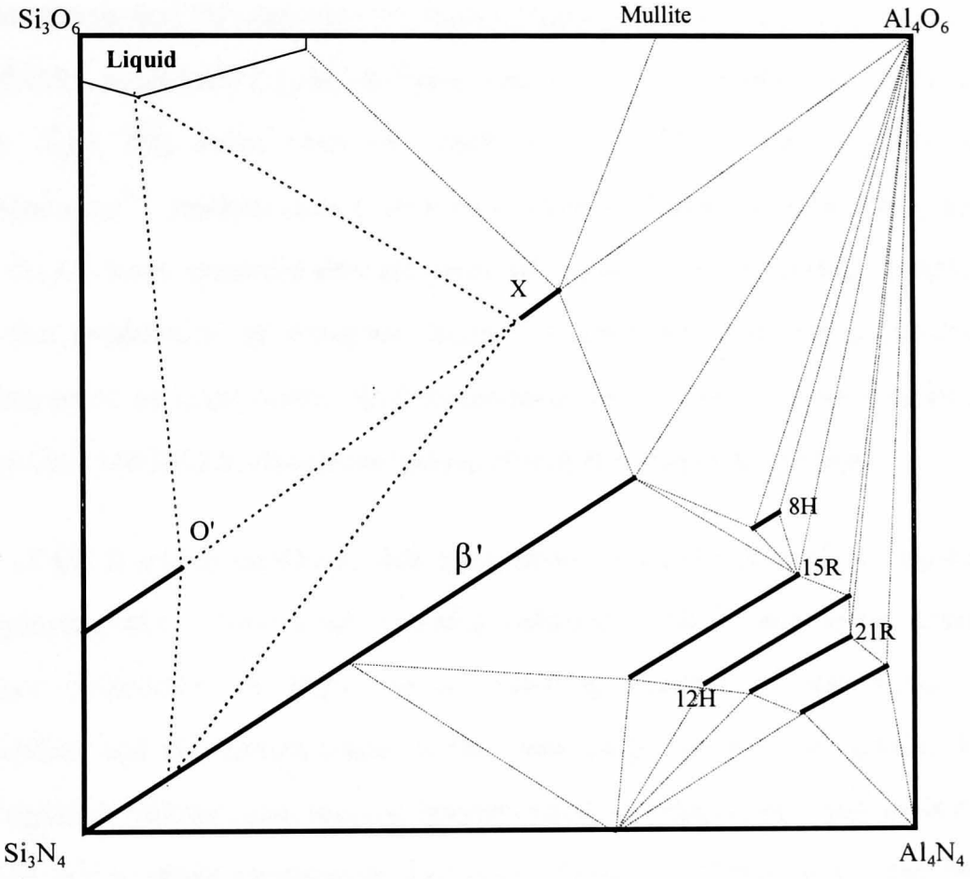

Figure 2.2 The square equivalence (iso-electric) diagram for the Si-Al-O-N system at 1800°C

The range of solid solution for the β Si_3N_4 based materials is demonstrated on a square equivalence diagram shown in Figure 2.2 with Si_3N_4, Al_2O_3, AlN and SiO_2 as the terminal compounds. The β sialon compositions lie along the Si_3N_4 - Al_3O_3N line. Sialons were originally produced by the sintering of appropriate mixtures of either Si_3N_4 - Al_2O_3 - AlN or Si_3N_4 - SiO_2 - Al_2O_3 - AlN but many more possible production routes are now used, many of them being proprietary.

From the liquid region shown in Figure 2.2 it should be possible to use this liquid phase to densify sialon materials without the addition of sintering aids[12]. Additions of equi-molar amounts of Al_2O_3 and AlN, followed by high

temperature sintering will result in β-sialon with little or no intergranular glass phase present.[13] However, in practice this is difficult to achieve and the divalent or trivalent oxide additives such as MgO or Y_2O_3 used for Si_3N_4 densification are still routinely used to achieve full density.

In the sialon system more liquid is formed at lower temperatures with the above oxide additives. This can have the advantages of producing a finer grain size microstructure and the amounts of liquid phase produced can lead to improved sinterability, especially by pressureless sintering. For example the addition of 1 to 3% Y_2O_3 has been seen to result in 2 to 6% residual glass in the microstructure[14]. Analysis has shown that reactions between Y_2O_3, SiO_2 and any added Al_2O_3 form considerable amounts of liquid at the sintering temperature. Since the production of complex shaped components requires a pressureless sintering route to limit costly final machining the ability of sialons to be easily pressureless sintered at moderate temperatures is a major advantage.

Many of the β sialon materials that have been successfully used in engineering applications have a low level of solid solution ($z<0.5$) and hence retain the excellent properties of Si_3N_4 while allowing control of the liquid phase sinterability and the composition of the remaining intergranular phase. Sialons with higher z values have shown deterioration in properties such as hardness, possibly due to grain coarsening. However, those with little or no intergranular glassy phase retain their properties up to about 1200°C. Materials with a significant amount of glassy phase have poor hot hardness properties and are limited to use below 1000°C, but at lower temperatures the presence of an intergranular phase allows a preferred crack path along grain boundaries and fracture toughness is enhanced as the crack is bifurcated at grain junctions. Oxidation is also affected in the presence of an amorphous phase. Normally Si_3N_4 ceramics are protected form excessive oxidation by the formation of a protective SiO_2 layer. However, when the intergranular amorphous phase contains Y_2O_3 the oxidation resistance is seen to decrease, possibly due to the differing composition of the oxide scale formed, allowing faster diffusion of oxygen through the oxide scale.

In addition to β sialon several other possible phases exist. α sialon, based on the α Si_3N_4 structure, occurs in the M-Si-Al-O-N system where M includes Li, Ca, Y and all the rare earths from Nd to Lu. The α unit cell contains 2 large interstitial sites that are capable of accommodating these ions which perform the role of valency compensation when the Si^{4+} is replaced by Al^{3+}. The structural arrangement can be pictured as similar to that achieved by stuffed quartz structures. There is considerable interest in composites containing both α and β sialon, the equiaxed α grains offer high hardness while the elongated β grains can contribute to fracture toughness. The control over the composition, allowing differing α:β ratios, gives the possibility of tailoring materials for specific applications.

As can be seen from Figure 2.2 there is a small range of solid solution of Al in silicon oxynitride Si_2N_2O and this phase is known as O' sialon and is formed by the same mechanism of solid solution as for β sialon. Also indicated are the polytypoid phases identified as 2H, 27R, 21R, 12H,15R and 8H found near the AlN corner. These were prepared by Gauckler et al. [15] and characterised by Roebuck and Thompson[16] and were found to be based on the wurtzite structure

2.2 Ceramic Composites

Much work has been done on increasing the strength and toughness of existing ceramics by improving processing conditions, purity of starting chemicals, the elimination of flaws and other factors. However, despite improvements in monolithic ceramic properties the practice of reinforcing ceramics by the inclusion of secondary compounds in the form of whiskers, fibres or particles, to form *ceramic composites*, has shown potential for improving the strength, toughness, hardness and influencing the failure modes of ceramics.

Ceramic composites can take many forms. Fibre and particulate reinforcements should be considered separately as their toughening mechanisms are quite different from those for particulate composites which form the basis of this work. In continuous fibre reinforced systems stressed parallel to the fibre direction there are two possibilities; (i) if the fibre is well bonded to the matrix then brittle fracture will occur as the crack propagates through both the matrix and whiskers, (ii) if the fibre is weakly bonded the crack is deflected along the interface between fibre and matrix and the fibre continues to bear the load. Continued loading leads to fibre pull out and fibre failure, all of which are energy absorbing processes. The failure mode for such composites changes from brittle to so called "graceful" failure due to the consecutive failure mechanisms of the fibres far too varied to discuss fully here.

While whisker reinforcement has provided an elegant and sometimes successful solution to some of the problems of ceramics, they are not ideal. The addition of the whiskers to the green body can interfere with the densification process and hence produce poorly sintered materials. The advantage of using particulate reinforcements is that they can be added in powder form in a way that does not overtly interfere with sintering. Particulate inclusions typically improve a material's hardness and toughness making then ideal for tribological materials.

2.2.1 Toughening Mechanisms in Particulte Reinforced Composites

There are several mechanisms that can improve hardness, toughness and strength in ceramics when particulates are introduced, the actual mechanism taking place will be dependent upon the nature of the composite, especially the properties of the particulate compound and its interaction with the matrix. If the inclusion is ductile then crack bridging by the ductile particles can inhibit crack progress, however, ductile materials usually have limited high temperature properties.

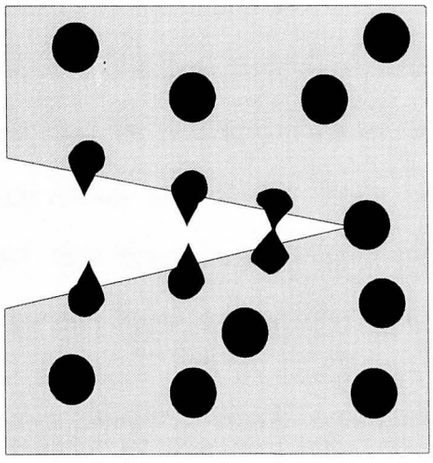

Figure 2.3 A crack interacting with ductile particles in a matrix. Plastically deformed particles bridge the crack, absorbing energy before finally failing.

For typical applications, where the high temperature and chemical properties of ceramics are important, the inclusions themselves are more usually ceramic materials.

In such a material there are several possible mechanisms:

1. The difference in thermal expansion (α) of the matrix and particles leads to a stress field which can be utilised to divert cracks around dispersed particles and hence increase the crack path length with a subsequent increase in toughness. A spherical particle of radius R in a matrix will experience a stress σ_r and the matrix will experience a radial stress of $\sigma_r R^3/r^3$ and a tangential stress of $\sigma_r R^3/2r^3$, where r is the distance from the particle centre to a point in the matrix. The stress can be calculated from:

$$\sigma_r = \frac{(\alpha_p - \alpha_m)\Delta T}{\frac{(1+\nu_m)}{2E_m} + \frac{(1-2\nu_p)}{E_p}}$$ **Equation 2.2**

where the subscripts p and m represent particle and matrix respectively, E is the Young's modulus, ν is Poison's ratio, α is the thermal expansion coefficient and ΔT is the temperature range. If $\alpha_p > \alpha_m$ then the matrix is in compression (after cooling from the sintering temperature) and this residual stress will tend to deflect cracks around particles.

2. Cracks can be deflected or multiplied around or even through particles by the orientation of preferred fracture surfaces such as weak grain boundaries. In moving the propagating crack out of the crack plane the driving force is reduced due to the fact that there is no longer pure mode I loading. This effect has been quantitatively demonstrated by Faber and Evans[17]

3. Crack bowing can occur when a crack encounters resistant particles or dispersoids in its path. The crack will then tend to bow between the two resistant particles.[18] Typically both bowing and deflection occur simultaneously.

4. Microcracking in the matrix (due to thermal coefficient or elastic modulus mismatch) can be responsible for inhibiting the growth of a crack. Microcracks lead to crack shielding by locally reducing the modulus at the crack tip and spreading the applied stress over many cracks rather than one primary crack.[19,20] Microcracking is difficult to demonstrate but predictions for a Si_3N_4/TiN material suggest a volume of 60% of TiN at 100μm particle size is needed[21]. Another evaluation suggests a size of only 17μm[22]. In real systems such as those where an intergranular phase is present in addition to the particles the energy of the grain boundaries strongly effects microcracking. The difference in sintering additives and processing conditions for materials such as Si_3N_4 or sialons may explain the varying predictions for the critical particle size to form microcracks.[28] Particle size is

Particle size is critical not only for microcracking to occur but if particles are too large then thermal cracking can occur and these cracks can limit the material's strength. The result is an enhanced toughness material with low strength.[23]

5. The passage of a crack around a particle or grain may lead to the pull out of the particle/grain from the matrix. The frictional interlocking of these partially removed grains with the matrix and the bridging of the crack by unbroken islands of material serve to shield the crack tip from the applied stress. Hence the opening force at the tip is reduced. While this phenomenon is most prominent in fibre reinforced systems it is also a significant factor in real composite microstructures.

All of the above mechanisms may take place in a composite and all can contribute to the enhanced properties of such a material. Estimates of the amount of toughening that can be achieved vary. Theoretical calculations for spherical particles[24] predict a 40-70% increase in toughness. Other studies[17] predict a factor of 2 increase for spherical particles, a factor of 3 for disc shapes and a factor of 4 for rod shaped particles. Another important factor is the vol% of the dispersed phase.

The choice of compound to be used as a particulate reinforcement depends upon several factors:

a) the chemical compatibility of the compound with the matrix

b) the difference in the coefficient of thermal expansion

c) the properties of the compound and its compatibility with the environment in which it may be used (e.g. oxidation resistance, chemical resistance, melting point)

d) the cost of the compound and the effect it may have on the cost of production of the composite offset against the magnitude of the improvement in properties.

2.3 Particulate Reinforced Si_3N_4 and Sialon Ceramics

It is consideration of the factors listed above and of the properties of matrix material that has led to the study of transition metal compounds as particulate reinforcements in Si_3N_4 and sialon matrices. Typically the nitrides and borides of transition metal compounds offer suitable properties such as high hardness, chemical inertness, high melting point, oxidation resistance, compatible Young's modulus and thermal expansion coefficients, low resistivity.

Several workers have examined the possibility of adding transition metal nitrides and borides to Si_3N_4 and sialon matrices[25], for example, TiN[26], ZrN[27], BN[28] and TiB_2[29]. The reasons for adding these compounds range from producing electro-discharge machinable ceramics to composites with improved tribological properties. The hardness (H_v) of Si_3N_4/TiN composites has been seen to increase[30] in some cases but decrease in others[31]. The actual variation depends upon the grain size and vol% of the TiN . The fracture toughness (K_{Ic}), however, was seen to rise, for all grain sizes, from 7.5 MPa $m^{1/2}$ to about 9 MPa $m^{1/2}$. A Si_3N_4 matrix with TiB_2 introduced as particles at a level of 35vol% showed an increase in K_{Ic} (Vickers indentation) from 5.2 to 6.3 MPa $m^{1/2}$.[32] Hillinger and Hlavacek[33] reported for a Si_3N_4/TiN material a maximum in K_{Ic} of 11.7 MPa $m^{1/2}$ at 20vol% (test method for K_{Ic} not reported). Silicon nitride reinforced with TiC, SiC (whiskers) and TiC & SiC were produced by Blanchard & Page[34] who measured the properties shown in Table 2.3

Material	H_V (GPa)	K_{Ic} (MPa $m^{1/2}$)	Flexural Strength (MPa)	E (GPa)
Si_3N_4	17.8	5.4	490	329
Si_3N_4/TiC	22.8	7.2	578	328
Si_3N_4/SiC	23.1	5.7	436	335
Si_3N_4/TiC/SiC	25.2	7.9	498	310

Table 2.3 Properties of composites produced for wear testing by Blanchard and Page

As can be seen from the above examples the addition of particulate inclusions into Si_3N_4 matrices has been successful, to some extent, in improving the properties over that of the matrix alone.

More recent work has investigated the toughening effects of so called "nanocomposites". Niihara has studied the effect of nanoscale additions of SiC in Si_3N_4 matrices.[35]

The methods employed in the production of such materials are varied as is the success of these materials. Traditional approaches to producing such composites consist of milling of powders of the compound to be added to a suitable size by conventional methods and then intimately mixing these powders with the raw materials for production of the matrix. This powder mix is then processed and sintered using similar methods to those used to produce the matrix phase alone. There are several factors associated with this approach that could make it undesirable for the successful and efficient production of such composites:

1. Achieving intimate mixtures and hence homogeneous microstructures may be complicated by the addition of these compounds.
2. Possible hindrance to sintering caused by the addition of the second phase.
3. Altered composition of the matrix due to impurities added via the second phase compound.
4. Increased wear to mixing and milling apparatus caused by the high hardness of these compounds.
5. Cost, an important factor when developing the material to a point where it is acceptable for use in commercial applications.

2.4 Tribology of Si_3N_4 And Sialon Ceramics

Much of the work done on the tribology of materials gives rise to results that differ significantly between studies. The differences are caused by several factors such as differing grades of the same material, different test methods, the type of equipment used, varying test conditions. The work carried out on silicon nitride and related systems such as SiAlON reflects this problem, with many workers reporting widely varying values for wear and friction. A critical, comprehensive literature review is therefore more difficult to achieve. For the sake of brevity the literature reviewed here is a representative cross section of worked carried out on Si_3N_4 based materials mated with themselves and with other materials such as diamond and steel.

In the following review the parameters under which tests are performed are described as follows: W= applied load (N), P= actual applied pressure when the load and contact area are known (Pa), RH= relative humidity (%), R= radius of pin (mm) when a rounded end is used, V= linear sliding velocity used (ms^{-1}) and A is the contact area (m^2) when known. Where appropriate the authors original data has been converted into the above "standard" quantities and units for ease of comparison.

2.4.1 Coefficient of Friction (μ)

The reported values for the coefficient of friction (μ) for Si_3N_4 and SiAlON systems vary widely but many of the variations can be explained or understood by considering the conditions under which they were measured. However, there remain conflicting reports in the literature on the value, and the variation, of μ with test conditions.

Gee and Butterfield[36] showed how the coefficient of friction can vary within an identical system by varying sliding speed and humidity for Si_3N_4 balls (85% Si_3N_4, 2%AlN, 8% Y_2O_3) sliding on identical discs. All tests exhibited a rapid

rise in μ from the start to a steady state level. The variation in μ with sliding speed and humidity for this system is demonstrated in Figure 2.4.

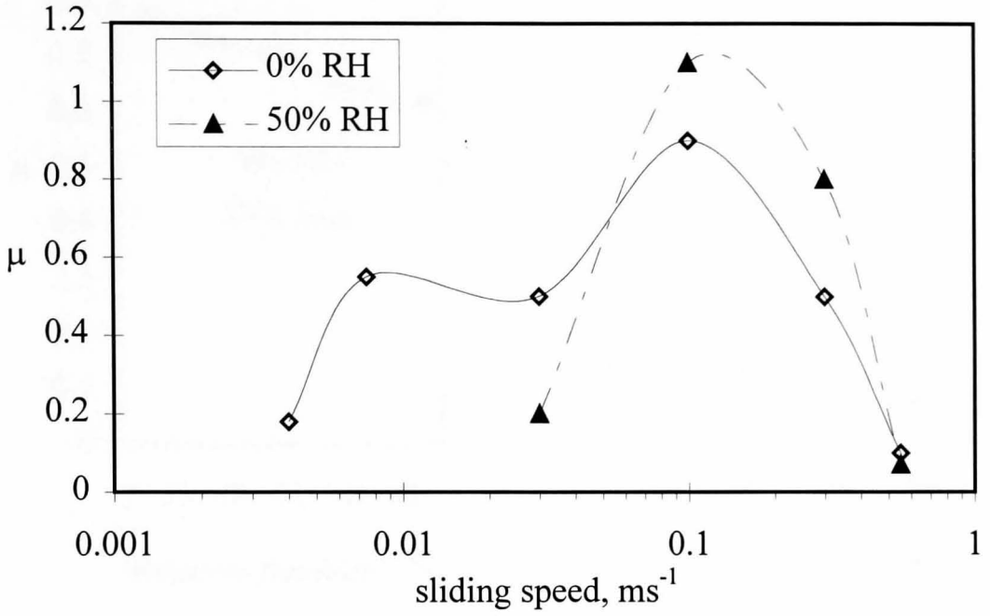

Figure 2.4 The variation of μ with sliding speed and humidity after Gee.[36]

Fischer and Tomizawa[37] examined the variation of μ in gaseous and liquid environments for Si_3N_4. The value of μ in air was seen to rise from the start of the test to ~0.7-0.8 under dry sliding conditions (V= 0.001m s^{-1}, W=0.3-30N, RH=0-98%). Variation with applied load showed only a weak dependence. They also found no great variation between dry and wet (98%RH) air or argon, with μ (dry Ar)=0.85, μ (wet Ar)=0.75, μ(dry air)=0.8 and μ(wet air)=0.75. Lubrication with water gave μ=0.7 and using a commercial lubricant μ was seen to fall to 0.15.

In examining the effects of sliding speed and humidity Sasaki[38] demonstrated the dependence shown in Figure 2.5

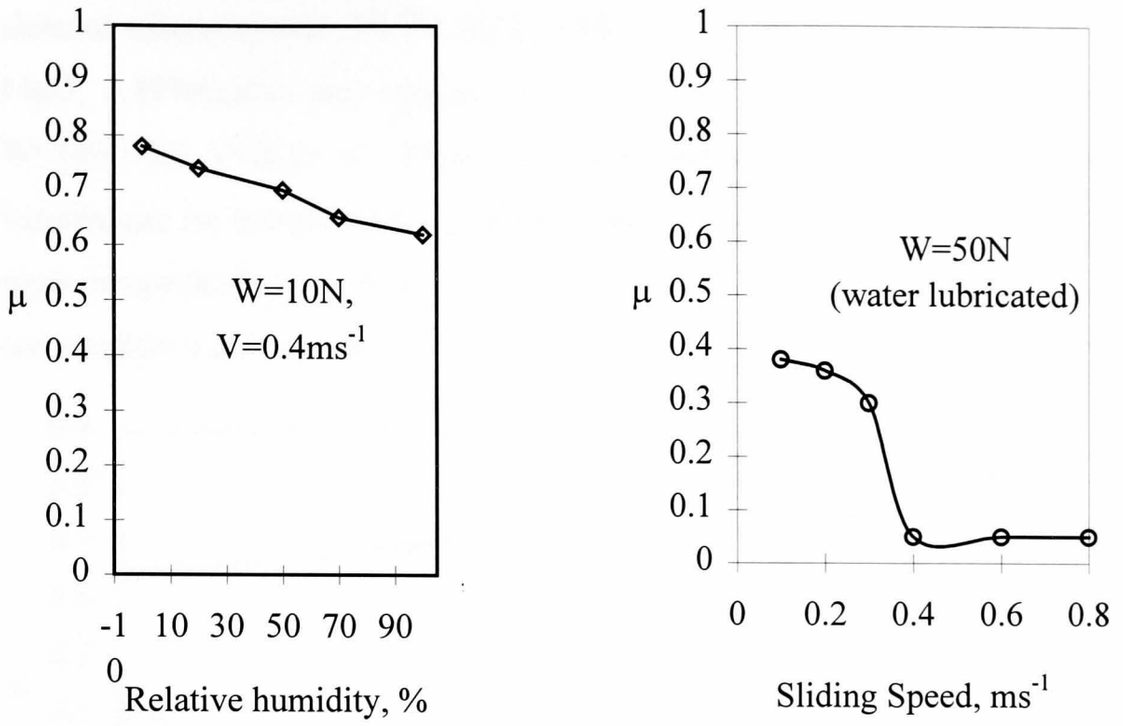

Figure 2.5 Variation with humidity and sliding speed (in water) for Si_3N_4 after Sasaki[38]

Furthermore the coefficient of friction may change during a test under constant conditions. Sliding Si_3N_4 on Si_3N_4 containing MgO densification aid (W=0.25N, V=10mm/min (0.00017 ms^{-1}) , R=0.2mm, RH=50%RH) Ishigaki[39] demonstrated a steady rise in μ with number of reciprocal slidings (0.2 to 0.8 over ~20 slidings) over the same area of material. This may be the same effect seen at the beginning of tests by Gee[36] and Sasaki[38]. When the pin slid over "virgin" material at each pass, μ remained constant at ~0.25. Ishigaki showed that the surface forms a protective layer by reaction with the atmosphere which plays a role both in the value of μ and the wear rate.

These variations are explained by considering the effects of tribochemical reactions in conjunction with other factors such as hydrodynamic lubrication. The formation of tribofilms or layers on Si_3N_4 is generally attributed to the formation of soft hydroxides between the sliding surfaces by the reaction of SiO_2 with H_2O forming $SiO_2.xH_2O$.

In another paper Gee[40] describes the measurement of μ with temperature of a sintered silicon nitride (79.5% Si_3N_4, 11% Y_2O_3, 1.8% SiO_2, 1.22% Si, 3.94% MgO, 2.19%Cr_2O_3) and reports a room temperature value of μ=0.42 with W=10N and V=0.2m s^{-1}. Figure 2.6 demonstrates the variation of μ with temperature for this material. A similar study by Czichos et. al.[41] demonstrated a room temperature μ=0.65 with W=10N and V=3 m s^{-1} and the variation with temperature is also shown.

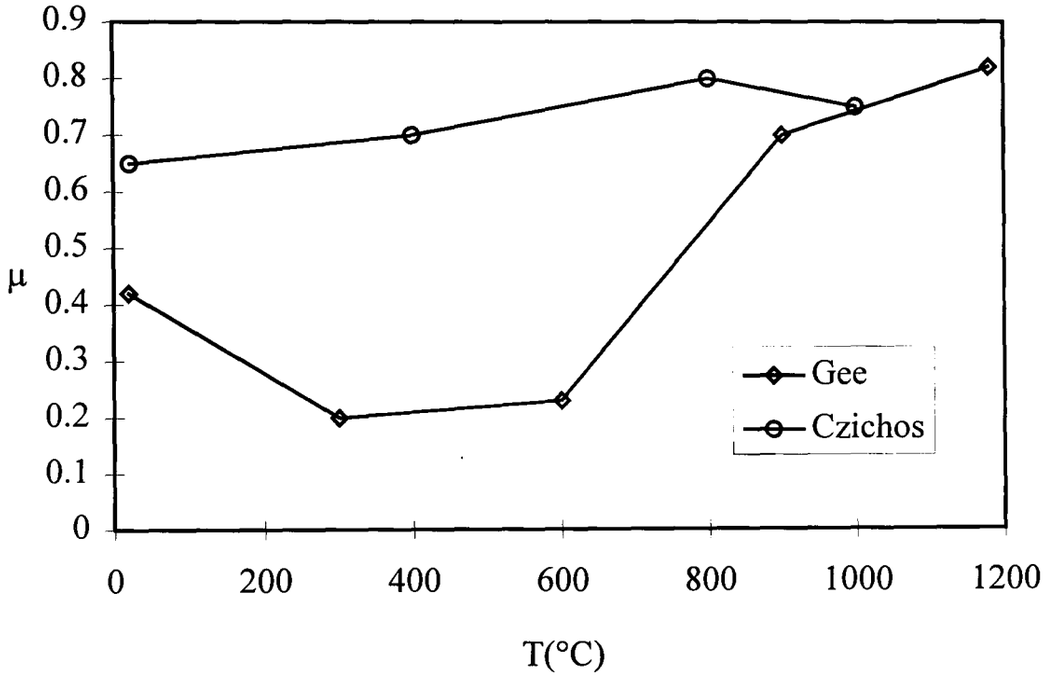

Figure 2.6 Variation of μ with temperature for a sintered silicon nitride after Gee[40] and Czichos[41]

As can be seen in all of the above, these nominally identical tests yield widely different results and are typical of such contradictions found in the literature.

Other material Systems

In studying the effects of humidity on the friction of WC(Co) balls on SiAlON (Kyon 2000, Kenametal Inc.) Komvopoulos[42] reports a μ of 0.45 at 50%RH. He also reported the presence of tribofilms at the wear surface due to the interaction with moisture and a variation in μ with relative humidity shown in Figure 2.7.

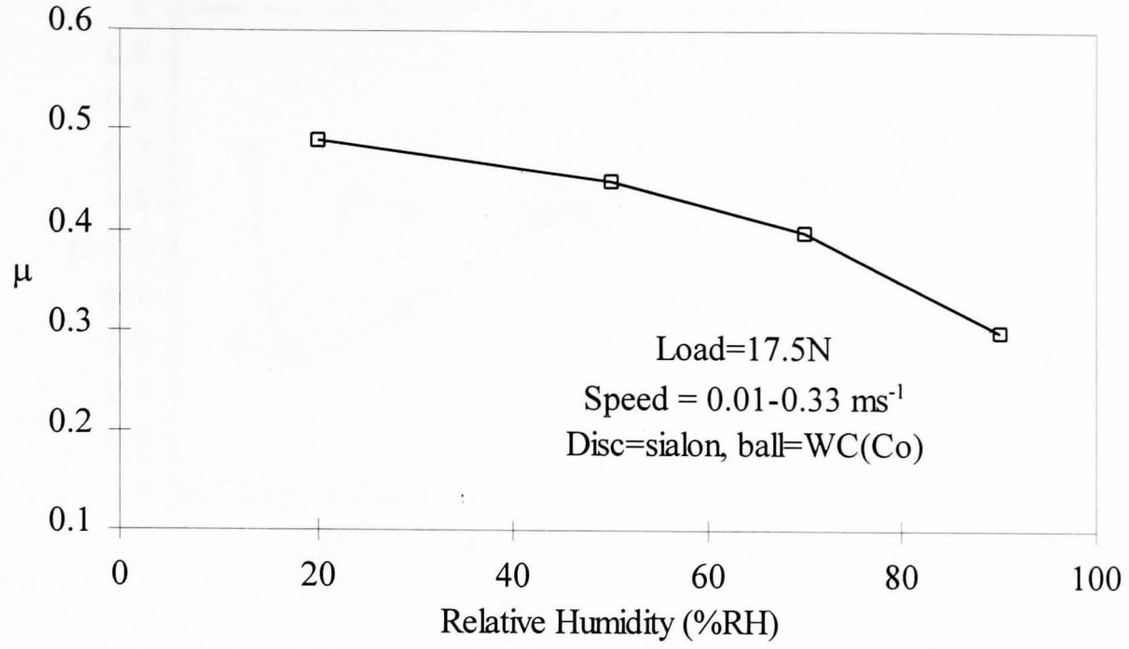

Figure 2.7 Variation of μ with relative humidity for SiAlON[42]

For diamond sliding on a hot pressed sialon Kapsa et. al.[43] measured μ to fall from ~0.1-0.2 at the start to >0.05 after 100,000 cycles (W=3,5,7.5N, RH=20%, R=100μm) for both a rough and smooth diamond tip.

A study of the wear performance of Si_3N_4 ceramic pins against steel discs was carried out by XingZhong et. al.[44] in order to assess the effects of load, lubrication and sliding speed. Although some facts are missing such as a report of RH for unlubricated tests and accounting for the rapid change of contact area with sliding distance it serves as a typical example of values found for Si_3N_4/steel sliding pairs. Unlubricated and in water μ~0.32 and was only weakly sensitive to applied load (60-235N). In oil μ dropped substantially to below 0.1 and remained insensitive to load. Not unlike the findings of Gee[36] the variation with sliding speed exhibits a maximum at a particular speed in dry sliding but such a maximum is not apparent in both water and oil lubricated tests where μ remains at ~0.3 and 0.1 respectively.

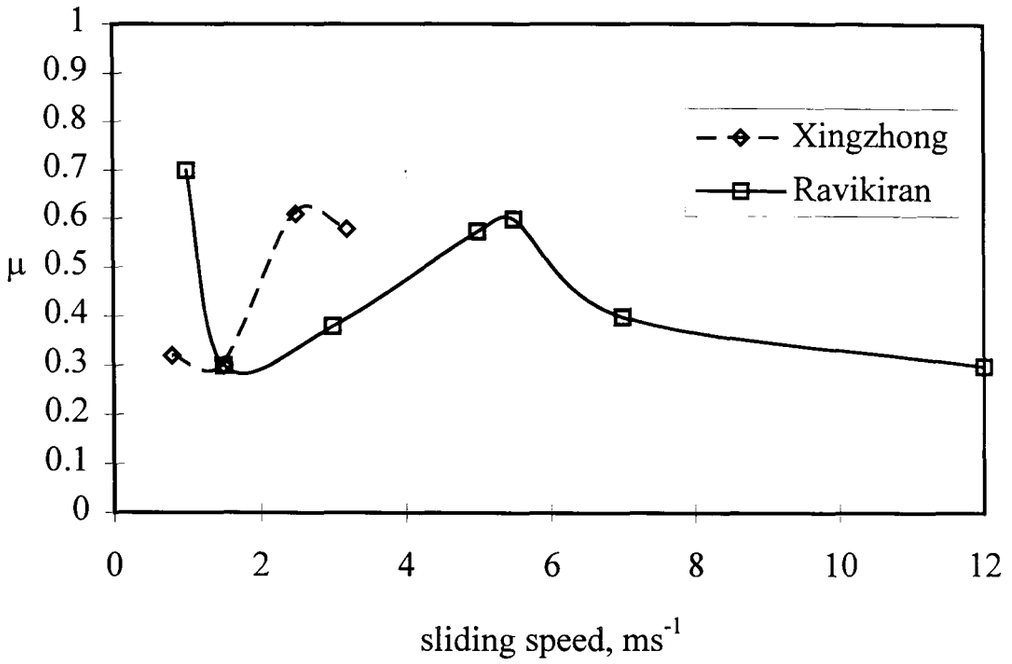

Figure 2.8 Si_3N_4 dry sliding on steel discs. Variations of μ with sliding speed from different researchers.

In attempting to characterise the tribochemical reactions occurring between Si_3N_4 and steel in dry sliding, Ravikiran and Pramila Bai[45] demonstrated the variation with sliding speed shown in Figure 2.8 . Differing wear regions were identified and tribochemical reactions played a role in all.

Table 2.4 shows a summary of some of the results for the value of μ reported in the literature reviewed. It is clear that while some investigations give similar results others can yield widely differing values. The probable cause of such variation is due to several factors. Incomplete control over all important parameters such as applied pressure, humidity, atmosphere, surface finish, material grade, test type and geometry can lead to significant differences.

Material Pair	Test	Conditions	μ*	Ref
Si_3N_4 / Si_3N_4	ball-on-ring	R=10mm, W=10N, RH=50%, V=0.3ms^{-1}	0.8	36
Si_3N_4 / Si_3N_4	pin-on-disc	R=3mm, W=10N, RH=40%, V=0.3ms^{-1}	0.65	41
Si_3N_4 / Si_3N_4	ring-on-flat	W=10N, V=0.2ms^{-1}, RH=?	0.42	40
Si_3N_4 / Si_3N_4	pin-on-disc	W=10N, R=3mm, RH= 0%, V=0.001ms^{-1}	0.8	37
Si_3N_4 / Si_3N_4	flat on rolling ball bearing	W=?, V=?, RH=?,	0.4	
Si_3N_4/Diamond	reciprocating pin-on-disc	W= 7.5N, R=100μm, RH=20%, V=0.002ms^{-1}	0.04	43
Si_3N_4/cast iron	ring (iron) on test bar (Si_3N_4)	W=1600N, V=3.56ms^{-1}, RH=?, Area of contact =1.12x10^{-6} m^2.	0.12	46
Si_3N_4 / Steel	pin-on-plate	W=117.6N, V=0.8ms^{-1}, RH=?	0.32	44
Si_3N_4/ Steel	pin-on-plate	P=15.5MPa, RH=50%, V=0.8ms^{-1}	0.7	45

** steady state μ values typical over sliding distances used.*

Table 2.4 Summary of friction coefficients from several similar studies on Si_3N_4 and sialon.

These results demonstrate the unpredictable nature of tribological behaviour with differing conditions. It further shows that researchers working with identical Si_3N_4 but using differing conditions could find radically differing results. Add to this the diverse number of grades and compositions of Si_3N_4 materials then the need for the reporting of all conditions accurately and the use of standard tests and conditions is obvious.

2.4.2 Wear

The wear of materials is reported in many ways in the literature and is plagued by the same inconsistencies as encountered for the coefficient of friction. In addition to the variation caused by differing test methods, material grades the quantification of wear is further confused by the variety of ways in which wear is reported. Common quantities are displacement, mass loss, wear volume, wear rate, specific wear rate, the wear constant/factor/coefficient with varying units

used for each. In reviewing the literature it is important to bear in mind these quantities, how they differ and how they are measured. Many studies are carried out purely as comparative studies between materials/lubricants but the results from such work cannot be easily used for comparison with data from other studies.

Firstly, it is appropriate to look at some of the suggested mechanisms of wear. Early studies suggested that Si_3N_4 sliding on itself underwent wear by intergranular cracking and delamination[47,48]. However, increasing work on characterising the worn surface has shown evidence for wear mechanisms that include tribochemical reactions [36,37,38,40,42]. Many researchers have shown evidence for such reactions such as tribofilms on wear surfaces and wear debris compositionally different to the parent materials. Since these tribofilms are formed and remain at the wear surface then the behaviour of the tribofilm governs wear more directly than the properties of the underlying materials. Whether these layers are trapped or removed from wear surfaces, hard or soft, strongly or loosely adhered, reformed or degraded with sliding distance determines the wear behaviour of the material system. In the case of Si_3N_4 against other material's tribochemical reactions, either with the atmosphere or with the mated materials, can also influence wear behaviour.[45,49,50].

Fischer and Tomizawa[37] describe two wear mechanisms: fracture and tribochemical reaction (with oxygen and water). These mechanisms occur simultaneously at intermediate humidity levels with fracture dominating in dry atmospheres and mostly tribochemical wear occurring in saturated environments. The fracture of the Si_3N_4 occurs by two mechanisms:

1. The removal of large grains and particles by intergranular fracture caused by fatigue cracks running parallel with the surface at ~3-5μm depth. These cracks, driven by relatively low stresses, follow grain boundaries until they emerge at the surface and cause grain removal as described by delamination wear theory[51].

2. Surface microfracture, producing fine wear debris, occurs by transgranular fracture of grains caused by the high stresses produced at asperity contacts or the impingement of sharp wear debris.

Kato[52] describes these two mechanisms as flake and powder formation respectively and introduced a criterion which describes the transition from one wear mode to the other. Hsu[53] describes differing wear regimes separated by wear transitions defined as "a sudden increase (and for accuracy we should include here a decrease) in wear due to small increments in either load or speed". Hsu demonstrates such transitions using "wear maps" which have as axis; speed (x), normal load (y) and wear volume (z). The collection of wear volume data over a range of normal loads and sliding speeds give a plot on which such transitions can be identified. Such maps are useful for comparing the performance of differing materials when considering them for engineering applications where operating conditions may vary.

Hsu identified 3 regimes of wear for silicon nitride which he labels A, B and C. In regime A, mild wear occurs at low speeds and low loads. At intermediate loads/speeds a wear transition occurs to regime B, severe wear. At the extremes of both load and speed Hsu identifies an ultra-severe wear regime C. In A the wear mechanism is identified as being dominated by tribochemical reactions producing tribofilms that plastically deform to produce rolls of wear debris leaving a polished surface resulting in low coefficients of friction. Repeated loading causes subsurface damage that builds up eventually leading to grain pull out. The change in contact geometry caused by the removal of grains can lead to high asperity loading and hence to a wear transition into the severe wear regime. Here Hsu suggests that stresses are not high enough to cause substantial fracture but that asperities abrade the surface forming grooves and hence wear controlling factors are hardness and surface conformity. Ultra-severe wear (C) is also dominated by brittle fracture of the silicon nitride but on a greater scale. Hsu's explanation leads to the conclusion that more effective microstructures can be designed to provide better wear resistant materials by moving the wear

transitions to higher loads and speeds. Improved fracture toughness, hardness and the chemical state of the surface should provide better wear resistance.

Tribochemical effects have been described by many workers, nearly all involving reactions with oxygen and consequentially with water (present as humidity). It has also been suggested that under some conditions high temperatures at asperity contacts can occur forming oxidation products at the surface.[54] The effect of the reaction with oxygen and water on wear is mixed and some examples are listed in Table 2.5

Materials	Test Type	Change in Wear (or Surface Damage)	Ref.
Si_3N_4 / diamond	pin-plate	increase	55
Si_3N_4 on itself	pin-on-disc	decrease	37
Hot pressed Si_3N_4	pin-on-disc	decrease	39
hot pressed Si_3N_4/diamond	pin-plate	increase	43
Sintered Si_3N_4/diamond	pin-plate	decrease	43
Si_3N_4 on itself	pin-on-disc	decrease	38
sintered Si_3N_4 on itself	ring-disc	decrease	56

Table 2.5 The effect of tribofilm formation on the wear of Si_3N_4 ceramics.

The reactions lead to the formation of ductile surface films which in "dry" sliding function as self-replenishing solid lubricants and reduce both friction and wear. If water or other aqueous solutions are used as lubricants then solubility of the oxides in the lubricant can lead to increased wear as material is dissolved away. Reduced wear and/or coefficients of friction may occur as perfectly smooth surfaces are formed allowing hydrodynamic lubrication. Which situation occurs depends upon the conditions (e.g. load, speed) , composition of the material and chemistry of the liquid used.

Table 2.6 lists some of the wear coefficients found by different researchers on different materials systems. Since no two have been carried out in an identical way or on identical materials it is difficult, if not impossible to draw any

conclusions from the results and comparison should be made with caution. However, an improved wear resistant material should at least match or better some of the values listed below under similar conditions.

Material Pair (reference)	**Conditions**	**Wear Coefficient, k ($mm^3N^{-1}m^{-1}$)**			
SSi_3N_4/SSi_3N_4 ([54])	W=10, V=varied, RH=20-40%,	2.5×10^{-5} (V=0.05)	3×10^{-5} (V=0.15)	4×10^{-6} (V=0.4)	7×10^{-5} (V=3.5)
HP Si_3N_4/ HP Si_3N_4 ([54])	W=10, V=varied, RH=20-40%,	2×10^{-5} (V=0.04)	1.5×10^{-5} (V=0.15)	1.5×10^{-5} (V=0.35)	3×10^{-5} (V=1)
SSi_3N_4/SSi_3N_4 ([57])	W=10, V=0.2, RH=50%,	Pin = 2.46×10^{-6}		Disc = 17.6×10^{-6}	
SSi_3N_4/SSi_3N_4 ([41])	W=10, V=3, RH=40%,	8×10^{-6}			
Steel/ SSi_3N_4 ([63])	W=10, V=0.2, RH=50%,	Pin = 1.45×10^{-6}		Disc = 10.2×10^{-6}	
β-Sialon/β-Sialon ([58])	W=13-43, V=0.24, RH=?,	Pin =$2\text{-}8\times10^{-6}$			
β-Sialon/β-Sialon [59]	W=10, V=0.1, in H_2O	Pin=9×10^{-6}		Disc=2×10^{-6}	
Sialon/Syndite	w=9.81, V=0.022, RH=50%	Pin= 5×10^{-6} (Pin = 6×10^{-5} in H_2O.)			

SSi_3N_4 =sintered Si_3N_4, HP =hot pressed. Syndite =diamond bonded disc.

Table 2.6 Some values for room temperature wear coefficients of Si_3N_4 and Sialon.

It has been suggested that an unlubricated tribological material should have a wear coefficient of better than 10^{-6} mm^3 N^{-1} m^{-1} and as low as possible a coefficient of friction[41]. All the above materials approach this value. However, since the value of k will vary significantly under different conditions for the same material this definition of a "good" wear material is not ideal and should be defined in terms of the conditions under which wear is likely to occur.

Since there does not appear to be a large gap between the tribological properties of Si_3N_4/Sialons and a "good" tribological material any small improvement in properties may be enough to produce a material that is suitable for use in wear applications.

2.4.3 Wear of Si_3N_4 Matrix Composites.

Several studies have been carried out on the tribological behaviour of Si_3N_4 based particulate composites. Silicon nitride containing 23vol% TiN[60] showed a slightly improved wear resistance over Si_3N_4 alone and also showed a strong dependence upon humidity where SiO_2 and TiO_2 containing tribofilms protected the surface. In the case of Si_3N_4 containing TiC particles[61] the friction and wear behaviour were improved. Again the improvements were attributed to the lubricating effects of tribofilms containing Si and Ti. The addition of SiC into a Si_3N_4 matrix improved bend strength and toughness but not friction and wear while BN in Si_3N_4 improved none of the materials properties[62]. The addition of TiB_2 to SiC showed no improvement in the wear but did improve the materials fracture toughness.[63]. Wear was primarily due to the pull out of TiB_2 grains form the matrix. A stronger matrix-TiB_2 interface would result in improved wear.

All of the above studies attribute the improved wear performance of the composites to the production of tribofilms that lubricate and prevent the surfaces from coming into direct contact. Wear in this situation is determined primarily by the properties of the tribofilm. The exact nature of these tribofilms is difficult to assess due to their thickness (a few microns) and the difficulty in removing them undamaged from the wear surface. Analysis in-situ is complicated by the presence of the underlying material.

2.5 Summary

Silicon nitride exhibits excellent engineering properties that it maintains to high temperatures making it suitable for many engineering applications. It can be

produced via several methods and with varying densification aids which provides a range of possible grades of material, each with properties tailored for specific applications. Its microstructure can be manipulated to achieve high hardness (small grain sizes) or high toughness (elongated grains) depending upon the demands of the application. Sialons retain, and in some cases improve on, many of the excellent properties of Si_3N_4 whilst allowing sintering at lower temperatures and/or less densification aid with all the advantages this entails.

Particulate composites with Si_3N_4 or sialon as the matrix phase have shown some improvement in material properties and have demonstrated improved wear resistance in some systems. The ability of sialons to absorb oxygen or nitrogen into their structure makes them suitable for in-situ reaction sintering of particulate composites where oxygen or nitrogen is a by-product of the reaction.

The tribological behaviour of Si_3N_4 and sialons has received limited attention from the ceramic community but they show some promise as tribological materials under some conditions. While exhibiting relatively high coefficients of friction under dry sliding conditions Si_3N_4 has been seen to respond well to lubricants with both friction and wear being reduced. It also exhibits tribofilm formation in the presence of water and oxygen which has been shown to reduce friction and wear rates for some materials.

No clear picture of how tribological properties change with changing conditions is apparent as the literature is plagued by inconsistencies caused by differing material grades and test methods.

2.6 References

[1] K.H. Jack, "Silicon nitride, sialons and realted ceramics", pp.256-288 in High Technology Ceramics-Past, Present and Future, Ceramics and Civilisation, Vol III, 1987, , The American Ceramic Society, Inc.

[2] N.L. Parr, G.F. Martin & E.R.W. May, "Study and applications of silicon nitride as a high temperature material", *Admiralty Materials Report* No. 1/75(S), 1959

[3] D. Hardie and K.H. Jack, "Crystal structure of silicon nitride", *Nature*, **180**, (1957), pp. 332

[4] G. Ziegler, J. Heinrich and G. Wötting, "Review:- Relationships between processing, microstructure and properties of dense and reaction bonded silicon nitride", *J. Mat. Sci.*, **22** (1987), pp. 3041-86

[5] L.J. Bowen, T.G. Caruthers & R.J. Brook, "Hot pressing of Si_3N_4 with Y_2O_3 ans Li_2O as ddditives", *J.Am. Ceram. Soc.*, **61** [7-8], pp335-39 (1978)

[6] T. Ekström & M. Nygren, "SiAlON Ceramics", *J. Am. Ceram. Soc.*, **75** [2]. pp259-76 (1992)

[7] R. Morrell, "Handbook of properties of technical & engineering ceramics, part 1, an introduction for the engineer and designer", NPL, HMSO,1985, pp.302-316

[8] K.H. Jack and W.I. Wilson, "Ceramics based on the Si-Al-O-N and related systems", *Nature Phys. Sci.*, **238**, (1972), pp.28-29

[9] Y. Oyama and O. Kamigaito, "Solid solutions of some oxides in Si_3N_4", *Jpn. J. Appl. Phys.*, **10**, (1971), pp1637

[10] Y. Oyama, "Solid solutions in the ternary system Si_3N_4-AlN-Al_2O_3", *Jpn. J. Appl. Phys.*, **11**, (1972), pp.760-71

[11] R.J. Lumby, B. North and A.J. Taylor, "Chemistry and creep in sialons", in Special Ceramics 6., Ed. P.Popper. The British Ceramic Research Association, Stoke-on-Trent, pp. 238-98, 1975

[12] S. Bandyopadhyay and J. Mukerji, "Sintering and properties of sialons without externally added liquid phase", *J. Am. Ceram. Soc.*, **70**[10], pp C273-277 (1987)

[13] T. Ekström, P.O. Käll, M Nygren and P.O. Olsson, "Dense single phase β-sialon ceramics by glass encapsulated hot isostatic pressing", *J. Mater. Sci.*, **24**, pp1853-61 (1989)

[14] T.Ekström and J. Pearson, "Hot hardness behaviour of yttrium sialon ceramics.", *J. Am. Ceram. Soc*, **73** [10], pp. 2834-38 (1990)

[15] L.J. Gauckler, H.L. Lucas and G. Petzow, "Contribution to the phase diagram Si_3N_4-AlN-Al_2O_3-SiO_2" *J. Am. Ceram. Soc.* **58**[7-8] (1975) pp346-47

[16] P.H.A. Roebuck and D.P. Thompson, "Polytypoids in the Si-Al-O-N and related systems", pp. 222-28 in *High Temperature Chemistry of Inorganic and Ceramic Materials*, Ed. F.P. Glasser and P.E.Potter, The Chemical Society, London, (1977)

[17] K.T. Faber & A.G. Evans, "Crack deflection processes: II, Experiment" *Acta. Metall.*, **31**, p577 (1983)

[18] BP Landa, FH Olivares, "Computer simulation of crack propagation in composite materials" *Engineering Fracture Mechanics*, 1989, Vol.34, No.4, pp.909-915

[19] D.J. Magely, R.A. Winholtz & K.T. Faber, "Residual stresses in a two phase microcracking ceramic.", *J. Am. Ceram. Soc.* , **73**, [6], pp51641-44, 1990

[20] N. Claussen, J. Steeb & R.F. Pabst, "Effect of induced microcracking on the fracture toughness of ceramics", *Am. Ceram. Soc. Bull.*, **56**, [6], pp559-62, 1977

[21] B.A. Galanov & O.N. Grigorev, "Failure of the elastic deformed heterophase material with a periodic microstructure", (IPM, Kiev,1990)

[22] D.J. Magely, R.A. Winholtz & K.T. Faber, "Residul stresses in a two phase microcracking system" *J. Am. Ceram. Soc.*, **73**, (1990), p1641

[23] M. Rühle, A.G. Evans, P.G. Charalambides, R.M Meeking, & J.W. Hutchinson, "Microcrack toughening in alumina/zirconia" *Acta Metall*, **35**, p2701, 1987

[24] J. Subrahmanyam & M. Vijaykumar, "Review: Self-propagating high temperature synthesis", *J. Mater. Sci.*, **27** (1992), p.6249

[25] J. C. Schuster and H. Nowotny in "Proceedings of the 11th Planese Seminar", Vol 1, pp. 899-91 (1985)

[26] F. Hong, R.J. Lumby and M.H. Lewis, "TiN/Sialon composites via in-situ reaction sintering", *J. Eur. Ceram. Soc.*, **11**, pp.237-39 (1993)

[27] G.G. Genesin, E.I. Gervits, L.A. Shipilova, V. Ya. Petrovskii and A.A. Kasyaneko, *Sov.* "Effect of production conditions on the structure formation and on the elctrical conductivity of hot pressed materials in the system silicon nitride-silicon carbide" *Powder Metall. Metal Ceram.*, **29** p.483 (1990)

[28] Yu. G. Gogosti, I.I. Osipova, S.I. Chugunova and V. Zh. Shemet, "Oxidation resistance of hot pressed ceramics based on silicon nitride" *Sov. Met. Metal Ceram.*, **26**, p.163 (1986)

[29] A. Tampieri, A. Bellosi and V. Baisini, in "Material Science Monographs", Vol 68, "Advanced structural inorganic composites", ed. P. Vincenzini (Elsevier, New York, 1991) pp. 409-20

[30] V. Yareshenko, Yu. Gogosti & I. Osipova, "Ceramics today-tomorrow's ceramics", ed. P. Vincenzini (Elsevier, Amsterdam, 1991) p. 2821

[31] V. Yareshenko, Yu. Gogosti I. Osipova & D. Pogorelova, "Tagunband IX Internationale Pulvermetallurgische Tagung", **B** 3, (Dresden, 1989), p.295

[32] Jow-Lay Huang, Fan-Jan Kuo & Shih-Yih Chen, "Investigation of microstructure and crack behaviours in hot pressed TiB_2 Si_3N_4 composites", *Mater Sci. Eng.* A174 (1994), pp157-164

[33] G. Hillinger & V. Hlavacek, "Direct synthesis and sintering of silicon nitride/titanium nitride composites", *J.Am. Ceram. Soc.*, **78** [2], pp495-96, (1995)

[34] C.R. Blanchard & R.A. Page, "Effect of silicon carbide whisker and titanium carbide particulate additions on the friction and wear behaviour of silicon nitride", *J. Am. Ceram. Soc.*, **73** [11], pp3442-52 (1990)

[35] A. Sawaguchi, K. Toda & K. Niihara, " Mechanical and electrical properties of Si_3N_4-SiC nanocompoites.", *J. Am. Ceram. Soc.*, **74** [5], pp1142-44 (1991)

[36] M.G. Gee and D. Butterfield, "The combined effect of speed and humidity on the wear of silicon nitride", *Wear*, 162-164 (1993) pp. 234-245

[37] T.E. Fischer & H. Tomizawa, "Interaction of tribochemistry and microfracture in the friction and wear of silicon nitride", *Wear*, Proc. Int. Conf. Wear of Material ASME, New York, 1985 pp.22-32

[38] S. Sasaki, "The effects of the surronding atmosphere on the friction and wear of alumina, zirconia, silicon carbide and silicon nitride.", *Wear*, 134 (1989). pp.185-200

[39] Hiroyuki Ishigaki, Ryo Nagata & Mikio Iwasa, "Effect of absorbed water on friction of hot-pressed silicon nitride and silicon carbide at slow speed sliding", *Wear*, 121, (1988) pp.107-16

[40] M.G.Gee, C.S. Matharu, E.A. Almond and T.S. Eyre, "The measurement of sliding friction and wear of ceramics at high temperature", *Wear*, 138, (1990) pp. 169-87

[41] H. Czichos, D. Klaffke, E. Santer and M. Woydt, "Advances in tribology: materials point of view", *Wear*, 190 (1995) pp. 155-61.

[42] K. Komvopoulos & H. Li, "The effect of tribolfilm formation and humidity on the friction and wear properties of ceramic materials", *J. Tribology*, Jan 1992, Vol 114, pp.131-40

[43] P. Kapsa, Y. Enomoto, "Sliding damage of hot-pressed and sintered silicon nitride caused by a diamond tip under controlled humidity", *Wear*, 127 (1998) pp.65-83

[44] Z. Xingxhong, L. Jiajun, Z. Baoliang, X Qunji, O. Jinlin, "The influence of lubrication on tribological properties of Si_3N_4/1045 steel sliding pairs", *J. Mater. Sci.*, **32**, (1997), pp.661-66

[45] A. Ravikiran & B.N. Pramila Bai, "Influence of the tribological reaction products and the associated transitions for the dry sliding of silicon nitride against steel", *J. Am. Ceram. Soc.*, **78** [11]. pp.3025-32, (1995)

[46] J. C. Conway Jr, R.N. Pangborn, P.H. Cohen, D.A. Love, "Dry sliding wear of a SiAlON ceramic", *Wear*, 126, No1, pp.79-90

[47] D.C. Crammer, "Friction and wear properties of monolithic silicon based ceramics", *J. Mater. Sci.*, 20, (1985), pp.2029-37

[48] O.O. Adewoye and T.F. Page, "Frictional deformation in polycrystalline SiC and Si_3N_4", *Wear*, 70 (1981), pp.37-51

[49] P.Gautier and K. Kato, "Wear mechanisms of silicon nitride, partially stabilized zirconia and alumina in unlubricated sliding against steel", *Wear*, 162-64, (1993), pp.305-13

[50] G.J. Tennenhouse, A. Ezis and F.D. Funkle, "Interaction of silicon nitride and metal surfaces.", *J. Am. Ceram. Soc.*, **68**[11], C30-C31, (1985)

[51] S. Jahanmir, N.P. Suh & E.P. Abrahamson, "Microscopic observations of the wear sheet formation by delamination wear", *Wear*, 28 (1974), p235

[52] K.Kato, "Tribology of ceramics", *Wear*, 136 (1990), pp.117-133

[53] Y.Wang, S.M. Hsu "Wear and wear transition mechanisms of ceramics", *Wear*, Vol.195, No.1-2, Jul 1996, , pp.112-122

[54] A. Skopp, M. Woydt, K.-H. Habig, "Tribological behaviour of silicon nitride materials under unlubricated sliding between 22°C and 1000°C", *Wear*, 181-183 (1995), pp.571-80

[55] O.O. Ajayi & K.C. Ludema, "Surface damage of structural ceramics: Implications for wear modelling", *Wear*, 124, pp237-57

[56] Y. Kimura, K. Okada & Y. Enomoto, "Sliding damage of Si_3N_4 in plane contact", 1989, *Proc. Int. Conf. Wear of Materials*, vol 1 (New York ASME) pp.361-68

[57] P.Andersson & K. Holmberg, "Limitations on the use of ceramics in unlubricated sliding applications due to transfer layer formation", *Wear*, 175 (1995), pp.1-8

[58] S.A. Horton, D. Dowson, F.L. Riley & N.C. Wallbridge, "The sliding wear of non-oxide ceramics", Ceramic Materials and Components for Engines, Proceedings of the Second International Symposium., Luebeck-Travemuende, West Ger, 14-17 Apr 1986, (Conf. code 09111), pp750-765, 1986.

[59] P. Andersson, "Water lubricated pin-on-disc tests with ceramics", *Wear*, 154 [1] pp.37-47, (1992)

[60] Y. Imada, K. Kamamura, F. Honda & K. Nakajima, "The tribological reaction accompanying friction and wear of silicon nitride containing titanium nitride", *Tans. of the ASME. J. Tribology*, April 1992 Vol. 114, pp.230-35

[61] C.R. Blanchard & R.A. Page, "Effect of silicon carbide whisker and titanium carbide particulate additions on the friction and wear of silicon nitride", *J. Am. Ceram. Soc.*, **73** [11], pp.442-52, (1990)

[62] R.A. Page, C.R. Blanchard-Ardid, W.Wei, "Effect of particulate additions on the contact damage resistance of hot-pressed Si_3N_4", *J. Mater. Sci.*, **23** (1988), pp.946-57

[63] O.O. Ajayi, A. Erdemir, R.H. Lee & F. Nichols, "Sliding wear of silicon carbide-titanium diboride ceramic matrix composite.", *J. Am. Ceram. Soc.*, **76** [2], pp.511-17, (1993)

Chapter Three

Experimental Techniques

3. Experimental Techniques

The production, characterisation and measurement of a ceramic material's properties requires the use of many techniques. An understanding of the operation and basic theory behind these techniques is essential if conclusions are to be drawn from the results and if they are to be compared with those produced by different methods. In the following sections the production and characterisation techniques used throughout this work are described.

3.1 Powder Preparation

Before synthesis of dense ceramic materials the raw materials, in powder form, must be processed. The aim of this processing is to produce homogeneous mixtures of the starting compounds in a form suitable for consolidation into green bodies and sintering. The following sections describe the techniques used in this work to process the starting compounds for sialon/TiB_2 ceramic composites and the methods used for consolidation.

3.1.1 Ball Milling

Ball milling techniques are frequently used not only to produce a range of small particle sizes but to create homogeneous, intimate mixtures of different raw materials[1,2] The powder mixture to be milled is placed inside a cylindrical container along with suitable milling media. The container is then rotated on two rollers for times usually in excess of 24 hours and most commonly for approximately 72 hours. The process can be carried out dry or wet. The major advantages provided by each method are summarised in Table 3.1

Wet Milling	Dry Milling
• Low power input	• Avoids powder drying stage
• No dust problems	• Avoids powder/liquid reactions
• Higher rotational speed achievable	• Less media and lining wear
• Good homogeneity of mixture	• Avoids contaminants introduced by liquids
• Smaller particle sizes	
• Wet sieving of slurry	

Table 3.1 Summary of advantages of wet and dry ball milling[3]

To avoid unwanted contamination hard media should be used which will not undergo significant wear and hence produce little contamination, however, chipping of the media can still occur contributing to contamination. Contamination can be further reduced using hard media of a similar composition to the charge. Wear resistant liners can be used inside containers but when dealing with hard materials (such as Si_3N_4, TiN) these liners are often ineffective or expensive. Containers made from polyurethane or various rubbers have been shown to be successful but the choice of liquids for wet milling is made so as to avoid attack of the polyurethane which may cause organic contamination. Organic contamination can be burnt off before sintering, other contaminants from hard liners are not removed so easily. Milling and mixing processes may increase the oxygen content of the powder, especially if there is significant formation of new surfaces by fracture.

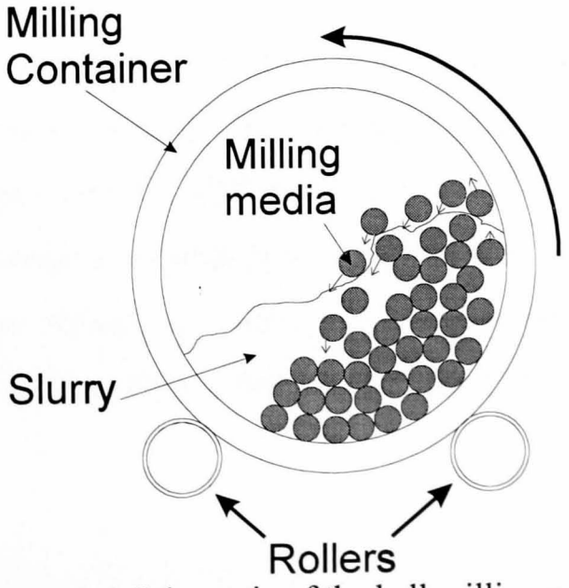

Figure 3.1 Schematic of the ball milling process

Powder batches of 100g were wet milled using 750g of cylindrical sialon media (10mm length, 5mm diameter) in polyurethane jars. The liquid used was iso-2-propanol (IPA) and was mixed with the powder charge in the ratio 2.5:1 respectively. The optimum speed for milling is ~65% of the critical speed (ω_c) above which media are held against the container wall for the whole rotation by centrifugal force:

$$\omega_c = \left(\frac{60}{2\pi}\right)\left(\frac{2g}{D}\right)^{\frac{1}{2}} \approx \frac{42.3}{D^{\frac{1}{2}}} \qquad \textbf{Equation 3.1}$$

where D = diameter of the container and g= acceleration due to gravity. Hence, for the 7.5cm diameter container used, the rotational speed was ~90rpm.

Another commonly encountered technique is that of *vibrational milling* in which the energy for milling is provided by the application of vigorous vibrational energy to a container containing the charge and milling media. Local impact on particles trapped between colliding media causes shear fracture. Vibrational milling was used where small quantities of powder were needed (e.g. 20g) primarily when making small additions to already mixed and milled composition to achieve optimum results. The milling media were cylindrical agate pieces ~5mm long by 4mm diameter and were arranged along the axis of the milling container so as to almost fill it. Vibrational milling was carried out for ~20-30 mins in IPA.

After milling and mixing the wet IPA/powder slurries were sieved through a 38μm sieve to remove any large scale contamination from the milling media. The slurry was then dried at ~50°C in a Pyrex dish for 24-48 hours. The dried product was broken up by passing it through 500 and 250μm sieves. Any large agglomerates were broken up either by brushing through by hand or by vibration sieving using milling media in the sieves to provide a breaking up action.

3.1.2 Consolidation

There are many available techniques for consolidating powders into green bodies. A simple and commonly used method of consolidating powder into simple shapes is uniaxial pressing. Uniaxial pressing was chosen over isostatic pressing because it provides discs of an appropriate size for the hot press. The powder is placed into a die (usually cylindrical) and pressure is applied in one direction either mechanically or hydraulically (see Figure 3.2(a)).

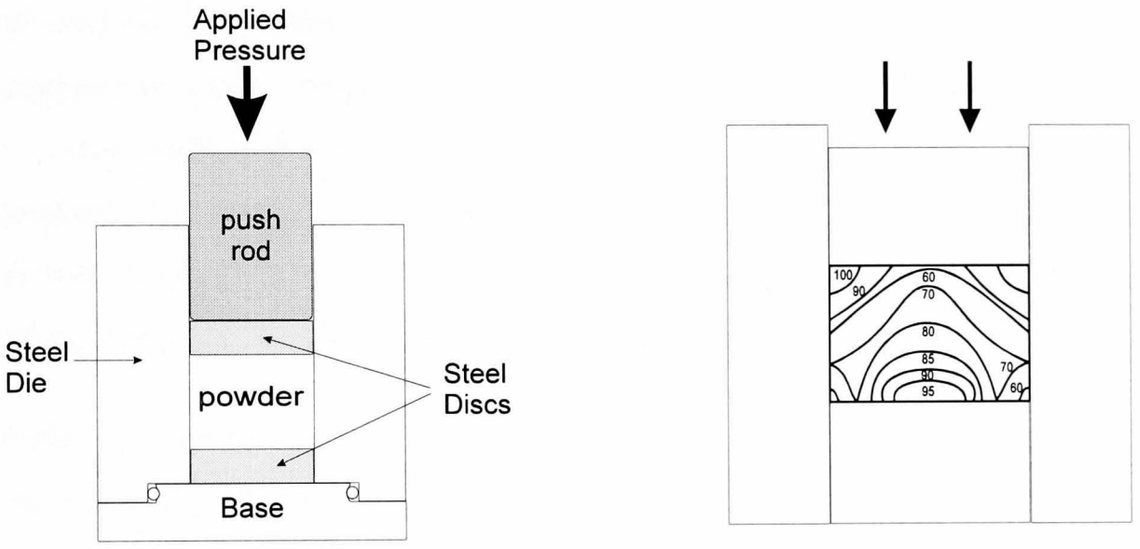

Figure 3.2 (a) Uniaxial pressing arrangement and (b) Density variations in a single ended uniaxially pressed green body. Figures are percentage of maximum density achieved.

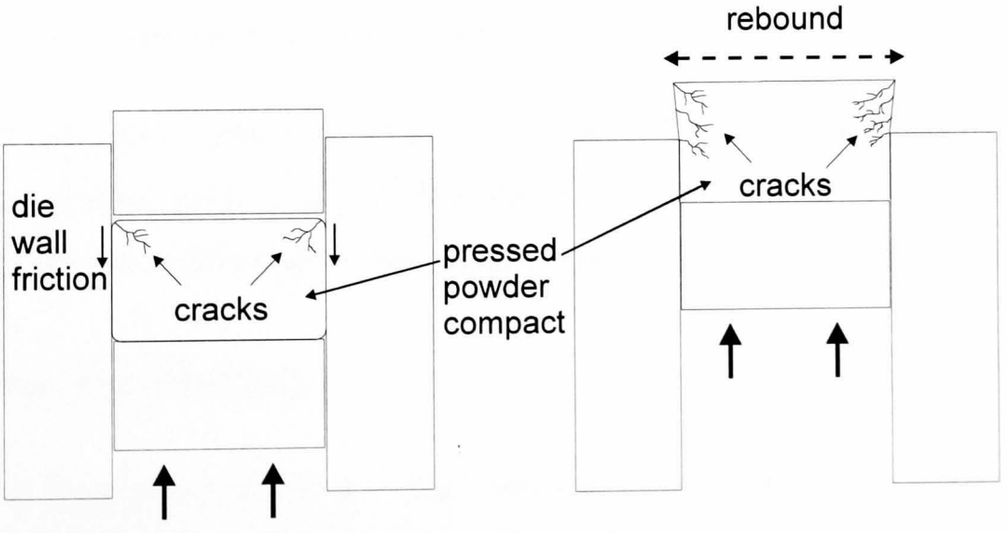

Figure 3.3 Cracking occurring in uniaxial pressed compacts due to die wall friction and rebound on removal from the die.

Particle rearrangement of agglomerate break up are responsible for the shrinkage of the component. There can be several problems associated with uniaxial pressing:

improper density or size
die wear
cracking
density variation.

In materials development the latter two are the most serious. The major causes of cracking are friction with the die wall and the rebound experienced by the compact on ejection from the die. The two mechanisms are illustrated in Figure 3.3. Non-uniform density, which may inhibit proper sintering of the compact, is primarily also caused by die wall friction. An example of density variation is shown in Figure 3.2(b). Non-uniform density can also be caused by uneven filling of the die and the presence of hard agglomerates.

Uniaxial pressing of prepared powders was carried out using a 25mm diameter steel die with pressure applied from one end. The correct pressures for each material were determined experimentally. (see chapter 5). In practice there were some inconsistencies in the results from uniaxial pressing. These were attributed to the following factors.

1. The removal rate after pressing was not controlled, it is possible that rebound is influenced by the speed at which the pellet is removed.

2. Die wall friction. Variation in die wall friction may have occurred due to contamination of the walls by other materials and the degradation with use of the die walls caused by the abrasive nature of the materials being pressed.

3.2 Hot Pressing

A description of the processes that take place during densification by hot pressing has been given in chapter 2. The following section describes the equipment used to hot press the composites and the way in which it was used.

Hot pressing was carried out using a Radyne radio frequency heated furnace (max. temp ~1900°C) equipped with a hydraulic ram system.. Heating was carried out by a water cooled copper coil which allowed the r.f energy to heat a graphite susceptor. Coil and susceptor were open to atmosphere and insulated by a large enclosure containing bubble alumina. A sketch of the set up is shown in Figure 3.4

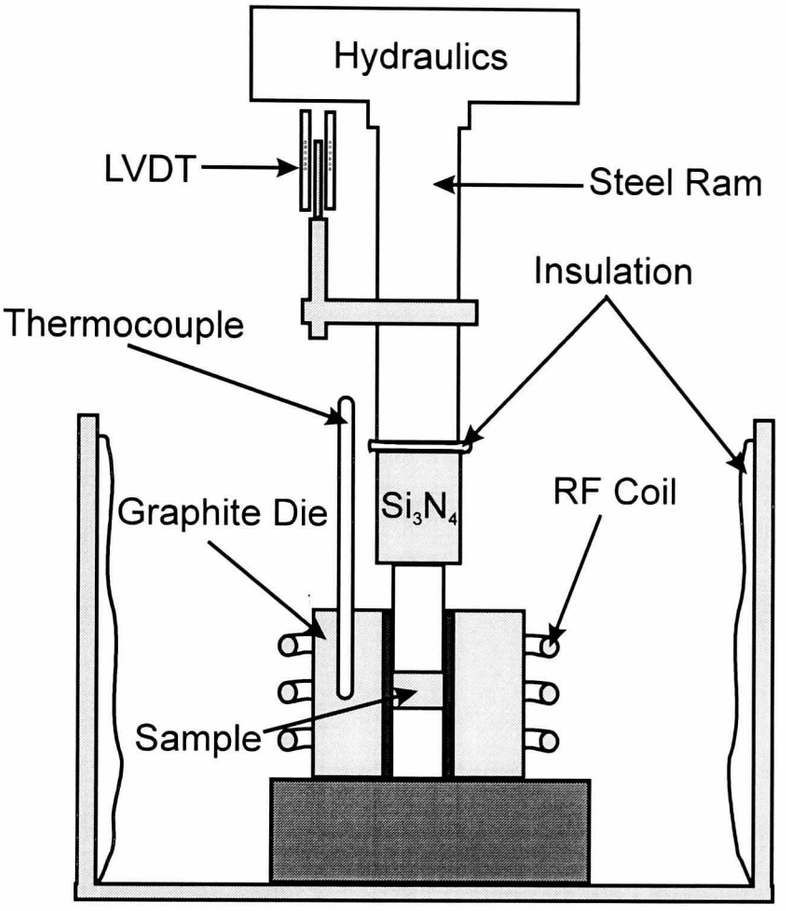

Figure 3.4 A schematic of the hot press apparatus

Because of the delicate nature of the green bodies and the cost and short supply of graphite dies a special "split" high density graphite die was manufactured to enable easy loading and unloading of the sample (see Figure 3.5). The die was of 25mm diameter and was surrounded by a receptor of ~15cm in diameter which was positioned with ~1cm clearance inside the copper coil. All punches and spacers were also made of high density graphite. The die was lined with an organic based BN paint to stop intimate contact between the sample and the graphite walls.

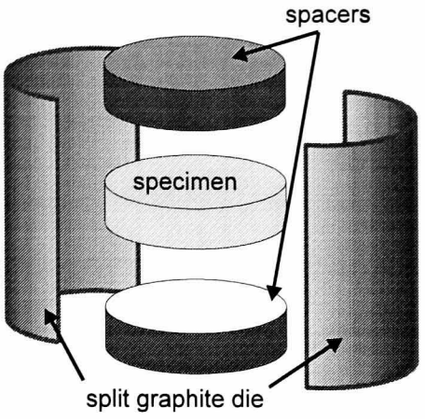

Figure 3.5 The arrangement of the sample in the split graphite die.

Initially, and for most composite production, the temperature was controlled via a computer and applied pressure was controlled manually. A system for automatically controlling the application of pressure was later added and was used for later composite production. The movement of the hydraulic ram, and hence the densification behaviour of the sample, was monitored by a linear variable displacement transformer (LVDT). Temperature was monitored by using a W_5* (tungsten 5% rhenium / tungsten 26% rhenium) thermocouple housed in an alumina tube and placed inside the graphite susceptor close to the sample.

Graphs of temperature, pressure and sample displacement were plotted from the recorded data. These plots were used to give information on the mechanisms and reactions occurring and at what temperatures they were active. The recording of the shrinkage of the sample was particularly useful for analysing densification behaviour but was only possible once the natural expansion of the system due to heating was subtracted from the LVDT data. The data from a "dry run" (i.e. no specimen present) with the same time/temperature/pressure profile was subtracted from real data to obtain the actual sample movement.

The actual compositions and time/temperature/pressure conditions used for composite production by hot pressing are given in chapter 5.

* Trade name of T.C., P.O. Box 130, Uxbridge, England.

3.3 Pressureless Sintering

Chapter 2 has described the processes that take place during the densification of these materials via pressureless sintering. Pressureless sintering was carried out in a resistance heated furnace (max. temp. 1900°C) which could be evacuated to a level of ~ $1x10^{-6}$ mbar. The element was composed of graphite and the specimen was contained in a graphite pot with a sialon lining. The chamber could be back filled with either nitrogen or argon. A schematic of the furnace is shown in Figure 3.4

The element is insulated from the steel container by carbon based insulation (not shown). The steel body is internally water cooled. Unlike hot pressing no information about sample densification was available during a run. Samples of the pressureless sinterable material could be sintered in the hot press under minimal pressure. While not achieving the required density or exact composition under these conditions, the sample densification behaviour could be monitored via the LVDT readout.

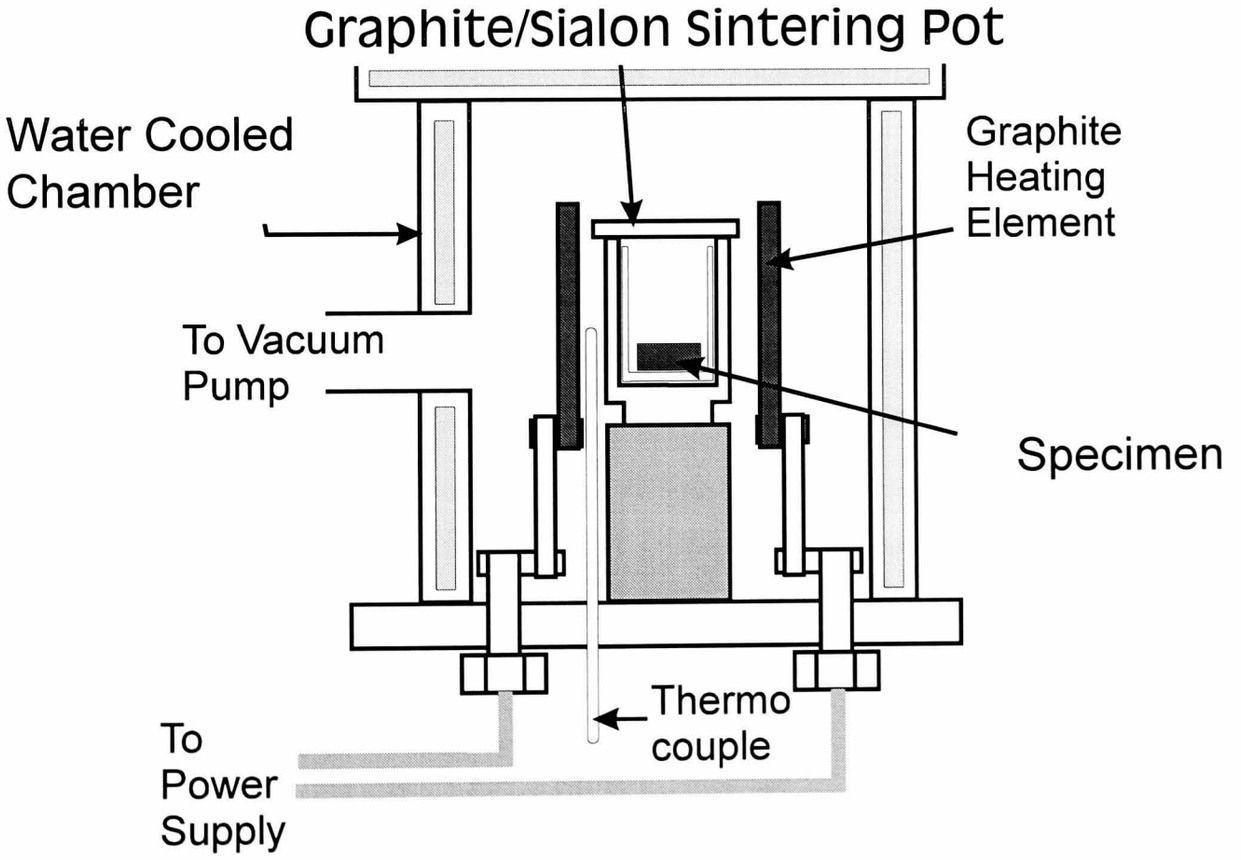

Figure 3.6 A schematic of the furnace used for pressureless sintering

Normal procedure was to evacuate the chamber to a good vacuum before heating began and to keep evacuating as the furnace was heated to a temperature of ~900°C. A hold at this temperature allowed the chamber and sample to be degassed without affecting the composition of the green compact.

After sintering the furnace cooled at its natural rate which is shown in Figure 3.7

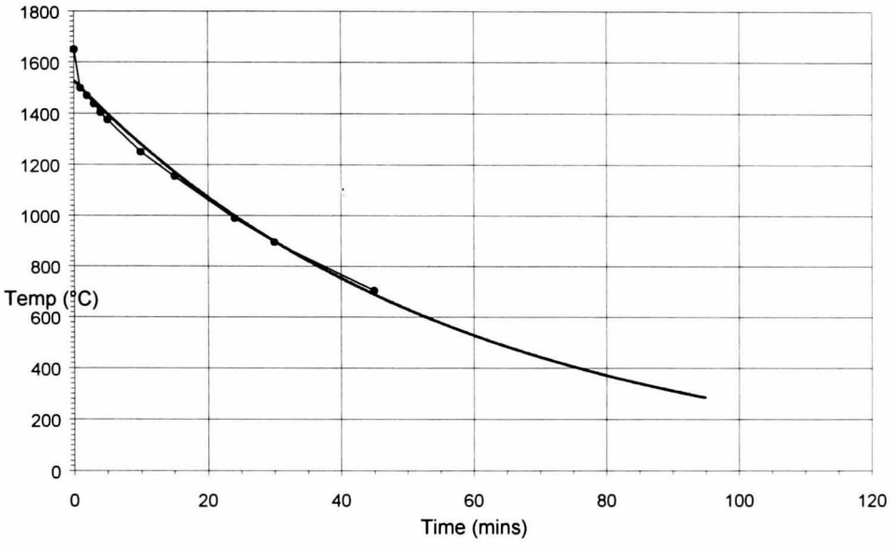

Figure 3.7 A typical cooling rate for the pressureless sintering furnace

The compositions and conditions for the pressureless sintering of sialon/TiB_2 composites are given in chapter 5.

3.4 Sintered Sample Preparation

In hot pressing, the BN lining of the graphite die impregnates the near surface region of any sample and the composition of the surface is affected by the presence of a reducing atmosphere caused by the reaction of O_2 with the graphite die (i.e.: $2C+O_2=2CO$). In pressureless sintering some dissociation may occur at the surface due to the absence of a nitrogen over pressure at the sintering temperature or there may be reaction at the surface between TiB_2 and the nitrogen atmosphere present during the later stage.

While the presence of such surface layers is undesirable from a production point of view it can be tolerated at research level but they must be removed to assess the properties of the underlying material. In all the techniques described in this

section these surface layers are removed as described below after analysis by XRD.

These unwanted layers were removed from the top, bottom and sides of each sample using a diamond grinding wheel (either automatically or by hand). Approximately 0.5 mm was removed from each surface or until all the outer layer was removed revealing a dense core of the required composition

Many techniques such as SEM and hardness and fracture toughness measurements require the sample to be perfectly flat and polished in order to observe the relevant features. Sample were thus further polished using water based diamond polishing solutions on felt polishing pads. After initial flattening using the coarsest diamond grades the samples were polished using 25, 6 and 1 μm diamond solutions and finally 0.25 μm colloidal silica. Polishing was performed by a combination of manual and automatic techniques.

3.5 Measurement of Density of Sintered Materials

The determination of the specific density of the sintered component and its comparison with the theoretical density of a fully dense body of the same material gives an indication of the porosity level in the sample. Clearly this is dependent upon knowing the phases present and their quantities. This information can be obtained from X-ray diffraction, electron microscopy and theoretical calculations.

The Archimedes method was used to determine the density of the sintered samples and to esimate the porosity level. The sample is firstly weighed in air (w_a) and then weighed in pure distilled water (w_w). For measurements of the bulk density of a body with porosity either the initial weight in water before significant penetration has occurred should be taken or the body should be encased in an impermeable coating.

A simple calculation, taking into account the density of the water (ρ_w) at the temperature at which measurement are taken (T), gives the actual density ρ_a. i.e.:

$$\rho_a = \frac{W_a \rho_w}{W_a - W_w} \qquad \textbf{Equation 3.2}$$

where $\rho_w = (-2.14\times10^{-4} \times T)+1.002457$ and where T= temperature of the water.

Weighing of the specimen in both air and water was carried out using a digital balance with an accuracy of ±0.002g. The balance was set up especially for the measurement of density and is shown schematically in Figure 3.8

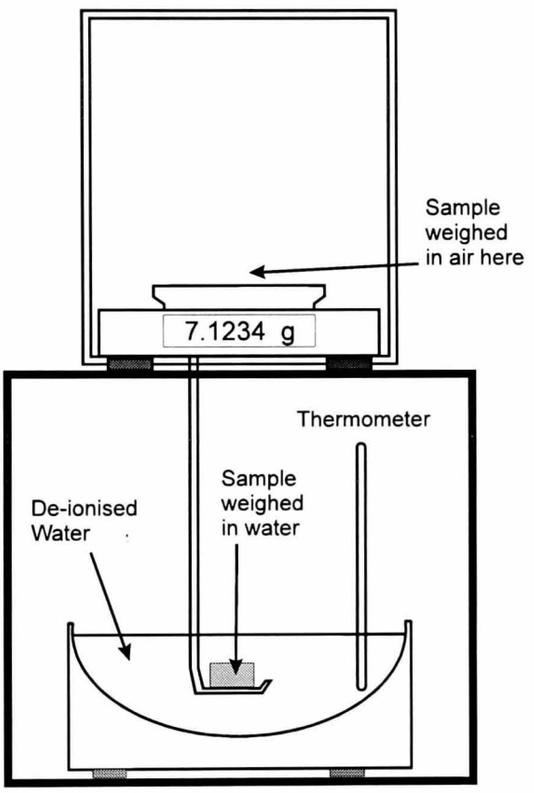

Figure 3.8 Apparatus for determining the bulk density of specimens.

Since information on the level of porosity was required the initial weights of the samples in water was taken for density calculations.

Closed porosity levels are difficult to measure without cutting the sample and examining the distribution and amount of the internal porosity. A non-

destructive approach is to compare the measured density with the theoretical density ρ_t to give a percentage value.

The bulk specific density of a solid of each sintered sample (ρ_a) was measured using the Archimedes method. Each result is reported in g/cc and as a percentage of the theoretical density (ρ_t) which is calculated from the compositional program used to generate the starting compositions.

Errors in the figures quoted come from several sources. Firstly, and probably the most significant, is the uncertainty of the initial weight of the sample in water before the water starts to penetrate the porous body. As the water is absorbed the value for density will move from the bulk density (including porosity) to the true density (open porosity is excluded by the penetration of the water.) Also the calculated theoretical density may not be correct due to slight variations in the amount and type of phases present in each sample.. Such variations can arise from any incorrect assumptions in the compositional calculations, errors at the powder weighing stage leading to non-stoichiometric mixtures and processing conditions that could lead to incorrect phase production.

Due to the nature of the production of the composites, the as-sintered specimens consist of a core of material with surface layers of a different and unwanted composition. These surface layers were always removed for key property measurement. Where a density is quoted this value corresponds to the density of the sample after the surface layers have been removed, unless otherwise stated. However, it was often impossible to determine whether all of this outer shell had been removed and since it is of a different composition then this may also lead to errors in the value of ρ_t.

3.6 X-ray Diffraction.

X-ray diffraction (XRD) is a powerful tool for the determination of the crystalline phase content of multiphase materials. Not only can it identify the phases present but it can give information on the level of solid substitution in

systems such as those under study (i.e.: SiAlON), grain size (from peak width) and some indication of the presence of anisotropic grain growth (intensity variation).

Diffraction from powdered samples is the normal procedure, however, when material is in short supply or cannot be easily reduced to a powder form, non-destructive methods can be used providing that the material has a small enough crystalline size and a random orientation of grains within the solid. XRD can therefore be performed on solid polycrystalline samples which have small enough crystallites and have flat surfaces aligned with the diffractometer axis.

There are some difficulties encountered when using this technique for identification:

a) encountering a new undocumented species.
b) shifts in peak position caused by solid solutions.
c) The presence of 3 or more species, when many peaks may coincide making identification difficult.
d) strong preferential orientation of the crystallites, leading to the reinforcement of some peaks and the absence of others

The x-ray source used in this work was a Philips 2kW, 60kV Cu tube operated at 40kV and 30mA filtered through a Ni filter to produce Cu $K\alpha_{1,2}$ radiation (λ Cu $K_{\alpha 1}$ = 1.5405Å and λ Cu $K\alpha_2$ = 1.5443Å). The peaks produced from these different wavelengths are not easily resolvable especially at low 2θ values and usually a weighted average is used of λ= 1.54178Å. However at higher values of 2θ the α_1 and α_2 peaks become resolvable and the peak position for calculation of d from 2θ should be taken with care. The detector was a Geiger Muller tube whose output was logged and plotted on computer , the scanning mode was 2θ for the detector and θ for the sample. Initial spectra were obtained over ranges from 10° to 80° 2θ at a continuous scan rate of 1° per minute and a data averaging rate of 30 readings per second. Later spectra were obtained by a stepping motor system that would typically dwell for 2 secs at 0.02° intervals over the same range.

XRD of powdered samples was carried out by placing a small amount of powder in a holder that presented a flat powder surface to the x-ray beam. Solid samples were simply ground flat before XRD.

Calibration of the equipment was carried out periodically using a polycrystalline silicon standard. However, unresolved equipment problems led to the use of a very thin layer of silicon powder being applied to the face of any sample to be examined. This provided a reference standard and allowed correction to be made for any error in 2θ.

The determination of peak position was carried out using a curve fitting procedure which, as a first approximation, fitted a Gaussian function to the data. This procedure was usually sufficiently accurate to allow phase identification. If the α_1-α_2 split was evident and a high degree of accuracy was necessary then a customised function that compensates for this split was used.

3.7 Electron Microscopy

The microstructure of a ceramic material is an important factor in its mechanical behaviour. Microstructural features on the scale of 100s of microns to 10s of nanometres can have significant effects on a material's properties. Examples are the morphology and size of individual grains, the level and size of porosity and the presence and composition of intergranular phases. The observation of fracture surfaces, indent sizes and crack length is also of interest and they exhibit features on similar scales to the microstructure. Observation and analysis of such features requires high magnifications and special techniques both of which can be provided by *electron microscopy.*

In scanning electron microscopy (SEM) there are many possible interactions between the incident electrons and the material under study which give rise to several analysis techniques. For imaging the electron beam is focused to a fine spot which is scanned in a raster pattern over the area of the sample being examined. For analysis of individual features such as grains, particles or intergranular phases it can be focused on a single point of the sample.

There are 3 main detection techniques. Secondary electron, back-scattered electron and x-ray detection.

3.7.1 Secondary electron detection

The high energy primary electrons that are incident on the sample, have an interaction volume as shown in Figure 3.9.

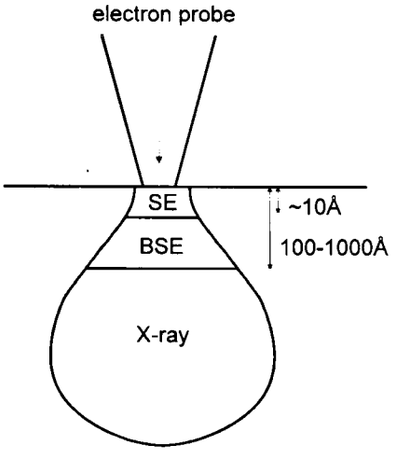

Figure 3.9 The interaction volumes for various detection modes of the SEM

Secondary electrons are emitted form the near surface regions (~10Å) and their intensity is proportional to the slope of the surface with respect to the incident electron beam. (see Figure 3.10) Hence detection of secondary electrons can provide an image which shows the topographic details of the specimen surface.

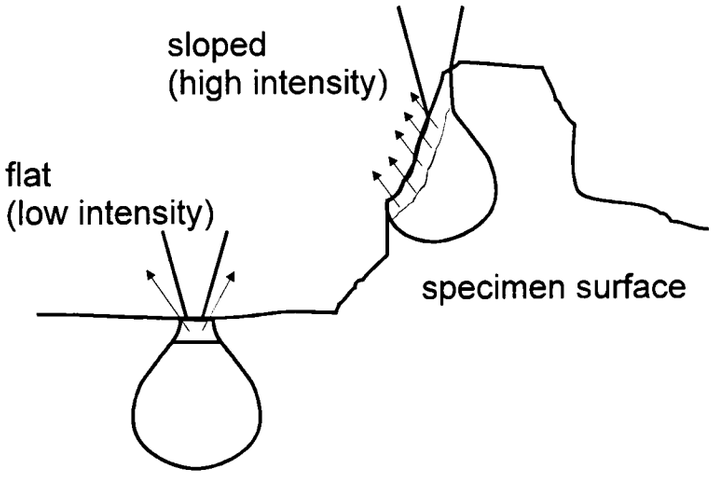

Figure 3.10 Schematic of the process giving rise to contrast in secondary electron detection.

In the study of ceramic materials secondary electron detection is a surface specific (~10Å) technique primarily used for the determination of porosity levels, some indication of microstructure (better images can be obtained by the method described in 3.7.2), examination of fracture surfaces and measurement of indent size and crack length and shape(for hardness and fracture toughness measurements). Topographic contrast is used extensively for the study of wear, for example the study of the wear damage to a surface.

3.7.2 Back Scattered Electron Mode

Primary electrons that undergo close interactions with the specimen atoms are expelled from the sample by the repulsive forces experienced close to a nucleus. These back scattered electrons can be used to image atomic contrast in materials. This technique is used extensively for the imaging of ceramic microstructures which are usually at least di-phasic.

To observe a purely compositional image the specimen should be polished perfectly flat to eliminate topographical effects which can dominate. The detector system, a disc shaped semiconductor device with a surface junction, usually consists of 4 quadrants allowing several imaging modes.

The resolution of back scattered electron images is less than that of secondary electrons because of the increased interaction depth (order of 100-1000Å in depth) involved for the elastic scattering process (see Figure 3.9) which leads to a resolution usually in the order of 100-500Å.

This imaging mode was used extensively to observe the microstructures of the composites and to quantify the amounts of TiB_2 present by using the image in conjunction with image analysis software. Back scattered contrast was also used to measure crack length when secondary electron contrast was not sufficient. Vickers hardness indents are often difficult to locate and observe using secondary electron contrast because low load indents are very shallow. The back scattered detector was used with two of its segments switched to provide inverse

contrast. In this condition topographical contrast is enhanced and makes small surface features easier to locate on a relatively large, flat and featureless specimen surface.

3.7.3 X-ray Emission, Energy Dispersive X-ray Analysis (EDX)

Further information about the sample is available via x-ray emissions from the specimen and this can be used to perform qualitative or quantitative analysis of its composition.

The x-rays arise from the interaction of primary electrons with core electron levels (usually the K and L shells) of the specimen. These electrons are ejected from the atom and electrons from the M or L shell are transferred to fill the subsequent gap. In doing so they emit an x-ray with energy E_K-E_L, for example, characteristic of the specimen atom involved. These x-rays can be detected and sorted either by their wavelength or by their energy, each technique using a different type of detector system. Commonly (and the technique used for this study) energy dispersive x-ray spectroscopy (EDX) is used, with a solid state, liquid nitrogen cooled detector system. The detector is protected from the condensation of species from the specimen chamber by the presence of a few micrometers thick beryllium window. However, the presence of this window absorbs many low energy x-rays and limits useful analysis to elements above sodium. This window can be exchanged for either an ultra-thin polymer based window or no window at all. In these circumstances analysis can be performed down to carbon at the risk of forming a condensed layer on the detector that may absorb incident x-rays.

The most serious limitation of EDX is the energy resolution possible. Each peak for a given element may have a width of 100-200eV making resolution of closely spaced peaks from different elements difficult to achieve. For example silicon and yttrium have peaks at 1.74keV ($K_{\alpha 1}$) and 1.92keV($L_{\alpha 1}$) which causes a problem if the silicon peak is significantly bigger than that of yttrium. (a common scenario in Si_3N_4 ceramics). The signal to noise ratio in a typical detector system is also a limiting factor to detectability and conditions such as

accelerating kV, spot size and specimen orientation with respect to the detector need to be set carefully to achieve a good enough signal to noise ratio when using quantitative analysis.

For qualitative analysis the x-ray emissions from the sample can be used in two ways. A distribution map (or x-ray map) of the elements of interest can be constructed from the emissions at each point as the electron probe scans the surface. Spot or probe analysis can be used to record a spectrum of the elements present at the probe position.

In the case of quantitative analysis the application of ZAF correction factors (Z= atomic number, A= absorption and F= fluorescence) along with careful calibration can provide quantitative information on the amounts of each atomic species present, giving the composition of the specimen. This technique requires careful calibration, choice of suitable operating conditions and the use of computer programs to perform the ZAF corrections.

The resolution for EDX is the lowest of the three techniques due to the large interaction volume for x-ray emission (see Figure 3.9). Again when using these techniques the specimen should be perfectly flat. Care should be taken when using any quantitative technique on bulk specimens as the large interaction volume may cause the sampling of a volume of specimen that differs compositionally to that which is visible to the operator, either by secondary or back scattered electrons, and hence lead to results that are incorrect. An example of this occurrence is shown in Figure 3.11.

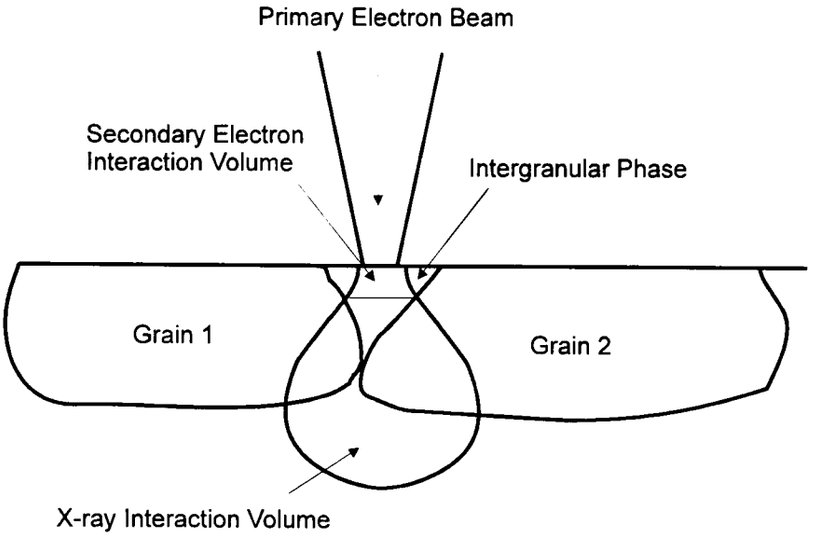

Figure 3.11 Interaction volume in a bulk specimen, regions below the visible surface contribute to the data collected and cause errors in quantitative analysis.

3.8 Hardness and Fracture Toughness Measurements

In the following sections the techniques for measuring the hardness and fracture toughness of ceramics are reviewed and the way in which these techniques were applied to the materials under study is described.

3.8.1 Hardness Measurement

The concept of hardness has no precise definition and can be measured in many different ways, and results from apparently similar tests can vary widely. It is thus essential that the appropriate test and conditions are used for the type of material being tested and that the conditions under which the test was performed are reported fully.

There are two commonly used tests for ceramic materials; (i) The Vickers hardness test and (ii) the Knoop hardness test. Both indent the surface but with a diamond of differing geometries. The diamond shapes are shown in Figure 3.12.

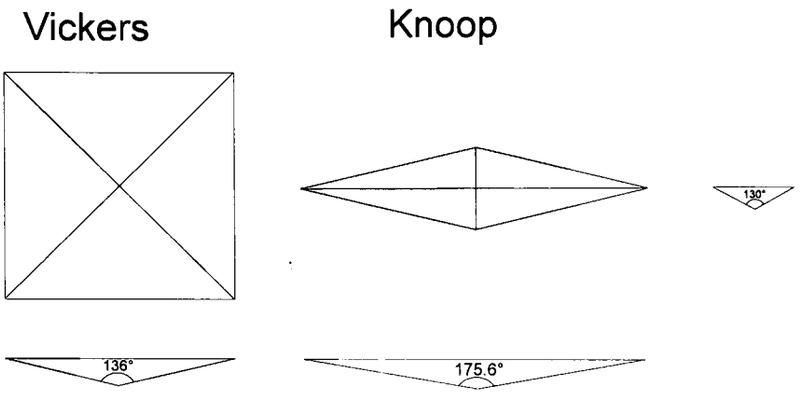

Figure 3.12 The geometries of Vickers and Knoop diamond indenters

The Vickers diamond is pyramidal with an angle of 136° between adjacent faces and produces a square indent. There is an inevitable chisel edge at the tip but most quality diamonds have a chisel edge length of 1-2μm. Errors involved in indenting with Vickers diamonds come from errors in the cut angle and from the size of the chisel edge, the most serious being from the chisel edge when loads (and hence indent sizes) are small.

Vickers Hardness (H_V) is calculated from the contact area of the indent by

$$H_V = \frac{P}{\text{contact area}} = \frac{0.322P}{a^2 \sin 136°} \qquad \textbf{Equation 3.3}$$

where P= load in Newtons and 2a= the diagonal length in metres. Units are therefore Nm^{-2} or more usually quoted in Pascals (Pa).

The Knoop diamond has a long and short axis with an angle of 175.6° between long axis faces and 130° between the short axis faces. The ratio between the long and short axis is ~7:1 and the Knoop can be used in different orientations to investigate the effect of anisotropy of the ceramic surface on hardness. The long axis also allows more accurate measurement at small penetration depths making it ideal for low or micro-hardness tests.

Knoop hardness (H_K) is calculated from the projected area and is hence not directly comparable with H_V. Its units can be quoted as for Vickers hardness but are also often found quoted as a "Knoop Number".

$$H_K = \frac{2P}{d_l^2(\cot 172.5° + \tan 130°)}$$ **Equation 3.4**

In choosing the correct load to use consideration should be given to the grain size of the material. It has been shown in some materials that, as the size of the indent approaches the grain size hardness is seen to increase as dislocations are blocked by grain boundaries. This has led to the arbitrary division of hardness measurements into 3 areas, all overlapping to some extent.

(i) Micro-hardness, ($\sim 10^{-1}$ to 10^{-4} kg applied load) - where loads produce indents close to the grain size. Care should be taken when experimenting in this region as variations in technique and microstructure have been seen to produce variations of 50 to 400% of the standard hardness values. In hard materials the shallow indents produced can be sensitive to and dominated by the condition of the surface.

(ii) Low hardness, ($\sim 10^{-1}$ to 10^{1} kg applied load) - where there is some dependence upon applied load but the problems associated with microhardness are less dominant.

(iii) Standard hardness ($\sim 10^{1}$kg and above), where there is no dependence upon applied load but results can be erratic because of the brittle response of the ceramic. Local cracking around the indent can absorb energy and lead to variations of the measured hardness.

In fact it is the cracks around high load indents that leads to the measurement of other ceramic properties such as fracture toughness (K_{Ic}).

Indentations for hardness measurements were carried out on smooth polished surfaces in order to be able to observe clearly and measure the indent by either optical or electron microscopy. Hardness measurements were carried out under several loads, mainly in the low load hardness regime. Indentation was performed on an Instron 1122 with a 500Kg load cell. Loading/unloading rates for all tests were 0.5mm/min and indent times were 30 secs. The load cycle was

load/stop/unload with no compensation for decreasing load as the material relaxed under the indenter. Indentations were measured on both optical and electron microscopes. There was a varied time delay between indentation and indent measurement, sometimes in excess of 24 hours. Results were taken as the average of the indent size from at least 5 indents with 10 being more typical.

Some Knoop measurements were carried out at low loads (5-200g) using a Vickers M12a microhardness tester. Loads were applied pneumatically for 30 secs duration and indent sizes were recorded optically.

3.8.2 Fracture Toughness Measurement

There are several techniques for measuring the fracture toughness and results can be method dependent, so care should be taken when comparing results between differing techniques. Non-destructive methods are preferred when there is a short supply of material therefore fracture toughness is measured by the indentation method using cracked indents formed by Vickers indentation (see Figure 3.13). Using indentation methods allowed a direct measurement of K_{Ic} of the materials to be wear tested without the need of the preparation of separate test bars.

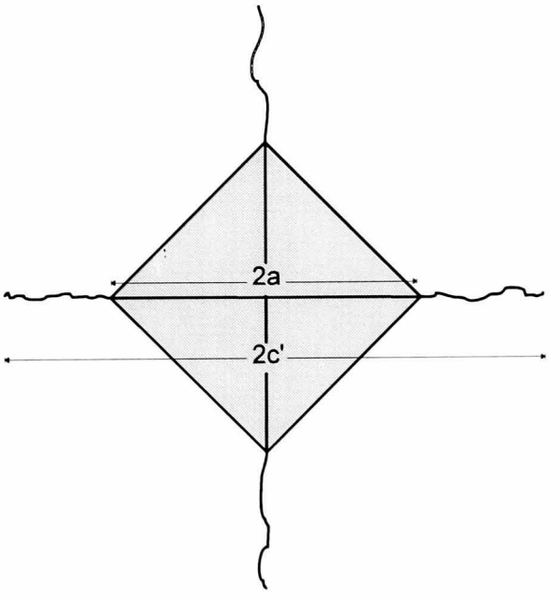

Figure 3.13 Cracks formed by the intersection of radial cracks intersecting the surface around a Vickers indent.

Evans and Charles[4] first empirically derived an expression for K_{Ic}. It was shown that K_{Ic} can be related to the crack length c', the indent diagonal 2a and the Vickers hardness by the expression:

$$K_{Ic} = \frac{S}{\phi} H_V a^{1/2} \left(\frac{c'}{a}\right)^{-3/2} \qquad \textbf{Equation 3.5}$$

where S is a surface correction factor found experimentally to be 3.2 and ϕ is a constraint factor which was originally 3.0 but has since been acknowledged as being too large. However, this expression still gives a measure of K_{Ic} to a confidence of level of 20-30% and can be used where E (the Young's modulus) of the ceramic is unknown. If E is known the full Charles and Evan's expression can be used:

$$K_{Ic} = 0.0732 \left(\frac{E}{H_V}\right)^{0.4} H_V a^{1/2} \left(\frac{c'}{a}\right)^{-1.5} \qquad \textbf{Equation 3.6}$$

Many other workers (Lawn et. al.[5], Niihara et.al.[6], Anstis et. al.[7]) have subsequently attempted to refine this model and make it less empirical but the dependence of $(c'/a)^{-1.5}$ remains throughout most relationships. The equations from each are shown below:

Lawn $$K_c = 0.028 \left(\frac{E}{H_v}\right)^{0.5} H_v a^{\frac{1}{2}} \left(\frac{c'}{a}\right)^{-3/2}$$

Niihara $$K_c = 0.067 \left(\frac{E}{H_v}\right)^{0.4} H_v a^{\frac{1}{2}} \left(\frac{c'}{a}\right)^{-3/2} \quad \text{for } c'/a > 3.0$$

Anstis $$K_c = 0.016 \left(\frac{E}{H_v}\right)^{0.5} P(c')^{-3/2}$$

This then makes it possible to measure readily the fracture toughness by making Vickers indentations at suitable applied loads on prepared ceramic surfaces and examining the crack length and indent size. Knowledge of E and H_v allows

more accurate measurement of K_{Ic}. The choice of applied loads is not a straight forward issue. Loads that produce significant cracking so that c' >a should be used but H_v for such measurements are better taken from non-cracked indents (i.e. lower applied loads.) The use of cracked indents to determine hardness (H_v) will produce artificially high hardness results since some of the energy has been expended on opening the cracks and not on plastically deforming the material. The use of these high hardness values affects the value for fracture toughness measured by indentation since E/H_v and H_v are factors in the calculation.

Another complicating factor is the determination of the crack system present under the indenter. Most models assume a radial crack intersecting the surface but it is also possible to have Palmqvist cracks which require a different treatment[6]. Both situations are demonstrated in Figure 3.14 Niihara also produced an equation for Palmqvist cracks[8]:

$$K_c = 0.018\left(\frac{E}{H_v}\right) H_v a^{\frac{1}{2}} \left(\frac{l'}{a}\right)^{-0.5} \qquad \textbf{Equation 3.7}$$

where l' is the surface length of the Palmqvist crack. Since Palmqvist cracks occur very close to the surface they are sensitive to surface stresses present from sample preparation.

Unfortunately determination of the crack system is not simple without destruction of the specimen and hence the choice of model to calculate K_{Ic} is problematic when the specimen needs to be preserved.

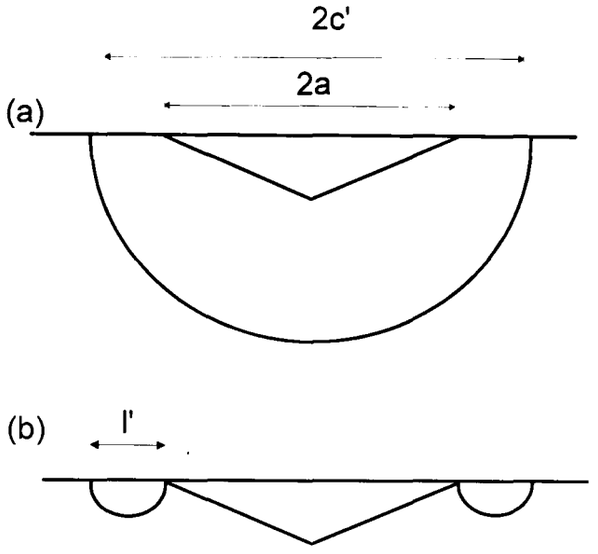

Figure 3.14 A cross sectional view of cracks formed under Vickers indents, (a) radial cracks and (b) Palmqvist cracks.

The measurement of fracture toughness was carried out using a combination of Vickers indents at various loads, to produce both cracked and uncracked indents, and Knoop indents (for the determination of H/E). Indentation was carried out as described for hardness measurements. The values of H_v were taken from the least cracked indents (i.e. lowest loads) and the indent size, 2a and crack length, c', were measured by electron microscopy. Each result was an average from at least 5 indents with 10 being more typical. E was also estimated by several other techniques to verify the results.

3.8.3 Estimation of Young's Modulus (E)

In composite materials it is often difficult to measure the elastic modulus, E, the material and hence the accurate determination of K_{Ic} is limited.

An estimate of E for a composite can be obtained from knowledge of E for the phases present and their amounts from the simple rule of mixtures for a sandwich like structure:

$$E_{\Uparrow} = E_a V_a + E_b V_b \qquad \textbf{Equation 3.8}$$

where E_a and E_b are the elastic moduli of the constituents and V_a and V_b are their volume fractions. This relationship is applicable for stress applied parallel to the

layers and there is a state of constant strain. Where constant stress is applied normally to the layers then the corresponding relationship is

$$E_{\perp} = \frac{E_a E_b}{E_b V_a + E_a V_b} \qquad \textbf{Equation 3.9}$$

These equations supply the upper and lower bounds for a material and practical materials usually have a value somewhere between the two.

The presence of porosity also effects E, always resulting in a decrease. MacKenzie[9] proposed the following relationship for E and the level of porosity:

$$E = E_0(1 - 1.9P + 0.9P^2) \qquad \textbf{Equation 3.10}$$

where E_0 is the modulus of the non-porous material and P is the volume fraction of pores.

A method of estimating H/E is by using Knoop indents. On unloading after a Knoop indentation there is some elastic recovery immediately below the plastic zone, the shape change in the Knoop indent can be estimated by assuming an elliptical hole subject to uniaxial stress and it can be shown that;

$$\frac{l'}{s'} = \frac{l}{s} - \chi\left(\frac{H_K}{E}\right) \qquad \textbf{Equation 3.11}$$

where l = size of long axis of Knoop indent, s = size of short axis and primed values are the relaxed dimensions of the indent. χ is a constant which has been determined from measurement of many ceramics, to be 0.45. Since for a Knoop diamond l/s = 7/1 values of H_K/E can be determined for use in K_{Ic} measurements.

Another method suggested by Marshall determines E (H_v is determined separately) when a Knoop hardness at 0.98N is inserted.

$$E = \frac{0.45H_K}{s/l - 0.1406}$$ **Equation 3.12**

E can also be estimated from work by Lawn on spherical indenters. When a spherical indenter of Young's modulus E and radius R is incident with applied load P the indenter deforms and the contact radius ,a, is given by:

$$a^3 = \frac{4\kappa PR}{3E}$$ **Equation 3.13**

where

$$\kappa = \frac{9}{16}\left[\left(1-\nu^2\right)+\left(1-\nu'^2\right)\frac{E}{E'}\right]$$ **Equation 3.14**

where ν and ν' are Poisson's ratio for the indenter and substrate respectively. The contact radius can be measured form the mark left in a thin sputtered gold coating.

All of these methods can be used to determine E and provide a level of confidence in the values for E and E/H for use in K_{Ic} measurements.

3.9 References

[1] Kondo Y, Hashizuka Y, Nakahara M, Yokota K & Ishizaki K, "Influence of combination of ball diameters and rotation speed on grinding performance of alumina by ball milling", *J. Ceram. Soc. Jap,* International Edition, Jul 1993, Vol.101, No.7, pp.797-801

[2] Yokota K, Hashizuka Y, Nakahara M, Kondo Y, "Characteristics of the ground alumina powders by wet rotation ball milling", *J. Ceram. Soc.Jap.,* Nov 1995, Vol.103, No.1203, pp.1167-1171

[3] Adapted from: S. Lukasiewicz, "Ceramic powder processing", *NICE Course*, American Ceramic Society, Ohio, 1982.

[4] A.G. Evans and E.A. Charles, "Fracture toughness determnation by indentation", *J. Am. Ceram. Soc,* **59**, p.371 (1976)

[5] B.R. Lawn, A.G. Evans and D.B. Marshall, "Elastic plastic indentation: The median/radial crack system", *J. Am. Ceram. Soc*, **63**, p.574 (1980).

[6] K. Niihara, R. Morena and D.P.H. Hasselman, " Indentation fracture toughness of brittle materials for Plamqvist cracks", *Fracture Mechanics of Ceramics*, 1983 vol. 5, p97

[7] G.R. Anstis, P. Chantikul, B.R. Lawn and D.B. Marshall, "Indentation techniques for measuring toughness of ceramics", *J. Am. Ceram. Soc*, **64**, p.539, (1981)

[8] K. Niihara, R. Morena & D.P.H. Hasselman, "Indentation fracture toughness of brittle materials for Palmqvist cracks", Fracture Mechanics of Ceramics,. Vol.5, pp97-105, 1983

[9] J.K. Mackenzie, "The elastic constant of a solid containing spherical holes", *Proc. Phys. Soc. (Lon)* B63, 2 (1950)

Chapter Four

The Pin on Disc Wear Test

4. The Pin on Disc Wear Test

There are many types of wear test suitable for the testing of small amounts of material such as produced at research level. Examples are shown in Figure 4.1

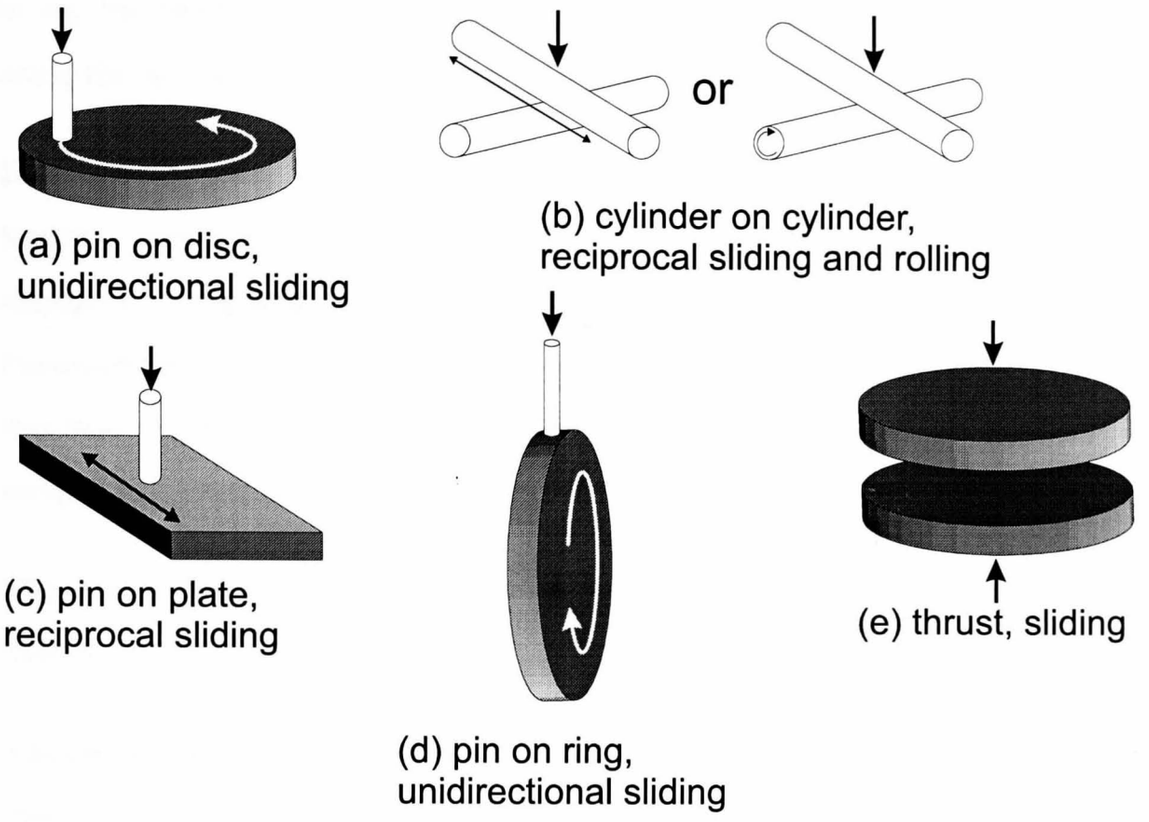

Figure 4.1 Different types of laboratory scale wear tests.

Simple geometries are preferred (such as pins and discs) because these are easily machined from the specimens produced by hot pressing or pressureless sintering.

The configuration chosen for tribological testing was the pin-on-disc test. Like all other wear tests it has both its advantages and disadvantages but as one of the most common tests used in the literature on wear testing of ceramics it was chosen for comparability of results.

4.1 General Description and Requirements

The pin on disc configuration is one of the simplest yet most versatile wear tests suitable for laboratory testing of materials under development. Its basic geometry consists of either a rounded or flat ended pin pressed against a flat,

rotating disc. There are several possible orientations of this arrangement such as the pin incident on the disc from above or below and the disc mounted in the vertical plane.

Loading systems and techniques for measuring friction and wear vary from rig to rig but there are some general requirements for unlubricated sliding tests using the pin on disc apparatus that are summarised below:[1]

Loading can either be by dead weight, pneumatic or hydraulic. For dead weight loading, frictional forces in the bearings of the loading system should be negligible compared to applied loads. Weights used should be calibrated. Pneumatic/hydraulic loads should be calibrated and the system should drift by less than 1% during the test. There should be no variation in loading caused by sample movement.

The motor drive should provide a constant speed of rotation under frictional loading (±1%) and should be monitored throughout the test.

Alignment of pin and disc: with rounded end pins alignment is not critical but should be within 2° of the axis of rotation of the disc. The disc itself should rotate in as flat a plane as possible.

Specimen mounting: The specimen should be mechanically clamped in position so that as little vibration/resonance as possible occurs. Adhesives should be avoided as they may deform, especially under frictional heating.

Machine dynamics: the dynamic response of the test machine can have large effects upon the results of friction and wear tests[2]. The test machine should be designed so that natural frequencies of the testing system are much higher than any vibrations generated from the motor and/or disc rotation system.

Environmental control: The surrounding environment should be kept constant throughout the test, this includes temperature, humidity and gas composition.

4.2 Specification of Pin on Disc Apparatus

Due to the highly varied nature of equipment design between laboratories it is important to clearly specify the type of apparatus used and its basic mode of operation to enable comparison with results from other workers.

The specific design and size of wear test apparatus depends upon factors including the range of loads to be used, specimen size and the amount of control required over environmental variables such as atmosphere, temperature and humidity.

The design parameters for the construction of the wear test apparatus to be used in this work were as follows:

a) A range of loads and sliding speeds should be possible.

b) Frictional force and measurement of the wear rate should be measurable continuously throughout the duration of the test

c) It should be capable of holding small specimen sizes such as the discs produced from hot pressing and pressureless sintering. (i.e. discs of between 18 and 25mm diameter and ~5-7mm in height and hence wear track radii of ~7-9mm.)

d) Pin sizes of approximately 3×3×15mm.

e) The apparatus should be capable of being enclosed to allow control and variation of the test environment with regards to ambient temperature, atmosphere and humidity.

f) Simple lubrication tests should be possible.

A schematic of the apparatus constructed for tribological testing is shown in Figure 4.2

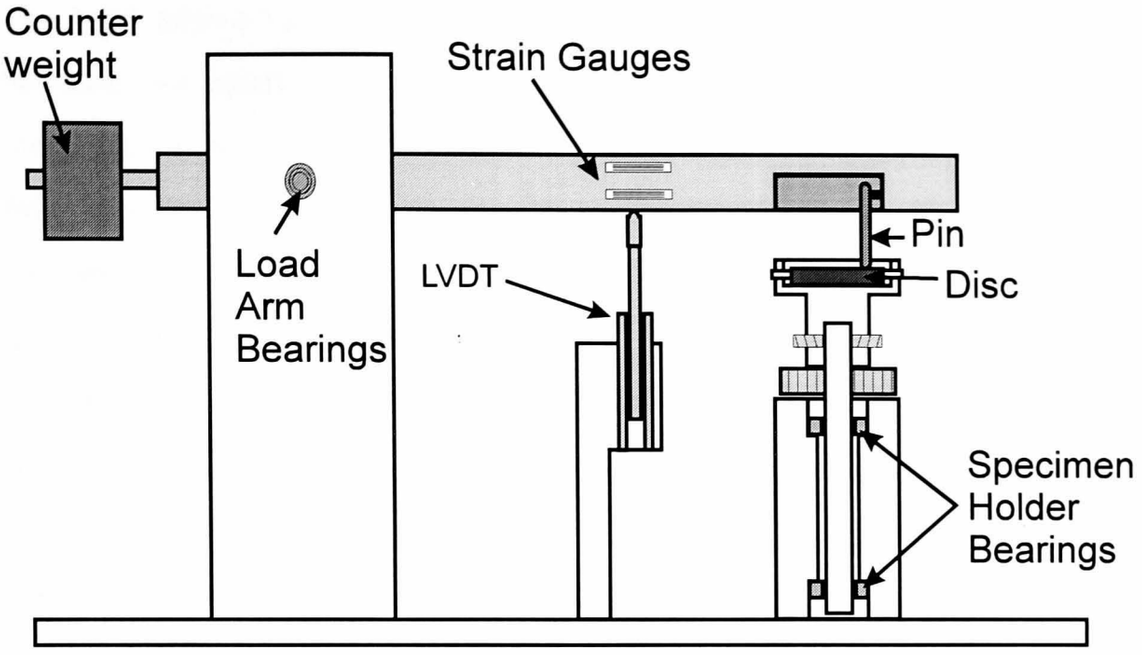

Figure 4.2 A schematic of the pin-on-disc wear test apparatus

For the control of the wear environment the whole apparatus was enclosed inside an adapted glove box with monitoring of humidity and ambient temperature achieved by a hygrometer with temperature resolution of 0.1° and an accuracy of ±1 and humidity resolution of 1% with an accuracy of ±5 in the range 10 to 95% RH.

The disc specimen was mechanically clamped into an aluminium holder via three equi-spaced steel grub screws. This arrangement provides good mechanical clamping and allows the rapid dissipation of any heat produced by friction. The holder is deep enough to allow liquid to be introduced to a level that covers the specimen thus making simple lubrication tests possible. The specimen holder is mounted centrally on a steel shaft fitted precisely into two vertically aligned bearings allowing free rotation of the disc with no significant frictional forces under the applied load. This precision arrangement also ensures no movement of the disc out of the plane of rotation during the test. The specimen is rotated by a d.c motor whose speed is adjustable via the input voltage, allowing variation of the sliding speed. The motor drive is rigidly coupled to the specimen holder directly by means of 2 hardened steel gears.

The load arm is constructed from aluminium and is supported on a pivot between two uprights that provide rigid support. Bearings in the load arm eliminate any movement of the load arm in the horizontal plane whilst allowing free movement of the arm in the vertical direction. A counter weight compensates for the weight of the load arm, important when lower applied loads are used. For ease of mounting the pin is housed in a separate holder. It is clamped in place via two steel grub screws and this holder is located in a recess at the end of the load arm. This arrangement allowed positioning of the pin at different lengths along the arm to accommodate different sized discs (i.e. wear tracks of differing radii).

Loading is achieved by the direct application of calibrated weights to the load arm directly above the pin position. To eliminate unwanted vibrations between the arm and the weights rubber and foam pads were used between the two components. Rubber padding is also used to isolate the motor and sample housing from the detection systems to eliminate motor dynamics and resonance from the results.

The environmental chamber was a converted glove box which allowed easy access for specimen removal and apparatus adjustment but also provided a closed environment with regards to temperature and humidity. The closed system also protects the operator from any fine powder produced as wear debris during the test. An internal fan circulated the air during a test to ensure constant conditions.

Data acquisition was performed using a computer which logged the voltage output from both friction and wear detection devices .Specially written software translated these voltages into force (for coefficient of friction) and displacement (for wear rate) whilst also logging time which was converted to sliding distance. Subsequent data processing such as noise reduction, graphical representations and curve fitting were performed after the test. A schematic of the data acquisition set up is shown in Figure 4.3

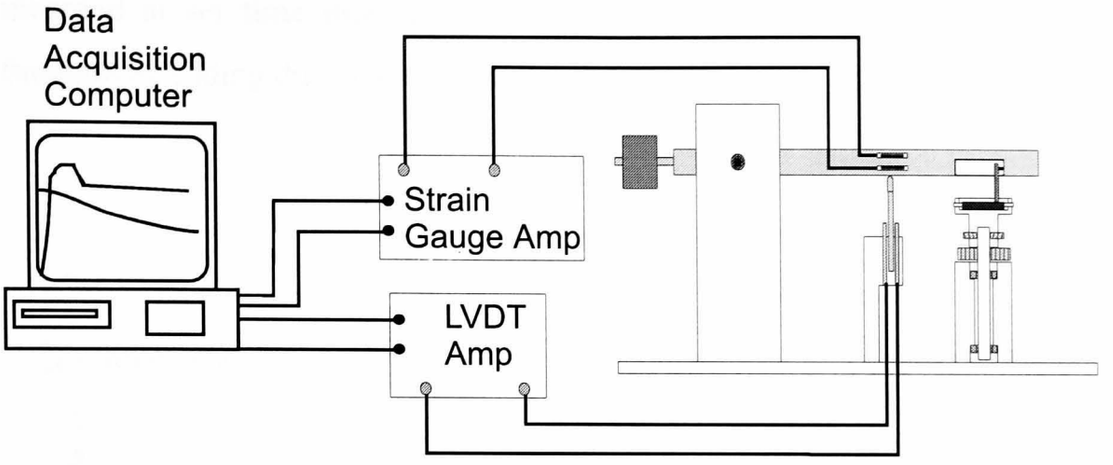

Figure 4.3 The data acquisition set up for wear and friction tests.

4.3 Measurement of Friction

The pin and disc were aligned so that rotation of the disc caused the frictional force to act perpendicular to the long axis of the load arm. This force causes the load arm to experience strain along its length. Measurement of this strain combined with calibration of the strain gauges provides a measure of the force acting on the arm which can then be simply related to the coefficient of friction, μ by the equation $F=\mu R$. Strain was measured using 4 strain gauges, two on each side of the arm experiencing equal and opposite strains, forming the bridge section of a strain gauge amplifier. A section of the load arm was thinned to provide an increased strain at this point and the strain gauges were mounted with epoxy adhesive on this section. All sharp corners were rounded after machining to remove stress concentration points. A schematic showing the direction of the frictional force and the strain gauge set up is shown in Figure 4.4

To calculate the coefficient of friction it was necessary to relate the voltage output from the strain gauges to force experienced by the load arm. Calibration was carried out using a range of weights to simulate the forces experienced during a test. Using this arrangement, a range of known weights were used to simulate the frictional force and the resultant voltage from the strain gauge arrangement was recorded. The recorded strain gauge output voltage was converted into the frictional force and the coefficient of friction. Friction was

recorded at set time intervals throughout the test and plots of friction as a function of sliding distance were obtained for each test.

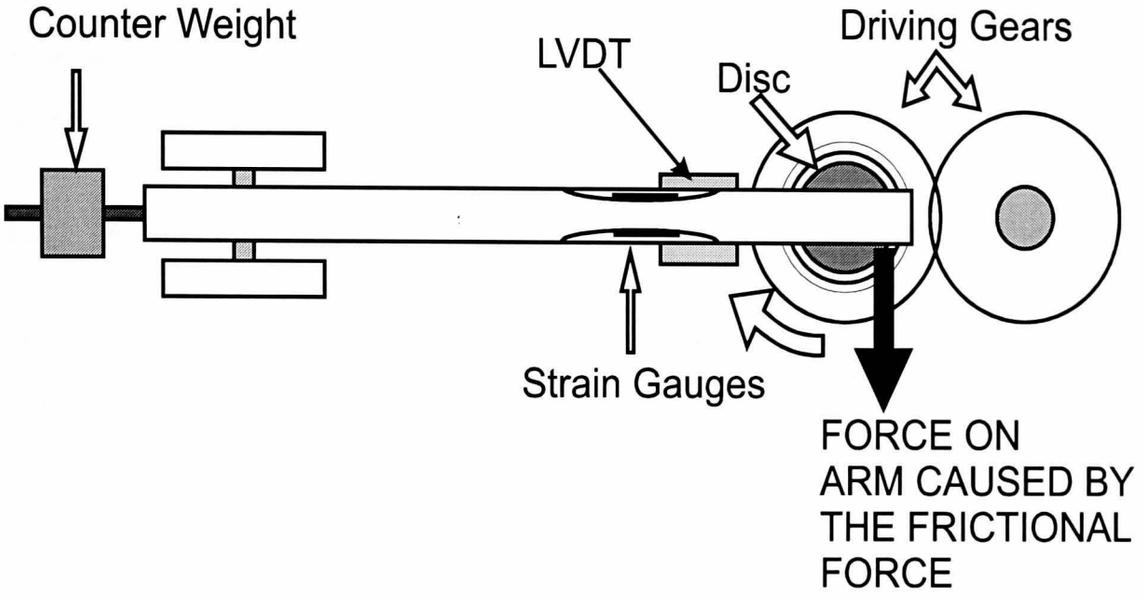

Figure 4.4 The measurement of the frictional force via strain gauges

4.4 Measurement of Wear.

The final amount of wear that has taken place can be determined by several methods after completion of the test. However, the wear rate is not necessarily constant with time/sliding distance and information on the dynamic wear rate requires continuous monitoring. This was attempted by measuring the displacement of the load arm in the vertical direction throughout the test by means of an LVDT mounted under the load arm (See Figure 4.2). This arrangement was also used to determine whether the specimen has been mounted correctly to avoid any movement of the disc out of the plane of rotation. The LVDT was calibrated using a micrometer arrangement, exhibiting a linear response over the working range of the LVDT and hence allowing simple conversion of output voltage into displacement. The displacement of the load arm was recorded at set time intervals during the test and plotted as a function of sliding distance.

The displacement of the arm is a function of the material removed from both the pin and the disc but is complicated by the entrapment of wear debris in the contact zone and the presence of any tribofilms. The build up of tribofilms of significant thickness can exhibit a decreased amount of wear. Hence measurement of the arm displacement, while giving some indication of the wear rate, is not directly related to the amount of material removed. To determine the wear volume removed from both the pin and the disc it is necessary to employ several techniques.

4.4.1 Wear Volume.

Provided the radius of the pin (R) is known at the beginning of the test the volume of material removed from the pin (V_p) can be calculated from optical microscopy measurements of the wear scar. The diameter of the wear scar 2r can be related to wear volume by the following relationship:

$$V_p = \frac{\pi r^4}{4R} \qquad \textbf{Equation 4.1}$$

Similar considerations can, in principle, be applied to any wear scar on the disc. The approximate volume of material removed from the disc (V_d) by a spherically capped pin of radius R is given by:

$$V_d = \frac{\pi d w^3}{12R} \qquad \textbf{Equation 4.2}$$

where d is the diameter of the wear track and w is the width of the wear track. However, for this to be an accurate approximation the assumption that the pin has maintained its radius and that the wear scar on the disc also has this radius are made. While this may be a good description of a hard pin on a soft disc for most material systems this is not the case and the above approximation should be used with caution, if at all.

In fact the situation is further complicated by the flattening of the rounded pin during the test. It is clear that as the test proceeds the pin will form a flat that

will not only make calculation of the worn disc volume more complicated but will also lead to a decreasing level of applied stress as the test progresses. In fact the applied stress may start at a high level but will soon decay to a significantly lower but much more constant level.

4.4.2 Wear Coefficient, k

Because wear testing can be carried out under many different conditions it is convenient to define a parameter that can be compared between dissimilar tests. Many papers report wear in differing ways, from $mm^2\ m^{-1}$ to $mm^3\ s^{-1}$ and other such quantities. Unless all parameters of the test are known these quantities are meaningless to other researchers and are only suitable for comparison of a material's performance within a particular study.

The wear coefficient, k, is the volume of material removed (in mm^3) per unit load per unit distance slid. Its units are most commonly quoted as $mm^3\ N^{-1}\ m^{-1}$ although it is sometimes found as $m^3\ N^{-1}\ m^{-1}$ (strictly this is more correct). This quantity is thus independent of the load used and distance slid provided that the same wear mechanism is active for both sets of data being compared.

4.5 Specimen Preparation

In order to ensure consistent results from different materials a standard preparation procedure was used to prepare specimens for the pin on disc test. Pins of material were cut from 25mm discs to approximately 3×3×15-20mm. The pin ends were shaped using a steel template that had been machined with "dimples" of the correct radii in its surface. Silicon carbide grinding powders were used in the dimple to remove material from the pin until it had obtained the correct radius.

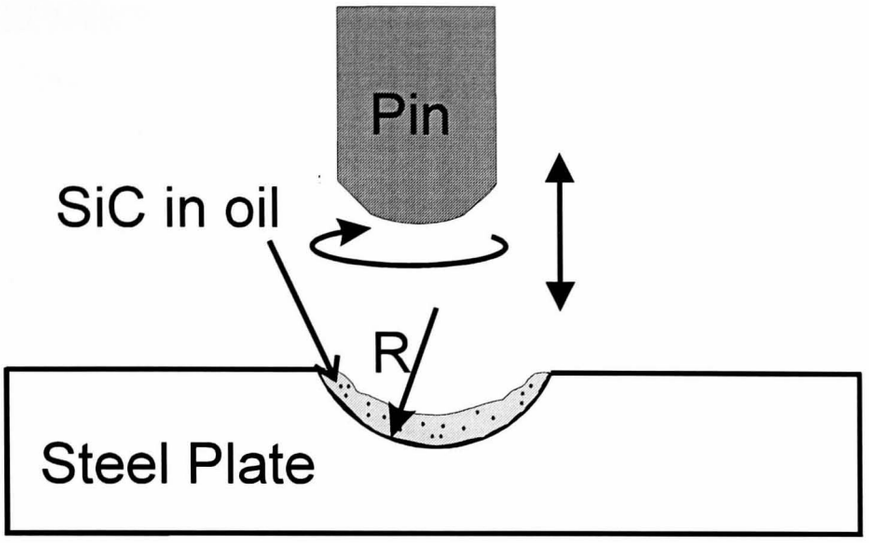

Figure 4.5 Schematic of the procedure for producing round ended pins.

This was followed by hand polishing of the pin using diamond polishing solutions of 25, 6 and 1μm. With practice the pin maintained its shape during the polishing procedure. Verification of the actual pin radius was carried out using optical microscopy techniques as shown in Figure 4.6. The measurement of 2r and x (see figure) gives a value of R, the pin radius from the equation $R= r^2/2x$. Both 2r and x were measured using a calibrated graticule in the microscope eyepiece.

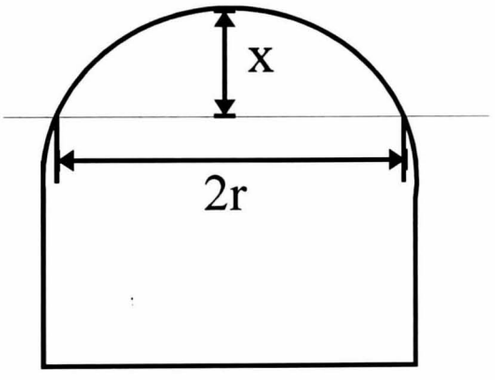

Figure 4.6 The method for measuring pin radius.

Discs consisted of either hot pressed or pressureless sintered materials with disc diameters from 18-25mm. The top and bottom faces of the discs of material were ground flat and parallel using a diamond grinding wheel and polished using 25, 6 and 1μm diamond polishing solutions. The usual pin radius was R=3mm.

Cleaning of components was carried out immediately before each test. Both pins and discs were cleaned ultrasonically in "Micro" cleaning solution followed by acetone and then methanol and all materials were dried on a hot plate and stored in clean containers. Handling of materials was carried out using tweezers and gloves to avoid organic contamination to the surface during specimen mounting.

4.6 Test Procedure

After specimen preparation as described in section 4.5 both pin and disc were mounted in their respective holders as described in section 4.2. The disc alignment was ensured by allowing the pin to run on the disc under a low load (<50g) enabling the arm movement to be monitored (via the LVDT) as the disc rotated. When satisfactory alignment had been achieved the pin was taken out of contact with the disc while the load was applied to the arm. With the pin still out of contact the rotational speed was set by altering the d.c. motor's supply voltage. With the disc again stationary the pin was then carefully lowered into position on the disc to avoid impact damage, ensuring that there was zero strain in the arm prior to the test beginning. All tests were started with the pin in contact with the stationary disc. The specimen chamber was then sealed and allowed to reach equilibrium (w.r.t. temperature and humidity). The speed of rotation was monitored after the test had started to ensure that it was not affected by the applied load and if necessary the speed was adjusted.

4.6.1 Data Collection

The data acquisition program allowed the collection of data over varying time intervals depending upon the time resolution needed. For example, to examine in detail the friction behaviour over the first few revolutions data was collected every 0.1 secs. For normal data collection over the duration of a complete run (~10,000 secs) data was collected every 2-3 secs and each data point was an average of 5 consecutive readings of each output device. The data (LVDT and

strain gauge output voltage) were simultaneously displayed on screen and all data was recorded to floppy disc for future analysis.

4.7 Variation of Test Parameters

As mentioned previously the most important parameters when measuring friction and wear are the load, sliding speed and wear environment (e.g. atmosphere, humidity, lubrication).

Sliding distance for most of the test was set at 500m. This distance was determined after initial test showed there to be no significant change in friction or wear after this distance but there was enough wear to be measurable by the above mentioned techniques.

4.7.1 Sliding Speed

The variation of sliding speed was simply achieved by the alteration of the d.c. motor's supply voltage. However, calibration of rotational speed (S) versus sliding speed (L) needed to be carried out for each wear track radius (R). Sliding speed was adjustable over the range 0.01 to 0.125ms^{-1} in steps of ~ 0.01.

4.7.2 Applied Load

Load is often used to refer to the applied load used in a wear test. However, this quantity is relatively meaningless unless converted into the applied stress that the ceramic experiences.

The maximum contact pressure P_0 at the axis of contact caused by a load W is

$$P_0 = \frac{3W}{2\pi r^2} \qquad \textbf{Equation 4.3}$$

The actual radius of the area of contact between a spherical surface and a flat, r, is described by the equation:

$$r = \left(\frac{3WR}{4E*}\right)^{1/3}$$ **Equation 4.4**

where W is the applied load, R is the radius of the pin and E* is

$$E* = \left[\left(\frac{1-\nu_1^2}{E_1}\right)+\left(\frac{1-\nu_2^2}{E_2}\right)\right]^{-1}$$ **Equation 4.5**

where ν_1 and ν_2 and E_1 and E_2 are Poisson's ratio and modulus for the indenter and substrate respectively[3].

Assuming that the contact between the spherically capped pin and the disc is Hertzian then the maximum radial tensile stress, σ_r is given by

$$\sigma_r = \frac{1-2\nu}{3}P_0$$ **Equation 4.6**

where P_0 is the applied force, ν is the Poisson's ratio. However, in sliding contact the maximum tensile stress is greater than this and occurs as the trailing edge of the sliding contact due to the frictional force. This maximum sliding stress is giving by

$$\sigma_s = \left\{\frac{(1-2\nu)}{3}+\left[\frac{(4+\nu)}{8}\right]\pi\mu\right\}P_0$$ **Equation 4.7**

This results in a magnification in the trailing edge tensile stress (and the leading edge stress becomes compressive) as illustrated Figure 4.7

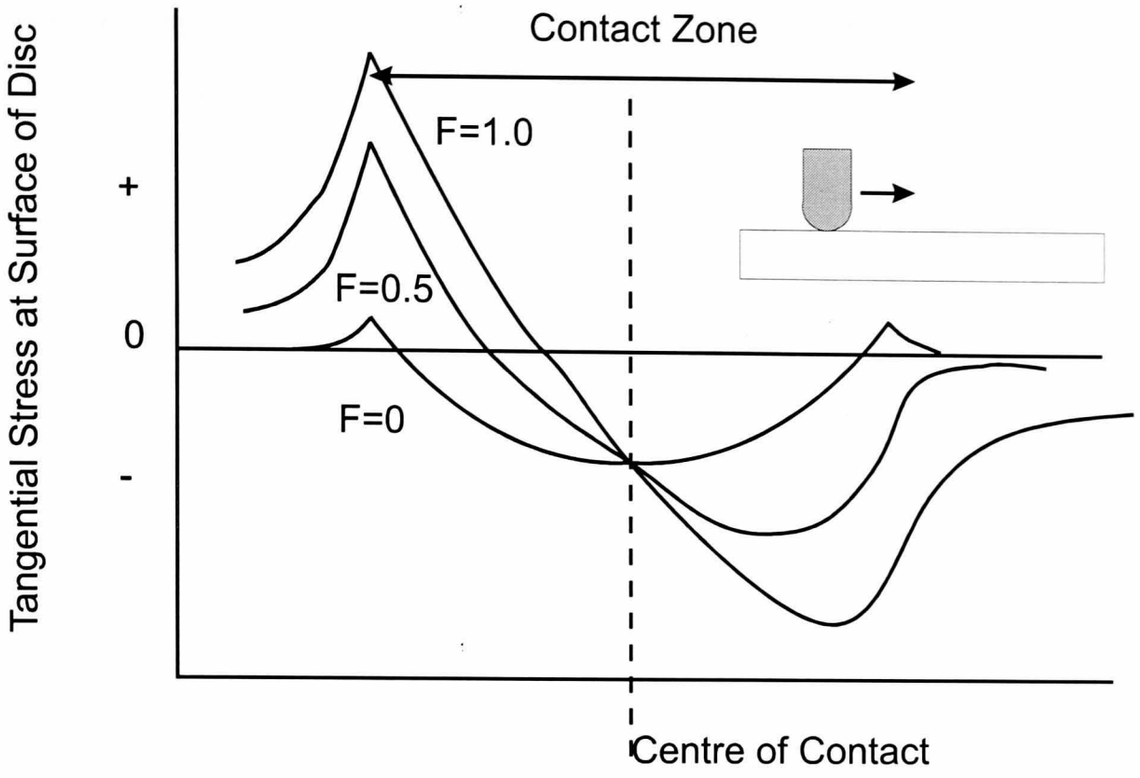

Figure 4.7 The effect of the frictional force on the stress distribution in a spherical sliding contact.

Therefore the applied load should be chosen to provide an appropriate level of applied stress for the contact being used, i.e. a pin with a small radius will provide higher stresses than a pin with a large radius. This also leads to the need for a degree of consistency in the radius of the pins being used. The production methods mentioned in section 4.5 provides adequate consistency between samples and the measurement technique described in section 4.5 provides an accurate assessment of pin radii.

As an example, consider a ceramic sliding on itself with E=300GPa, ν=0.22, P=9.81N, R=3mm and μ=0.7. The maximum contact pressure P_0 is 1.7GPa. The maximum tensile stress at the trailing edge is 2.3GPa caused by a contact area of radius ~52μm.

Clearly then to have an accurate assessment of the contact area, and hence the applied stress, it is necessary to know the E modulus of the material. This in itself can cause some problems as the E modulus for these materials has not been measured accurately and can only be inferred from knowledge of the amounts of phases present, including porosity as described in chapter 3. This

gives an upper and lower limit for E which in turn gives an upper and lower limit for the applied stress.

The initial applied stress is soon reduced due to the formation of a flat contact area between the pin and the disc. As this area increases so the stress falls. In the example given, if the pin wear scar at the end of the test is ~ 400μm in radius then the maximum tensile stress at the trailing edge has been reduced from 2.3GPa to 397MPa. The stress may soon fall below a level where significant wear of the pin occurs and the stress level becomes constant. Below the level of stress needed to cause fracture in the pin or disc, material is removed by the much slower action of polishing or abrasion.

It can be seen from the above arguments that only the initial applied stress can be accurately assessed and that reduction in this stress occurs rapidly after the start of the test. In addition, the stresses experienced under sliding conditions are augmented by the frictional force and this makes the exact measurement of stress in the material at any one time difficult to determine. If possible some indication of the variation on the applied stress from that experienced at the beginning of the test should be given. This problem must be one commonly encountered by researchers but pin-on-disc still continues to be used without proper consideration of this complicating factor.

Constant cross section pins (i.e. square flat ended) can be used to overcome this problem but this makes alignment of the pin with the disc critical otherwise the above problem re-occurs but with a differing geometry.

It should be possible to predict the rate of change of the cross sectional area but this requires knowledge of the material removal (wear) rate. Since this is often the quantity that the test is being used to determine this is not usually possible. One solution is to monitor the vertical displacement of the load arm as the test progresses and to dynamically calculate from this the area of contact. This, however, requires excellent resolution in the measurement system and perfect alignment of the disc in the horizontal plane, neither of which was achieved to a level that made this calculation possible.

To summarise, the variation of applied stress was achieved by simply changing the load applied to the arm. However, the determination of exact stress level caused by this load throughout the test could not be accurately measured and all figures are hence approximate.

4.7.3 Lubrication

Due to the complicated nature of wear a comprehensive study of lubricated wear was not a major objective of the research. However, the pin-on-disc apparatus was used to perform simple lubricated tests, to compare with other workers results for lubricated wear of Si_3N_4 and SiAlON systems.

The sample holder was designed to be able to hold both the specimen and a small reservoir of liquid which could cover the contact zone between pin and disc as shown in Figure 4.8

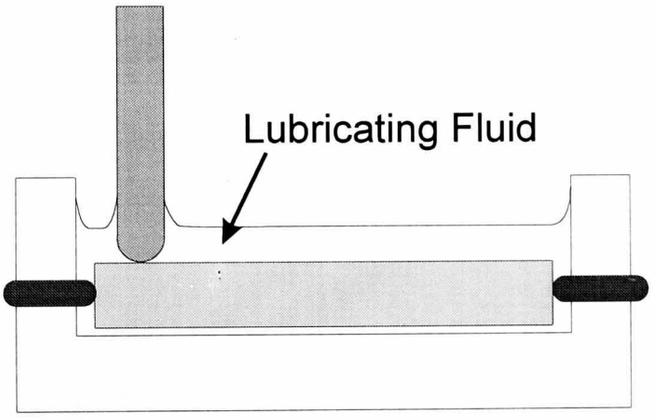

Figure 4.8 Pin-on-disc lubricated test conditions.

4.7.4 Humidity & Atmosphere

Both the humidity and the composition of the atmosphere in which the wear test takes place can play an important role in the tribological behaviour of a material. In tests in which other parameters were varied the humidity in the chamber was kept constant at 40-45%RH. Humidity could be varied by either filling the chamber with compressed air which lowered the humidity to less than 10%RH or by using saturated aqueous solutions of various chemicals which are designed to provide varying levels of humidity (up to a maximum of ~95%RH)

when placed in a confined space. Table 4.1 gives some examples of these solutions.

Solid Phase	% Humidity (@ r.t.)
$Pb(NO_3)_2$	98
$(NH_4)_2SO_4$	81
$NaClO_3$	75
$NaBr.H_2O$	58

Table 4.1 Aqueous solutions used to give varying humidities in a closed environment.

The atmosphere composition was limited to either static laboratory air, flowing compressed air or flowing nitrogen. Both the latter were provided by placing a nozzle providing the gas close to the contact zone as shown in Figure 4.9. Since the chamber could not be evacuated the nitrogen atmosphere was not pure but contained small amounts of laboratory air (i.e. oxygen was still present).

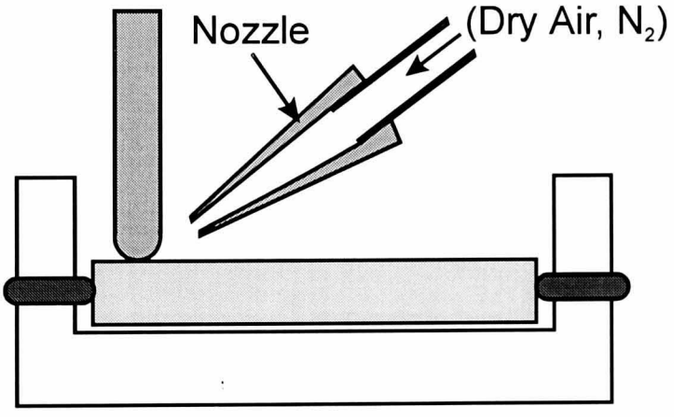

Figure 4.9 Set up for providing different atmospheres at the contact zone.

4.8 Summary

The configuration chosen for tribological test is pin-on-disc with the pin incident on the disc from above. The apparatus is capable of performing tests with the following parameters being variable: sliding speed (0.01-0.125ms^{-1}), applied load (1.96-20N), humidity (10-95%RH), lubrication (water, paraffin) and atmosphere (flowing air or nitrogen.) Sliding distance for the majority of

tests was ~500m. The equipment is capable of measuring the coefficient of friction with an accuracy of ±0.05 and can determine the rate of material movement from the pin and disc combined during a test via the displacement of the load arm.

Wear coefficients for the materials tested can be calculated by measurement of wear scars using optical and electron microscopy. Wear mechanisms can be determined by examination of wear surfaces by electron microscopy.

The test is subject to the same limitations and problems as all pin-on-disc tests. The stress experienced by the material is not constant but decays as a function of wear rate that itself may be a function of applied stress. The analysis of wear mechanisms may be complicated by the entrapment of wear debris under the contact zone.

4.9 References

[1] M.G. Gee, "Guidelines for unlubricated sliding wear tests: Part 2, procedures for pin on disc testing.", NPL report DMM(A)97, National Physical Laboratory, Teddington, Middx, UK, TW11 0LW. (April 1993)

[2] M.G. Gee, "Effects of test machine dynamics on the sliding wear of alumina.", Wear Testing of Advanced Materials, ASTM STP 1167, Ed. R. Divakar and P.J. Blau, American Society for Testing and Materials, pp22-44, (1992)

[3] O.O. Ajayi, A. Erdemir, R.H. Lee, and F.A. Nichols, "Sliding wear of silicon carbide-titanium diboride ceramic matrix composites", *J. Am. Ceram. Soc.*, **76** [2], pp. 511-17, 1993

Chapter Five

Synthesis & Properties of Sialon/TiB_2 Ceramic Composites

5. Synthesis and Properties of Sialon/TiB_2 Ceramic Composites.

Previous work by Hong[1] had investigated several reactions that would form ceramic matrix composites via in-situ reaction sintering. This chapter describes how such reactions were used to produce compositions suitable for hot pressing and pressureless sintering. After determination of the conditions needed to produce dense composites with the desired phase content, the resulting materials were characterised with respect to microstructure, hardness and fracture toughness. The oxidation resistance of the materials was also examined to a limited extent.

5.1 Synthesis of Sialon/TiB_2 Ceramics

An objective of this work was to investigate the possibility of producing sialon/TiB_2 composites via in-situ reaction sintering using both hot pressing and pressureless sintering. Choice of raw materials was followed by the calculation of compositions. The results from sintering trials were used to refine the compositions until the phase content and density of the resulting materials were optimised.

5.1.1 Raw Materials

The powders used as precursors were commercially available grades of suitable particle size and purity. The list of manufacturers and grades of materials is shown in Table 5.1. Fine powder are needed for pressureless sintering and with proper processing help to produce homogeneous microstructures.

Powder	Manufacturer /Supplier	Grade	Particle size (μm)
α Si_3N_4	UBE, (Japan)	SN E-10	~0.2 [D50=0.5]
TiN	Tioxide Chemicals (UK)	TTN70	0.05 [D50=0.74]
BN	BC&C, UK	HQ	[D50=0.4]
Si	Kemanord, Sweden	4E	[D50=3]
AlN	H.C. Stark GMBH, Germany	C	[D50=0.55]
Sintering Aid	Y_2O_3 or a pre-prepared glass*	-	not measured

*the glass consisted of Y_2O_3:Al_2O_3:SiO_2 in the ratio 40:25:35

Table 5.1 Suppliers and Grades of powders used for production of Sialon/TiB_2 composites.

Figures are quoted as manufacturers figures and as measured in water with ultra sonic agitation on a Malvern instruments particle size analyser. D50 is the figure for 50% of the particles being less than this size and is thus larger than many of the optimistic values quoted by manufacturers.

5.1.2 Composition Calculation

Previous work has defined the reactions that could be used to form TiB_2 and sialon simultaneously. In order to produce the composites with the required phase content, the amounts of starting compounds were calculated from consideration of the reactions that are being used to form TiB_2. Also considered is the required balance of oxides and nitrides present to form β sialon after densification. In order to calculate the starting composition the following factors were taken into consideration.

- The following reaction was assumed to occur and by setting the volume of TiB_2 required in the final product the amount of TiN, BN and Si needed can be calculated :

$$4TiN + 8BN + 9Si = 4TiB_2 + 3Si_3N_4.$$

An example for 20vol% TiB_2 is shown in Table 5.2

Vol % TiB_2	Wt% TiB_2	Wt % TiN	Wt% BN	Wt% Si
20	30.3867 (20.936 Ti, 9.4506 B)	27.058	21.695	29.199

Table 5.2 an example of calculation or raw materials to form 20vol% TiB_2.

This reaction produces Si_3N_4 (~48wt% in the above example), the remaining amount needed to form the matrix is added as α Si_3N_4 powder.

- To form sialon, oxygen and aluminium are introduced by Al_2O_3 and SiO_2 introduced as surface oxides on AlN, Si and Si_3N_4 powders. AlN is added to create a stoichiometric mixture that will form the β sialon phase.

- Densification aids e.g. Y_2O_3:Al_2O_3:SiO_2 glass, affect the final composition of the sialon and hence the amounts of AlN added needs to be increased in order to produce β sialon.

- In addition to the reaction to form TiB_2 from the nitrides it is also possible to use the oxide impurities introduced as surface layers on powders. The oxides TiO_2 and B_2O_3 can react with Si and AlN to form SiO_2 or sialon as shown below.

$$2TiO_2 + 2B_2O_3 + 5Si = 2TiB_2 + 5SiO_2,$$

$$2TiO_2 + 2B_2O_3 + 5Si + 10AlN = 2TiB_2 + Si_5Al_{10}O_{10}N_{10}$$

These reactions require the addition of silicon and AlN to balance the overall composition.

From the above considerations the exact amounts of starting compounds (i.e. Si, α Si_3N_4, AlN, BN, TiN and sintering aid) needed for any vol% of TiB_2 could be calculated. The z value and density of the sialon were estimated from the assumed Si:Al and O:N ratios. Knowledge of the densities and amounts of phases present allows the calculation of a theoretical density for the densified composite.

5.1.3 Green body formation

Uniaxial pressing from one direction was used with a 25mm steel die. Typically each sample was pressed from ~6 to 8g of powder, resulting in discs of ~6 to 8mm in height. The correct applied pressure for forming green bodies without significant cone cracking was found to be ~60-80MPa. These applied pressures typically produced discs with green densities of 1.5-1.7 g/cc (~48-54% of the theoretical 3.13g/cc). It was found that lower pressures produced poor green densities and above 80MPa the presence of cone cracks often led to the separation of the compact into two halves.

No lubricant was used in the die as un-cracked green bodies were found to be possible without the need for lubrication, hence avoiding organic contamination. Some damage, such as the removal of small chips from the corners, was common and some specimens exhibited limited cone cracking.

5.1.4 Hot Pressing

The use of in-situ reaction sintering requires two hold temperatures during the firing process. The first is used to synthesise TiB_2 from TiN and BN along with the simultaneous production of Si_3N_4. The second is the conventional hold for densification and transformation of α Si_3N_4 to β sialon.

The temperature for reaction was initially set at 1380°C after thermodynamic calculations predicted that this was high enough to allow the formation of TiB_2 from TiN and BN to proceed. Above this temperature the silicon present in the sample could become liquid and coalesce effecting the homogeneity of the sample and hence distributing the simultaneous formation of TiB_2 and Si_3N_4.

The temperature for densification by liquid phase sintering was initially set at 1650°C after previous experience of sialon systems showed that liquid phase sintering was possible at these temperatures. Higher temperatures are to be avoided because of possible reactions of TiB_2 with nitrogen, reforming TiN.[2]

The optimisation of the production of hot pressed sialon/TiB_2 composites followed the following steps. The main objective of each step is stated.

1. **Hot pressing with no sintering aids**. The determination of whether predicted reactions can take place in a real system and whether densification occurs without externally added liquid formers.

2. **Hot pressing under varying time/temperature/pressure profiles**. For the determination of optimum conditions.

3. **Investigation of the effect of oxide additions**. Identification of a suitable sintering aid.

5.1.4.1 Hot Pressing with No Sintering Aid

Preliminary experiments on these systems, conducted before the beginning of this work, used no sintering additives as would usually be found in sialon materials. It was predicted that the liquid region in the sialon square equivalence diagram (see chapter 2) could be used to form liquids from the existing oxides present as surface layers on the powders. Initial hot press compositions were calculated using this assumption and hence no sintering aid was added. Powders were mixed for compositions that would produce 5,10,15 and 20vol% TiB_2 composites.

Preliminary experiments with the hot press resulted in fracture of the graphite punches. Experience with several runs attributed this failure to the application of too high a load at temperatures below 1000°C, hence applied loads were kept below 10MPa until 1000°C was reached. Above 1000°C the pressure was increased manually while monitoring the sample compression via the LVDT. Pressure was applied as needed to sustain the densification process until no more compression of the sample was observed with increasing pressure. This was carried out at both hold temperatures with the maximum applied pressure being ~30MPa. This was both the limit of the equipment and the point at which no more compression of the sample was seen.

Four samples (5,10,15 and 20vol% TiB_2) were hot pressed in this way. The density was measured and phase content examined by XRD as described in chapter 3. The results are shown in Figure 5.1 and Table 5.3.

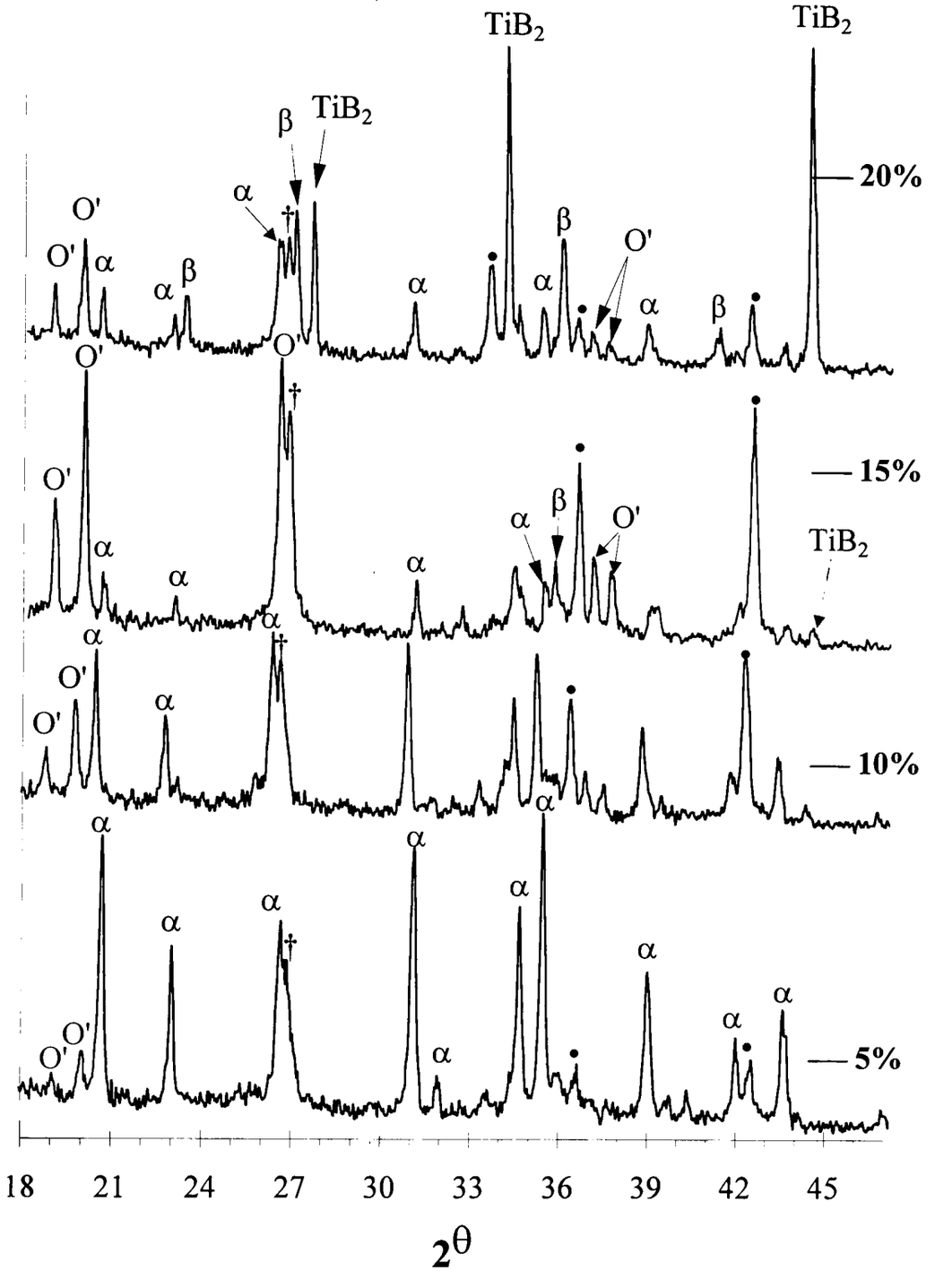

Figure 5.1 XRD for 5,10,15 and 20 vol% TiB_2 materials hot pressed with no densification aid. • = TiN. † = BN, α = α Si_3N_4, β = β Sialon, O' = O` Sialon.

Vol% TiB_2	5	10	15	20
Density, g/cc (% of theoretical)	2.586 (79%)	2.582 (78%)	2.664 (78%)	2.650 (76%)
Phases Present (in descending order)	α- Si_3N_4, TiN, BN	α, TiN, BN, O', β', TiB_2	O', α, BN, TiN, β', TiB_2	TiB_2, O', β', TiN, α Si_3N_4, BN

Table 5.3 Phases present in samples by XRD. α= α Si_3N_4, β = β sialon, O'=O' sialon

The low densities and the presence of α Si_3N_4 in all samples implies that liquid phase sintering has not occurred. Only the highest vol% TiB_2 composition showed significant TiB_2 formation. Either the reactions have not occurred or atmospheric gases were able to penetrate the porous samples and react with any TiB_2 to reform TiN and BN. Clearly there is insufficient liquid phase being formed under these conditions. In order to both encourage liquid formation and to investigate whether the reaction temperature is sufficient the temperatures for both stages were varied.

5.1.4.2 Variation of Temperature for Reaction and Densification

Identically prepared specimens were hot pressed under the following conditions: (i) 1350/1650°C, (ii) 1400/1650°C, (iii) 1400/1670°C and (iv) 1380/1650°C using pressure applied as described earlier up to a maximum of ~30MPa.

Temp Profile⇒	1360/1650	1400/1650	1400/1670	1380/1650
Density, g/cc	3.13	3.06	3.02	3.02
(% t.d.)	(78%)	(77%)	(76%)	(76%)
Phase Content	O', BN, TiN, TiB_2, α	O', TiB_2, BN, TiN, α, β	O', TiN, BN, TiB_2, α, β	TiB_2, O', TiN, BN, β, α

Table 5.4 Variation with reaction/sintering temperature of density and phase content of hot pressed 20vol% samples. α= α Si_3N_4, β = β sialon, O'=O' sialon.

As can be seen from Table 5.4 the samples show no significant improvement in density. However, the phase content of the sample hot pressed at 1380/1650°C

shows the best result in terms of amount of TiB_2 produced and the presence of β sialon.

The melting of the silicon at the reaction temperature and possible reactions between TiB_2 and nitrogen at the densification temperature prevent further increases in temperature.

5.1.4.3 The Effect of Oxide Additions on Densification and Phase Content

Since the pressures used were at the maximum achievable by the equipment and variation of temperature did not produce any significant improvements, the effect of additives on densification behaviour was examined.

Continuing to use the assumption that the preliminary samples that had been produced had densified without using a metal oxide sintering aid (e.g. CaO, MgO, Y_2O_3), SiO_2 was added to a 20vol% TiB_2 compositions in order to supplement the oxides present and thus produce more liquid phase at the sintering temperature. Any SiO_2 additions were balanced with extra AlN in order to form β sialon. Hot pressing was carried out using the 1380/1650°C temperature profile and pressure was applied as before.

Density and XRD results from these materials showed no significant improvement. A 20vol% TiB_2 composition resulted in a density comparable to previous runs and a phase content of O' sialon, TiN, TiB_2 and α Si_3N_4. Similar additions to several other compositions also resulted in no improvement.

It is clear that despite the additional oxides the temperatures used do not produce enough liquid to allow liquid phase sintering and the lack of density leads to reactions that produce the observed phases. Under such conditions the use of a known sintering aid is required. Yttria (Y_2O_3) is known to produce large amounts of liquid phase at relatively low densification temperatures[3] and is commonly used in the sintering of silicon nitride and sialons.

A densification aid consisting of 1 wt% Y_2O_3 was added by vibrational milling to a 20vol% composition. Hot pressing was carried out with the 1380/1650°C

temperature profile with pressure applied to a maximum of 30MPa as described previously. The sintering profile and sample densification is shown in Figure 5.2

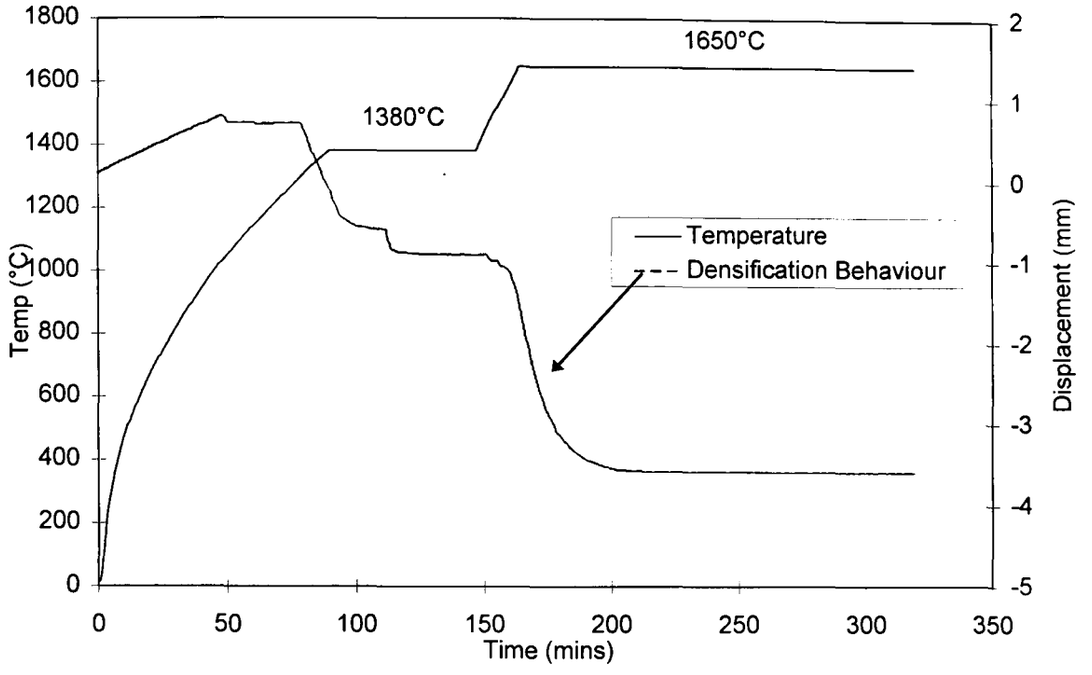

Figure 5.2 Temperature profile and densification behaviour of hot pressed 20vol% TiB_2 material with 1wt% Y_2O_3.

The densification behaviour exhibited by this sample suggests that some liquid is formed as low as 1250-1300°C which is close to the eutectic of Y_2O_3:SiO_2 systems. Some densification had taken place by the end of the reaction hold and further substantial shrinkage begins at ~1500°C. After ~1 hour at 1650°C no further densification is observed. This behaviour corresponds to the well known liquid phase densification process for silicon nitrides with the α Si_3N_4 to β sialon transformation taking place through solution-precipitation processes in the liquid phase.

The density of this sample (measured by Archimedes method) was 3.378 g/cc which is ~96±2% of the theoretical (3.5041g/cc). The XRD spectra from the material is shown in Figure 5.3

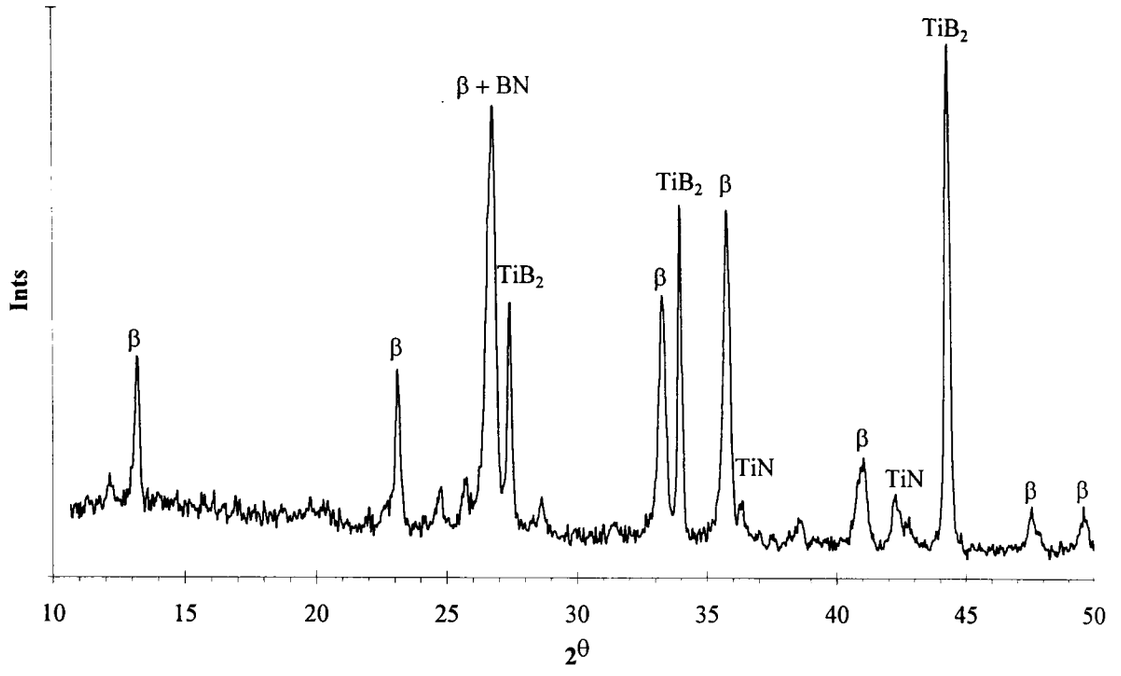

Figure 5.3 XRD from 20vol% TiB_2 containing material hot pressed with 1wt% Y_2O_3. (β = β sialon).

The sample consists of the required phases β sialon & TiB_2 but also contains small amounts of TiN and BN. Whether these phases are present because they did not react to form TiB_2 or because they are the product of the reaction of TiB_2 with nitrogen is unclear. It was noted that the TiN peak positions are significantly different from the JCPDS values possibly because of the substitution of oxygen, carbon or boron into the TiN structure.

The addition of an yttria alumina silicate glass has been shown to allow densification of sialons at lower levels of yttria content than by the addition of yttria alone. This approach avoids the formation of yttrium aluminium garnet which consumes some of the yttria making it no longer available for liquid formation[4]. A 20vol% TiB_2 composition was mixed with a glass containing Y_2O_3, Al_2O_3, and SiO_2 in the proportion 45:25:35 respectively by weight. 0.625wt% of this glass was added by vibrational milling and hot pressing was carried out as previously.

The XRD for this sample, after two stages of surface removal is shown in Figure 5.4

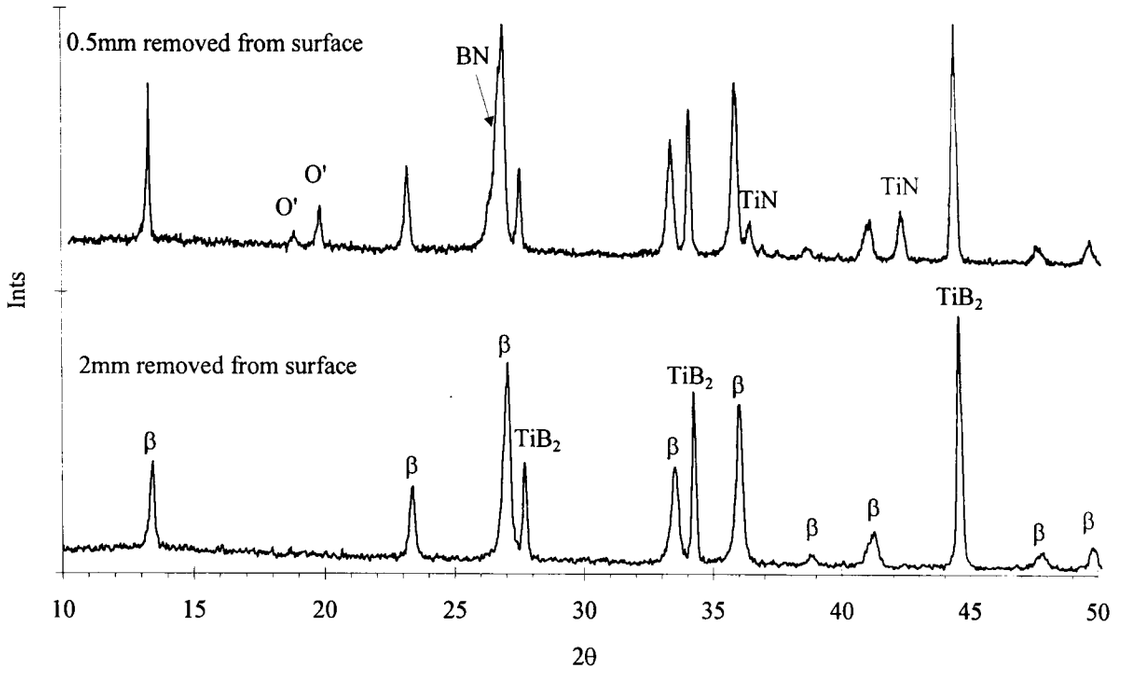

Figure 5.4 XRD from a 20vol% material hot pressed with 0.625wt% glass. The two surfaces x-rayed were exposed by removing 0.5 and 2mm from the sample after hot pressing.

XRD of the near surface regions of this sample show the presence of O' sialon, TiN and probably BN. However, the removal of an extra 2mm reveals that the centre of the material is dense and contains only β sialon and TiB_2. This is evidence of atmospheric interactions with the surface of the sample and shows that the presence of TiN and BN both here and in previous samples is most likely a product of nitrogen reacting with TiB_2 at the sintering temperature. The density of the specimen once the surface was removed was ~97% of the theoretical density.

Thus a very small amount of sintering aid facilitates the production of composites in which both the reaction to form TiB_2 and matrix phase has fully proceeded and densities close to the theoretical have been achieved. After removal of surface layers the phase content appears, by XRD, to be purely di-phasic.

5.1.5 Discussion of hot pressed material production.

For compositions where no sintering aid was used the density and XRD data show that not only were the correct phases not being formed but that

densification was not taking place. This has been explained by the lack of liquid present at the sintering temperatures used. The resulting open structures allow the penetration of atmospheric gases which react with the sample producing the phases observed by XRD.

The presence of O' sialon also indicates an excess of SiO_2. It is possible that estimations for the levels of oxides on the starting powders were too low and the reaction

$$2TiO_2 + 2B_2O_3 + 5Si = 2TiB_2 + 5SiO_2,$$

takes place leading to O' Sialon formation on combination with AlN. In which case a re-estimation of the oxide levels and re-calculation of starting compositions should lead to better results. In dense specimens O' is limited to the surface layers suggesting that it may arise from reactions with the sintering atmosphere. Reactions with the atmosphere also explain the presence of TiN and BN by the reaction of TiB_2 with nitrogen.

The densification of hot pressed samples was possible with the use of a very small amount of yttria (<0.25wt%) and implies that the limited number of samples prepared by Hong[5] were successful because of yttria contamination at a very low level. It is possible that the mixing and milling techniques used were contaminated with enough yttria to produce dense composites. This explains the failure of the initial attempts to produce sialon/TiB_2 composites without the addition of a sintering aid.

Using a densification aid containing yttria the optimum conditions for hot pressing have been identified as a reaction temperature of 1380°C and a sintering temperature of 1650°C for ~1 hour each. For densification and the exclusion of atmospheric gases pressure should be applied to 10MPa before 1000°C and then increased gradually to a maximum of 30MPa by the sintering temperature.

After removal of the surface layers, caused by the impregnation of the BN coating and reactions with the atmosphere, the remaining material consists of β

sialon (of a low level of substitution of $z \approx 0.5$), and TiB_2 with a density of 3.30-3.35 g/cc (~97-98% of the theoretical). Dense hot pressed materials were used for the determination of key engineering properties such as hardness, and fracture toughness and were used as specimens for the study of tribological behaviour.

Only a limited volume of hot pressed material was produced before the hot press was taken out of commission for conversion into an environmental hot press capable of being used under vacuum or other atmospheres.

5.1.6 Pressureless Sintering

Previous work had only concentrated on hot pressing and it was not known if the same composites were possible via pressureless sintering. Unknown factors were whether the glass would allow sintering without applied pressure and whether it would inhibit the reaction between TiN and BN. Having shown that a glass of yttria, alumina and silica is suitable for densification by hot pressing the same glass was used in larger amounts in an attempt to pressureless sinter sialon/TiB_2 composites.

In order to determine whether sialon/TiB_2 composites were viable via pressureless sintering the following procedure was followed.

1. **Composition calculation**. As for hot pressed materials but taking into consideration the presence of large amounts of densification aid.

2. **Verification that the required reactions still take place**. The addition of sintering aid may effect the production of TiB_2 by separating the reactive species.

3. **Determination of a sintering cycle**. The times, temperature and atmospheres needed to successfully pressureless sinter were determined.

Starting compositions were re-calculated to take into account the presence of Al_2O_3 and SiO_2 introduced in the form of the sintering aid. These additions

significantly affect the balance of the reactions used to form the sialon matrix. The presence of large amounts of residual sintering aid also affects the theoretical density. For simplicity the remaining sintering aid was assumed to re-crystallise as YAG. This leads to inaccuracy in the theoretical density if all the residual glass is not re-crystallised because of the differences in the densities. (YAG=4.47 g/cc, Glass ~3.32 g/cc).

From the work on hot pressing it was known that the presence of nitrogen at the reaction temperature (1380°C) is undesirable as it can penetrate the specimen and react with silicon forming Si_3N_4. The Si would then no longer be available to take part in the reaction to form TiB_2 and excess nitrogen would be present in the composition. To avoid this problem the procedure for pressureless sintering used two stages, as for hot pressing, but with an argon atmosphere present. The sintering furnace allows the use of a vacuum, argon or nitrogen as the sintering atmosphere.

In order to burn off any organic impurities in the sample and to achieve a pure argon atmosphere the sample was first heated to 900°C under vacuum. A hold at 900°C for ~1 hour allowed proper de-gassing of the sample. The argon atmosphere was introduced only when a vacuum of better than 5×10^{-5}mbar was achieved. The 900°C hold had no noticeable effect on the specimen.

To verify that the presence of the sintering aid did not inhibit the reaction between TiN and BN a composition made for hot pressing (15vol% TiB_2) was mixed with 15wt% glass and 8wt% AlN by vibrational milling. This composition was uniaxially pressed and heated in the pressureless sintering furnace to 1380°C in argon for 1 hour. XRD reveals that the reaction to form TiB_2 still occurred in the presence of the sintering aid. Other phases present were α Si_3N_4, β sialon, YAG and possibly small amounts of TiN and BN. The presence of YAG indicates that the glass is crystallising on cooling and the presence of β sialon indicates that some liquid phase sintering has already begun at 1380°C. Hence the reaction to produce TiB_2 and Si_3N_4 is not inhibited

by the glass phase or the use of a vacuum to 900°C and argon at the reaction temperature.

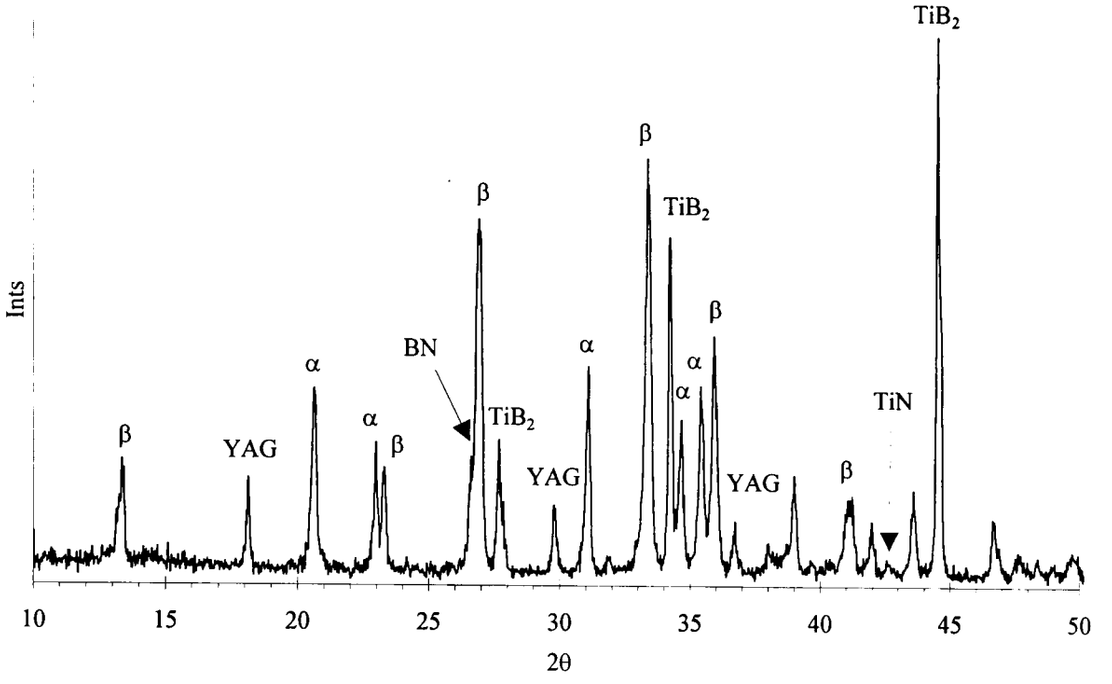

Figure 5.5 XRD of a sample with 15wt% glass fired at 1380°C in argon.

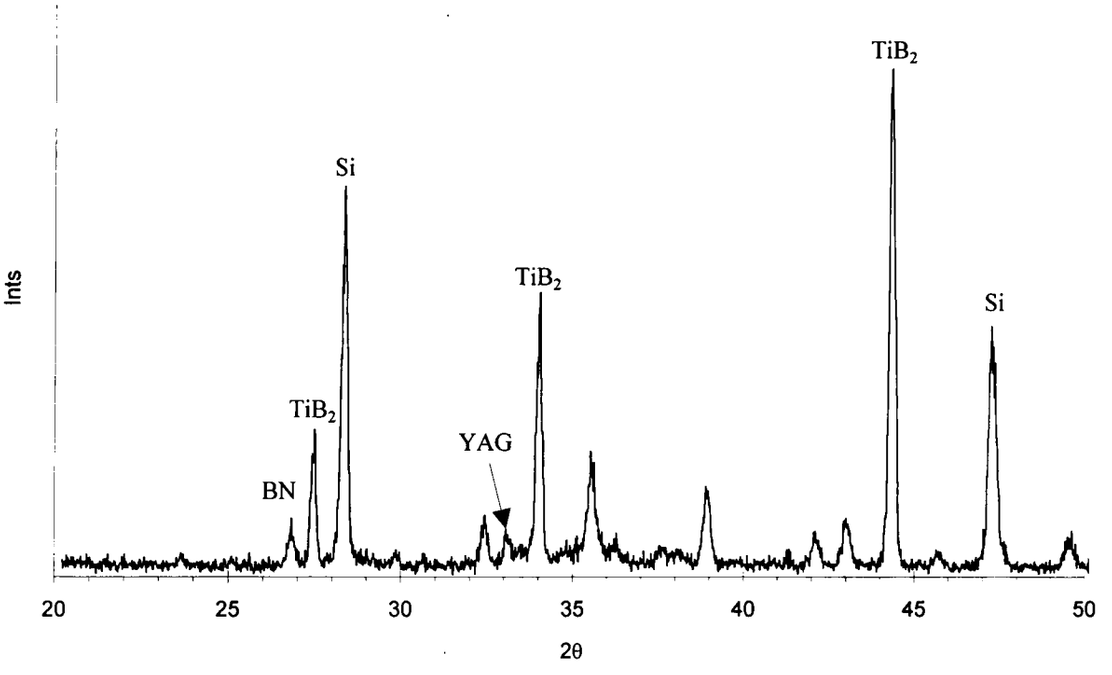

Figure 5.6 XRD from the as sintered surface of a pressureless sintered sample. At 1650°C in argon the Si_3N_4 has dissociated to form liquid silicon.

An identical specimen was subject to the full sintering cycle of 900°C for degassing, 1380°/1hr for reaction and 1650°C/1hr for densification. Argon was used during the whole of the run after de-gassing. In Figure 5.6, XRD of the as-sintered surface reveals that while TiB_2 has been formed there is also silicon

present. This silicon was seen in the form of balls or droplets on the surface indicating that it had been cooled from a liquid.

The presence of silicon is explained by the dissociation of the Si_3N_4 or sialon. In the absence of a nitrogen overpressure at the higher sintering temperatures Si_3N_4 or sialon has decomposed into Si and N via the reaction

$$Si_3N_4 \Leftrightarrow 3Si(l) + 2N_2(g) \qquad \textbf{Equation 5.1}$$

At 1600-1700°C, for Si_3N_4, at least 10^{-1} to 1 atm of N_2 is needed to prevent decomposition.[6]. Unfortunately there is a possible reaction between TiB_2 and nitrogen that will re-form TiN and produce BN & TiN in the composite. The reaction itself may effect the interface between the matrix and TiB_2 influencing the composite's properties[2].

$$2TiB_2 + 3N_2 \Rightarrow 2TiN + 4BN,\ \Delta G_{1900^\circ} = -831kJ / mol \qquad \textbf{Equation 5.2}$$

If nitrogen is introduced while the sample has open porosity this reaction could occur throughout the whole of the specimen and the desired sialon/TiB_2 composite would not be produced. A compromise is the introduction of nitrogen only after the sample has achieved closed porosity. In this way re-conversion only takes place at the surface.

Because the pressureless sintering furnace gave no information on the densification of the sample the point where closed porosity occurs was determined by sintering pressureless sinterable materials in the hot press. Using minimal pressure and the LVDT to monitor shrinkage the behaviour in Figure 5.7 was observed. The phase content of the specimen after surface grinding was β sialon, TiB_2, TiN, YAG and some small amounts of α and its density was ~3.2g/cc (94% t.d.).

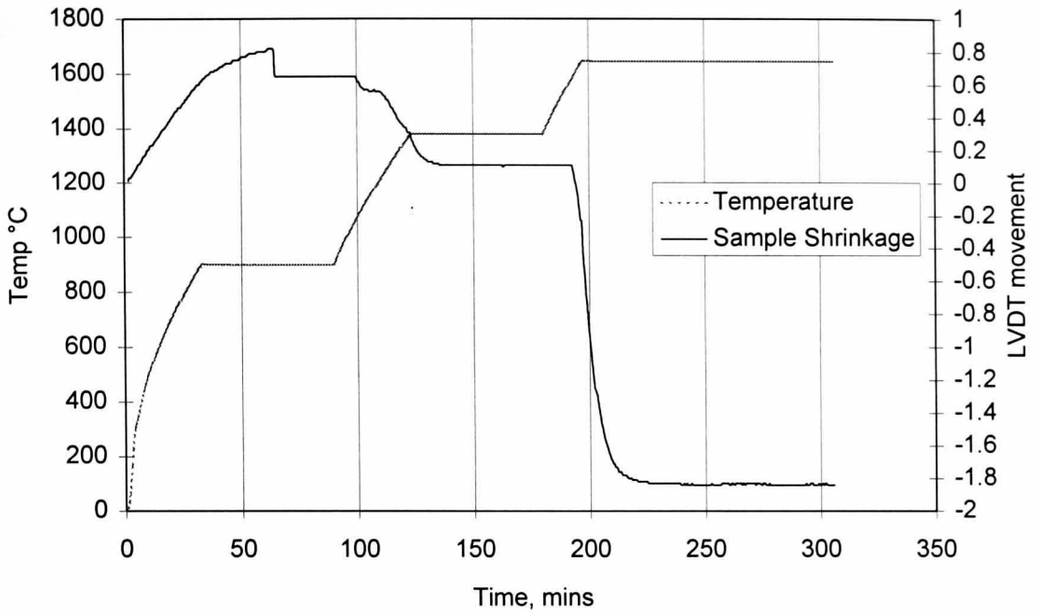

Figure 5.7 Sample shrinkage with time/temp for a pressureless sinterable sample (15wt% glass) sintered in the hot press under 10MPa .

From this information it was predicted that a closed pore structure would form at some point above 1500°C. The determination of the correct point at which to change the atmosphere from argon to nitrogen is crucial to the successful production of dense sialon/TiB_2 composites by pressureless sintering

With the above information the sintering profile for pressureless sinterable materials was as shown in Figure 5.8.

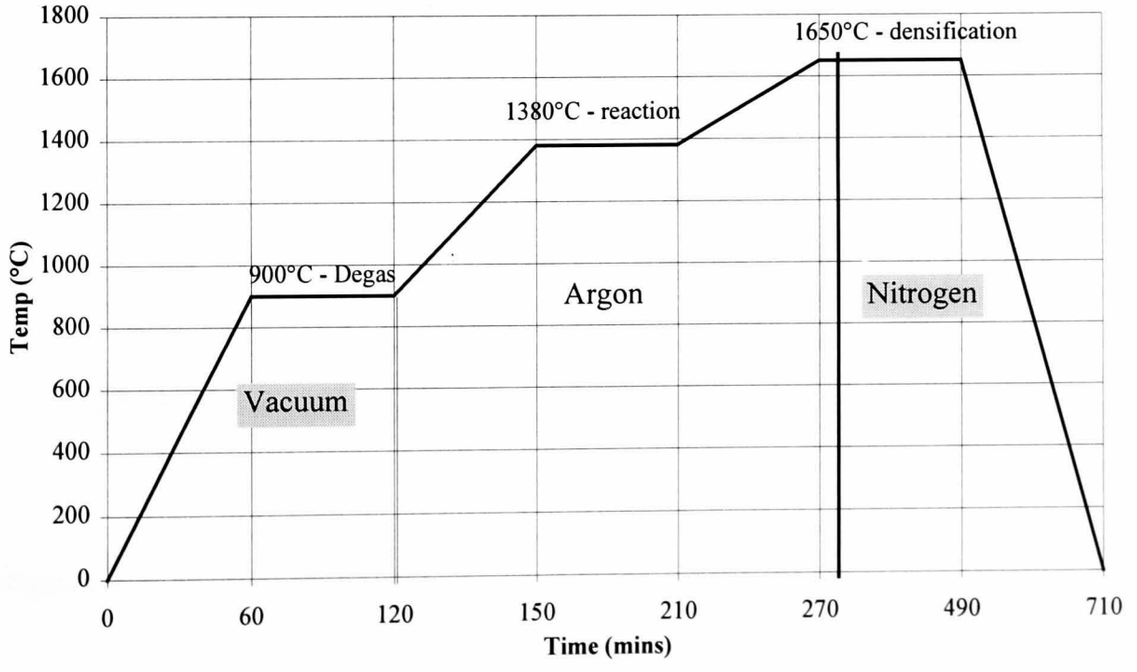

Figure 5.8 A typical sintering profile for pressureless sintering

Using the above profile several 10vol% TiB_2 compositions were sintered but with the atmosphere changed from argon to nitrogen at 1500°C, 1600°C and after 20mins at 1650°C.

Atmosphere Change @	Phases identified by XRD	Density, g/cc
1500°C	Y-α' sialon, TiN, BN	2.5
1600°C	β sialon, TiN, BN, small amount TiB_2	2.7
1650°C (20mins)	β sialon, TiB_2, YAG.	3.33 (97%)

Table 5.5 Phases and densities of pressureless sintered samples with the argon to nitrogen change point.

It is clear that after only 20 mins at the sintering temperature the samples were densified enough to resist the ingress of nitrogen and the associated reactions. This procedure was adopted for the rest of materials production. The surface layers of even the most dense samples are still compositionally different from the interior, usually consisting of Y-α sialon, TiN and BN. The XRD in Figure 5.9 shows the phases present at the surface of a sample sintered at 1650°C in nitrogen.

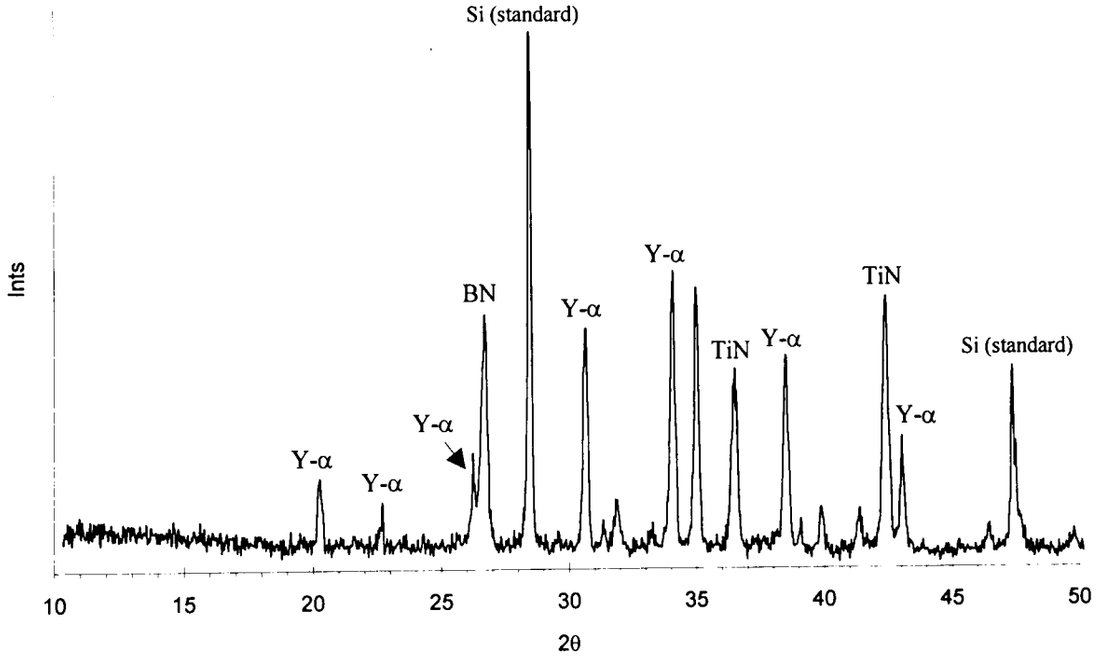

Figure 5.9 XRD from the surface of a sample sintered in 1650°C in nitrogen. Y-α = Yttria α sialon.

The removal of these surface layers reveals the phases shown in Figure 5.10. By using a nitrogen atmosphere after closed porosity has been achieved the samples form dense sialon/TiB_2/YAG composites.

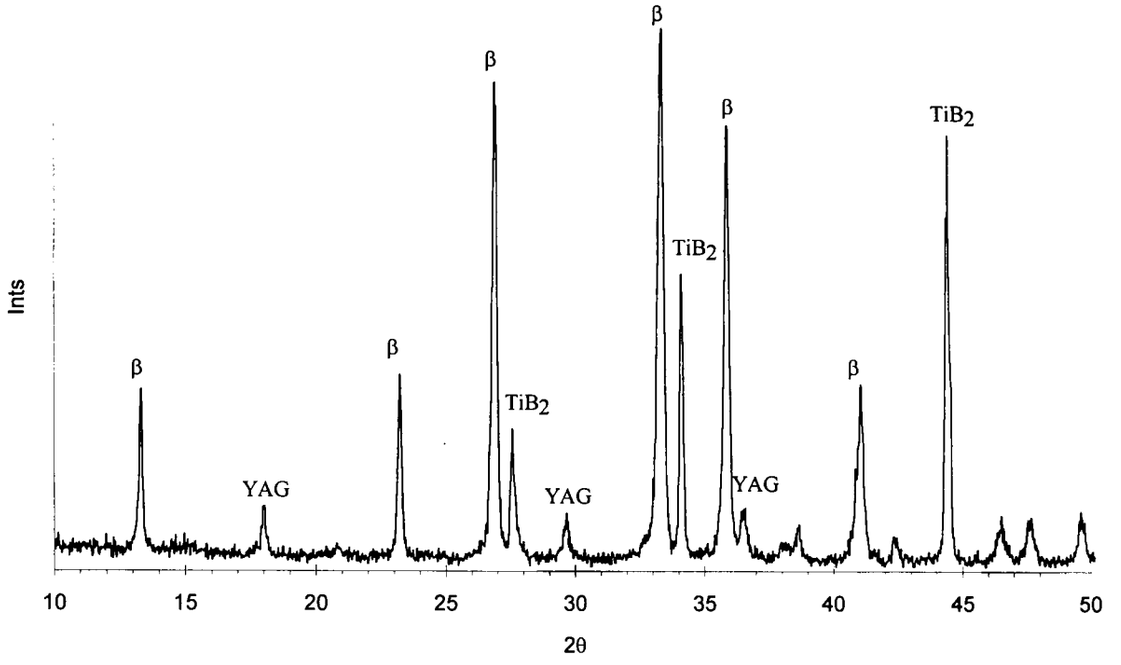

Figure 5.10 XRD form the dense bulk of a pressureless sintered specimen after optimising the sintering procedure.

In order to try and minimise or even eliminate the surface layer a combination of atmosphere changes and powder beds were used as listed in Table 5.6.

Atmosphere	Powder bed	Phases present by XRD	Density, g/cc
Ar	α Si_3N_4	β sialon, TiB_2, TiN, YAG	3.22 (94%)
Ar/N_2(20min at 1650°C)	α Si_3N_4	β sialon, TiB_2, TiN, YAG	3.21 (94%)
Ar/N_2 (20min at 1650°C)	above α Si_3N_4	β sialon, TiB_2, TiN, YAG	3.25 (95%)

Table 5.6 Phases and densities of samples sintered in α Si_3N_4 powder beds with varying atmospheres.

The α Si_3N_4 was used to provide a partial pressure of nitrogen around the sample at the sintering temperature. The stability of sialon means that the α Si_3N_4 should dissociate first providing a localised atmosphere of nitrogen.

Whilst all samples exhibited good densities and the required phase compositions the surface layers of Y-α sialon, TiN and BN were still present under powder

bed conditions. Whilst improving the composition and density of samples sintered in argon alone the presence of an α Si_3N_4 powder bed did not significantly decrease the surface layers formed and they were not used in subsequent runs.

Some warpage of specimens was encountered as shown in Figure 5.11 which is a schematic of a sectioned sample showing the warpage and the surface layers.

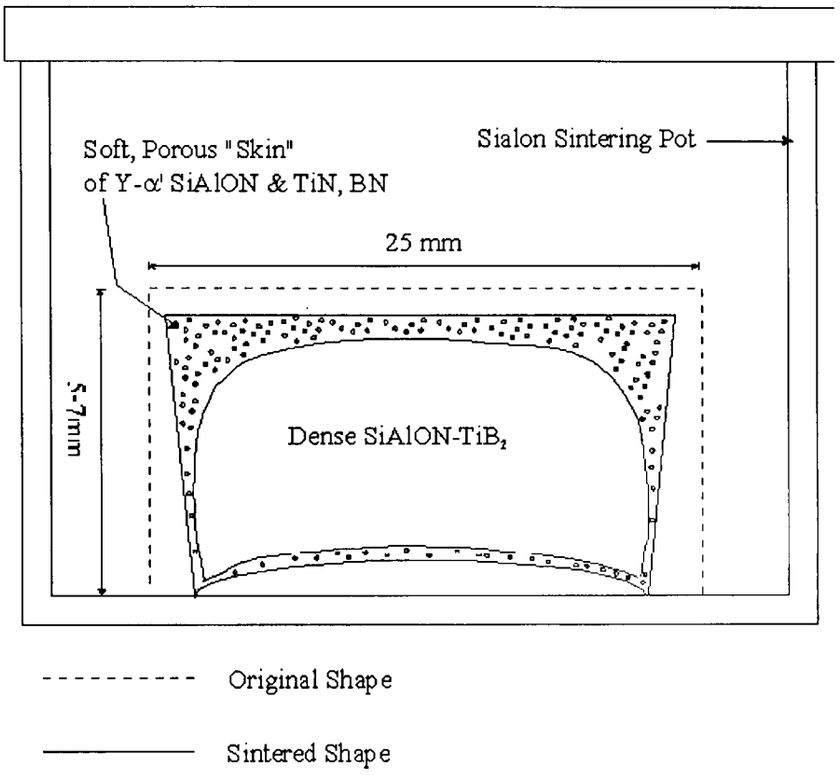

Figure 5.11 Schematic of a cross-sectioned pressureless sintered material.

5.1.7 Discussion of Pressureless Sintered Material Production

The procedure for pressureless sintering is necessarily more complex than for hot pressing. The temperature used for hot pressing (1380°C and 1650°C) were also found to be suitable for pressureless sintering. The reaction to form TiB_2 is uninhibited in the presence of a glassy phase and an argon atmosphere. A dual atmosphere sintering run is required in order to avoid (a) reactions with the starting compounds and (b) the dissociation of sialon at the densification temperature. As a consequence of the reaction between nitrogen and TiB_2 the atmosphere change can only take place once closed porosity has been achieved. This point has been determined as being ~20mins after the sample has reached

the sintering temperature. The presence of nitrogen at the sintering temperature is proposed as the cause of a surface layer being formed on all specimens which consists primarily of Y-α sialon, TiN & BN.

The thickness of these layers was inconsistent between specimens sintered in exactly the same way. It was concluded that the sintering kinetics must vary between samples and that some have not achieved close porosity when the gas is changed. Possible explanations are that the sintering conditions varied from run to run or that sample preparation produced varying green densities that lead to some specimens densifying earlier than others. Individual densification rates could not be monitored with the equipment used and hence neither of these explanations could be confirmed.

Removal of the surface layers reveals a material of ~ 95±3% of the theoretical density. The presence of residual sintering aid makes the uncertainty in the calculated theoretical density higher than for hot pressed materials. The samples consisted of β sialon, TiB_2 and YAG. The presence of YAG is due to the crystallisation of the intergranular phase. The reaction temperature used (1380°C) is close to the crystallisation temperature of the glass and YAG has been seen after cooling from this temperature. It is possible that some crystalline phase may remain at the densification temperature and lead to reduced amounts of liquid for densification. It is also possible that crystallisation on cooling is not complete and there is some remaining yttria based glass in the structure.

Once the surface layers had been removed, the density and phase content of these materials was suitable to allow the materials to be used in the measurement of hardness, fracture toughness and wear resistance.

5.2 Microstructure

The microstructure of ceramics is of prime importance because of the dependence of properties on certain microstructural features. For example properties such as strength, hardness and toughness are dictated by matrix grain size and morphology, particulate inclusion distribution, size and morphology and the presence of any intergranular phase.

Composites produced by both hot pressing and pressureless sintering were examined using SEM to determine:

1. The amount, distribution and morphology of the TiB_2 particulate phase in the matrix.

2. The grain size and morphology of the sialon matrix.

3. The amount and distribution of intergranular phase arising from residual sintering aid.

The TiB_2 is homogeneously distributed throughout the sialon matrix with a range of particle sizes of ~0.25 to 3μm - the mean size is ~1.5μm. The average centre to centre distance was ~6±0.5μm. The particle size distribution is shown in Figure 5.12. The microstructure of a composite designed to contain 20vol% TiB_2 imaged in back scattered electron mode is shown in Figure 5.13 and Figure 5.14. The TiB_2 particles appear as the lighter phase with the darker area being the sialon matrix. Digital imaging techniques were used to estimate the amount of TiB_2 present and for the hot pressed material shown the result was 20±3 area%. The error comes from the difference in results achievable by changing the contrast of the image to be analysed.

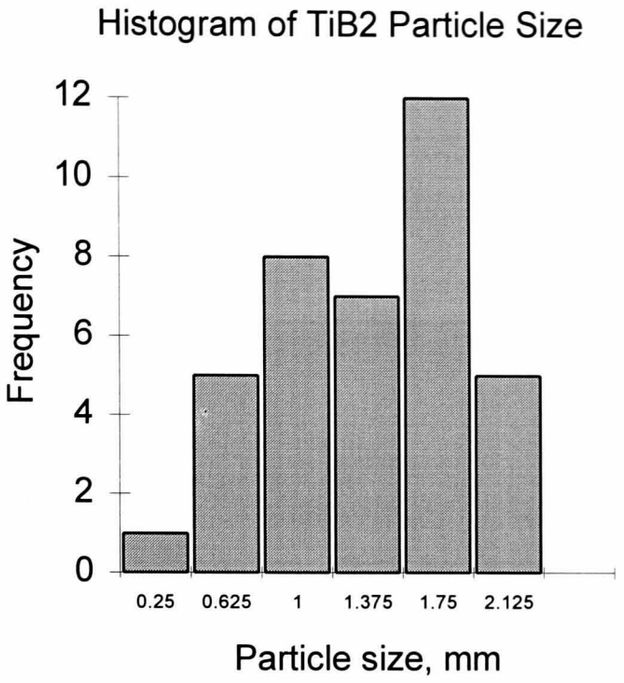

Figure 5.12 Particle size distribution of TiB_2 for a hot pressed 20 vol % composite.

At 20 vol% many of the TiB_2 grains are in contact forming effectively bigger particles. A common feature is a dark inclusion (in back scattered electron contrast) in many of the TiB_2 grains. Their size is too small for these to be meaningfully analysed but it is probable that these are Si_3N_4 or sialon entrapped by the growth of TiB_2 around them.

There is no evidence for chemical interaction between the sialon and the TiB_2 particles. Other workers have reported a reaction zone or porosity around TiB_2 particles in sialon composites formed by conventional methods. There is also no detectable intergranular phase. Only very small amounts of yttria are present in the starting composition but no yttria was imaged or detected by EDX.

The absence of detectable intergranular phases in hot pressed materials makes imaging the microstructure of the sialon matrix difficult. Individual grains cannot be detected so no information on grain shape and size is available. A plasma etch technique was used to try and image the matrix microstructure but the plasma merely produced etch pits in the material and it was not clear if these corresponded to the outlines of sialon grains.

The level and form of the porosity in the hot pressed material is shown in Figure 5.14. The porosity appears at higher levels than those calculated from the theoretical density. The shape of these pores suggests that they may have been enlarged by grain pull out and damage introduced by sample preparation (i.e. grinding and polishing).

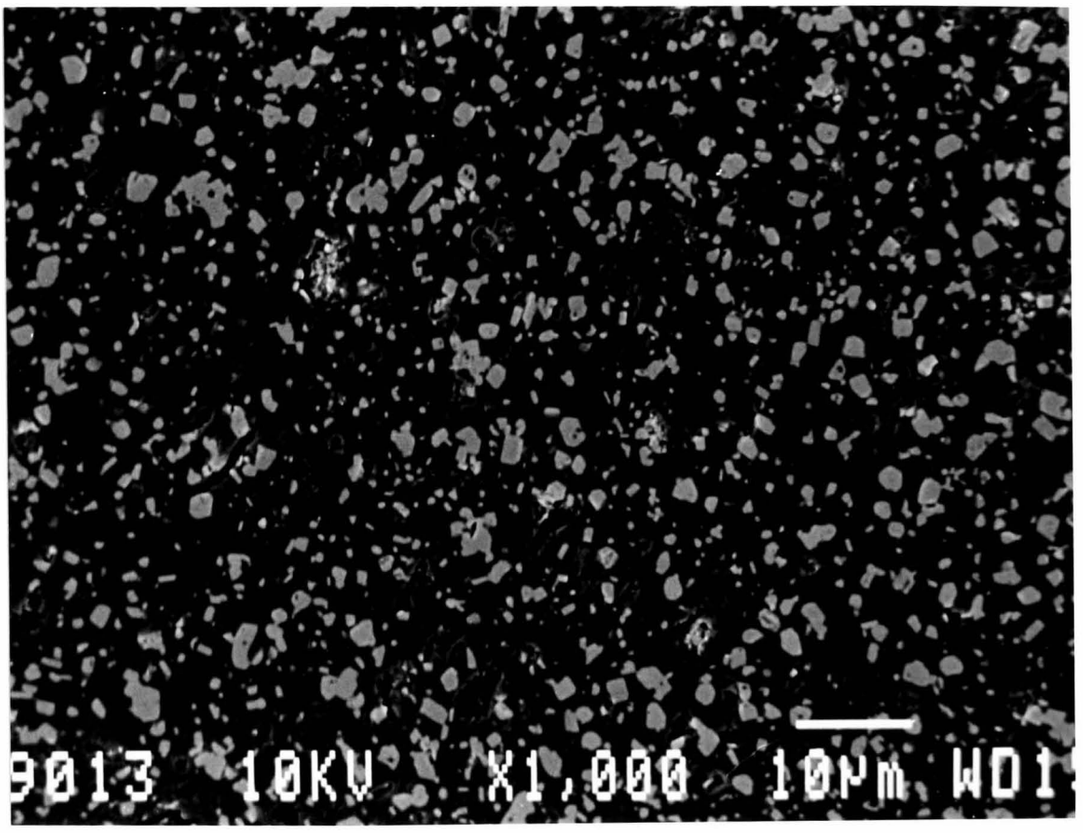

Figure 5.13 The microstructure of a hot pressed 20vol% TiB_2 material. Lighter particulate phase is TiB_2.

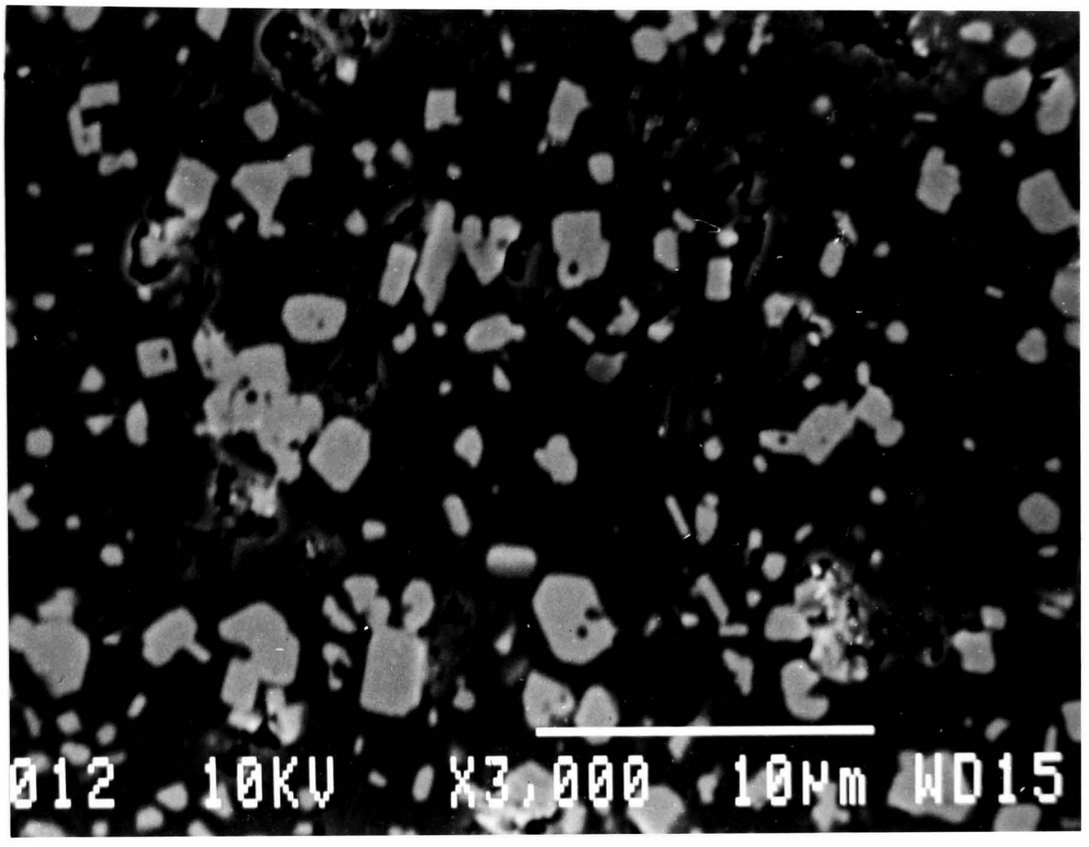

Figure 5.14 Higher magnification of Figure 5.13, TiB_2 grains show no reaction zone or porosity around particle. Good particle-matrix interface.

Pressureless sintered materials contain an additional phase of YAG and possibly some glassy phase. SEM micrographs taken in back scattered mode are shown in Figure 5.17 and Figure 5.18. As for hot pressed materials, the darkest phase is the sialon and the mid grey phase is TiB_2. The bright intergranular phase has been identified by EDX as being yttria rich and indicates that the YAG has crystallised from the intergranular glassy phase.

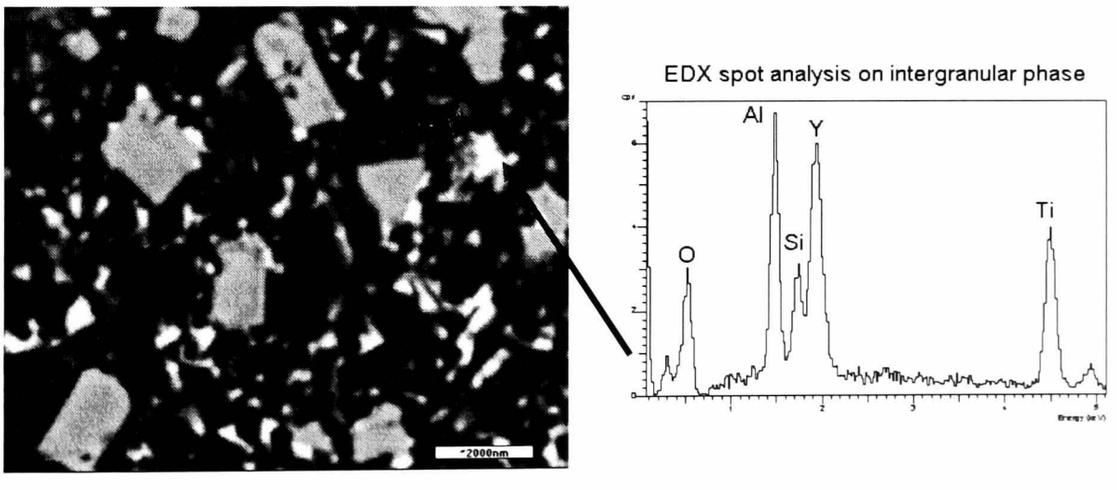

Figure 5.15 Microstructure of pressureless sintered 10vol% TiB_2 material. EDX reveals bright phase to be yttria rich. (micron bar =2000nm)

The sample shown contains only 10vol% TiB_2 which is homogeneously distributed in the matrix. The lower vol% results in fewer TiB_2 particles being in contact. The TiB_2 particle size distribution is shown Figure 5.16. The mean particle size was ~1μm with an average centre to centre particle distance of ~8 ±1μm.

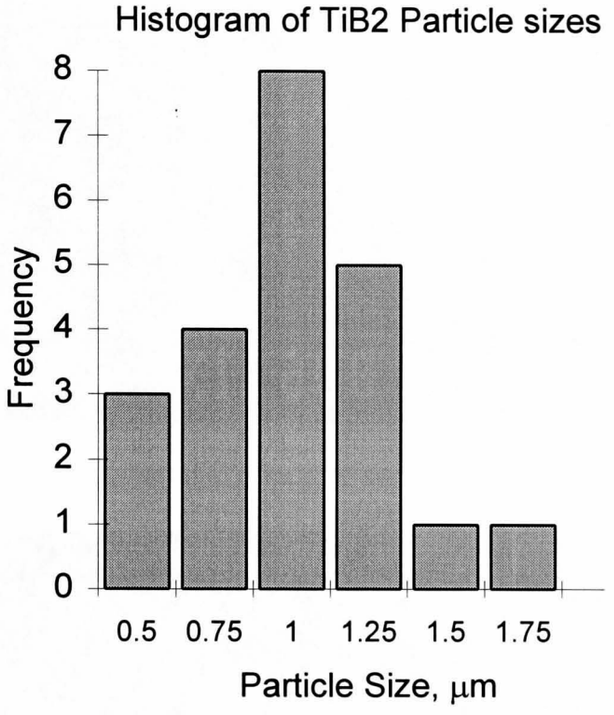

Figure 5.16 Particle size distribution of TiB_2 particles in a pressureless sintered 10vol% material

The intergranular phase allows the sialon grain structure to be observed. It consists of a small grain size with many grains <1μm. Many of the grains are of a spherical or hexagonal appearance but there is some evidence for small elongated grains in the structure, typical of a β sialon. The "soak" times at the densification temperature were short and no pronounced grain growth of the β sialon was expected. The small grain size is expected to contribute to the hardness of the material but such small grains cannot confer the structure with a high fracture toughness. No reaction zones or porosity surrounding the TiB_2 particles in the pressureless sintered materials were observed.

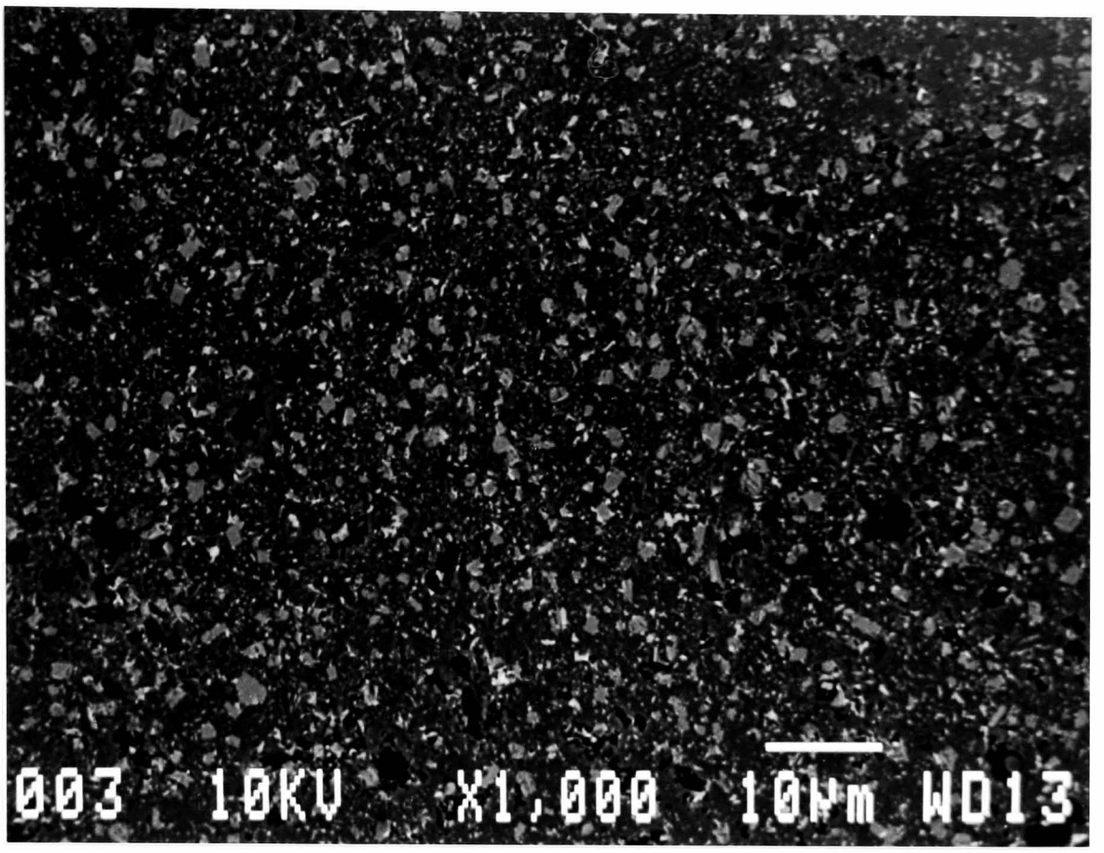

Figure 5.17 Pressureless Sintered composite containing 10 vol% TiB_2.

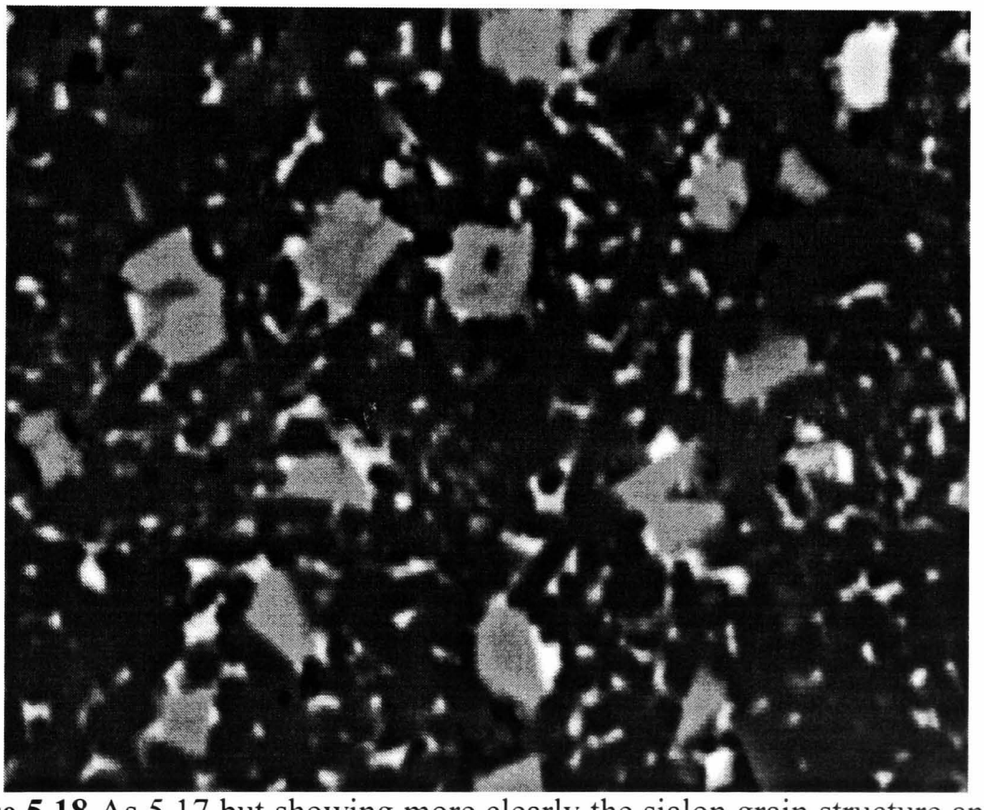

Figure 5.18 As 5.17 but showing more clearly the sialon grain structure and the intergranular phase.

2μm

The porosity of the pressureless sintered material is best illustrated by secondary electron contrast and is shown in Figure 5.19. This level of porosity is consistent with estimates from density measurements. The pressureless sintered

samples, despite having the outer layers removed by grinding, have an area of increased porosity around the edge of the disc. This is shown in Figure 5.20, a micrograph taken within the outer 0.5mm of a pressureless sintered disc. While the top and bottom surfaces of the disc have been ground sufficiently to remove any material effected by the reactions with the sintering atmosphere, the sides of the disc have not had as much material removed and still exhibit the microstructure of these layers. The same effect was visible in hot pressed materials but to a much lesser extent.

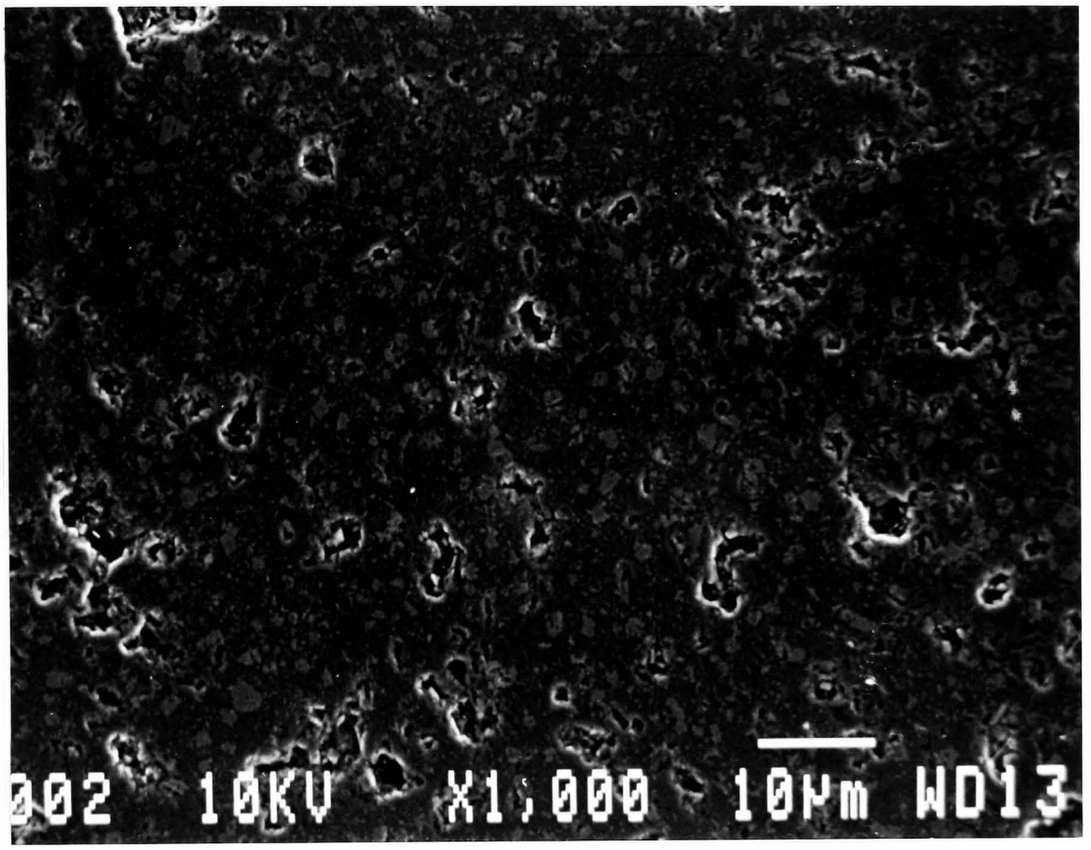

Figure 5.19 The porosity found in a typical pressureless sintered sample.

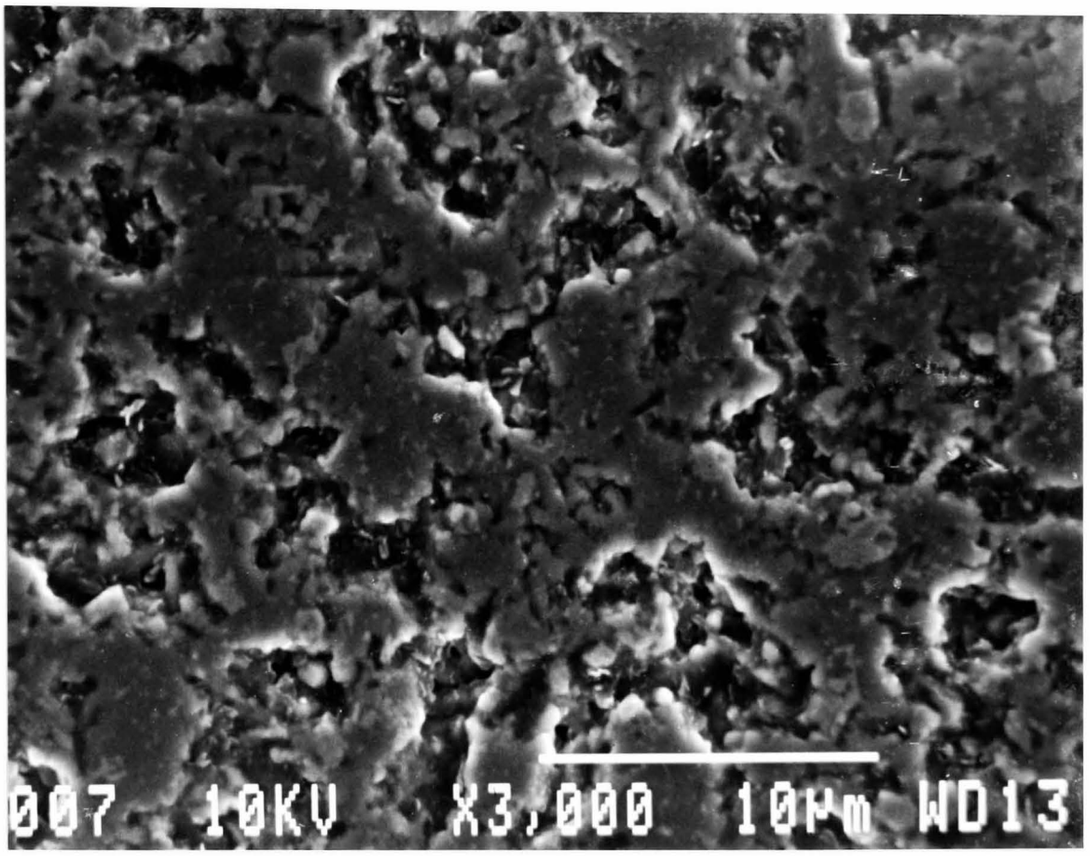

Figure 5.20 Porosity at edge of pressureless sintered disc.

5.2.1 Discussion of Microstructure of Sialon/TiB_2 Composites

The microstructure of both grades of material show that TiB_2 has been formed in particulate form from the reaction between TiN and BN. The particles are of a range of sizes form <0.5µ to ~3µm. Larger particles occur where adjoining grains have coalesced. The particles are homogeneously distributed throughout the matrix phase. In hot pressing there is no intergranular phase detectable by SEM or EDX whereas pressureless sintered materials contain an intergranular phase that is yttria rich and is probably YAG with some residual glass. The sialon has a small grain size in the pressureless sintered material with many grains being sub-micron. In hot pressed materials the matrix grains cannot be observed but are expected to be not unlike those of the pressureless sintered material.

The porosity observed in the materials approximately agrees with that implied from density measurements. The exaggerated size of some pores is attributed to their enlargement by grain pull out caused by the specimen preparation. (i.e.

grinding.) The pore sizes range from <1μ to >10μm with the larger pores being more significant from a properties point of view.

Potential improvements in microstructure would be : the elimination of as much residual porosity as possible, the development of the sialon matrix to include high aspect ratio β grains or mixed α/β microstructures and the inclusion of a greater vol% of TiB_2 or the growth of TiB_2 to form high aspect ratio inclusions.

5.3 Hardness

Hardness and fracture toughness were measured by indentation methods for the reasons described in chapter 3. Both hot pressed and pressureless sintered materials were tested. In addition a commercial grade of sialon was also tested in an identical way for comparison.

The samples on which hardness was measured and a description of their composition is given in Table 5.7

Sample	Composition	Density	Tests used
20OXYAG	0.625wt% glass. 20vol% TiB_2.	96%	Vickers, Knoop, K_{Ic}.
HP20OXY	1wt% Y_2O_3. 20vol% TiB_2	97%	Vickers, Knoop, K_{Ic}
HP20Y1	1wt% Y_2O_3, 20vol% TiB_2	84%	Vickers
PS10R2	15wt% glass. 10vol% TiB_2.	94%	Vickers, Knoop, K_{Ic}
PS10R6	15wt% glass, 10vol% TiB_2	97%	Vickers, Knoop, K_{Ic}
PS15R1	15wt% glass , 15vol% TiB_2	96%	Vickers, Knoop, K_{Ic}

Table 5.7 Samples used for hardness testing, densification aids and vol% of TiB_2, densities and methods of testing.

20OXYAG and HP20OXY were hot pressed samples with differing densification aids but similar densities. HP20Y1 was a yttria densified sample that had not fully densified and was used to demonstrate the effect of porosity on the measurement of hardness. PS10R2, PS10R6 and PS15R1 were pressureless sintered samples with varying densities and vol% of TiB_2.

Various applied loads (1.96 to 10N) were used to investigate the material's hardness. It was found by experiment that no significant cracking occurred at 5N. Because of the small grain size the small indents formed under such a low load still sampled the average microstructure. The results of hardness measurements under several loads by both Vickers and Knoop are shown in Table 5.8

Sample	Method	Load (N)	Hardness (GPa) [±2]	~% porosity
20OXYAG	Vickers	10	**19**	4
" "	Vickers	5	**22**	4
" "	Knoop	10	**17**	4
" "	Knoop	1.96	**16**	4
HP20OXY	Vickers	5	**20**	3
	Knoop	1.96	**16**	3
HP20Y1	Vickers	10	**8**	16
" "	Knoop	10	**8**	16

Table 5.8 Hardness measured by Vickers and Knoop for hot pressed composites.

No 5N Vickers were carried out on HP20Y1 because the level of porosity was such that a significant amount of the indent intersected porosity.

As a comparison Vickers indentation was carried out on a commercial grade of sialon with varying loads. The results are shown in Table 5.9

Sample	Vickers Load (N)	H_v (GPa) [±2]
Syalon 101	80	**17.5**
	50	**17.4**
	30	**15.3**
	10	**15.3**
	5.6	**16.2**

Table 5.9 Hardness of Syalon 101 tested under several Vickers loads.

An accepted value for syalon101 is H_v(60N)=16MPa and the above results agree with this figure within experimental error. Another commercial grade (not tested here) of the same material that contains TiN particulates has a reported hardness of H_v(60N)=16MPa.

Residual porosity affects the measured hardness of the hot pressed composites but they are still significantly harder than Syalon 101, a commercial Si_3N_4 material.

It is clear that the less porosity present the higher the measured hardness. A suggested method for compensating for the presence of porosity and calculating the true hardness at zero porosity is to use the equation:

$$H_{measured} = H_0 \exp(-bp) \qquad \textbf{Equation 5.3}$$

where H_0 is the hardness at zero porosity, p is the volume fraction of porosity and b is a constant that is usually 7 for ceramics[7]. Using this relationship for the hot pressed materials gives **H_v(5N)=25-29GPa**. Usually such corrections should be treated with caution because of the low level of porosity and uncertainty in determining the value of b. However, it can be used with some confidence here since, if used for HP20Y1, where there is a high level of porosity (16%), it yields H_v(10)=24GPa which is comparable with the results for the other materials. These results show that elimination of the final few percent of porosity would yield a very hard material.

Pressureless sintered materials were expected to be less hard because they contain less TiB_2 and also contain residual sintering aid. The hardness measured by Knoop and Vickers for several pressureless sintered materials is shown in Table 5.10

Sample	Method	Load (N)	Hardness (GPa) [±2]	~ % porosity
PS10R2	Vickers	57	**15**	6
" "	" "	10	**16**	6
" "	" "	5	**17**	6
" "	Knoop	10	**13**	6
" "	Knoop	1.96	**18**	6
PS10R6	Vickers	10	**19**	3
" "	Knoop	10	**14**	3
PS15R1	Vickers	55	**12**	4
" "	Knoop	1.96	**17**	4

Table 5.10 Vickers and Knoop hardness of pressureless sintered materials.

The hardness of pressureless sintered materials is ~80% of the hot pressed materials but still comparable with the fully dense Syalon 101. Again there is

dependence upon the porosity level and adjusting for the presence of porosity gives **H_v(10)=19 to 24 GPa**.

Typical errors in these measurement arise from variations in the load applied between each indentation. Typically for 5 and 10 N loads the error was ~5-10%. Each measurement is an average of the diagonals of about 10 indentations and a typical standard deviation for measurement of the diagonal 2a was ±3 to 5% (the larger error being associated with the smaller indent). Combined these errors give an uncertainty in hardness of about 10 to 15% which translates to typical values of ±2 to 3 GPa in the highest harnesses. Low Knoop loads have larger errors caused by optical measurement of small Knoop indents. For a 1.96N load a typical error in the reported hardness is ±15%.

Sialon/TiB_2 composites exhibit high hardness values which have the potential for further improvement if the materials can be produced with less residual porosity. Hot pressed specimens exhibit the highest hardness due to the larger volume of TiB_2 present and the absence of intergranular phases.

5.4 Fracture Toughness

The measurement of fracture toughness by indentation methods is not ideal but was necessary in this instance because of the low volume of materials available and the need to correlate hardness and fracture toughness of surfaces to tribological performance. Generally, results from indentation methods can be expected to yield lower values than pre-cracked beam tests.[8].

5.4.1 Estimation of E for use in K_{Ic} Calculations.

The only method of calculation that does not require knowledge of E, the Young's Modulus, is from Evans and Charles[9] and this only gives a 20-30% confidence in the value of K_{Ic}. All other methods require a value for E. As mentioned in chapter 3 there are several methods for determining E.

The upper and lower limits for a 20vol% hot pressed material are given by: $E_{\Uparrow} = E_a V_a + E_b V_b$ and $E_{\perp} = \frac{E_a E_b}{E_b V_a + E_a V_b}$. Using E_{sialon}=300GPa, E_{TiB2}=500GPa and V_{sialon}=0.8 and V_{TiB2}=0.2, the limits become $E_{\Uparrow}$=340GPa and $E_{\perp}$=326GPa. However the presence of porosity effects the actual E of the material. One suggested relationship is $E = E_0(1 - 1.9P + 0.9P^2)$ where P is the fraction of porosity. For a typical hot pressed sample with ~4% porosity this makes the limits 313 and 300GPa respectively. Such estimation can be used to evaluate E for each material for the calculation of K_{Ic}.

Sample	Porosity (%)	E, Upper Limit (GPa)`	E, Lower Limit (GPa)
HP20OXY	3	320	307
20OXYAG	4	313	300
PS20R2	6	282	275
PS10R6	3	301	293
PS15R1	4	330	320

Table 5.11 Estimation of E for materials used in K_{Ic} measurements.

With the above values K_{Ic} can be calculated from the measurement of H_v and the length of the cracks around an indent.

5.4.2 Fracture Toughness Measurements

Fracture toughness was measured using Vickers indents which exhibited significant cracking at indent corners. Measurement of the surface crack lengths, c', were carried out by SEM after the tests had taken place. Each measurement is the result of ~10 indents. K_{Ic} was calculated using the method of Anstis et.al.[10] in order to be comparable with the majority of other research.

Sample	E (GPa)	H_v(5N) GPa [±2]	K_{Ic} MPa $m^{½}$ [±1.1]
20OXYAG	305	19	**4.23**
HP20Y1	225	8	**3.44**
PS10R2	279	16	**4.41**
PS10R2	279	16	**3.9**
PS10R6	297	19	**4.33**
PS15R1	300	12	**4.20**
Syalon 101	300	17	**4.4**

Table 5.12 Fracture toughness by indentation for hot pressed and pressureless sintered materials

An accepted value for syalon101 measured by a notched edge beam techniques is 7.7MPam$^{-½}$. By comparison the commercial grade of the same material that contains TiN (syalon501) has an accepted value for K_{Ic} of 5.7MPam^{½}. The value found here for sialon101 is lower and as such values for sialon/TiB_2 composites can be considered to be subject to the same increase if tested by similar techniques. A fuller discussion of the origin of the lower values measured by indentation techniques follows.

5.4.3 Discussion of K_{Ic} of Sialon/TiB_2 composites

K_{Ic} by Vickers indentation is known to produce lower values than by other methods such as single edge notched beam (SENB). For SiC the difference was found to be ~30% lower than the SENB results.[11] In work on in-situ reinforced Si_3N_4, Choi[12] measured K_{Ic} by several methods and found the measurement of indentation crack size to yield the lowest results by 46 to 83% (indentation measurement; K_{Ic}= 5.8MPa $m^{½}$, indentation strength; K_{Ic}=8.5MPa $m^{½}$ and chevron notched beam; K_{Ic}=10.7MPa $m^{½}$). Finally tests carried out on sialon101 in this work reveal a K_{Ic} that is substantially lower than the accepted value measured by notched beam techniques. Hence in comparing these results with others reported in the literature care should be taken to make compensation for the techniques. For example if the results of Choi are taken for Si_3N_4 materials then sialon/TiB_2 composites could be expected to have K_{Ic} values of between

6.0MPa $m^{1/2}$ and 8.0MPa $m^{1/2}$ when measured by other techniques. Fully dense specimen values for K_{Ic} depend upon the increase of hardness and modulus achieved by the fully dense material and in some K_{Ic} may actually be lower.

In some materials the crack system can continue to grow slowly after the load has been removed and such crack growth is enhanced in the presence of water vapour (humidity)[13]. Such crack growth could produce results that vary between specimens that were measured at different times after indentation and which produce lower values for K_{Ic} as c' increases with time. A growth of 13% has been observed in glasses in a period of 24 hours[14]. Post indentation slow crack growth will be more prominent in pressureless sintered materials where there may be some intergranular glass.

As a comparison indentation toughness was measured on Syalon 101 and found to be comparable under these conditions. Like hardness and modulus the presence of porosity can be expected to effect the measured K_{Ic} when compared to the K_{Ic} achievable by the zero porosity material. However, no simple relationship exists to compensate for porosity.

Values for K_{Ic} are subject to a range of errors arising from assumptions made in the calculations. Firstly, there are errors in E arising from estimation of the modulus of sialon and TiB_2. Reported values of E for sialon range form 290-320GPa and for TiB_2 common figures quoted are 500-550GPa. This is further complicated by the presence of intergranular phases in the case of pressureless sintered materials. Nothing is known about E or V for this phase since it difficult to measure and could be glass or crystalline. There are errors arising from the measurement of hardness (10-15%) and from the measurement of crack length (typically <10%). In addition there are inconsistencies between the available models for calculating K_{Ic} by indentation. For example, using values for 20OXYAG the Evans and Charles[9] model that does not require knowledge of E gives K_{Ic}=4.86 MPa $m^{1/2}$ and when estimates of E and H_v are included this rises to 6.89 MPa $m^{1/2}$. A method described by Lawn[15] yields K_{Ic}=3.43 MPa $m^{1/2}$ for the same material. The crack system for all these models is assumed to be

radial. If the cracks are Palmqvist in nature then the model proposed by Niihara[16] yields slightly increased values for K_{Ic} (between 4 and 17%) in all cases except for 20OXYAG. Finally, the models all assume a simple semi circular crack shape, in real systems this crack will be complex in nature and this will inevitably effect the applicability and accuracy of the model[17].

Thus K_{Ic} values measured for these materials should be regarded as having errors of ~25% (~±1.1 MPa $m^{½}$) in the worse case scenario.

Consideration of the above factors lead to the conclusion that sialon/TiB_2 composites have reasonable fracture toughness at least comparable with other Si_3N_4 materials and potentially greater that commercial particulate composites (syalon501). Measured values should only be compared with tests done in identical ways on similar materials. From comparison with work on similar materials using both indentation and other techniques the composites are expected to have a K_{Ic} in the region of 6-8 MPa $m^{½}$ when measured in these ways. Due to the small volumes of materials involved and the destructive nature of these tests no such experiments were performed.

5.4.4 Proposed Toughening Mechanisms in Sialon/TiB_2

SEM observations of the cracks around Vickers indents reveal that the crack follows an intergranular path through the matrix. The crack encounters TiB_2 particles and is either diverted around them or in some cases passes through them. A typical crack encounters several such events in its total length and interactions are frequently with 2 or more particles. The exact extent to which the crack is diverted is dependent on the particle size, morphology and orientation with respect to the crack. Even where the crack encounters no TiB_2 it follows the sialon grain boundaries which divert it from the straightest path.

Examples of this crack behaviour are shown in Figure 5.21.

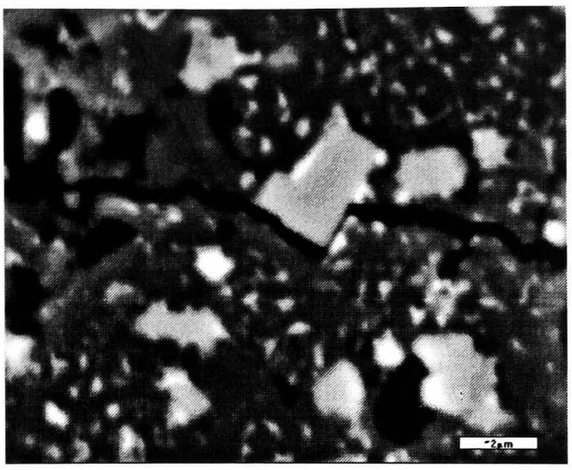

(a) micron bar =2μm

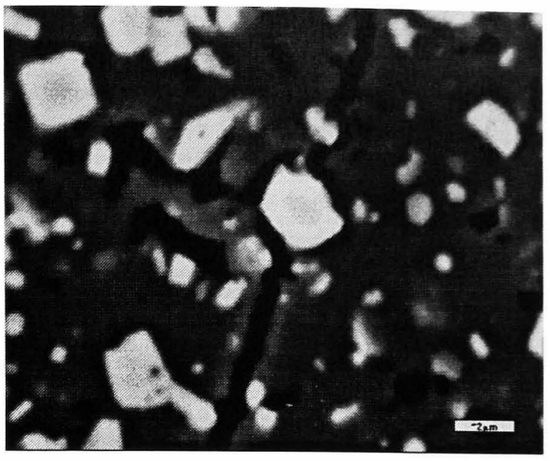

(b) micron bar =2μm

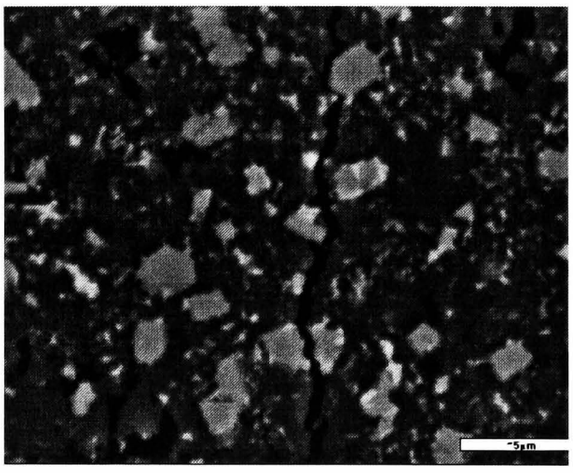

(c) micron bar =5μm

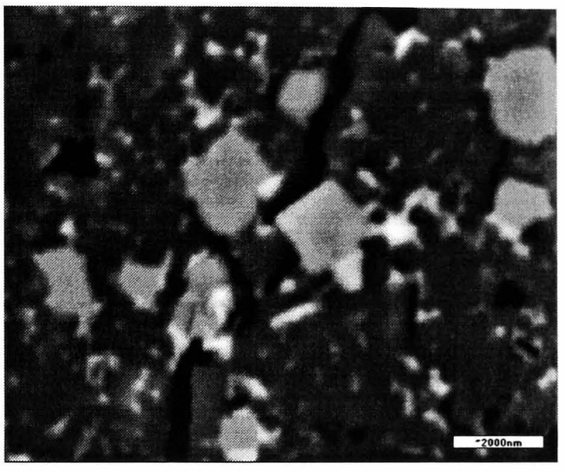

(d) micron bar =2μm

Figure 5.21 Several examples of crack interaction with TiB_2 particles in both hot pressed and pressureless sintered materials.

In addition to crack diversion the pull out of such grains from the matrix and the accompanying grain boundary friction and mechanical interlocking is also a possible toughening mechanism. The magnitude of the mis-match in thermal expansion coefficients for sialon/ TiB_2 composites is relatively large and gives rise to compressive radial stresses in the matrix of up to 1GPa. These stresses can act to resist crack growth and to close the crack front. The stresses are also anisotropic due to the anisotropy of the coefficient of thermal expansion in TiB_2 ($a=6.6x10^{-6}/K$, $c=8.7x10^{-6}/K$). This will also contribute to the deflection of the crack.

The presence of microcracks is difficult to demonstrate but the magnitude of the thermal coefficient mis-match is such that microcracks are possible.

5.5 Oxidation

The oxidation of Si_3N_4 ceramics can begin as low as 800°C forming a thin protective layer of SiO_2 according to:

$$Si_3N_4 + 3O_2 \Rightarrow 3SiO_2 + 2N_2$$

This describes low temperature oxidation of dense Si_3N_4 but at higher temperatures and in materials containing densification aids the situation is more complex. Oxidation is controlled in these materials by the rate of diffusion of oxygen into the material and metal ions to the surface. Some densification aids or their oxidation products can have high diffusions rates, allowing the Si_3N_4 to oxidise more quickly. In materials where the intergranular phase is a crystalline oxynitride the oxidation products can undergo large volumetric changes causing cracking of the surface, exposing fresh surface for oxidation.

Oxidation tests were not a major objective of this research but if the composites suffered from severe oxidation at low temperatures then they would be less useful for many applications. Many workers report oxidation of sialons during dry sliding wear tests and knowledge of the oxidation temperature of the specimens can give some indication of the flash temperatures achieved in dry sliding.

Two pressureless sintered samples containing 10 & 15 vol% TiB_2 and Y_2O_3 Al_2O_3 and SiO_2 glass densification aid were tested at 800°C, 900°C and 1000°C for upto 100 hours. Oxidation was measured by weight change and surface appearance.

PS15R1 was heated to 800°C in static air for 100 hours and weighed periodically. There was no significant weight change and no change in the optical appearance of the sample. Total weight gain over 100 hours was ~2.4mg. It is possible that there was some slight SiO_2 formation at the surface.

The same specimen was then heated at 900°C for 100 hours under the same procedure an gained and extra 2mg.

PS10R12 (96.5% t.d.) containing 10 vol% TiB_2 was heated at 1000°C in static air for 100 hours and weighed periodically throughout. The specimen did appear a lighter grey colour on the surface after a few hours in the furnace but measurement throughout the run showed no significant weight gain with the total gain after 100 hours of only 1.5mg. The approximate surface area of the sample was 8.4cm^2 making the oxidation resistance $1.8x10^{-5}$ g/cm^2 hours @ 1000°C. The oxidation resistance of TiB_2 is quoted as $3x10^{-4}$ g/cm^2 hours. If 10% of the surface is assumed to be TiB_2 then the expected gain from TiB_2 alone is 25mg. Clearly this is not occurring and is an indication that at least to 1000°C the oxidation resistance of sialon is retained in the presence of TiB_2 particles and yttria based sintering aid.

Despite there being no significant weight change there was some change on the surface of the material. SEM of the disc surface reveals the structures shown in Figure 5.22

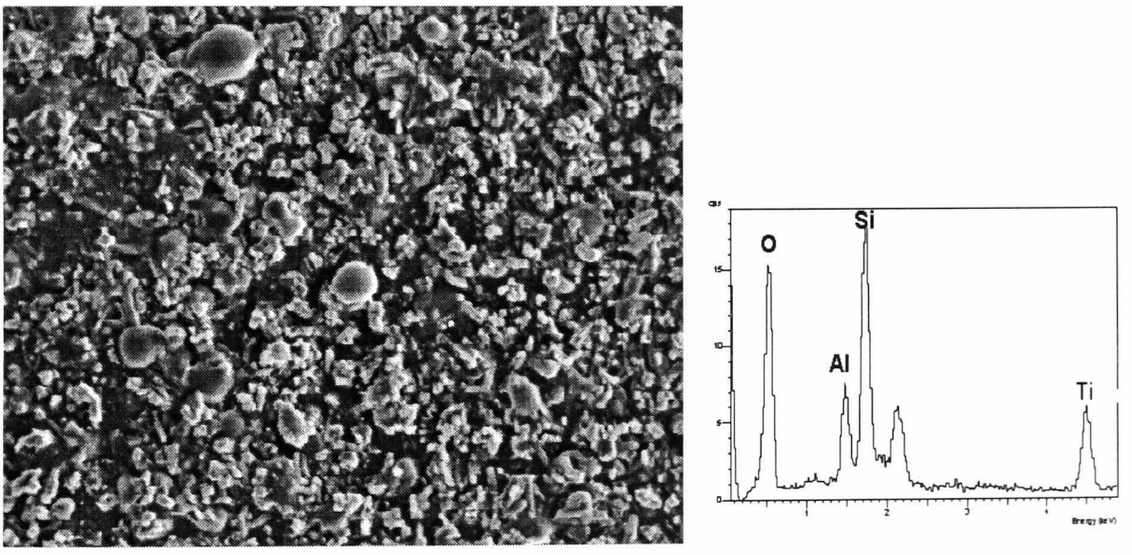

Figure 5.22 The surface of a pressureless sintered specimen after 100 hours in static air at 1000°C. EDX spectrum from area scan shows an increased oxygen content.

EDX analysis of these phases show that they have an increased oxygen content compared to the un-oxidised surface. Oxidation has occurred at the surface but has not penetrated the sample, probably due to the formation of a protective oxide layer through which the diffusion of oxygen is slow thus preventing further oxidation. XRD of the surface (Figure 5.23) did not show any oxidation

products because of the small amounts present and the possibility that they may be amorphous.

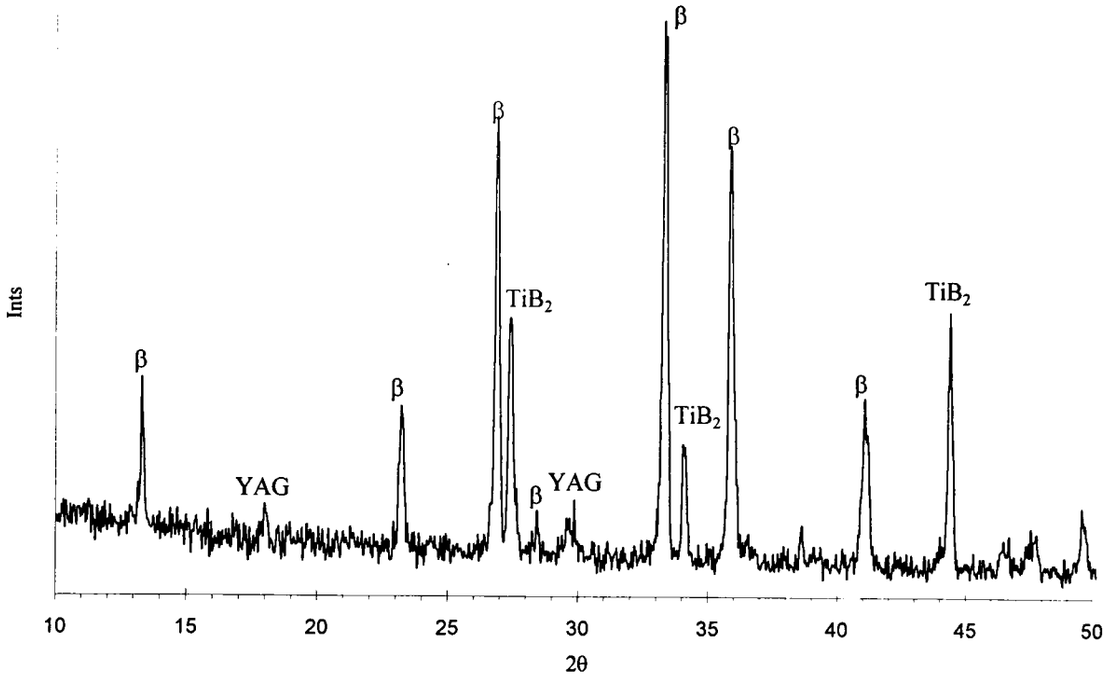

Figure 5.23 XRD from oxidised surface showing no crystalline oxidation products are evident.

5.6 References

[1] F. Hong, R.J. Lumby and M.H. Lewis, "TiN/sialon composites via in-situ reaction sintering", *J. Eur. Ceram. Soc.*, **11**, pp.237-39 (1993)

[2] Bor-Yuan Shew & Jow-Lay Huang, "Investigation of chemical reactions in TiB_2/Si_3N_4 composites", *Mater. Sci & Eng.*, A159, (1992), pp.127-33

[3] T. Eksröm & J. Persson, "Hot hardness behaviour of yttrium sialon ceramics", *J. Am. Ceram. Soc.*, **73** [10], pp.1722-24, 1989

[4] R.J. Lumby, University of Warwick, Private communication, May, 1994

[5] F. Hong, M.H. Lewis, "Ceramic matrix composites via in-situ reaction sintering", *Ceram. Eng. & Sci. Proc.*, **14**, 1993, p131

[6] S. Prochazka and C.D. Greskovich, "Development of a sintering process for high performance silicon nitride", AMMRC Tr., 78-32 (1978)

[7] V.S. Kirillov, V.I. Kovalenko, V.G.Marinin, I.T. Ostpenko and V.P. Podtykan, " Erosion of boron carbide under the action of cavitation", *Sov. J. Superhard Mater.*, **5**, 21, (1983)

[8] N. Miyahara, Y. Mutoh, K. Tanaka & M. Takahashi, "Fracture toughness evaluation of structural materials by various testing methods", *Trans. Japan. Soc. Mech. Eng.*, Part A, Vol 57, No.538, pp.1326-33, 1991

[9] A.G. Evans and E.A. Charles, "Fracture toughness dteremination by indentation", *J. Am. Ceram. Soc,* **59**, p.371 (1976)

[10] G.R. Anstis, P. Chantikul, B.R. Lawn and D.B. Marshall, "Indentation techniques for measuring toughness of ceramics", *J. Am. Ceram. Soc*, **64**, p.539, (1981)

[11] M. Srinivasan & S.G. Seshadri, "Application of single edged notched beam and indentation techniques to determine fracture toughness of alpha sic", *Fracture Mechanics of Ceramics Rocks and Concrete,* ASTM STP, 745, S.W Freiman & E.R. Fuller eds. American Society for Testing and Materials. 1981, pp46-68.

[12] S.R. Choi, J.A. Salem, "Crack-growth resistance of in-situ toughened silicon nitride", *J. Am. Ceram. Soc.* , **77** [4], pp.1042-46(1994)

[13] S.W. Freiman, "Brittle fracture of ceramics", *Bulletin. Am. Ceram. Soc.* Vol. 67, No. 2, pp.392-402, 1988

[14] S.S. Smith, P. Magnusen & B.J. Pletka, "Fracture toughness of glass using the indentation fracture technique", *Fracture Mechanics of Ceramic, Rocks & Concrete*, ASTM STP, 745, S.W Freiman & E.R. Fuller eds. American Society for Testing and Materials. 1981, pp. 33-45.

[15] B.R. Lawn, A.G. Evans and D.B. Marshall, "Elastic plastic indentation damage in ceramics: the median/radial crack system." *J. Am. Ceram. Soc*, **63**, p.574 (1980).

[16] K. Niihara, R. Morena & D.P.H. Hasselman, "Indentation fracture toughness of brittle materials for Palmqvist cracks", *Fracture Mechanics of Ceramics*,. Vol.5, pp97-105, 1983

[17] S.M. Smith & R.O. Scattergood, "Crack shape effects for indentation fracture toughness", *J. Am. Ceram. Soc.*, **75** [2], pp305-15, (1992)

Chapter Six

Tribology of Sialon/TiB_2 Composites

6. Tribology of Sialon/TiB_2 Composites

The tribological behaviour of sialon/TiB_2 composites was studied using the pin-on-disc apparatus described in chapter 4. Dry sliding and limited lubricated tests were performed with both self mated couples and other materials. Both the friction and wear of the materials were studied, including SEM observation and EDX analysis of wear surfaces, wear debris and tribofilms. The test conditions were varied to investigate the effect of load, speed and humidity on tribological behaviour.

6.1 Measurement of Friction

The magnitude of the frictional force experienced is important because it can influence wear and may be important in applications where low frictional forces are desired such as bearings. In order to understand the wear properties of a material system and to decide whether a material is suitable for a particular application it is necessary to know the value of μ and to understand how μ varies with different conditions.

To allow comparisons between different materials a standard set of test conditions was adopted. Except where it was deliberately varied the sliding speed was set at $0.05ms^{-1}$. The standard load used was a 1kg weight (actually 1008g) providing a force of 9.88N. The humidity in the apparatus enclosure was kept as close to 40%RH as possible during the tests. All specimens were finished to a 1μm finish, using water based diamond polishing, unless otherwise stated.

Measurement of friction was via the strain experienced by the load arm during the test and was continuously monitored. As is shown in Figure 6.1 the variation in the measured frictional force could be large. This is explained by consideration of the processes taking place at the pin-disc interface. The maximum force cannot be sustained indefinitely and the arm, once strained to the maximum, springs back. However, it never returns to its original zero strain position because of the continuing frictional force caused by the rotating disc.

Hence continuous monitoring of the strain in the load arm exhibits a range of values between the maximum and the minimum.

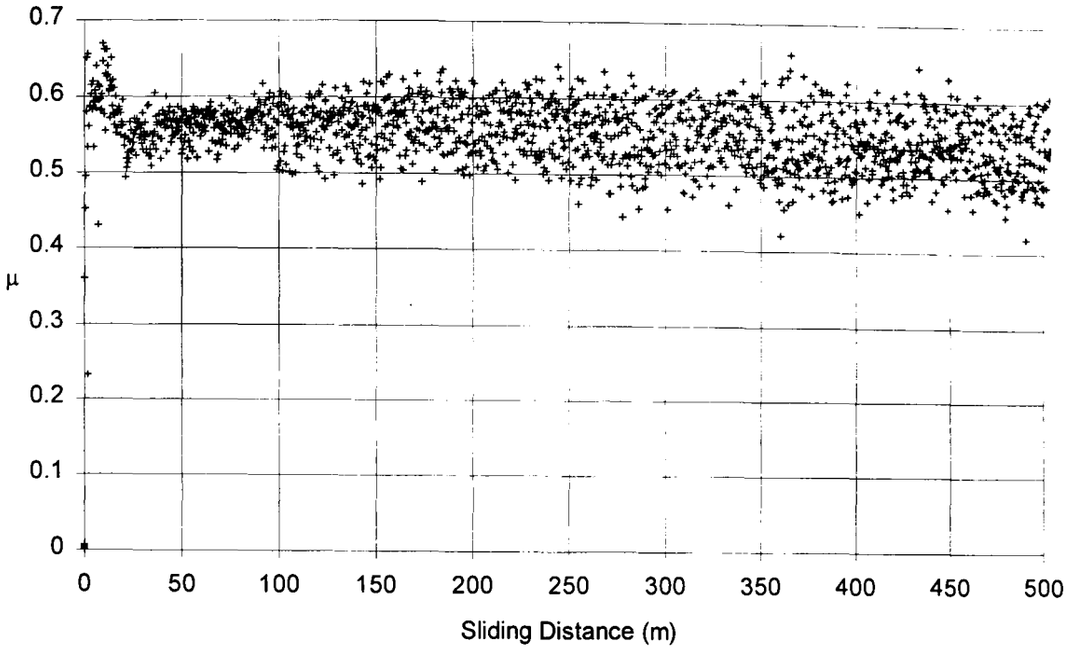

Figure 6.1 An example of the variation in the force experienced by the load arm during a test, giving rise to "variation" in the coefficient of friction (μ)

This variation can make reporting the coefficient of friction ambiguous. Although many researchers must experience the same problems they do not always report how they calculate μ from such data, the maximum or average being the two most obvious choices. As can be seen the difference between the two in the example given is as much as 0.15 (~30% error). In this work the value of μ reported is that calculated from the maximum frictional force experienced over a fixed time period (e.g. every 5 secs/0.25m during a test the maximum frictional force in that time/distance is used to calculate the coefficient of friction). Each point on a friction versus distance graph represents one such measurement. Error bars on each point vary slightly between tests, depending upon the amount of noise in the system, but generally are ~0.02-0.04.

6.1.1 Dry Sliding Friction:- Ceramic on Ceramic

Dry sliding pin-on-disc tests were carried out on several combinations of materials under the conditions listed in Table 6.1. Their microstructure and other properties are given in chapter 5.

Friction/sliding distance plots for the materials listed above are shown in Figure 6.2. The data recorded over the first few revolutions were recorded at more frequent intervals to improve resolution.

For a hot pressed material containing 20vol% TiB_2 (HP20) sliding on itself the value of μ rises rapidly from the start of the test and quickly acquires a steady state value of ~0.78±0.02 over 500m sliding. For the identical pin sliding on a pressureless sintered material containing 10vol% TiB_2 (PS10), μ was found to be significantly lower at μ=0.40±01 and also did not change with sliding distance. In the reverse situation, with a PS10 pin sliding on a HP20 disc, μ=0.56±0.01 and again was invariant with sliding distance.

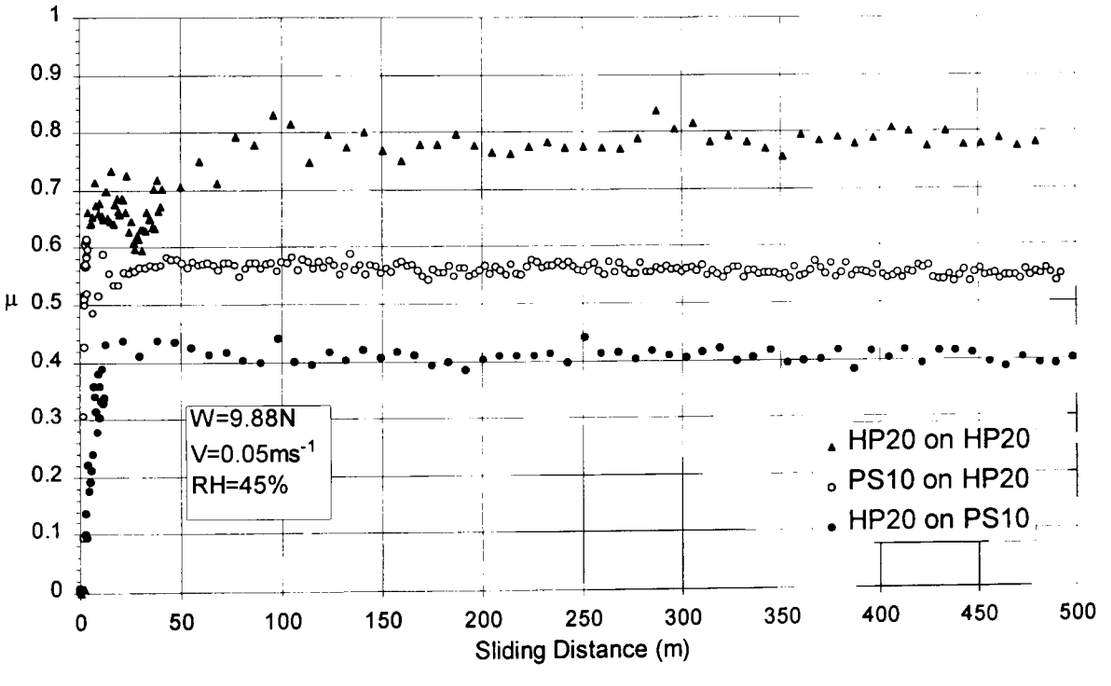

Figure 6.2 The coefficient of friction with sliding distance for HP20 on itself, HP20 on PS10 and PS10 on HP20.

Pin	Disc	Load (N)	Speed (ms^{-1})	RH (%)	μ	Figure number
HP20	HP20	9.88	0.05	40	**0.78**	6.2
HP20	PS10	9.88	0.05	43	**0.4**	6.2
PS10	HP20	9.88	0.05	45	**0.56**	6.4
Syalon 101	Syalon 101	9.88	0.05	37	**0.69**	6.5

Table 6.1 Coefficient of friction for sialon/TiB_2 composites. (HPx = hot pressed sialon with x vol% TiB_2, PSx = pressureless sintered sialon with x vol% TiB_2 [PS materials made with 15wt% sintering aid])

As a comparison material a commercial grade of sialon was tested under identical conditions. The Syalon 101 (Lucas Syalon Ltd) dry sliding on itself produced the trace shown in Figure 6.3. The μ reaches a steady state of 0.69±0.02 after an initial rapid rise similar to that found in sialon/TiB_2 composites.

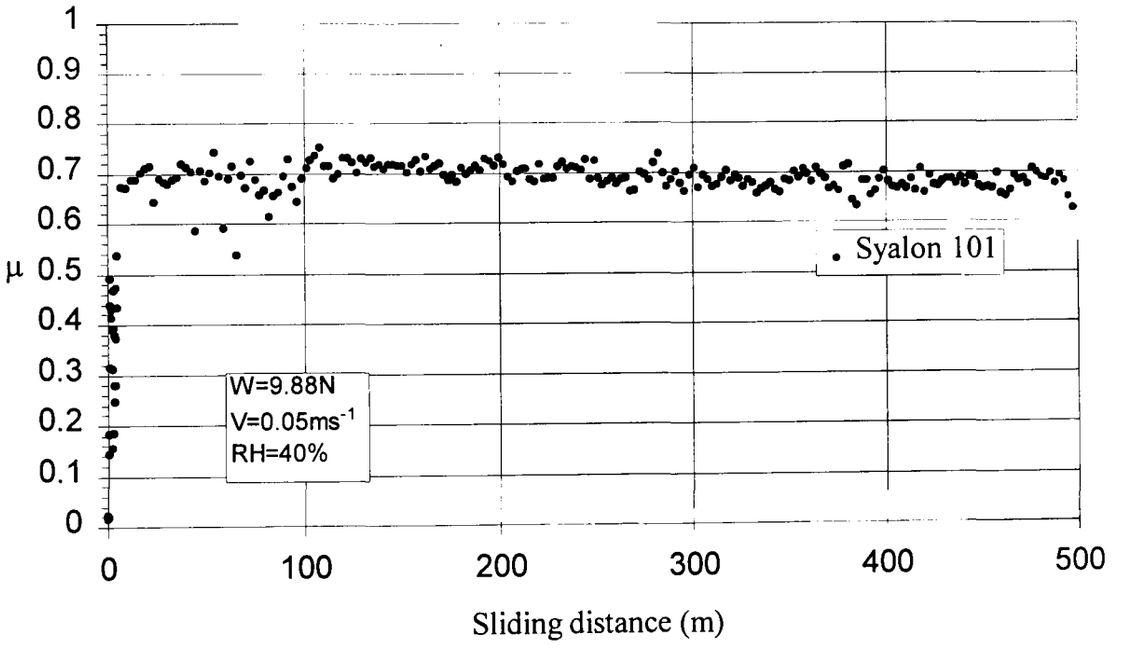

Figure 6.3 A commercial sialon grade tested under identical conditions to the sialon/ TiB_2 composites.

The coefficient of friction for these materials is seen to depend upon the type of material being tested i.e. hot pressed or pressureless sintered. Coefficients of friction are seen to be substantially lower when pressureless sintered materials are used as either the pin or the disc. These microstructures contain less TiB_2

and an yttria rich intergranular phase (YAG + glass). It is possible that the yttria phase contributes toward some form of solid lubricant that reduces friction more than for hot pressed materials, where very little yttria is present. Glassy phases[1], oxides and hydroxides[2,3] have all been observed on silicon nitride wear surfaces and it is the properties of these films that determine friction. The study of any tribofilm formation is carried out in later sections.

6.1.2 The Effect of Humidity

The humidity in the enclosure could be maintained at ambient (~40%RH) or it could be set at intermediate levels by the use of saturated aqueous chemical solutions. To test whether humidity would have some effect on the dry sliding friction a saturated solution of lead nitrate ($Pb_2(NO_3)_2$) was placed in the apparatus enclosure. When equilibrium was reached the chamber had a level of >95%RH.

Both hot pressed and pressureless sintered specimens were tested under standard test conditions (Table 6.2) and the results for friction are shown in Figure 6.4

Hot pressed materials exhibit an immediate rise to ~0.8 followed by a sharp drop to 0.6 in the first few metres of sliding, μ then rises throughout the test reaching a steady state of 0.80±0.02 between 120 and 500m. Pressureless sintered materials exhibited a noisy signal which may have been due to unresolved equipment noise. The noise obscures the detail of the change with sliding distance but it can be seen that μ reaches a steady level of ~0.55±0.07 after 100m.

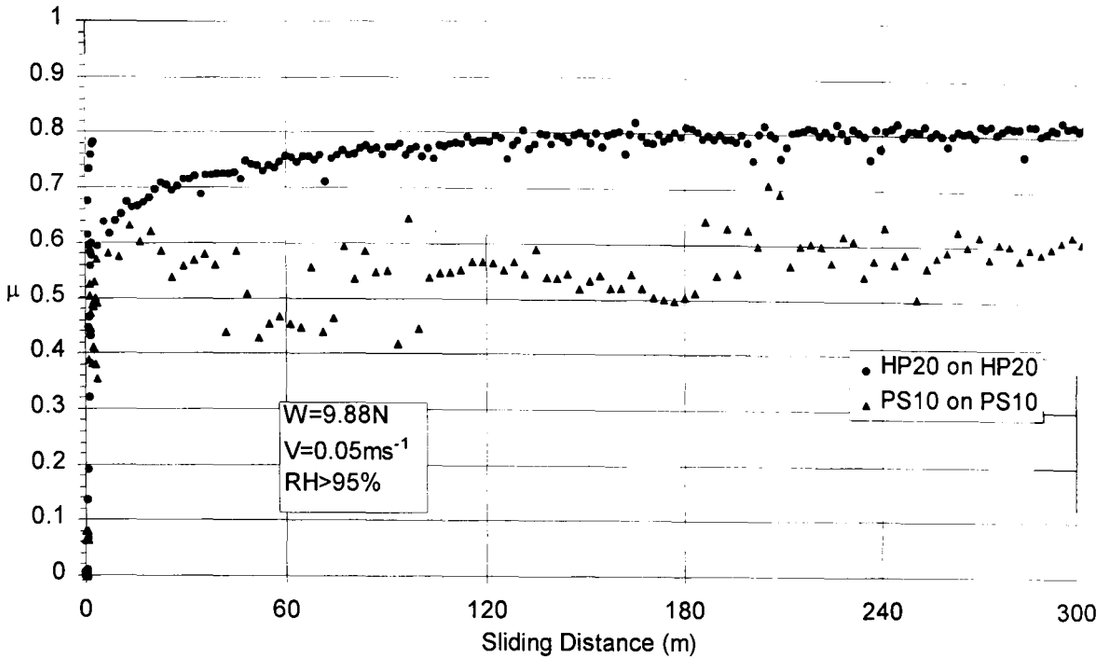

Figure 6.4 HP20 and PS10 materials sliding on themselves with >95%RH.

To test the materials under low humidity, compressed gases were used which have very low water contents. Since the chamber could not be evacuated compressed air was directed onto the sample via a nozzle that allowed the dry air to reach the pin/disc contact area before being contaminated with humidity from the surrounding air. This set up did, however, blow away much of the wear debris from the contact zone. The effect which removing the wear debris has on wear will be discussed in the later sections.

The friction versus distance plot is shown in Figure 6.5. The initial value of μ=0.79±0.02 was reached after ~50m and fell slowly throughout the test to a final level of 0.69±0.01 after 500m. Again this is comparable with the dry sliding at 40%RH of μ=0.78. The only discernible difference is the variation with sliding distance. For >95% both hot pressed and pressureless sintered materials exhibit a slight rise in μ with sliding distance. At 10%RH μ fell with sliding distance, but at 40%RH (Figure 6.2) μ reached a steady state value over the sliding distance used.

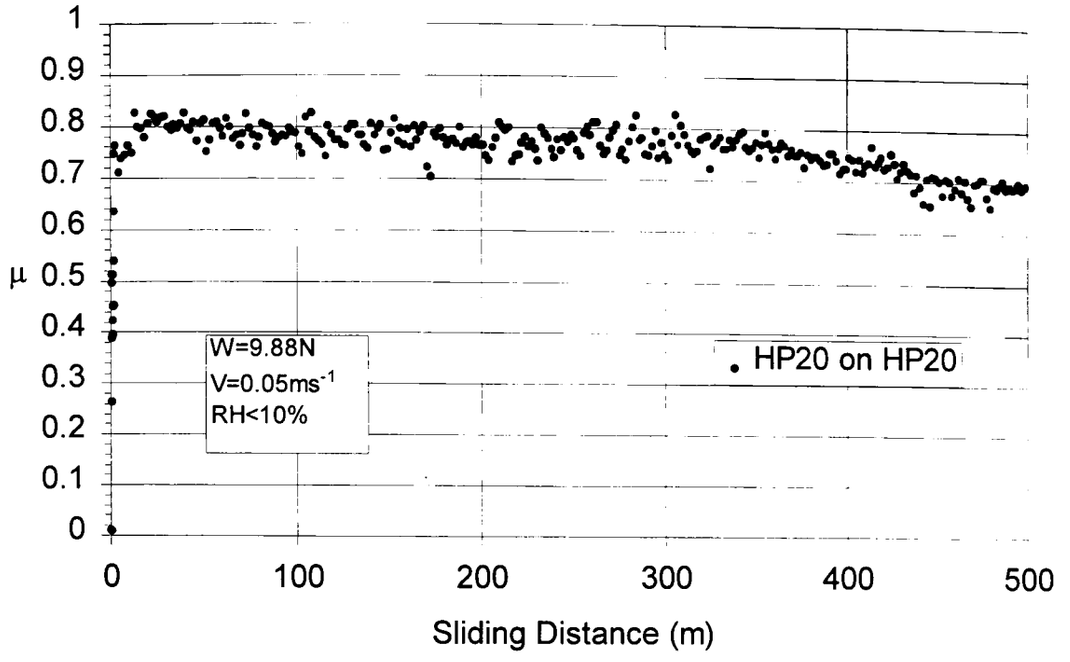

Figure 6.5 HP20 sliding on HP20 in flowing dry air (<10%RH).

Pin	Disc	Load (N)	Speed (ms^{-1})	RH (%)	μ	Figure number
HP20	HP20	9.88	0.05	>95	**0.80**	6.4
PS10	PS10	9.88	0.05	>95	**0.55**	6.4
HP20	HP20	9.88	0.05	<10	**0.79↓ 0.69**	6.5

Table 6.2 The effect of relative humidity on the sliding coefficient of friction.

6.1.3 Lubricated Sliding

Simple lubricated tests were possible by filling the sample holder with the lubricating fluid as shown in Figure 4.8.

Pin	Disc	Load (N)	Speed (ms^{-1})	Lub.	μ	Figure number
HP20	HP20	9.88	0.05	H_2O	**0.67**	6.7
HP20	HP20	9.88	0.05	Paraffin	**0.1-0.15**	6.8
PS10	PS10	9.88	0.05	Paraffin	**0.15-0.2**	6.9

Table 6.3 Materials and conditions for lubricated tests

De-ionised water was used with hot pressed 20vol% TiB_2 sialons sliding on themselves. The test was started under dry sliding conditions to record the dry sliding μ and the water was added at the point indicated. The results for the coefficient of friction are shown in Figure 6.6

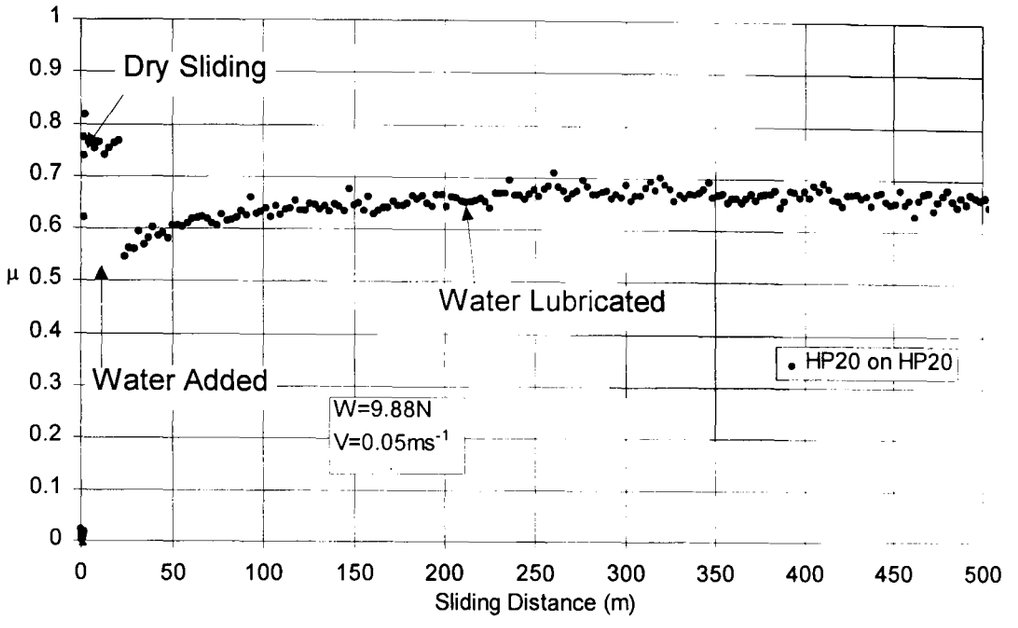

Figure 6.6 The effect of water lubrication on sliding friction of HP20.

The dry sliding value of μ was ~0.76, the addition of water reduced μ to 0.56 initially but μ slowly rose throughout the test to a steady state value of μ=0.67±0.01 after 500m. This is contrary to reports by other workers who describe a rapid reduction in friction with sliding distance from an initial value of μ=0.7 [4] (W=10N, R=10mm,V=0.1ms^{-1}) This was accompanied by the production of a very smooth surface finish by chemical wear leading to boundary lubrication. The high value seen here is most likely due to the initial damage caused by the dry sliding part of the test. This damage will have introduced an uneven wear track that could not be smoothed by chemical polishing. Hence lubricated sliding is sensitive to the initial state of the surface. If the surface is damaged then boundary lubrication breaks down and higher friction (and wear) occur,

Paraffin was also used as a lubricant for both hot pressed and pressureless sintered sialons containing 20vol% and 10vol% TiB_2 respectively. The results are shown in Figure 6.7 and Figure 6.8

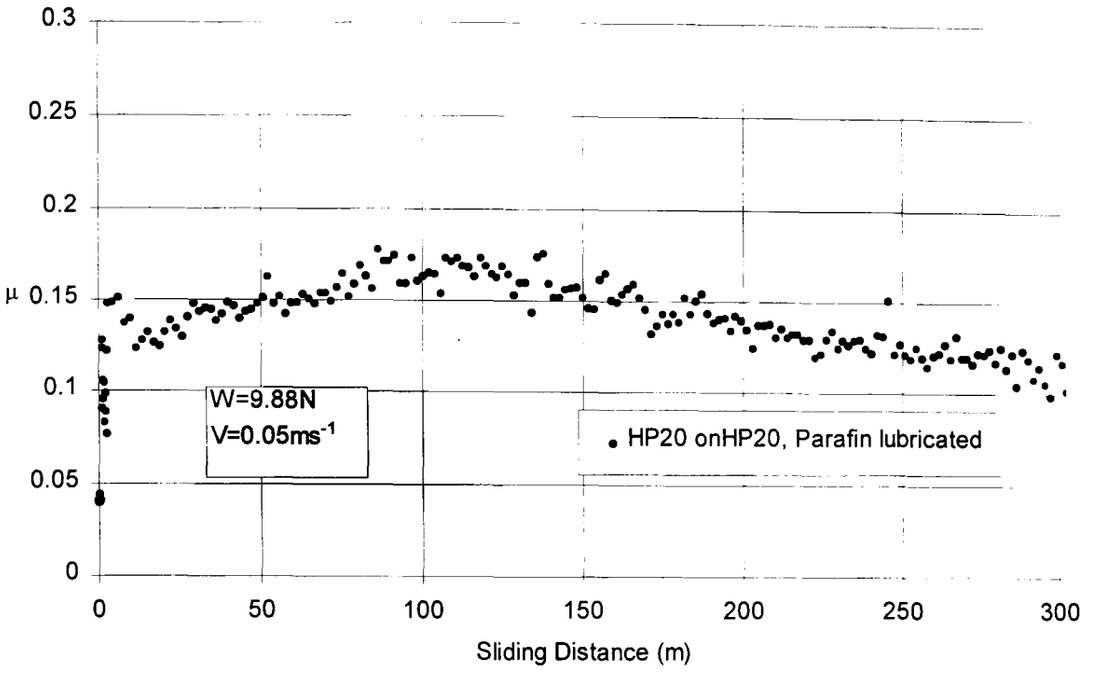

Figure 6.7 HP20 sliding on itself in paraffin.

The value of μ for both is significantly lower than for dry or water lubricated sliding. For the hot pressed material μ reached a peak of 0.17 after 120m and then slowly falls to ~0.12 after 300m. For the pressureless sintered material μ rises to a peak of 0.25 before experiencing a minimum of 0.12 at 150m followed by a slow rise to 0.18 after 500m. Examination of the apparatus showed that a component rubbing against the specimen holder may account for the initial rise to 0.25.

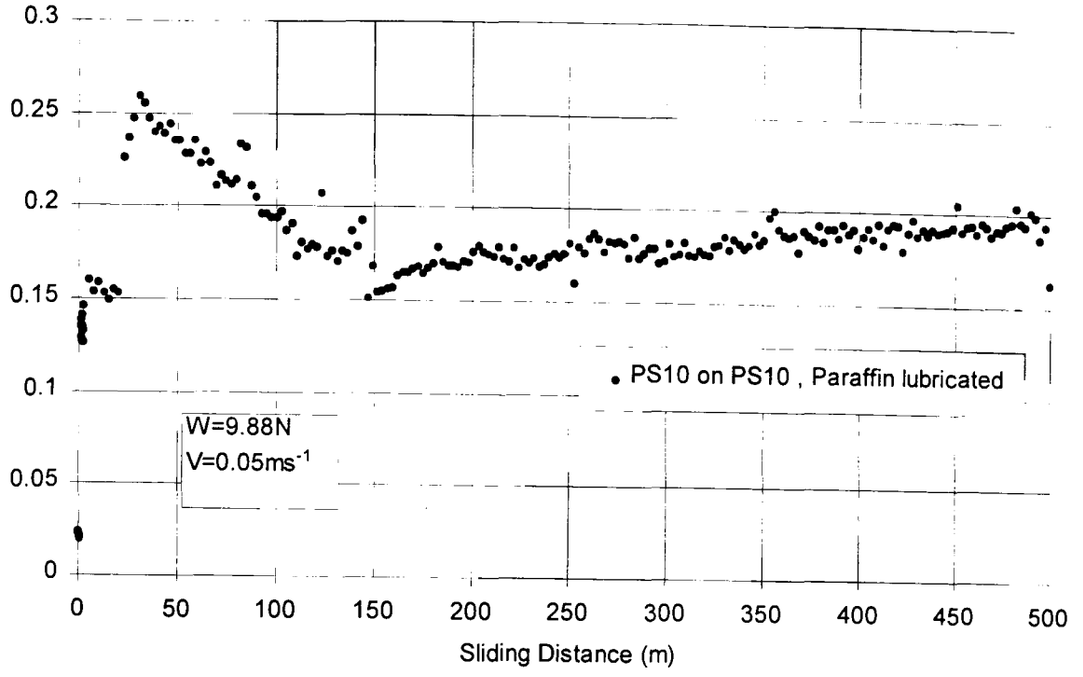

Figure 6.8 PS10 sliding on itself in paraffin.

Unlike for water these samples were not subject to dry sliding before lubrication was added. Hence, boundary lubrication is active from the beginning of the test.

6.1.4 The Effect of Load.

A hot pressed composition was tested under different loads to examine the dependence of friction on load.

The conditions for the tests are shown in Table 6.4. The results for 9.88N have been shown in Figure 6.2.

Pin	Disc	Load (N)	Speed (ms^{-1})	RH (%)	μ	Figure number
HP20	HP20	**9.88**	0.05	40	**0.78**	6.2
HP20	HP20	**4.91**	0.05	47	**0.71**	6.14
HP20	HP20	**1.96**	0.05	44	**0.6↓0.4**	6.15

Table 6.4 Materials and conditions for load variation test on HP20 materials.

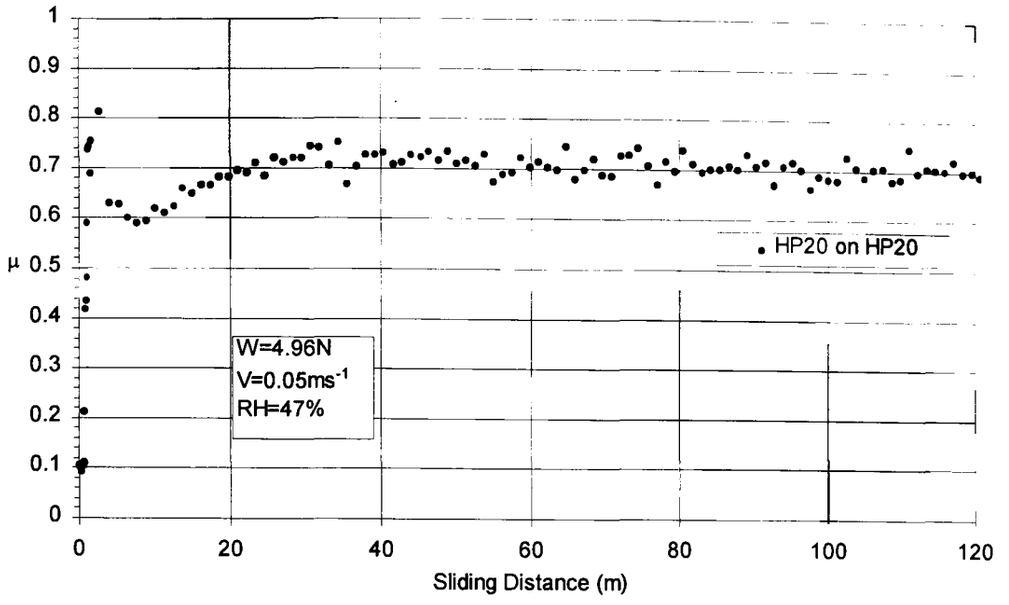

Figure 6.9 The coefficient of friction for HP20 under 4.91N load.

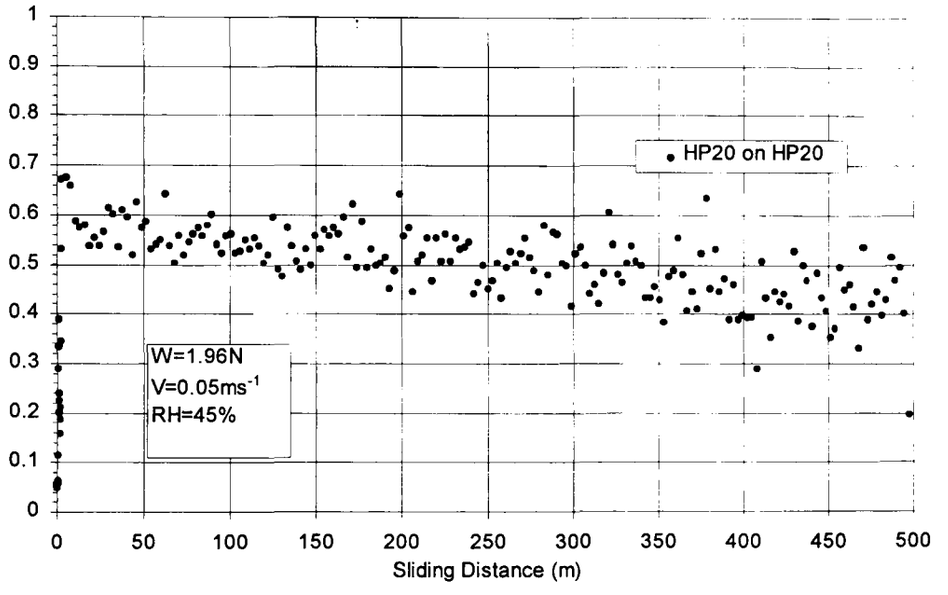

Figure 6.10 The coefficient of friction for HP20 under 1.96N load.

For 9.88N the steady state μ=0.78 (see Figure 6.2), under 4.96N load μ attained a steady state value of 0.71 and under 1.96N μ was lower with an initial steady state of μ=0.6 initially but falling over 500m to μ=0.4. The increased noise in the lowest load result is due to the reduced magnitude of the frictional force and this load is the lowest practical with the current apparatus. Hence there is a weak dependence of μ with load for hot pressed materials and under the lowest load friction fell with sliding distance.

6.1.5 The Effect of Sliding Speed

In order to assess the effect of sliding speed on μ the sliding speed was increased to 0.1ms^{-1} for a hot pressed sialon with 20vol% TiB_2 sliding on itself. The results are shown in Figure 6.11. The value of μ sliding at 0.05ms^{-1} was ~0.78, at 0.1ms^{-1} steady state μ=0.6±0.04 after an initial peak of 0.68.

Pin	Disc	Load (N)	Speed (ms^{-1})	RH (%)	μ	Figure number
HP20	HP20	9.88	**0.1**	43	**0.6**	6.13

Table 6.5 Material and conditions for variation of sliding speed.

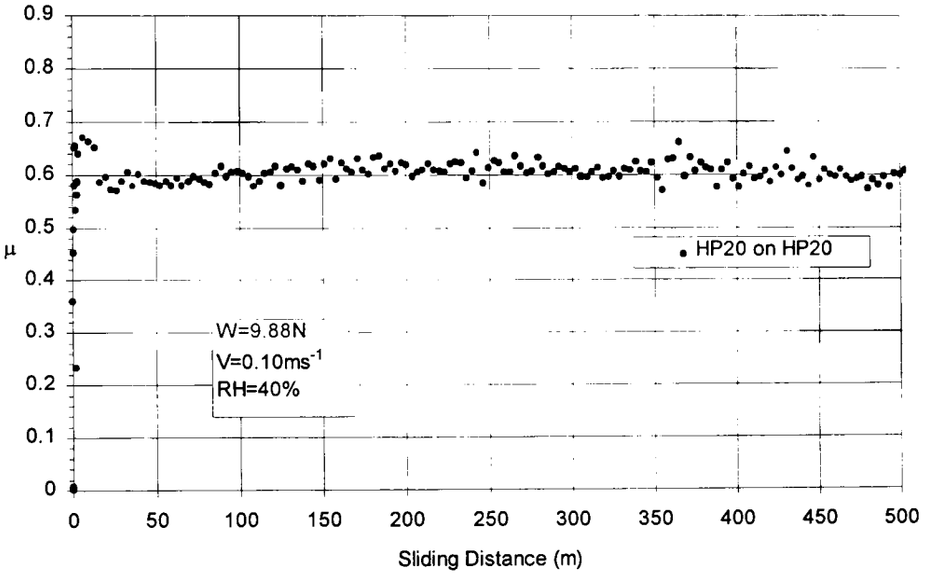

Figure 6.11 HP20 pin sliding on itself at 0.1ms^{-1}

The sliding speed was also varied from 0.01 to 0.125ms^{-1} continuously during a test in the sequence 0.01, 0.025, 0.05, 0.075, 0.1, 0.125. The coefficient of friction was recorded over 20m at each speed and the speed was then increased. To test for any change in the surface condition that takes place at higher speeds the sliding speed was then reduced in the same increments and friction recorded. The results are shown in Figure 6.12 & Figure 6.13.

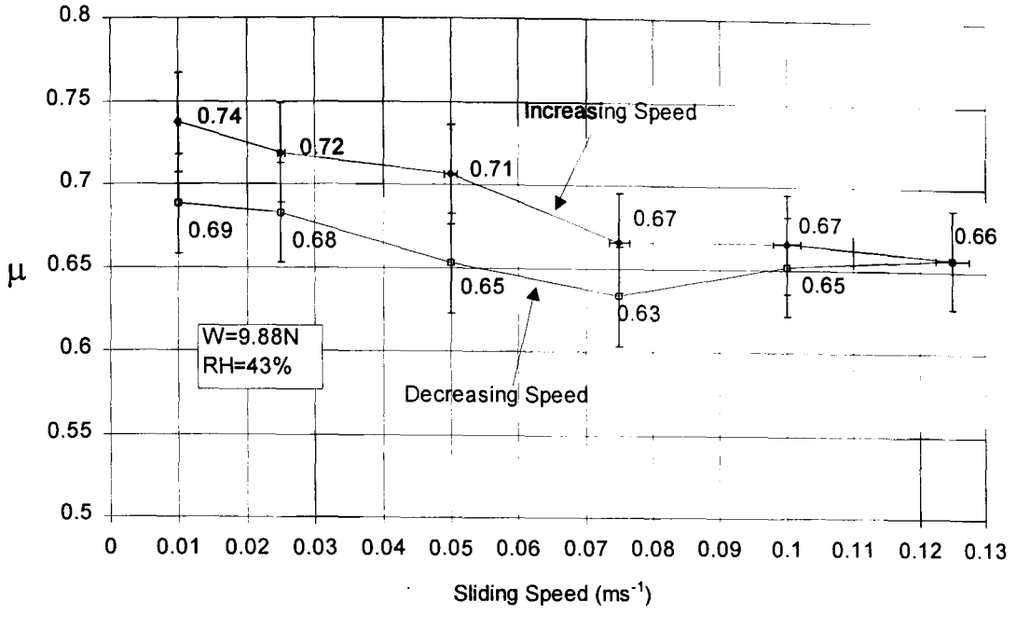

Figure 6.12 Variation of μ with sliding speed for HP20 material.

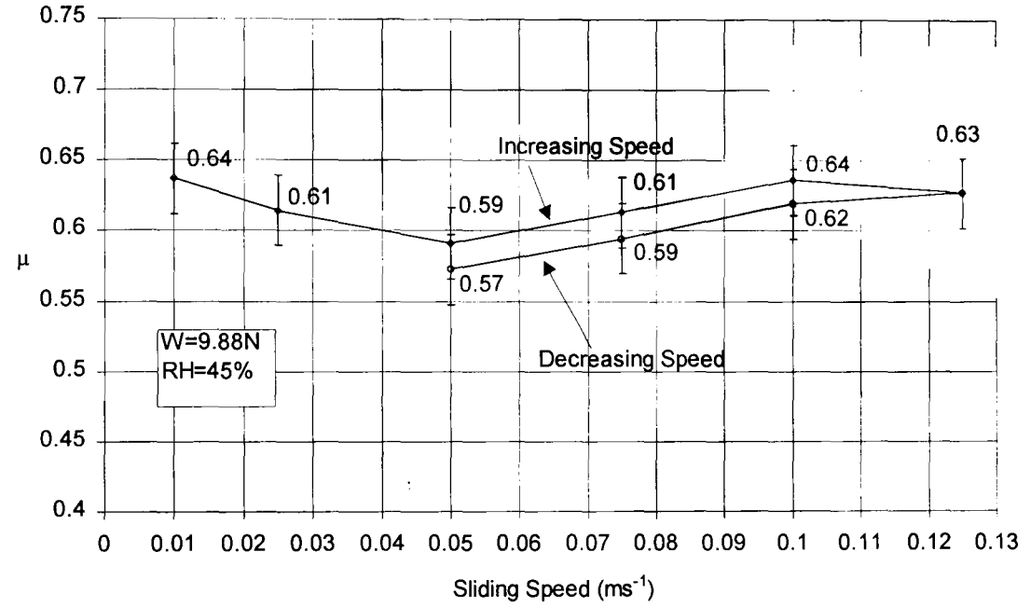

Figure 6.13 Variation with sliding speed for PS10 material

The results for pressureless sintered materials at $0.05ms^{-1}$ are higher than that recorded previously. It is possible that the sliding at slow speeds preceding the measurement at $0.05ms^{-1}$ has changed the nature of the surface, affecting the coefficient of friction. As will be shown later tribofilm formation occurs in these materials and in this case the slow sliding speeds and short sliding distances may not have produced the same conditions at the interface experienced in the previous test.

The results demonstrate a fall with sliding speed of μ for hot pressed material. As the speed was reduced the measured values of μ were consistently lower than those measured with increasing speed. This is attributed to changes in the nature of the contact at the higher speeds which then remain in place during the reduction of speed. The flash temperature at asperity contacts has been shown to vary greatly with increasing sliding speed[3] by as much as 1350°C. It is proposed that it is this temperature difference that is responsible for the change in interface at higher speeds and that the properties of the modified surface affect the friction of the system.

For pressureless sintered materials there is an initial drop but a minimum occurs at $0.05ms^{-1}$ before μ rises again. On the reduction of speed a similar, but less pronounced, effect is observed to that seen in hot pressed materials. These materials contain less TiB_2 and more yttria phase than hot pressed materials and this may be contributing to the nature of the interface between the tribopair resulting in slightly differing behaviour between the two grades.

6.1.6 Pre-oxidised Surfaces

The examination of wear surfaces (see later sections) shows the presence of wear debris and tribofilms that have a high oxygen content. It is possible that these films can protect the surface from wear and reduce friction. To test this proposition a PS10 specimen that had been used in an oxidation test (100hrs @ 1000°C) and had been seen to have an oxide surface layer (see figure 5.22) was tested under standard conditions.

The results for friction are shown in Figure 6.14. Initially $\mu=0.5$ but rises steadily throughout the test to $\mu=0.67\pm0.02$ after 100m. It is apparent that pre-oxidising the surface does not form a low friction coating. In fact μ reaches higher values than for smooth un-oxidised surfaces. It is proposed that the oxidised surface is soon sheared away by high initial stresses and fresh un-oxidised surface is revealed. It is possible that this surface may have been affected by the oxidation and this may explain the slightly higher friction than for non-oxidised surfaces.

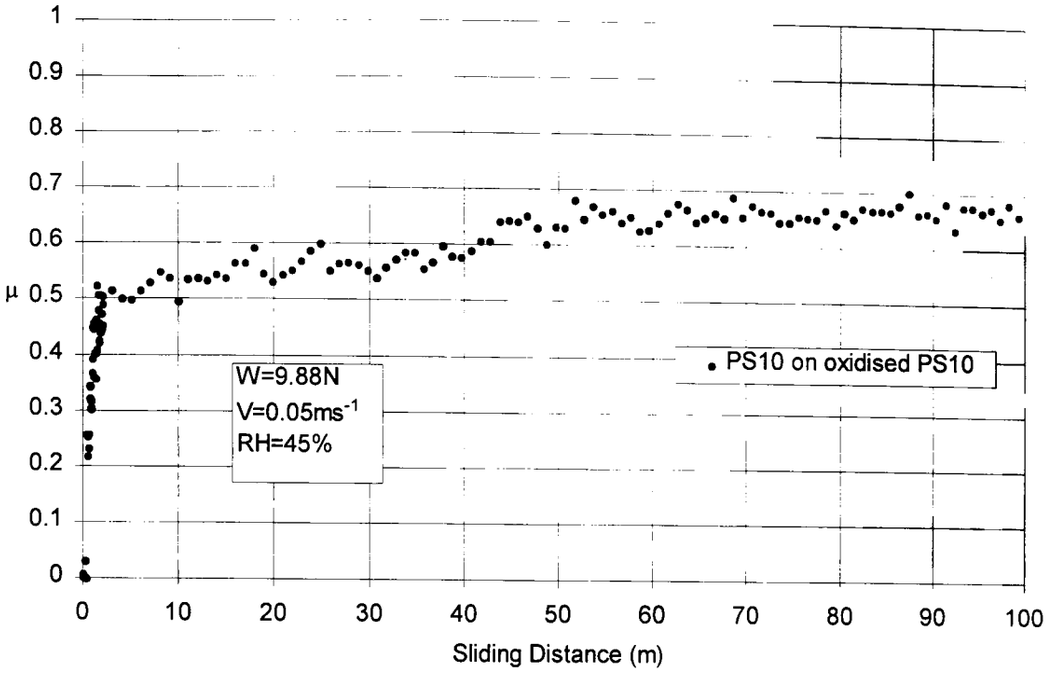

Figure 6.14 The coefficient of friction for a PS10 pin sliding on an oxidised surface of a PS10 disc.

6.1.7 Dry Sliding Friction:- Steel on Ceramic.

In the literature on the subject many workers use steel pins or discs to investigate the wear of ceramics[5,6]. Silicon nitride ceramics are often used as cutting tools for steel and hence the interaction of steel with the ceramic is of interest. A number of steel pins were prepared to the same specification as the ceramic specimens and were used with standard test conditions to determine the friction and wear of the sialon/TiB_2 composites on dry sliding with steel.

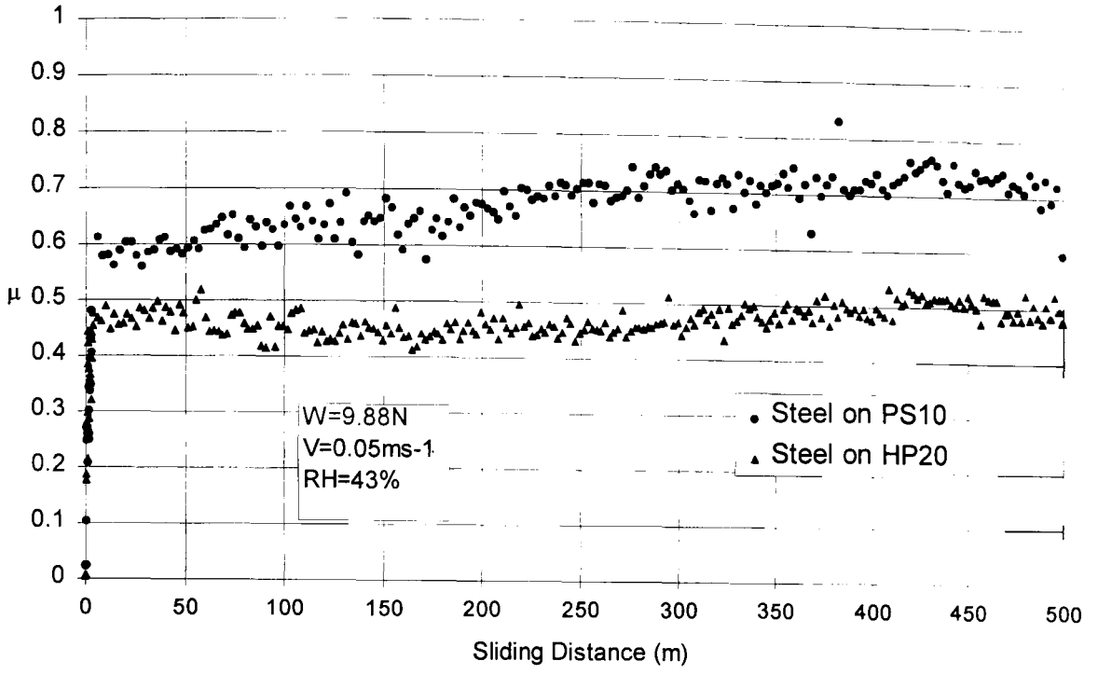

Figure 6.15 Steel pin sliding on HP20 and PS10 discs.

Steel on a hot pressed material exhibits μ=0.47±0.03 while on pressureless sintered materials μ=0.60±0.04 rising to 0.71±0.03 after 500m. These result closely agree with values reported by Zhao for HP Si_3N_4 of μ=0.41 (W=58N, V=1.6ms^{-1}) and Andersson[2] for a sintered Si_3N_4 of μ=0.68 (R=9.5-11mm, W=10N, V=0.2ms^{-1}, RH=50%). Thus the friction against a steel pin of a sialon/TiB_2 composite is comparable to silicon nitride materials containing no particulate inclusions.

Pin	Disc	Load (N)	Speed (ms^{-1})	RH (%)	μ	Figure number
Steel	HP20	9.88	0.05	40	**0.47**	6.15
Steel	PS10	9.88	0.05	44	**0.6↑0.71**	6.15

Table 6.6 Materials and conditions for dry sliding of steel on ceramics

Summary of the Study of Friction.

The values of the coefficient of friction for sialon/TiB_2 composites sliding on themselves are comparable with those found by other workers for silicon nitride and sialon ceramics[7,8]. Tests on syalon 101 using the same apparatus also shows comparable levels of friction. Tribological studies under similar conditions on other Si_3N_4 particulate composites have found that the change in μ is dependent

upon the type of reinforcement used. e.g Si_3N_4-SiC & Si_3N_4-BN had a higher μ but Si_3N_4-TiC had a lower μ than the matrix material alone.[9]

It appears that the TiB_2 content does not play a major role in determining the coefficient of friction but that the presence of yttria in the pressureless sintered material is responsible for a lower coefficient of friction. In fact pressureless sintered materials show a significantly lower μ than hot pressed materials. It can be seen that it is the disc material that influences the lower friction results with the lowest values achieved when the disc was a pressureless sintered material.

Similarly the friction of steel on sialon/TiB_2 composites exhibits values similar to those reported in the literature[10]. Again the two grades of material exhibited slightly different values for μ. In fact for steel on ceramic the pressureless sintered material exhibited the higher coefficient of friction, the inverse of the ceramic on ceramic situation.

The effect of relative humidity on the coefficient of friction was small. At 10, 40 and 95%RH the value of μ did not significantly change. (μ=0.8@>95%RH, μ=0.78@40%RH and μ=0.7@<10%RH). These results are in good agreement with work by Fischer and Tomizawa[7] who demonstrated a similar effect for Si_3N_4.

When lubricated with water, tests on hot pressed materials demonstrate a reduction in μ of only 0.1. This is in agreement with Fischer and Tomizawa (μ=0.7) but is in contrast to other workers who reports a rapid decrease in μ for sialon sliding in water.[4] This effect is linked with the production of perfectly smooth surfaces by tribochemical wear allowing boundary lubrication by the water. In this work either the conditions (i.e. speed, load etc.) were insufficient for boundary lubrication to take place or the surface damage imposed initially by the dry sliding prevented it occurring. The materials are seen to respond well to lubrication by paraffin with a large reduction in the coefficient of friction for both materials. The paraffin is providing boundary lubrication between the two materials reducing friction and wear.

For varying loads between 9.88 and 1.96N the coefficient of fiction was seen to decrease slightly with decreasing load for hot pressed materials. It should be noted that in tests with a fixed load the actual stress experienced by the material falls rapidly because of the increased area of contact formed by wear of the pin. In such a situation μ is independent of decreasing stress where a steady state coefficient of friction is observed. However, stress varies most at the beginning of the test where the measured friction is increasing and these two effects, "wearing in" and the change of friction with decreasing applied stress, cannot be observed independently.

One feature that is found in many friction/sliding distance plots is the initial high value of μ followed by a fall to a lower steady state level. It is possible that this is caused by the high stresses resulting from the initial small area of contact. Calculations show that the maximum pressure applied at the beginning of a test is of the order of 2 to 3GPa. The resulting high stresses may cause fracture and grain pullout leading to rough surfaces and high friction. The formation of tribofilms soon after sliding has begun can reduce friction by "healing" the rough surface by filling damage with wear debris and providing a smoother sliding surface. A discussion and evidence for such mechanism is given in the next section which examines the nature of wear in these materials.

6.2 Wear of Sialon/TiB_2 Ceramic Composites

The tests described in section 6.1 for the study of friction were also used to study the wear behaviour of the composites. Primarily this consisted of the measurement of the volume of material lost during a test and calculation of the wear coefficient, k. Also of interest were the actual mechanisms of wear that take place in these composites. This involved SEM observation of wear surfaces and EDX analysis of any wear debris and tribofilms.

6.2.1 The Wear Coefficient, k

The wear coefficient has been defined as the amount of material removed per unit load per unit sliding distance and has units of $mm^3\ N^{-1}\ m^{-1}$. The lower the

value of k the better the material's resistance to wear. Ideally k is calculated from the volume removed from the pin and the disc. However, it was found in practice that the measurement of the volume removed from the disc was not practically possible. Attempts were made to measure the wear scar depth and profile but inconsistencies resulted in widely varying results for the same sample. The formation of tribofilms, the small volumes removed and the uneven nature of the worn surface all make measurement of disc wear too inaccurate to be of practical use. A schematic of the problems encountered is shown in Figure 6.16 Even with the tribofilm removed by careful polishing the wear scar itself was filled with debris and could not be easily measured.

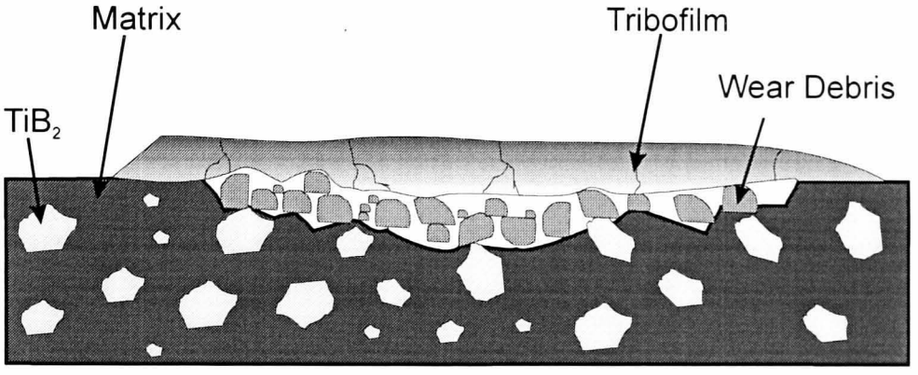

Figure 6.16 Cross section through a wear track showing the obscuration of the worn volume by wear debris and tribofilms.

The worn volume of the pin was therefore used as a performance indicator for wear tests and was measured by optical and electron microscopy as described in chapter 4. The wear coefficients measured for several combinations of sialon/TiB_2 materials under standard test conditions are given in Table 6.7

Pin	Disc	Conditions W(N), V(ms^{-1}), RH(%), d(m)	Volume (mm^3)	Wear Coefficient, k $x10^{-6}$ ($mm^3 N^{-1} m^{-1}$)
PS10	HP20	W=9.88, V=0.05, RH=48, d=500	$5.5x10^{-3}$	**1.1**
HP20	PS10	W=9.88, V=0.05, RH =41, d =658	$16.4x10^{-3}$	**2.5**
HP20	HP20	W=9.88, V=0.05, RH=40, d=300	$14x10^{-3}$	**4.6**
HP20	HP20	W=9.88, V=0.05, **RH=95**, d=700	$30.4x10^{-3}$	**4.4**
PS10	PS10	W=9.88, V=0.05, **RH=95**, d=500	$49x10^{-3}$	**9.8**
HP20	HP20	**W=4.1**, V=0.05, RH=45, d=250	$13x10^{-3}$	**23**
PS10	PS10	**W=4.1**, V=0.05, RH=45, d=250	$26x10^{-3}$	**21**
HP20	HP20	**W=1.96**, V=0.05, RH=45, d=500	$7.2x10^{-3}$	**7.4**
Syalon 101	Syalon 101	W=9.88, V=0.05, RH=40%, d=500	$31x10^{-3}$	**6**

Table 6.7 Wear coefficients measured for different material pairs under "dry" sliding conditions. Calculations are for the pin material. Characters in bold indicate conditions varying from the standard test.

The material with the best wear resistance under the conditions used was seen to be a pressureless sintered 10vol% materials sliding on a hot pressed 20vol% material, with the next best being the inverse situation. This suggests that the pressureless sintered material does not wear as much as the hot pressed material despite the lower volume % of TiB_2 present. These results correspond with the results for friction where the lowest friction was observed for these two material combinations. Hot pressed materials sliding on themselves show reasonable values for k of the order of 10^{-6} $mm^3N^{-1}m^{-1}$.

Sliding in an atmosphere at >95% humidity affected the wear resistance of the two grades of material differently. Sliding on itself, PS10 showed increased

wear while HP20 remained effectively unchanged. At lower loads both HP20 and PS10 exhibited an *increased* wear coefficient. For the lowest load practical (1.96N) there was also an increase over the value found at 10N for hot pressed materials. As a comparison Syalon 101 sliding on itself exhibited a value of k of 6 $mm^3 N^{-1} m^{-1}$ which is comparable with the results for the composites. Again it must be noted that syalon 101 is fully dense whereas all composite samples contained 3-7% residual porosity which has been shown to affect other properties.

Under lubricating conditions the following wear coefficients were measured.

Pin	Disc	Conditions	Volume (mm^3)	Wear Coefficient, k ($mm^3 N^{-1} m^{-1}$)
HP20	HP20	W=9.88N, V=0.05ms^{-1}, H_2O	$1.5x10^{-3}$	**$8.7x10^{-6}$**
HP20	HP20	W=9.88N, V=0.05ms^{-1} Paraffin	$20x10^{-6}$	**$6x10^{-9}$**
PS10	PS10	W=9.88N, V=0.05ms^{-1}, Paraffin	$43x10^{-6}$	**$8.8x10^{-9}$**

Table 6.8 Wear coefficient for sialon/TiB_2 composites under lubricated conditions.

For water the value of k is slighter higher than for dry sliding suggesting that water was not capable of separating the two surfaces.

Clearly the paraffin is separating the two surfaces with boundary lubrication for most of the sliding as shown by the friction results for these tests. In fact most of the material lost was probably removed in the first few metres of sliding where the stresses were high and the contact areas small and the materials may have been in contact.

The test carried out on a pre-oxidised surface (W=9.88N, V=0.05ms^{-1}, RH=45%, d=100m) showed a value of k of $13x10^{-6}$ $mm^3N^{-1}m^{-1}$ which is substantially higher than sliding on an un-oxidised smooth surface. This may be

due to the increased roughness of the surface caused by the formation of surface oxides (see figure 5.22).

The wear of ceramic materials has been shown to be complex and involve more than one mechanism. The possible processes taking place include: wear by brittle fracture and grain removal, the formation of wear debris and their subsequent interaction within the contact zone, the tribo-chemical reaction between materials and with the atmosphere and the formation of tribofilms. To examine the wear processes that take place in these composites the techniques described in chapters 3 and 4 were used for the examination of wear surfaces, wear debris and tribofilms.

Initial evidence for the influence that tribo-chemical reactions may have on the wear performance comes from experiments performed in dry flowing gases of nitrogen and air. The results for these tests are shown below.

Pin	Disc	Conditions	Volume, mm^3	**k, ($mm^3 N^{-1} m^{-1}$) x10^{-6}**
HP20	HP20	W=09.88, V=0.05, RH<10%, d=540, **DRY NITROGEN**	1.2	**220**
HP20	HP20	W=09.88, V=0.05, RH<10%, d=500, **DRY AIR**	0.34	**70**

Table 6.9 Wear coefficients for HP20 materials with different dry flowing gases present at the contact zone.

Clearly in low levels of oxygen (the atmosphere was not pure nitrogen) and in the absence of water vapour (low humidities) the wear of these materials is much greater. The presence of a flowing gas at the contact zone also swept away any lose wear debris formed thus making them unavailable for re-cycling through the contact zone.

6.3 Observation of Wear Surfaces, Debris and Tribofilms.

After each test performed in section 6.1 the specimens were examined both optically and by SEM. The appearance of both the pin and the disc were examined with regard to the appearance of the wear track, the presence and

morphology of wear debris, the presence of tribofilms, the size of wear scars and the severity of damage to the material.

The general appearance of a wear track from a HP20 material sliding on itself is shown in Figure 6.17

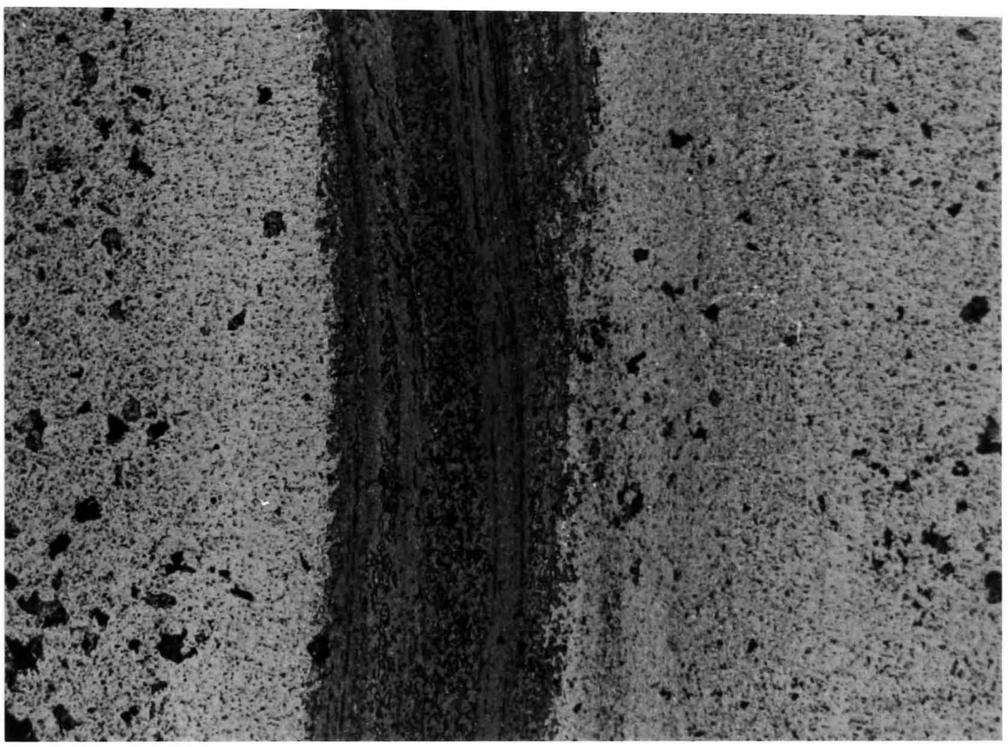

Figure 6.17 Optical micrograph of the wear scar on a disc formed from HP20 sliding on itself for 100m at V=0.05ms^{-1} under a load of 9.88N. Agglomerated wear debris can be seen to the left and right of the wear track

This optical image reveals the presence of wear debris either side of the wear track and what appears to be some form of damage in the middle. For HP20 sliding on itself under the standard conditions these features are shown by SEM to be tribofilms adhered to the surface as shown in Figure 6.18. These layers have been extensively cracked by the repeated passage of the pin but also show a very smooth finish. It can be seen that the film is thin and appeared transparent under optical microscopy.

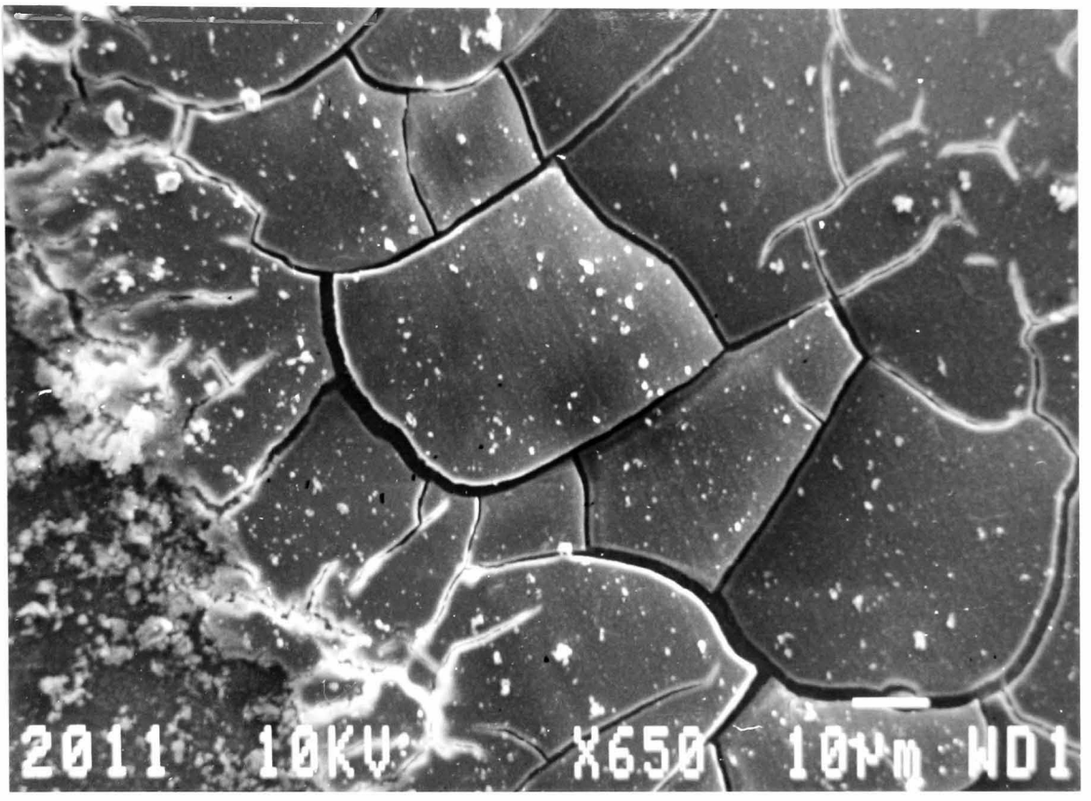

Figure 6.18 SEM image of the wear track shown in Figure 6.17. The disc is covered by a tribofilm that has been extensively cracked by repeated passage of the pin.

The thickness of the tribo film is demonstrated in Figure 6.19& Figure 6.20 where a small piece has peeled away from the surface. The underlying surface was seen to be slightly damaged on some areas and almost undamaged in others as shown in Figure 6.21 & Figure 6.22. The damage observed has probably occurred before the tribofilm formed. This indicates that the tribofilms are forming adhered protective layers preventing further wear of the disc.

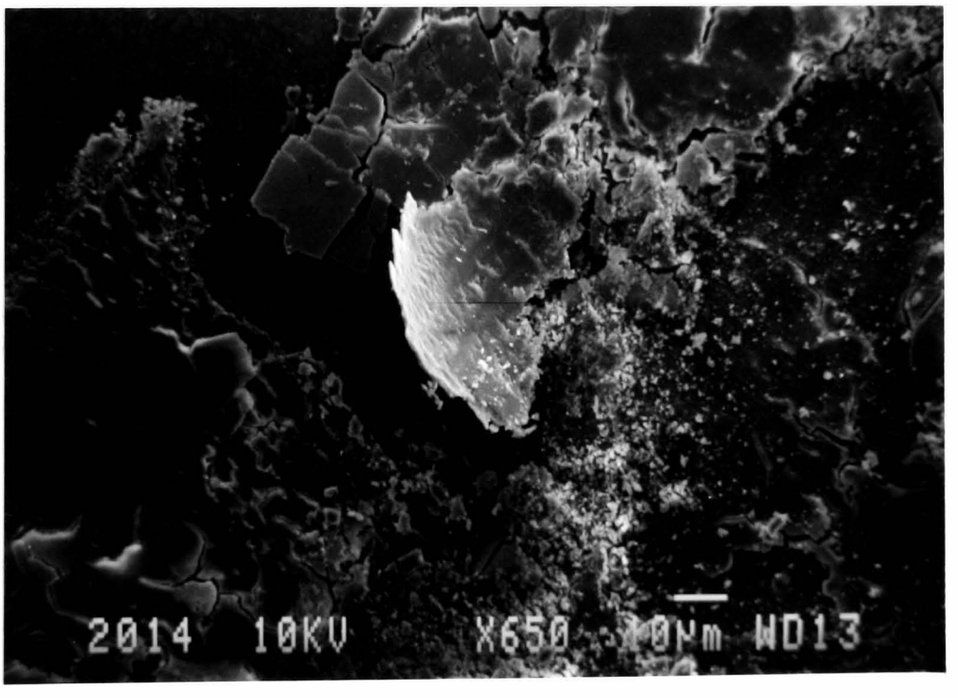

Figure 6.19 Extensively cracked tribofilm that has begun to peel away from the disc revealing undamaged surface underneath.

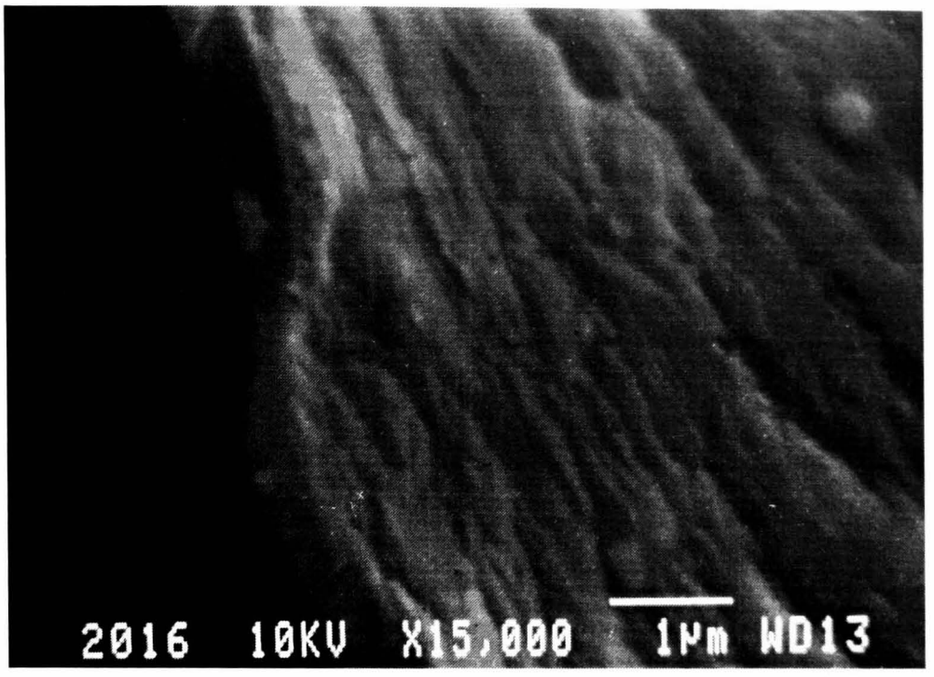

Figure 6.20 The thickness of the tribofilm shown in Figure 6.19, the film appears homgeneous and shows markings on its surface from the passage of the pin.

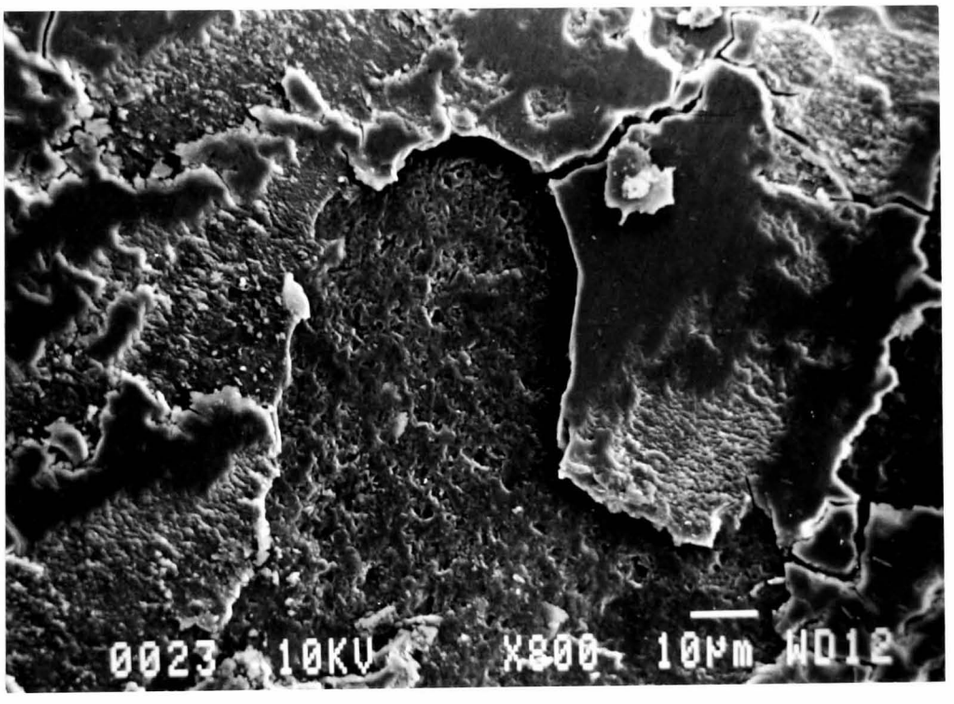

Figure 6.21 The removal of some areas of tribofilm reveal the underlying surface to have suffered some damage prior to the formation of the film.

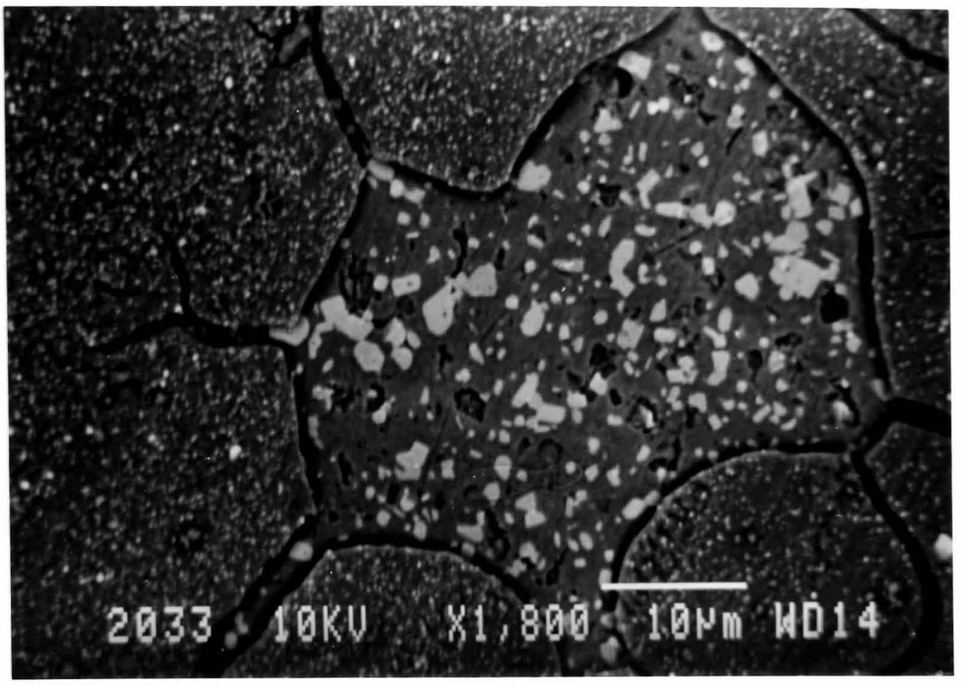

Figure 6.22 (back scattered mode) Another area where tribofilm has been removed. The underlying surface shows no signs of damage. Note that the surrounding tribofilm has many small bright inclusions.

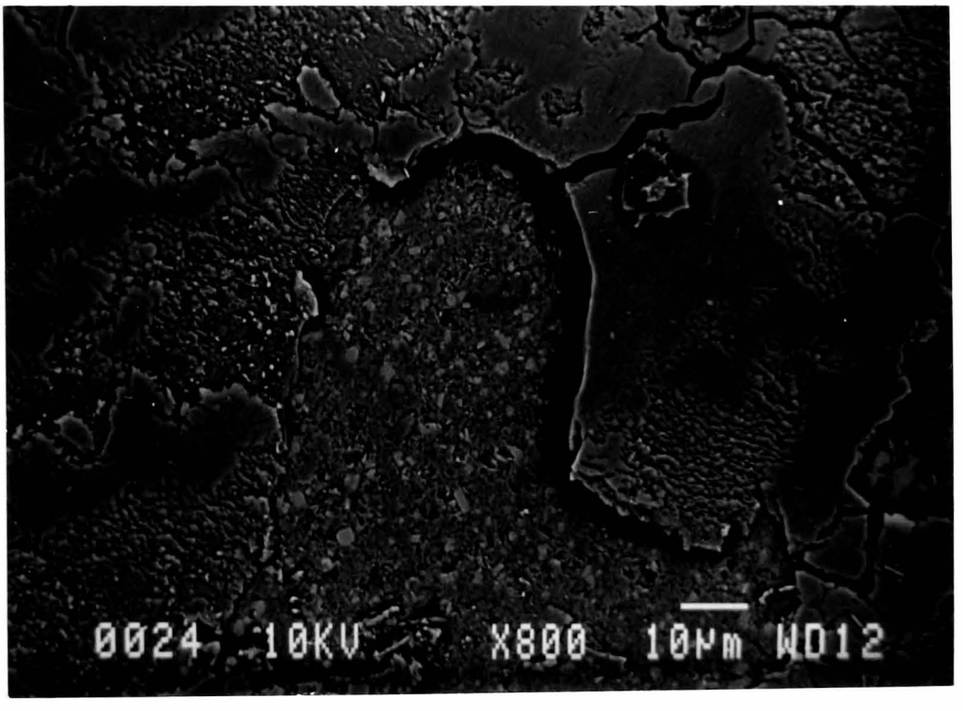

Figure 6.23 Back Scattered electron image of Figure 6.21 showing that this tribofilm has no bright inclusions.

Back scattered imaging of tribofilms reveals (Figure 6.22 & Figure 6.23) that some contain many fine particles while some are relatively homogeneous and single phase. EDX analysis of both tribofilms and wear debris was carried out. The wear debris and some fragments of tribo film were removed from the

surface so they could be analysed independently of the bulk material. Examination of wear debris shows them to be of a small particle size and to have a high oxygen content as shown in Figure 6.24. Also commonly encountered are the flake-like debris and these also have high oxygen content. These are not pieces of the original surface but fragments of tribofilm that have been cracked and removed. This analysis shows that both the films and wear debris contain all the elements found in the material plus elevated levels of oxygen. The small bright particles in the tribofilms were too small for meaningful analysis but because of their bright appearance in back scattered mode they are assumed to contain titanium. From this observation it was concluded that tribofilms and the fine wear debris were the product of tribo-chemical reactions between the materials in contact and the surrounding atmosphere forming a mixed oxide product.

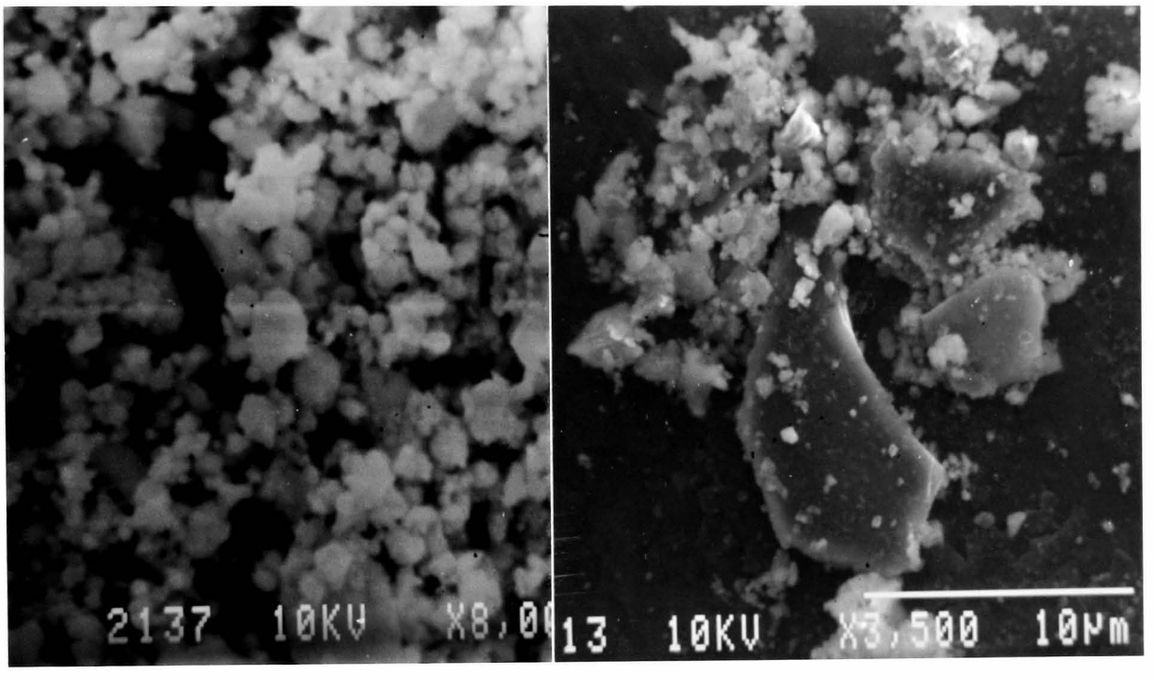

Figure 6.24 SEM images and EDX analysis of typical wear debris, both particles and flakes.

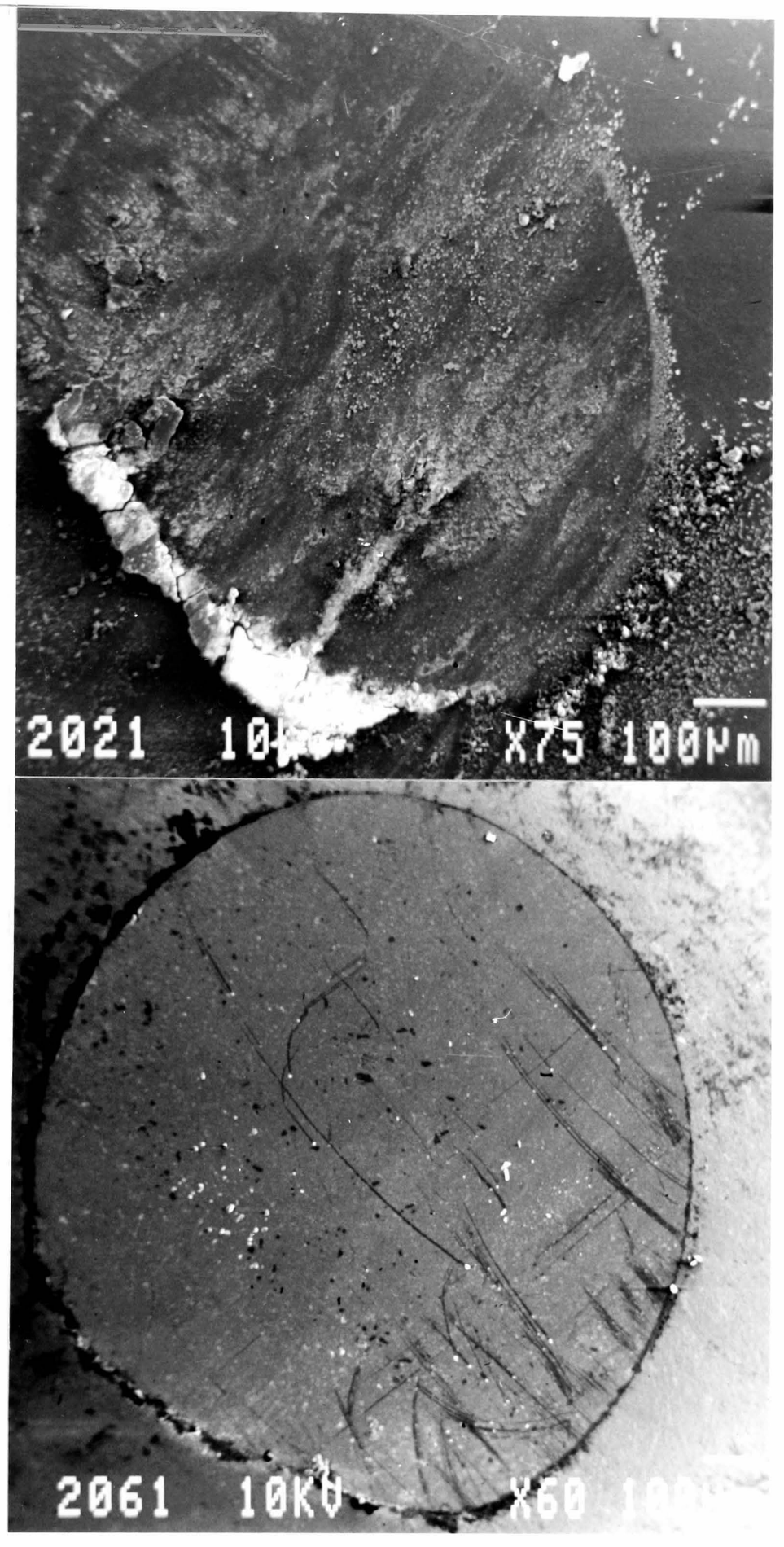

Figure 6.25 The appearance of the pin scar (a) as tested and (b) afetr removal of loosely bound wear debris.

The surface finish of the wear scar on the pin is shown in Figure 6.25. In the as-worn state the surface shows many adhered wear debris and tribofilm. After

gentle cleaning to remove loose debris the surface appears to have a very smooth finish.

Paraffin lubricated tests exhibited very little wear and smooth surfaces. Water lubricated tests showed just as much tribofilm formation (Figure 6.26) and wear in the presence of high humidity produced smooth pin wear surfaces as shown in Figure 6.27 where any pores in the original microstructure have been filled and are no longer visible.

When dry flowing air was used the damage to both the pin and the disc was observed to be more severe. (see figure 6.29). This could be due to the absence of water, hindering tribofilm formation and/or the removal of wear debris by the jet of air, making them unavailable to be form protective layers.

The large amounts of wear experienced for tests run in flowing dry nitrogen confirm that both oxygen and water vapour need to be present to form the protective tribofilms. While the damage observed is not severe the lack of protection has allowed both wear of the pin and disc to a much greater extent. The scar on the disc was observed to have a measurable profile, unlike other tests in air with 40%RH.

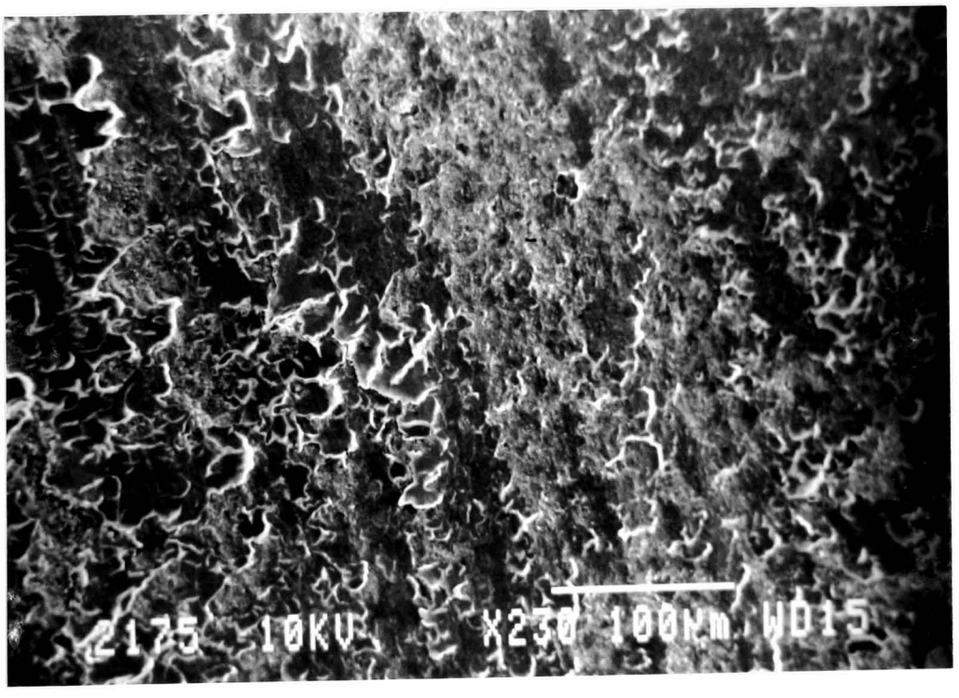

Figure 6.26 The worn surface of the disc after sliding in water. There is some tribofilm formation and some exposed, damaged disc surface.

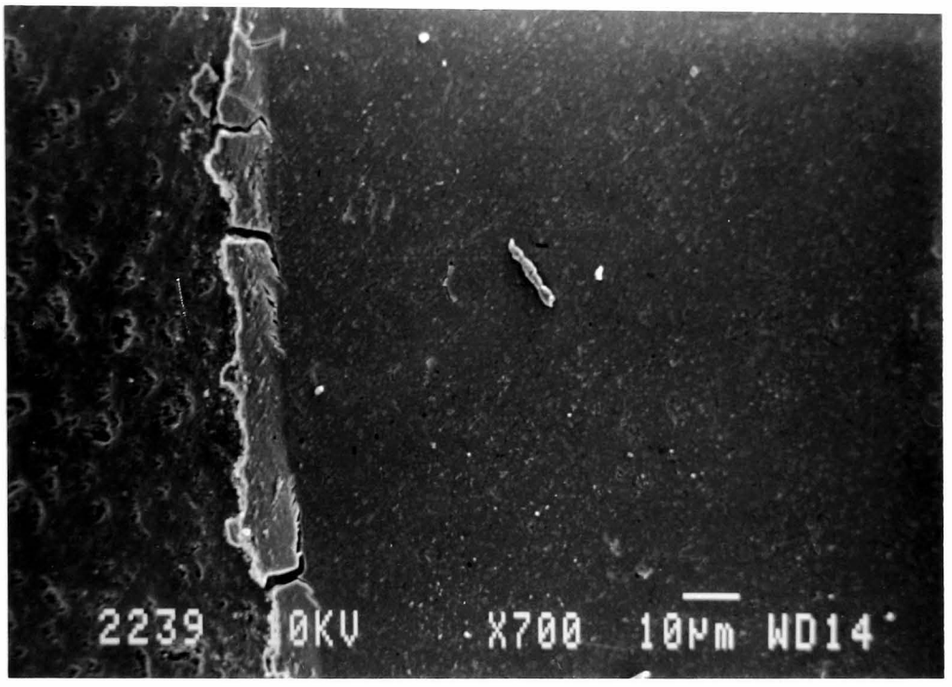

Figure 6.27 The smooth finish produced on the pin after sliding at >95% humidity. Note the porosity of the original unworn material on the left and the lack of apparent porosity on the pin wear scar.

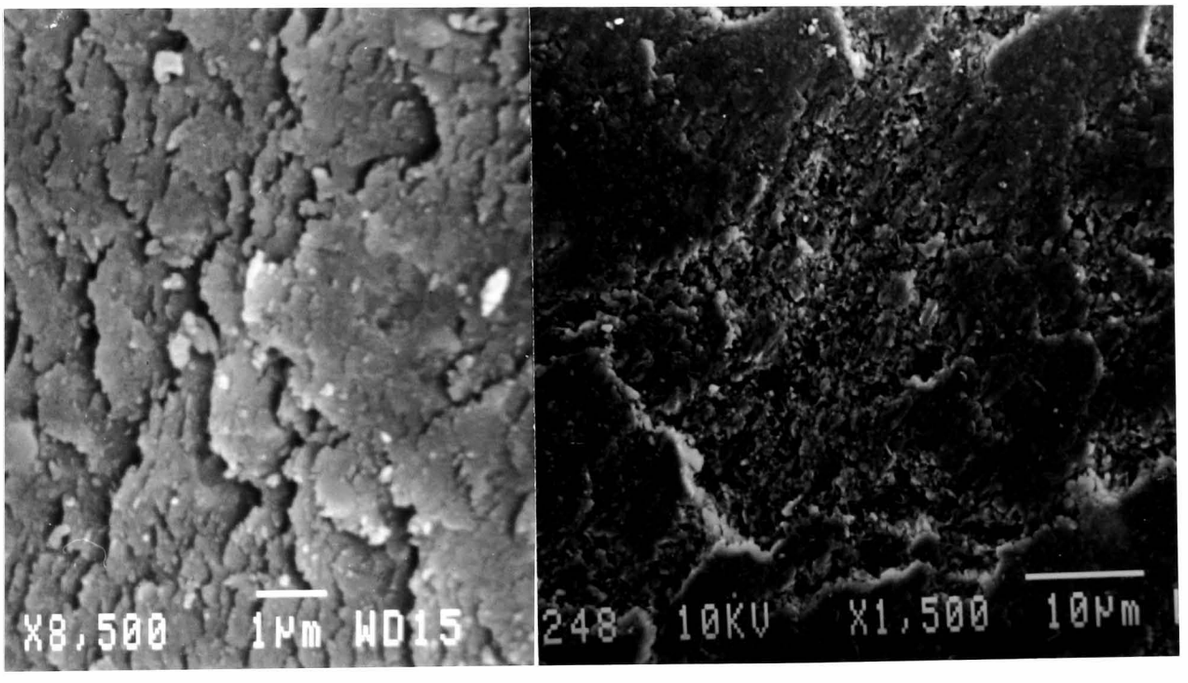

Figure 6.28 The damage on the pin (left)and disc (right) after sliding at <10% humidity in flowing air.

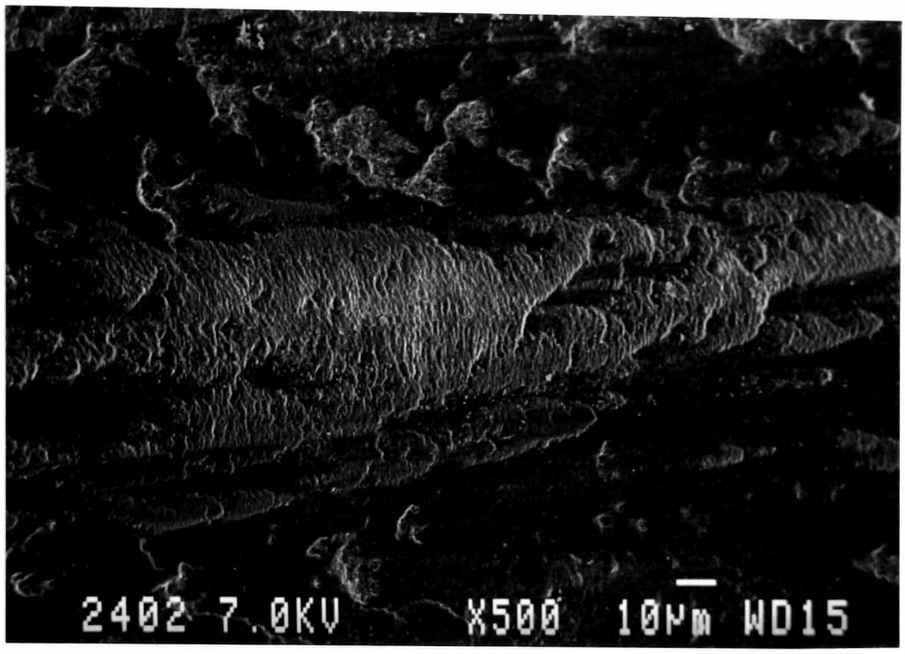

Figure 6.29 The wear surface of a disc of sialon101 after a standard test.

The wear surface of a disc of syalon101 is shown in Figure 6.29. The surface has been smoothed in places but has a "rippled" texture in others. EDX of the wear surfaces reveals them to also have a high oxygen content implying that the same wear mechanisms are active.

Steel pins sliding on the composites produced little or no apparent damage to the surface of the material and all material removal had occurred from the pin. Figure 6.30 shows the wear surface with no apparent damage. The small cylinders on the surface have been observed by other workers and determined to be hydroxylated silicon oxide formed from the tribochemical reaction with air and water vapour.[11] These debris have also been observed in sialon/TiB_2 tests at higher sliding speeds as shown in Figure 6.31.

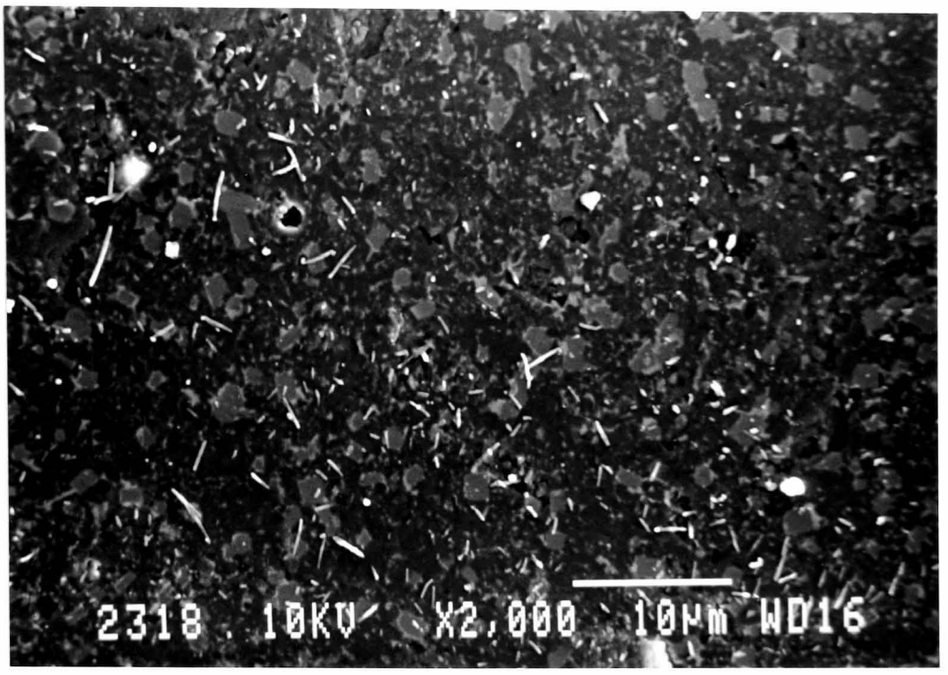

Figure 6.30 The surface of discs after sliding under a steel pin. No damage has been done to the disc, the cylindrical features have been identified as hydroxylated silicon oxide..

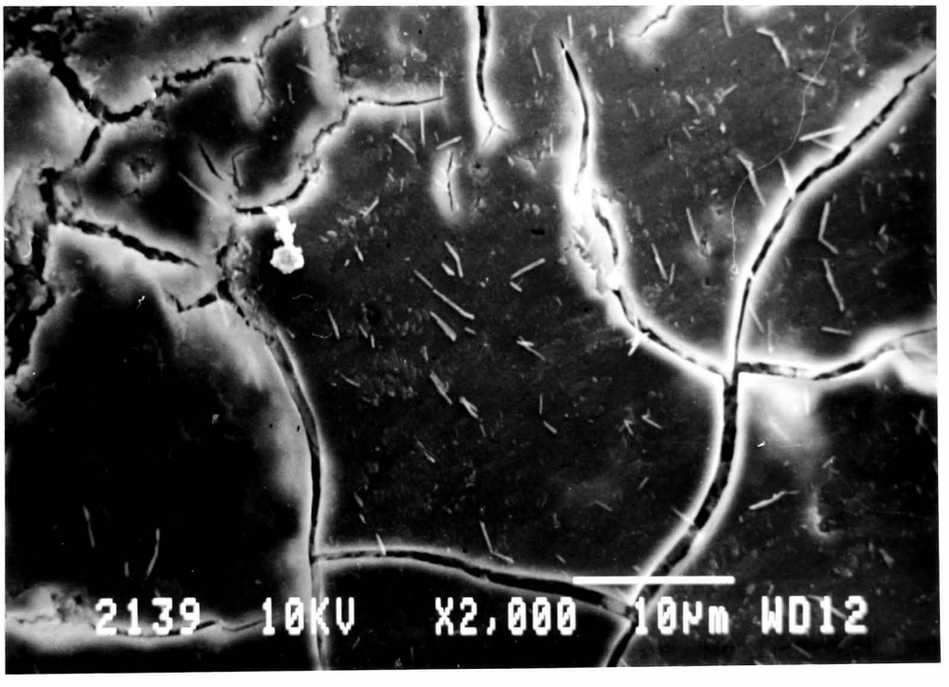

Figure 6.31 Hydroxylated silicon oxide wear debris produced at $0.1ms^{-1}$ sliding of HP20 on HP20.

6.3.1 The Variation of Applied Stress with Sliding Distance

The applied load reported on its own gives no indication of the stresses experienced by the material and often in the literature, tests carried out under the same load will actually be applying substantially different stresses. The stress induced by a spherical sliding contact is a function of applied load, Young's modulus (E), Poisson's ratio(ν), the pin radius(R) and coefficient of friction(μ). The equation previously given in chapter 4 is:

$$\sigma_s = \left\{ \frac{(1-2\nu)}{3} + \left[\frac{(4+\nu)}{8} \right] \pi\mu \right\} P_0$$

where

$$P_0 = \frac{3W}{2\pi r^2},\ r = \left(\frac{3\mathrm{WR}}{4\mathrm{E}^*} \right)^{1/3} \text{ and } E^* = \left[\left(\frac{1-\nu_1^2}{E_1} \right) + \left(\frac{1-\nu_2^2}{E_2} \right) \right]^{-1}$$

using this with the estimated values for E and ν and the measured value of μ the maximum tensile stress at the trailing edge of the contact for these composites during sliding is σ_s~ 2 to 3GPa. This, however, is soon reduced by the increase in contact area as the spherical pin forms a flat. Typically at the end of a test σ_s been reduced to ~20-30MPa. An example of real data obtained from the LVDT read-out on a hot pressed material test is shown below in Figure 6.32

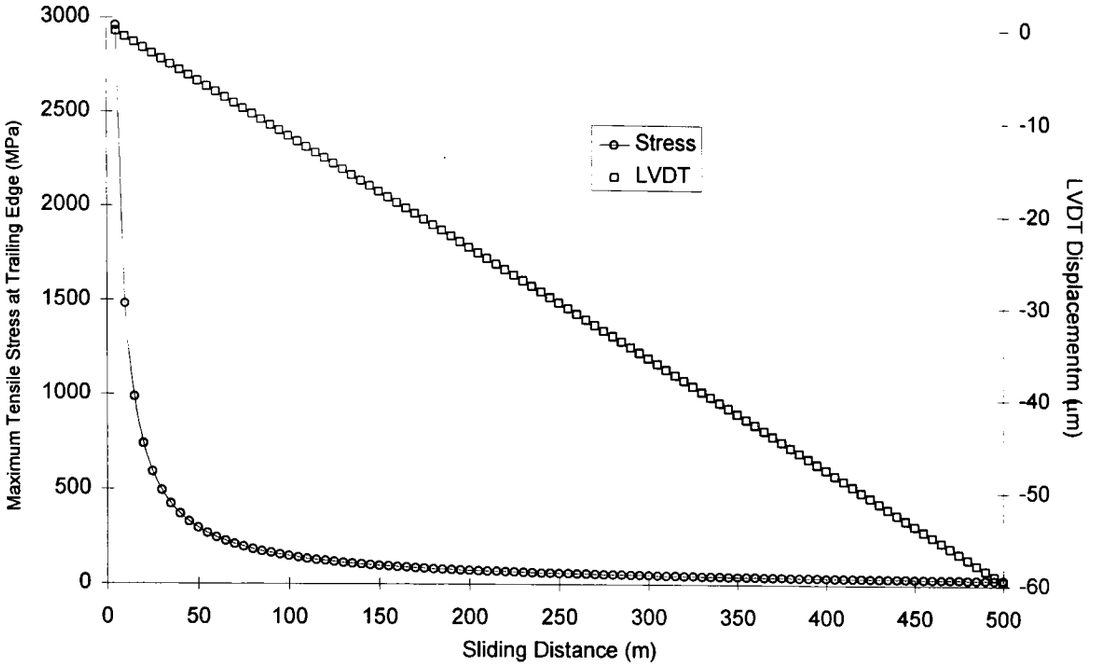

Figure 6.32 The variation in the maximum stress experienced at the trailing edge of a sliding contact with sliding distance, calculated from LVDT data from a real test.

It is clear then that unless a uniform contact area is used throughout the test then the actual stresses experienced by the disc vary with sliding distance. It is worth noting that to avoid this problem the alignment of the two surfaces to be in contact is critical and poses a difficult engineering problem, especially for small specimens.

The most severe damage and wear is expected to occur at the beginning but the rapidly decaying stress will soon fall to levels where much less severe damage is done. Thus in a single test it is possible that the material may experience several wear modes and that wear becomes less severe as the test progresses.

This situation implies that the wear coefficient, k, despite its form of $mm^3N^{-1}m^{-1}$, is not independent of sliding distance or load since the stress that causes damage varies with distance. In fact after the initial 50m the stress has been reduced to a point where much less wear should occur. Using k under such circumstances leads to misleading results suggesting that a material has a good wear resistance under a certain load when in fact over the last 400m or so of sliding very little wear has occurred. Compare this to a test run only over 100m and the results

will seem much worse as the same amount of damage has been done but only 100m is used in the calculation of k.

Unfortunately the full extent of this problem was not realised at the outset and some test have been performed over distances <500m. Consideration of the above points means that values of k for these tests should be expected to appear high when compared to 500m tests. This situation has important implications for the use of the pin-on-disc test as a standard wear test.

It also implies that observation of wear mechanisms at the end of a test does not necessarily give the full picture since the damage caused at the beginning of the test has been obscured by the less severe wear processes.

6.4 Wear Mechanisms of Sialon/TiB_2 Ceramic Composites.

Many researchers suggests the pin sliding on the disc causes microfracture and grain pull out due to the high stresses at the trailing edge. Most of the wear debris examined are high in oxygen content suggesting that they have formed by reaction with atmospheric oxygen and are not fragments of the original material removed by fracture. This is supported by their morphology which does not reflect the morphology of the original material. Under examination by TEM the wear debris are seen to be amorphous in nature, Figure 6.33. There were no diffraction spots when selected area diffraction was used on individual particles. It is proposed that while some microfracture and grain removal occurs at the beginning of sliding the formation of the majority wear debris observed is tribochemical in nature.

The fine wear debris produced are trapped under repeating sliding of the pin and tend to fill pores and craters formed by grain removal. The formation of a tribofilm then covers the surface. This process is shown schematically in Figure 6.34

Figure 6.33 TEM image of typical wear debris. No diffraction pattern was obtained form these particles showing them to be amorphous.

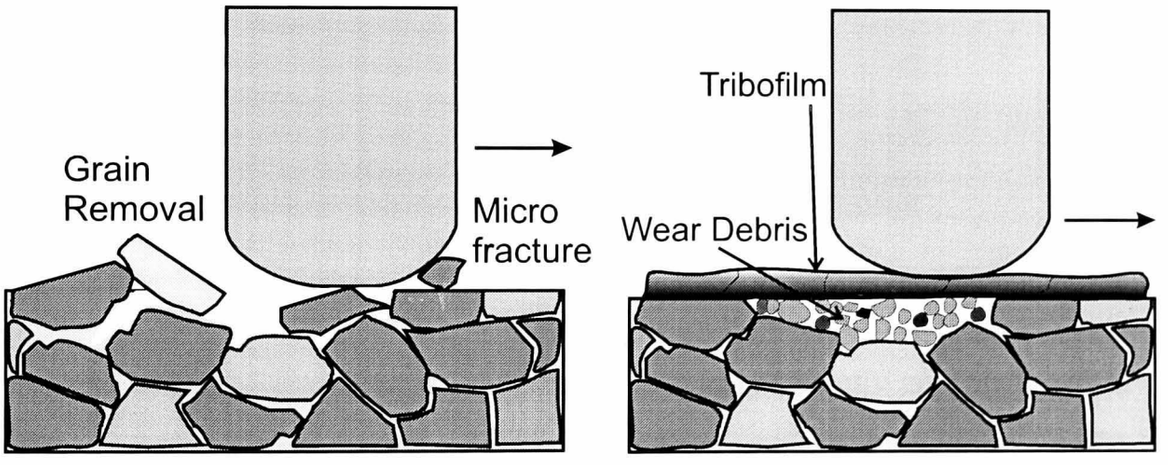

Figure 6.34 (a) Formation of wear craters by initially high stresses and (b) the filling of such craters by wear debris and the formation of a "protective" tribofilm.

It is clear that the surfaces quickly form tribofilms stopping further intimate contact. It is the wear of these films that is the source of the oxygen rich wear debris. This process is probably self perpetuating as some tribofilms observed clearly consist of compacted and coalesced wear debris (fig 6.36).

Wear is then dominated by the removal of the tribofilm by cracking. Large areas of tribofilm have to be removed before the pin can come into contact with the disc. The small gaps formed by the removal of pieces of tribofilm are quickly filled with more wear debris making further intimate contact between the pin and the disc unlikely. The wear mechanism after tribofilm formation is likely to be a polishing action on the pin by the wear debris formed and further reaction with oxygen.

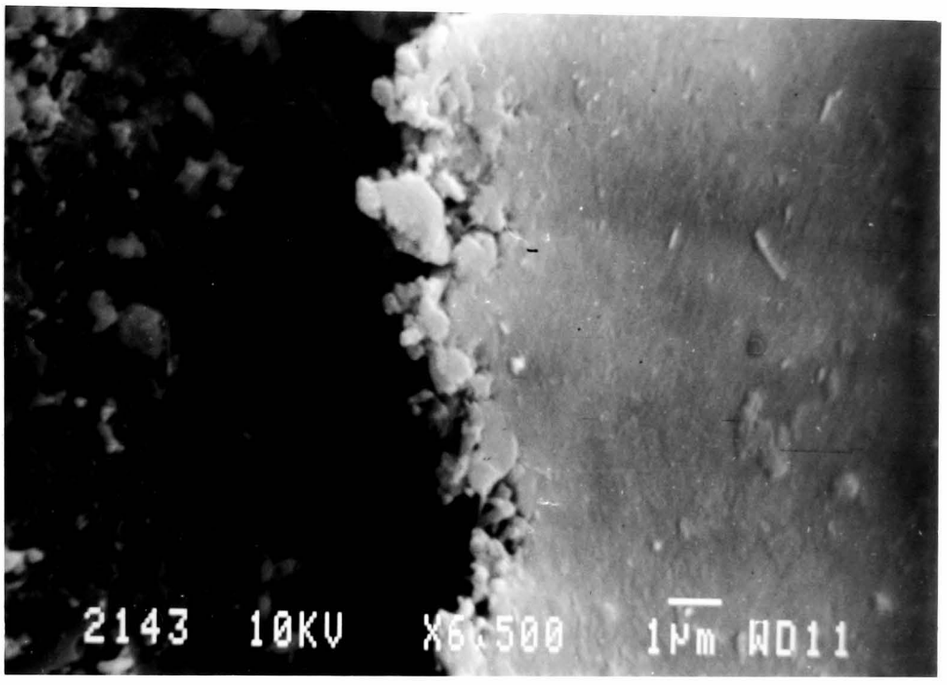

Figure 6.35 Tribofilm formed from compacted wear debris

It should be noted that the pin sliding on the disc is not strictly unidirectional in nature as demonstrated by the variation in the friction readout (see fig 6.1). The rebound of the arm under frictional loading produces a small scale reciprocal motion of the pin over the disc and the frequency and displacement is close to the conditions used in fretting wear test. This will complicate the situation over that of simple unidirectional sliding.

6.5 Summary of Wear

Generally, the wear coefficients of the pins measured for sialon/TiB_2 ceramic composites are comparable to other reported values for Si_3N_4 and sialon systems. Work on other Si_3N_4 or sialon composites has been carried out in a way that makes the results difficult to compare directly. The inherent difficulty

in comparing wear results between different experimental systems and differing materials makes it difficult to draw precise conclusions about the relative performance of these materials. However, the performance under the conditions used indicates that they are at least as good as Si_3N_4 and sialon systems when consideration is given to the fact that they are still at the development level and have not achieved their optimum properties.

The wear of these materials has been identified as being primarily dominated by tribochemical reactions with water and oxygen. These reactions form tribofilms and wear debris at the interface where conditions allow the formation of oxides and/or hydroxides. These conditions include high pressures and possibly high flash temperatures at asperity contacts. The tribofilms form protective layers adhered to the disc which prevent contact between the pin and the disc and wear takes place primarily of the pin by further tribochemical reaction and the polishing action of wear debris passing into the contact zone. Tribofilm removal by cracking is also a contibuting factor to wear.

As for friction, when one of the tribopair contains Y_2O_3 in the form of residual sintering aid the wear resistance is seen to improve. The exact nature of this effect is unclear but is most likely linked to the effect that yttria has on the properties and formation of oxide wear debris and tribofilms.

6.6 References

[1] M.G. Gee, "The formation of glass in the wear of reaction-bonded silicon nitride", *J. Phys. D: Appl. Phys*, **25** (1992) A182-A188

[2] P. Andersson & K. Holmberg, "Limitations on the use of ceramics in unlubricated sliding applications due to transfer layer formation.", *Wear*, 175. pp1-8, (1994)

[3] A. Skopp,, M. Woydt & H.-H. Habig, "Tribological behaviour of silicon nitride materials under un-lubricated sliding between 22°C and 1000°C",*Wear*, vol.181-183, No. 2, 1995, p.571

[4] P. Andersson, "Water Lubricated pin-on-disc tests with ceramics.", *Wear*, Vol 154, No.1, pp.37-47, Apr 1992

[5] Z. Xingxhong, L. Jiajun, Z. Baoliang, X Qunji, O. Jinlin, "The influence of lubrication on tribological properties of Si_3N_4/1045 steel sliding pairs", *J. Mater. Sci.*, **32**, (1997), pp.661-66

[6] A. Ravikiran & B.N. Pramila Bai, "Influence of the tribological reaction products and the associated transitions for the dry sliding of silicon nitride against steel", *J. Am. Ceram. Soc.*, **78** [11]. pp.3025-32, (1995)

[7]T.E. Fischer & H. Tomizawa, "Interaction of tribochemistry and microfracture in the friction and wear of silicon nitride.", *Wear*, Proc. Int. Conf. Wear Materials, ASME, New York, pp22-32, 1985

[8] M.G. Gee and D. Butterfield, "The combined effect of speed and humidity on the wear of silicon nitride", *Wear*, 162-164 (1993) pp. 234-245

[9] R.A. Page, C.R. Blanchard-Ardid, W. Wei, "Effect of particulate additions on the contact damage resistance of hot pressed Si_3N_4", *J. Mater. Sci.*, **23** pp946-57, 1988

[10] M.H. Wani, J. Mukerji, B. Prakash & S. Bandopadhay, "Friction and wear behaviour of hot pressed sialon-steel ball tribopair under reciprocating sliding conditions", *Am Ceram Soc. Bull.*, **72** [9], pp82-87 (1993)

[11] S. Jahanmir and T.E. Fischer, "Friction and wear of silicon nitride lubricated by humid air, hexadecane and hexadecane+0.5% stearic acid", *Tribology. Trans.*, **32** (1989) pp32-43

Chapter Seven

Conclusions and Further Work

7. Conclusions and Further Work

The 3 main objectives of this research were:

1. To investigate the production of sialon/TiB_2 particulate reinforced ceramic matrix composites via an in-situ reaction sintering route by both hot pressing and pressureless sintering.

2. To measure some of the key engineering properties of these composites with special attention to those properties that can influence wear.

3. To design and build a wear test apparatus suitable for testing small volumes of material and to use this apparatus to test the composite's tribological properties.

By achieving these objectives a critical assessment of the potential for particulate reinforced composites has been performed.

7.1 Synthesis of Sialon/TiB_2 Ceramic Matrix Composites

Using the reactions identified by Hong[1], compositions were calculated that produced both TiB_2 and sialon simultaneously from TiN, BN and Si. The production of a sialon/TiB_2 composite also required the use of α Si_3N_4 and AlN where the oxide components for sialon production were present as oxide impurities on the surfaces of powders.

The use of in-situ reaction sintering requires a two stage process. The first hold temperature is required for the synthesis of TiB_2 from TiN and BN and the simultaneous production of Si_3N_4. The reaction temperature was found to be critical, too low and the reactions did not fully occur and too high and the silicon present liquified and was no longer available for reaction. The optimum temperature was found to be 1380°C and hold times of ~1 hour were sufficient to complete the reaction.

Once reaction was complete, a second hold at a higher temperature was used for the densification of the sialon matrix via liquid phase sintering. Again the temperature was limited by the possible reactions that could occur between nitrogen (present from the surrounding atmosphere or from the dissociation of Si_3N_4) and the TiB_2 in the sample. The optimum temperature for densification was found to be 1650°C for times of 1 to 2 hours.

In hot pressing, applied pressures of up to 30MPa were required to densify the sample. It was found that the pressure should be applied as soon as possible to prevent the penetration of nitrogen into the sample which could consume the silicon before it had reacted to form Si_3N_4 in the reaction to form TiB_2.

It was not possible to produce dense composites without the addition of a sintering aid containing Y_2O_3. This contradicted preliminary work which had successfully densified a limited number of samples via hot pressing without any externally added sintering aid. It had been thought that the levels of oxide impurities present were sufficient to form a liquid phase at the sintering temperature. This was found to be incorrect by a series of experiments in which both the levels of oxides present and the sintering temperatures were varied. Eventually the addition of a small amount of Y_2O_3 (1wt%) allowed the densification process to occur and produced composites close to the theoretical density (95-97%). Y_2O_3 is known to produce large volumes of liquid, in reaction with SiO_2 and Al_2O_3, from very small additions. It was assumed that in the preliminary work samples had been contaminated with small amounts of Y_2O_3, most probably from the mixing and milling procedures.

To avoid the formation of Yttrium Aluminium Garnet (YAG) the yttria for subsequent samples was added in the form of a glass consisting of Y_2O_3, Al_2O_3 and SiO_2. This means that the level of yttria added was reduced to 0.25wt%. Hot pressed samples using this additive still achieved good densities of 95-97% of the theoretical.

XRD of the specimens produced reveals them to consist of only the desired phases of sialon (a low substitution β sialon) and TiB_2. No yttria containing

phase was detectable. Like most hot pressed materials there were surface layers that had to be removed to reveal this underlying material.

Pressureless sintering of the above compositions was carried out using ~15wt% of the yttria containing glass. The presence of the glass did not effect the reaction to form TiB_2. Pressureless sintering required the two stage temperature process as described for hot pressing but also required the presence of an inert atmosphere at the reaction temperature to avoid nitridation of the silicon. Argon was used after an initial evacuation of the furnace to $>5x10^{-5}$mbar to degas the sample and produce a pure argon atmosphere. At the sintering temperature the presence of a nitrogen atmosphere was found to be necessary to avoid the dissociation of the sialon. However, if introduced before the sample had achieved closed porosity the TiB_2 could reconvert to TiN throughout the whole sample. The point at which to change from argon to nitrogen was determined by experiment to be ~20 mins after the sintering temperature had been reached. Under these conditions pressureless sintered materials achieved densities of 95-97% of the theoretical with phase contents of β sialon, TiB_2 and YAG. The YAG is thought to have formed from crystallisation of the yttria rich intergranular phase on cooling from the sintering temperature. The presence of YAG can be beneficial in terms of high temperature strength and creep but detrimental in terms of room temperature fracture toughness.

All pressureless sintered materials consisted of a dense core of the required phases surrounded by soft, porous layers of Y α sialon, TiN and BN formed from the dissociation of the sialon and the reaction between nitrogen and TiB_2 at the surface. Attempts to limit the extent of this surface layer with the use of powder beds were not successful.

Some inconsistencies were found in the production of pressureless sintered materials. Many samples sintered in identical ways had differing amounts of surface layers, some with only thin layers and some where the layers consisted of the majority of the sample. This can be attributed to several factors, inconsistencies in the composition from sample to sample, variations in the

furnace conditions, variations in the green density or some unknown variable. The powder processing stages are well known and produce homogeneous mixtures consistently for other materials and the furnace was generally found to be reliable by other workers. It is possible that uniaxial pressing was not sufficiently controlled to produce constant green densities, resulting in differing densification rates which would explain the observed results. It is also possible that combination of factors, including unknown variables, contribute to the problem.

Thus it was found to be possible to produce sialon/TiB_2 composites with close to full density using in-situ reaction by both hot pressing and pressureless sintering. The technique avoids many of the problems found in producing such composites via conventional methods.

7.2 Microstructure of Sialon/TiB_2 Composites

Study of the microstructures by SEM reveals that both production methods produce homogeneous distributions of TiB_2 in a sialon matrix. The particle sizes are spread over the range 0.5 to 3 μm with some larger particles being produced from the joining of two adjacent particles. TiB_2 morphology varies from near spherical to hexagonal with some rectangular higher aspect ratio grains. All observed morphologies reflect the hexagonal crystal structure of TiB_2. All particles appear well bonded with the matrix with no porosity or reaction zone around each particle. This fact is important if the properties of TiB_2 are to influence those of the matrix material.

In hot pressed materials the matrix grain size and morphology was not observed due to the absence of any intergranular phase to highlight the microstructure. No yttria containing phase was detected by SEM.

In pressureless sintered materials there was a significant amount of intergranular phase which was rich in yttria. It is known from XRD that this phase must contain YAG but it is also possible that some glass remains. The intergranular phase allows the observation of the sialon grain size and morphology. Generally

the grains are small(<1μm in many cases) with a mixture of spherical/hexagonal and some elongated grains. This small grain microstructure is expected to confer the material with high hardness while the presence of TiB_2 may toughen the material.

The level of porosity observed by SEM concurs with that inferred from density measurements. Pressureless sintered materials are seen to have increased porosity around the edges where dissociation and reaction had occurred during sintering.

7.3 Hardness and Fracture Toughness of Sialon/TiB_2 Ceramics

The hardness and fracture toughness can be key factors in determining the wear behaviour of materials. In addition they are also important in many potential applications for this material.

Hardness was measured by Vickers (H_v) and Knoop (H_k) diamond indentation at various loads. It is important to note that the values reported were those measured at loads where cracking at the corners of the indents did not occur. This is a more accurate assessment of hardness than those where a high load is used to achieve an easily visible indent. At such loads the cracks are formed under the indenter making the assessment of hardness inaccurate.

Under such conditions the hardest hot pressed materials had a value of $H_v(5N)=22\pm2GPa$ while pressureless sintered materials achieved a maximum of $H_v(5N)=19\pm2GPa$. When correction for the presence of porosity was applied the values rise to a potential of $H_v(5N)=29GPa$ and $H_v(5N)=24GPa$ respectively. The measurement technique was validated by the parallel measurement of a sialon of known hardness. Syalon101 hardness was measured as $H_v(50N)=17\pm2GPa$ and $H_v(5N)=16\pm2GPa$ and these values compare well with the accepted value of $H_v(60N)=16GPa$.

These high hardnesses were attributed to the inclusion of TiB_2 ($H_v(0.3N)=33GPa$) and the small grain size of the sialon. These materials thus

applications where high hardness is required, including tribological applications.

Fracture toughness was measured by the indentation method which has been shown to consistently produce lower K_{Ic} values than precracked beam methods. In order to calculate K_{Ic} the value of E for these materials was first estimated from the rules of mixtures while compensating for the presence of porosity. Using these estimated values K_{Ic} was found to vary from specimen to specimen but generally K_{Ic} was found to be in the range 4 to 4.3MPa $m^{½}$. The parallel testing of syalon 101 by this method resulted in a value of K_{Ic}=4.4MPa $m^{½}$ which compares with accepted values of K_{Ic} measured by notched beam techniques of 7.7MPa $m^{½}$. Hence from this and other comparisons of techniques in the literature[2,3] the expected value for the K_{Ic} of these materials measured by other techniques is ~6-8MPa $m^{½}$. Other factors such as time dependent slow crack growth and the applicability of the model used to calculate K_{Ic} all act to reduce the measured value of K_{Ic}.

7.4 Toughening Mechanisms in Sialon/TiB_2 Composites

The fracture toughness of these materials is relatively high when considering the small grain size of the matrix and the non-optimised properties. It is thus reasonable to assume that the some toughening mechanisms are in action. It is clear from SEM images that cracks do interact strongly with TiB_2 particles, which are considerably larger than the matrix grains. The cracks are seen to be deflected around the TiB_2 and are often deflected through large angles of up to 90°. Some cracks are also seen to fracture TiB_2 particles intra-granularly. A typical crack is seen to interact with many TiB_2 grains throughout its length. Thus crack deflection is a possible toughening mechanism.

The SEM studies of microstructure have shown that TiB_2 is well bonded in the matrix phase. The pullout of the larger TiB_2 grains from the matrix is likely to absorb some of the of the crack energy. Some TiB_2 particles are seen to bridge the crack after the crack front has passed and may absorb some energy by intergranular friction and mechanical interlocking.

Finally, while there is no direct evidence for it, the mismatch of thermal expansion coefficients of TiB_2 (α=6.63 to 8.7x10^{-6}/K) and Si_3N_4/sialon (α~3x10^{-6}/K) will cause the particles to be in tension and the matrix to be in overall compression. This compressive force may suppress the crack growth through the matrix. Thermal expansion mismatch can also give rise to microcracking which can toughen by spreading the stress over several crack fronts and lowering the local modulus.

7.5 Oxidation Resistance

Not only is oxidation resistance important in high temperature applications but many researchers have reported the oxidation of ceramics at room temperature under tribological conditions.

The limited tests conducted show that at 1000°C for 100 hours no catastrophic oxidation occurs and that only the surface layers appear to have undergone oxidation.

7.6 Tribology of Sialon/TiB_2 Ceramics

For the study of tribology a wear test apparatus was constructed to the NPL guidelines for dry sliding pin-on-disc tests.[4] The composites produced were tested with respect to their friction and wear properties.

7.6.1 The Wear Test Apparatus

The wear test apparatus constructed was of the pin-on-disc configuration as it was the most suitable for application to small volumes of material and is commonly encountered in the literature. The apparatus was capable of testing specimens of diameters as low as 15mm with pins of ~3x3x10-20mm. This is ideal for materials development where material may be limited. Loads were also limited to those that did not damage the material to the extent where it could not be used for subsequent tests.

The accuracy of the apparatus was limited by the magnitude of the frictional force, low coefficients of friction produced low signal to noise ratios. This was not a problem for dry sliding where $\mu>0.5$ for most of the time. The accuracy of the measurement of wear was limited by the ability to produce accurate spherically ended pins and by the ability to measure the worn volume of the disc. This was seen to be made practically impossible by the formation of tribofilms in the majority of tests. The wear volume of the pin was used as a performance indicator for these materials.

7.6.2 Friction

Tests were carried out under a range of conditions including varying sliding speed, load and humidity. Friction was measured for both hot pressed and pressureless sintered materials. Generally, for dry sliding of like tribopairs the value of μ was ~0.7 to 0.8 for hot pressed materials and μ~0.4 to 0.5 for pressureless sintered materials with values between these extremes when different grades were run on each other.

These compared well with other researchers working with similar conditions on Si_3N_4 and sialon materials. Syalon101 tested in the same way was found to have a value of $\mu=0.7$.

A weak dependence with load was observed for hot pressed ceramics with μ falling with decreasing loads. The variation of sliding speed also exhibited a decreasing μ with increasing speed for hot pressed materials. Pressureless sintered materials did not behave in such a simple manner with varying speed, exhibiting a minimum in μ at $0.05ms^{-1}$.

The level of humidity did not seem to have a large effect on the level of μ and water lubricated tests also demonstrated only a slight decrease in μ. Paraffin lubricated tests show that these ceramics respond well to conventional lubricants. The level of μ was reduced to <0.25 and shows that boundary lubrication is occurring at the interface. The use of pre-oxidised discs did not lower μ and may have even increased it by roughening the surface.

It was noted that in tests with a fixed load the actual stress experienced by the material fell rapidly because of the increased area of contact formed by wear of the pin. In such a situation μ is independent of decreasing stress where a steady state coefficient of friction is observed. However stress varies most at the beginning of the test where the measured friction is increasing and these two effects, "wearing in" and the change of friction with decreasing applied stress, cannot be observed independently.

One feature that is found in many friction/sliding distance plots is the initial high value of μ followed by a fall to a lower steady state level. It is possible that this is caused by the high stresses resulting from the initial small area of contact. Calculations show that the maximum pressure applied at the beginning of a test is of the order of 2 to 3GPa. The resulting high stresses may cause fracture and grain pullout leading to rough surfaces and high friction. The formation of tribofilms soon after sliding has begun can reduce friction by "healing" the rough surface by filling damage with wear debris and providing a smoother sliding surface (see figure 6.19)

The difference in μ between hot pressed and pressureless sintered materials is attributed to the presence of yttria containing phases in the pressureless sintered grade. It was shown that the interface between pin and disc is occupied by oxide products resulting from tribochemical reactions. It is proposed that the presence of yttria effects the properties of the tribofilms and wear debris and that this influences the interface in such a way as to reduce friction.

The variation with sliding speed and the lower values of μ measured on reduction of the speed suggest that the sliding interface is subject to change with increasing speed possibly due to the increase in flash temperatures at asperity contacts[5]. Again the difference between hot pressed and pressureless sintered is attributed to the presence of yttria.

7.6.3 Wear

Wear coefficients for the composites under dry sliding conditions with varying tribopairs were measured from the worn volume of the pin. The best results obtained were for pressureless sintered pins on hot pressed discs with $k=1.1x10^{-6}$ $mm^3N^{-1}m^{-1}$ with hot pressed on pressureless sintered being the next best with $k=2.5x10^{-6}$ $mm^3N^{-1}m^{-1}$. Hot pressed material on itself exhibited $k=4.6x10^{-6}$ $mm^3N^{-1}m^{-1}$. The increase of humidity increased wear as did *decreasing* the load. The former result can be explained by the increased amount of tribochemical wear due to increased amounts of water vapour. However, the increase of wear with decreasing load has not been explained. It is possible that under decreased loads the conditions to form protective layers are not present and more wear occurs this way or that the decreased pressure at the contact zone does not repair the tribofilm by consolidation of wear debris.

The wear behaviour of sialon/TiB_2 ceramics was found to be dominated by tribochemical reactions with oxygen and water. These reactions formed oxide or hydroxide wear debris and tribofilms which adhered to the disc surface and hence protected the disc from further significant wear. The high stresses caused by the initial contact geometry caused some damage to the disc, probably by the extension of surface cracks caused by the tensile stress at the trailing edge of the pin contact zone. This damage was observed in some areas where tribofilms had been removed from the surface. However, tribofilm formation soon builds up and stops direct contact between pin and disc. Other areas where tribofilms had been removed showed an underlying undamaged disc surface.

Wear of the material is then by cracking and removal of the tribofilm and tribochemical wear and polishing of the pin by the small wear debris.

Consideration of the stresses produced by a sliding spherical contact has shown that the actual stress experienced by the material decreases rapidly with sliding distance. (see figure 6.17). This leads to the conclusion that different wear modes maybe present during a single test. The most severe wear will occur at the beginning when stresses are high but this period is short lived (50-100m in

tests described here) as stresses are reduced and tribofilms form. This makes the initial state of the surfaces important because it is these surfaces that undergo the most wear. For the rest of the test the stresses will be much lower and vary little with sliding distance and a less severe wear mechanism is expected. This situation makes use of the wear coefficient k unsuitable as it is supposed to measure the wear of a material independent of load and sliding distance. As has been demonstrated it is not independent of either if non-uniform areas of contact are used. This has implications for pin-on-disc testing using spherically capped pins (or other geometries where the contact area increases with wear).

7.7 Summary

The objectives of this research have been achieved in that composites have been produced successfully and tested with regards to hardness, fracture toughness and tribological properties. However, despite satisfactory results for all of the above properties the addition of TiB_2 has been seen to play no major role in these properties with the possible exception of fracture toughness. Much emphasis is placed on the high hardness of TiB_2 of 33GPa but it should be noted that this is a microhardness quoted at 0.3N load and it can be expected to be much lower at higher indentation loads (e.g. $H_v(5N)=20.8GPa$)[6] It is the excellent properties of the sialon matrix that contribute to the properties measured and sialon matrices can be tailored (by grain growth) to achieve fracture toughness of the same level and higher and have the advantage of being easier to process (i.e. no surface layer problems). The role of TiB_2 in the wear resistance of these composites is unclear and oxidation characteristics, which contribute to the formation of protective tribofilms, may be influenced by the presence of titanium and boron but the most obvious effect has been shown to be caused by the presence of intergranular phases containing yttrium.

Considering the above points further development of these types of composites should be pursued in parallel with other Si_3N_4 based materials such as α'/β' sialons to ensure that property improvements are significant and could not be more easily achieved by simpler, more well established routes.

7.8 Further Work

The elimination of the final few percent of porosity would allow the composites to realise their true potential with respect to hardness and fracture toughness. The use of HIPing or sinter-HIPing has the potential to produce fully dense composites. The problem of the reaction of the nitrogen with the TiB_2 forming TiN and BN at the surface also needs to be addressed. It is possible that better green densities may help minimise the effect and isopressing of green bodies can be used to achieve this. The use of powder beds of a more complex composition may also allow the minimisation of this surface effect.

The production of greater volumes of material would allow testing of the strength of the materials and also the measurement of fracture toughness by destructive methods that are more directly comparable to other materials.

Originally it was envisaged that the tribological study would involve the construction of wear maps for these materials. However, the apparatus was not capable of the range of variation of load and speed needed to investigate the differing wear modes. Modifications to the apparatus that would allow a greater variation in loads and speeds while maintaining accuracy is one objective of further work. As has been shown the use of spherically capped pins reduces the meaningfulness of pin-on-disc tests so the use of uniform cross section pins would be another objective. This requires perfect alignment of the pin and disc and requires re-engineering of the apparatus.

7.9 References

[1] F. Hong, M.H. Lewis, "Ceramic matrix composites via insitu reaction sintering", *Ceram. Eng. & Sci. Proc.*, **14**, 1993, p131

[2] S.R. Choi, J.A. Salem, "Crack-growth resistance of in-situ toughened silicon nitride", *J. Am. Ceram. Soc.* , **77** [4], pp.1042-46(1994)

[3] M. Srinivasan & S.G. Seshadri, "application of single edged notched beam and indentation techniques to determine fracture toughness of alpha SiC", *Fracture Mechanics of Ceramics Rocks and Concrete,* ASTM STP, 745. S.W Freiman & E.R. Fuller eds. American Society for Testing and Materials. 1981. pp46-68.

[4] M.G. Gee, "Guidelines for unlubricated sliding wear tests: Part1, general approach", & "Guidelines for unlubricated sliding wear tests: Part 2. procedures for pin-on-disc testing", DMM(A)96, National Physical Laboratory (NPL), Teddington , Middlesex, UK., April 1993.

[5] M.H. Wani, J. Mukerji, B. Prakash & S. Bandopadhay, "Friction and wear behaviour of hot pressed sialon-steel ball tribopair under reciprocating sliding conditions", *Am Ceram Soc. Bull.*, **72** [9], pp82-87 (1993)

[6] S.K. Chung, "Fracture characterisation of armour ceramics", *Am.Ceram Soc. Bull.*, **69** [3], pp358-66, 1990